SLAC-PUB-9498
September 2002
CERN-EP/2001-098
hep/0112021

A Combination of Preliminary Electroweak Measurements and Constraints on the Standard Model

The LEP Collaborations, ALEPH, DELPHI, L3, OPAL,
the LEP Electroweak Working Group
and the SLD Heavy Flavour and Electroweak Group

Stanford Linear Accelerator Center, Stanford University, Stanford, CA 94309

Work supported by Department of Energy contract DE–AC03–76SF00515.

EUROPEAN ORGANIZATION FOR NUCLEAR RESEARCH

CERN-EP/2001-098
LEPEWWG/2001-02
ALEPH 2001-078 PHYS 2001-028
DELPHI 2001-131 PHYS 906
L3 Note 2723
OPAL PR 350
hep-ex/0112021
December 17th, 2001

A Combination of Preliminary Electroweak Measurements and Constraints on the Standard Model

The LEP Collaborations* ALEPH, DELPHI, L3, OPAL,
the LEP Electroweak Working Group†
and the SLD Heavy Flavour and Electroweak Groups‡

Prepared from Contributions of the LEP and SLD Experiments to the 2001 Summer Conferences.

*The LEP Collaborations each take responsibility for the preliminary results of their own.

†WWW access at `http://www.cern.ch/LEPEWWG`

The members of the LEP Electroweak Working Group who contributed significantly to this note are:
D. Abbaneo, J. Alcaraz, P. Antilogus, A. Bajo-Vaquero, P. Bambade, E. Barberio, M. Biglietti A. Blondel, S. Blyth, D. Bourilkov, P. Casado, D.G. Charlton, P. Checchia, R. Chierici, R. Clare, B. de la Cruz, M. Elsing, P. Garcia-Abia, M.W. Grünewald, A. Gurtu, J.B. Hansen, P. Hansen, R. Hawkings, J. Holt, R.W.L. Jones, B. Kersevan, N. Kjaer, E. Lançon, L. Malgeri, C. Mariotti, M. Martinez, F. Matorras, C. Matteuzzi, S. Mele, E. Migliore, M.N. Minard, K. Mönig, A. Oh, C. Parkes, U. Parzefall, Ch. Paus, M. Pepe-Altarelli, B. Pietrzyk, O. Pooth, G. Quast, P. Renton, H. Rick, S. Riemann, J.M. Roney, H. Ruiz, K. Sachs, S. Spagnolo, A. Straessner, D. Strom, R. Tenchini, F. Teubert, E. Tournefier, A. Valassi, S. Villa, H. Voss, C.P. Ward, N.K. Watson, P.S. Wells.

‡N. de Groot, P.C. Rowson, V. Serbo, D. Su.

Abstract

This note presents a combination of published and preliminary electroweak results from the four LEP collaborations and the SLD collaboration which were prepared for the 2001 summer conferences. Averages from Z resonance results are derived for hadronic and leptonic cross sections, the leptonic forward-backward asymmetries, the τ polarisation asymmetries, the $b\overline{b}$ and $c\overline{c}$ partial widths and forward-backward asymmetries and the $q\overline{q}$ charge asymmetry. Above the Z resonance, averages are derived for di–fermion cross sections and forward-backward asymmetries, W–pair, Z–pair and single–W production cross section, electroweak gauge boson couplings, W mass and width and W decay branching ratios. For the first time, total and differential cross sections for di–photon production are combined.

The main changes with respect to the experimental results presented in summer 2000 are updates to the Z-pole heavy flavour results from SLD and LEP and to the W mass from LEP. The results are compared with precise electroweak measurements from other experiments. Using a new evaluation of the hadronic vacuum polarisation, the parameters of the Standard Model are evaluated, first using the combined LEP electroweak measurements, and then using the full set of electroweak results.

Chapter 1

Introduction

This paper presents an update of combined results on electroweak parameters by the four LEP experiments and SLD using published and preliminary measurements, superseding previous analyses [1]. Results derived from the Z resonance are based on data recorded until the end of 1995 for the LEP experiments and 1998 for SLD. Since 1996 LEP has run at energies above the W-pair production threshold. In 2000, the final year of data taking at LEP, the total delivered luminosity was as high as in 1999; the maximum centre-of-mass energy attained was close to 209 GeV although most of the data taken in 1999 was collected at 205 and 207 GeV. By the end of LEP-II operation, a total integrated luminosity of approximately 700pb^{-1} per experiment has been recorded above the Z resonance.

The LEP-I (1990-1995) Z-pole measurements consist of the hadronic and leptonic cross sections, the leptonic forward-backward asymmetries, the τ polarisation asymmetries, the $b\overline{b}$ and $c\overline{c}$ partial widths and forward-backward asymmetries and the $q\overline{q}$ charge asymmetry. The measurements of the left-right cross section asymmetry, the $b\overline{b}$ and $c\overline{c}$ partial widths and left-right-forward-backward asymmetries for b and c quarks from SLD are treated consistently with the LEP data. Many technical aspects of their combination are described in References 2, 3 and references therein.

The LEP-II (1996-2000) measurements are di–fermion cross sections and forward-backward asymmetries; di–photon production, W–pair, Z–pair and single–W production cross sections, and electroweak gauge boson self couplings. W boson properties, like mass, width and decay branching ratios are also measured.

Several measurements included in the combinations are still preliminary.

This note is organised as follows:

Chapter 2 Z line shape and leptonic forward-backward asymmetries;

Chapter 3 τ polarisation;

Chapter 4 Measurement of polarised asymmetries at SLD;

Chapter 5 Heavy flavour analyses;

Chapter 6 Inclusive hadronic charge asymmetry;

Chapter 7 Photon-pair production at energies above the Z;

Chapter 8 Fermion-pair production at energies above the Z;

Chapter 9 W and four-fermion production;

Chapter 10 Electroweak gauge boson self couplings;

Chapter 11 W-boson mass and width;

Chapter 12 Interpretation of the Z-pole results in terms of effective couplings of the neutral weak current;

Chapter 13 Interpretation of all results, also including results from neutrino interaction and atomic parity violation experiments as well as from CDF and DØ in terms of constraints on the Standard Model

Chapter 14 Conclusions including prospects for the future.

To allow a quick assessment, a box highlighting the updates is given at the beginning of each section.

Chapter 2

Z Lineshape and Lepton Forward-Backward Asymmetries

Updates with respect to summer 2000:
Unchanged w.r.t. summer 2000: All experiments have published final results which enter in the combination. The final combination procedure is used.

The results presented here are based on the full LEP-I data set. This includes the data taken during the energy scans in 1990 and 1991 in the range[1] $|\sqrt{s} - m_{\mathrm{Z}}| < 3$ GeV, the data collected at the Z peak in 1992 and 1994 and the precise energy scans in 1993 and 1995 ($|\sqrt{s} - m_{\mathrm{Z}}| < 1.8$ GeV). The total event statistics are given in Table 2.1. Details of the individual analyses can be found in References 4–7.

$\mathrm{q\overline{q}}$					
year	A	D	L	O	all
'90/91	433	357	416	454	1660
'92	633	697	678	733	2741
'93	630	682	646	649	2607
'94	1640	1310	1359	1601	5910
'95	735	659	526	659	2579
total	4071	3705	3625	4096	15497

$\ell^+\ell^-$					
year	A	D	L	O	all
'90/91	53	36	39	58	186
'92	77	70	59	88	294
'93	78	75	64	79	296
'94	202	137	127	191	657
'95	90	66	54	81	291
total	500	384	343	497	1724

Table 2.1: The $\mathrm{q\overline{q}}$ and $\ell^+\ell^-$ event statistics, in units of 10^3, used for the analysis of the Z line shape and lepton forward-backward asymmetries by the experiments ALEPH (A), DELPHI (D), L3 (L) and OPAL (O).

For the averaging of results the LEP experiments provide a standard set of 9 parameters describing the information contained in hadronic and leptonic cross sections and leptonic forward-backward asymmetries. These parameters are convenient for fitting and averaging since they have small correlations. They are:

- The mass m_{Z} and total width Γ_{Z} of the Z boson, where the definition is based on the Breit-Wigner denominator $(s - m_{\mathrm{Z}}^2 + is\Gamma_{\mathrm{Z}}/m_{\mathrm{Z}})$ with s-dependent width [8].

[1] In this note $\hbar = c = 1$.

- The hadronic pole cross section of Z exchange:

$$\sigma_{\rm h}^0 \equiv \frac{12\pi}{m_{\rm Z}^2}\frac{\Gamma_{\rm ee}\Gamma_{\rm had}}{\Gamma_{\rm Z}^2}\,. \tag{2.1}$$

  Here $\Gamma_{\rm ee}$ and $\Gamma_{\rm had}$ are the partial widths of the Z for decays into electrons and hadrons.

- The ratios:

$$R_{\rm e}^0 \equiv \Gamma_{\rm had}/\Gamma_{\rm ee},\quad R_\mu^0 \equiv \Gamma_{\rm had}/\Gamma_{\mu\mu} \text{ and } R_\tau^0 \equiv \Gamma_{\rm had}/\Gamma_{\tau\tau}. \tag{2.2}$$

  Here $\Gamma_{\mu\mu}$ and $\Gamma_{\tau\tau}$ are the partial widths of the Z for the decays $\mathrm{Z}\to\mu^+\mu^-$ and $\mathrm{Z}\to\tau^+\tau^-$. Due to the mass of the τ lepton, a difference of 0.2% is expected between the values for $R_{\rm e}^0$ and R_μ^0, and the value for R_τ^0, even under the assumption of lepton universality [9].

- The pole asymmetries, $A_{\rm FB}^{0,\rm e}$, $A_{\rm FB}^{0,\mu}$ and $A_{\rm FB}^{0,\tau}$, for the processes $\mathrm{e^+e^-}\to\mathrm{e^+e^-}$, $\mathrm{e^+e^-}\to\mu^+\mu^-$ and $\mathrm{e^+e^-}\to\tau^+\tau^-$. In terms of the real parts of the effective vector and axial-vector neutral current couplings of fermions, $g_{\rm Vf}$ and $g_{\rm Af}$, the pole asymmetries are expressed as

$$A_{\rm FB}^{0,\rm f} \equiv \frac{3}{4}\mathcal{A}_{\rm e}\mathcal{A}_{\rm f} \tag{2.3}$$

  with

$$\mathcal{A}_{\rm f} \equiv \frac{2g_{\rm Vf}g_{\rm Af}}{g_{\rm Vf}^2+g_{\rm Af}^2} = 2\frac{g_{\rm Vf}/g_{\rm Af}}{1+(g_{\rm Vf}/g_{\rm Af})^2}\,. \tag{2.4}$$

The imaginary parts of the vector and axial-vector coupling constants as well as real and imaginary parts of the photon vacuum polarisation are taken into account explicitly in the fitting formulae and are fixed to their Standard Model values. The fitting procedure takes into account the effects of initial-state radiation [8] to $\mathcal{O}(\alpha^3)$ [10–12], as well as the t-channel and the s-t interference contributions in the case of $\mathrm{e^+e^-}$ final states.

The set of 9 parameters does not describe hadron and lepton-pair production completely, because it does not include the interference of the s-channel Z exchange with the s-channel γ exchange. For the results presented in this section and used in the rest of the note, the γ-exchange contributions and the hadronic γZ interference terms are fixed to their Standard Model values. The leptonic γZ interference terms are expressed in terms of the effective couplings.

The four sets of nine parameters provided by the LEP experiments are presented in Table 2.2. For performing the average over these four sets of nine parameters, the overall covariance matrix is constructed from the covariance matrices of the individual LEP experiments and taking into account common systematic errors [2]. The common systematic errors include theoretical errors as well as errors arising from the uncertainty in the LEP beam energy. The beam energy uncertainty contributes an uncertainty of ±1.7 MeV to $m_{\rm Z}$ and ±1.2 MeV to $\Gamma_{\rm Z}$. In addition, the uncertainty in the centre-of-mass energy spread of about ±1 MeV contributes ±0.2 MeV to $\Gamma_{\rm Z}$. The theoretical error on calculations of the small-angle Bhabha cross section is $\pm0.054\,\%$ [13] for OPAL and $\pm0.061\,\%$ [14] for all other experiments, and results in the largest common systematic uncertainty on $\sigma_{\rm h}^0$. QED radiation, dominated by photon radiation from the initial state electrons, contributes a common uncertainty of $\pm0.02\,\%$ on $\sigma_{\rm h}^0$, of ±0.3 MeV on $m_{\rm Z}$ and of ±0.2 MeV on $\Gamma_{\rm Z}$. The contribution of t-channel diagrams and the s-t interference in $\mathrm{Z}\to\mathrm{e^+e^-}$ leads to an additional theoretical uncertainty estimated to be ±0.024 on $R_{\rm e}^0$ and ±0.0014 on $A_{\rm FB}^{0,\rm e}$, which are fully anti–correlated. Uncertainties from the model-independent parameterisation of the energy dependence of the cross section are almost negligible, if the definitions of Reference [15] are applied. Through unavoidable remaining Standard Model

		correlations								
		m_Z	Γ_Z	σ^0_h	R^0_e	R^0_μ	R^0_τ	$A^{0,e}_{FB}$	$A^{0,\mu}_{FB}$	$A^{0,\tau}_{FB}$
χ^2/N_{df} = 169/176		ALEPH								
m_Z [GeV]	91.1891 ± 0.0031	1.00								
Γ_Z [GeV]	2.4959 ± 0.0043	.038	1.00							
σ^0_h [nb]	41.558 ± 0.057	−.091	−.383	1.00						
R^0_e	20.690 ± 0.075	.102	.004	.134	1.00					
R^0_μ	20.801 ± 0.056	−.003	.012	.167	.083	1.00				
R^0_τ	20.708 ± 0.062	−.003	.004	.152	.067	.093	1.00			
$A^{0,e}_{FB}$	0.0184 ± 0.0034	−.047	.000	−.003	−.388	.000	.000	1.00		
$A^{0,\mu}_{FB}$	0.0172 ± 0.0024	.072	.002	.002	.019	.013	.000	−.008	1.00	
$A^{0,\tau}_{FB}$	0.0170 ± 0.0028	.061	.002	.002	.017	.000	.011	−.007	.016	1.00
χ^2/N_{df} = 177/168		DELPHI								
m_Z [GeV]	91.1864 ± 0.0028	1.00								
Γ_Z [GeV]	2.4876 ± 0.0041	.047	1.00							
σ^0_h [nb]	41.578 ± 0.069	−.070	−.270	1.00						
R^0_e	20.88 ± 0.12	.063	.000	.120	1.00					
R^0_μ	20.650 ± 0.076	−.003	−.007	.191	.054	1.00				
R^0_τ	20.84 ± 0.13	.001	−.001	.113	.033	.051	1.00			
$A^{0,e}_{FB}$	0.0171 ± 0.0049	.057	.001	−.006	−.106	.000	−.001	1.00		
$A^{0,\mu}_{FB}$	0.0165 ± 0.0025	.064	.006	−.002	.025	.008	.000	−.016	1.00	
$A^{0,\tau}_{FB}$	0.0241 ± 0.0037	.043	.003	−.002	.015	.000	.012	−.015	.014	1.00
χ^2/N_{df} = 158/166		L3								
m_Z [GeV]	91.1897 ± 0.0030	1.00								
Γ_Z [GeV]	2.5025 ± 0.0041	.065	1.00							
σ^0_h [nb]	41.535 ± 0.054	.009	−.343	1.00						
R^0_e	20.815 ± 0.089	.108	−.007	.075	1.00					
R^0_μ	20.861 ± 0.097	−.001	.002	.077	.030	1.00				
R^0_τ	20.79 ± 0.13	.002	.005	.053	.024	.020	1.00			
$A^{0,e}_{FB}$	0.0107 ± 0.0058	−.045	.055	−.006	−.146	−.001	−.003	1.00		
$A^{0,\mu}_{FB}$	0.0188 ± 0.0033	.052	.004	.005	.017	.005	.000	.011	1.00	
$A^{0,\tau}_{FB}$	0.0260 ± 0.0047	.034	.004	.003	.012	.000	.007	−.008	.006	1.00
χ^2/N_{df} = 155/194		OPAL								
m_Z [GeV]	91.1858 ± 0.0030	1.00								
Γ_Z [GeV]	2.4948 ± 0.0041	.049	1.00							
σ^0_h [nb]	41.501 ± 0.055	.031	−.352	1.00						
R^0_e	20.901 ± 0.084	.108	.011	.155	1.00					
R^0_μ	20.811 ± 0.058	.001	.020	.222	.093	1.00				
R^0_τ	20.832 ± 0.091	.001	.013	.137	.039	.051	1.00			
$A^{0,e}_{FB}$	0.0089 ± 0.0045	−.053	−.005	.011	−.222	−.001	.005	1.00		
$A^{0,\mu}_{FB}$	0.0159 ± 0.0023	.077	−.002	.011	.031	.018	.004	−.012	1.00	
$A^{0,\tau}_{FB}$	0.0145 ± 0.0030	.059	−.003	.003	.015	−.010	.007	−.010	.013	1.00

Table 2.2: Line Shape and asymmetry parameters from fits to the data of the four LEP experiments and their correlation coefficients.

assumptions, dominated by the need to fix the γ-Z interference contribution in the $q\overline{q}$ channel, there is some small dependence of ± 0.2 MeV of m_Z on the Higgs mass, m_H (in the range 100 GeV to 1000 GeV) and the value of the electromagnetic coupling constant. Such "parametric" errors are negligible for the other results. The combined parameter set and its correlation matrix are given in Table 2.3.

If lepton universality is assumed, the set of 9 parameters is reduced to a set of 5 parameters.

without lepton universality		correlations								
$\chi^2/N_{\rm df} = 32.6/27$		$m_{\rm Z}$	$\Gamma_{\rm Z}$	$\sigma^0_{\rm h}$	$R^0_{\rm e}$	R^0_μ	R^0_τ	$A^{0,\rm e}_{\rm FB}$	$A^{0,\mu}_{\rm FB}$	$A^{0,\tau}_{\rm FB}$
$m_{\rm Z}$ [GeV]	91.1876 ± 0.0021	1.00								
$\Gamma_{\rm Z}$ [GeV]	2.4952 ± 0.0023	$-.024$	1.00							
$\sigma^0_{\rm h}$ [nb]	41.541 ± 0.037	$-.044$	$-.297$	1.00						
$R^0_{\rm e}$	20.804 ± 0.050	.078	$-.011$	.105	1.00					
R^0_μ	20.785 ± 0.033	.000	.008	.131	.069	1.00				
R^0_τ	20.764 ± 0.045	.002	.006	.092	.046	.069	1.00			
$A^{0,\rm e}_{\rm FB}$	0.0145 ± 0.0025	$-.014$	.007	.001	$-.371$	.001	.003	1.00		
$A^{0,\mu}_{\rm FB}$	0.0169 ± 0.0013	.046	.002	.003	.020	.012	.001	$-.024$	1.00	
$A^{0,\tau}_{\rm FB}$	0.0188 ± 0.0017	.035	.001	.002	.013	$-.003$	.009	$-.020$	.046	1.00

with lepton universality

$\chi^2/N_{\rm df} = 36.5/31$		$m_{\rm Z}$	$\Gamma_{\rm Z}$	$\sigma^0_{\rm h}$	R^0_ℓ	$A^{0,\ell}_{\rm FB}$
$m_{\rm Z}$ [GeV]	91.1875 ± 0.0021	1.00				
$\Gamma_{\rm Z}$ [GeV]	2.4952 ± 0.0023	$-.023$	1.00			
$\sigma^0_{\rm h}$ [nb]	41.540 ± 0.037	$-.045$	$-.297$	1.00		
R^0_ℓ	20.767 ± 0.025	.033	.004	.183	1.00	
$A^{0,\ell}_{\rm FB}$	0.0171 ± 0.0010	.055	.003	.006	$-.056$	1.00

Table 2.3: Average line shape and asymmetry parameters from the data of the four LEP experiments, without and with the assumption of lepton universality.

R^0_ℓ is defined as $R^0_\ell \equiv \Gamma_{\rm had}/\Gamma_{\ell\ell}$, where $\Gamma_{\ell\ell}$ refers to the partial Z width for the decay into a pair of massless charged leptons. The data of each of the four LEP experiments are consistent with lepton universality (the difference in χ^2 over the difference in d.o.f. with and without the assumption of lepton universality is 3/4, 6/4, 5/4 and 3/4 for ALEPH, DELPHI, L3 and OPAL, respectively). The lower part of Table 2.3 gives the combined result and the corresponding correlation matrix. Figure 2.1 shows, for each lepton species and for the combination assuming lepton universality, the resulting 68% probability contours in the R^0_ℓ-$A^{0,\ell}_{\rm FB}$ plane. Good agreement is observed.

For completeness the partial decay widths of the Z boson are listed in Table 2.4, although they are more correlated than the ratios given in Table 2.3. The leptonic pole cross-section, σ^0_ℓ, defined as

$$\sigma^0_\ell \;\equiv\; \frac{12\pi}{m^2_{\rm Z}}\frac{\Gamma^2_{\ell\ell}}{\Gamma^2_{\rm Z}}\,, \tag{2.5}$$

in analogy to $\sigma^0_{\rm h}$, is shown in the last line of the Table. Because QCD final state corrections appear twice in the denominator via $\Gamma_{\rm Z}$, σ^0_ℓ has a higher sensitivity to α_s than $\sigma^0_{\rm h}$ or R^0_ℓ, where the dependence on QCD corrections is only linear.

2.1 Number of Neutrino Species

An important aspect of our measurement concerns the information related to Z decays into invisible channels. Using the results of Table 2.3, the ratio of the Z decay width into invisible particles and the leptonic decay width is determined:

$$\Gamma_{\rm inv}/\Gamma_{\ell\ell} \;=\; 5.942 \pm 0.016\,. \tag{2.6}$$

without lepton universality		correlations			
		$\Gamma_{\rm had}$	$\Gamma_{\rm ee}$	$\Gamma_{\mu\mu}$	$\Gamma_{\tau\tau}$
$\Gamma_{\rm had}$ [MeV]	1745.8 $\pm$2.7	1.00			
$\Gamma_{\rm ee}$ [MeV]	83.92$\pm$0.12	$-$0.29	1.00		
$\Gamma_{\mu\mu}$ [MeV]	83.99$\pm$0.18	0.66	$-$0.20	1.00	
$\Gamma_{\tau\tau}$ [MeV]	84.08$\pm$0.22	0.54	$-$0.17	0.39	1.00

with lepton universality		correlations		
		$\Gamma_{\rm inv}$	$\Gamma_{\rm had}$	$\Gamma_{\ell\ell}$
$\Gamma_{\rm inv}$ [MeV]	499.0 $\pm$1.5	1.00		
$\Gamma_{\rm had}$ [MeV]	1744.4 $\pm$2.0	$-$0.29	1.00	
$\Gamma_{\ell\ell}$ [MeV]	83.984$\pm$0.086	0.49	0.39	1.00
$\Gamma_{\rm inv}/\Gamma_{\ell\ell}$	5.942 $\pm$0.016			
σ^0_ℓ [nb]	2.0003$\pm$0.0027			

Table 2.4: Partial decay widths of the Z boson, derived from the results of the 9-parameter averages in Table 2.3. In the case of lepton universality, $\Gamma_{\ell\ell}$ refers to the partial Z width for the decay into a pair of massless charged leptons.

The Standard Model value for the ratio of the partial widths to neutrinos and charged leptons is:

$$(\Gamma_{\nu\nu}/\Gamma_{\ell\ell})_{\rm SM} \quad = \quad 1.9912 \pm 0.0012\,. \tag{2.7}$$

The central value is evaluated for $m_{\rm Z} = 91.1875$ GeV and the error quoted accounts for a variation of $m_{\rm t}$ in the range $m_{\rm t} = 174.3 \pm 5.1$ GeV and a variation of $m_{\rm H}$ in the range 100 GeV $\leq m_{\rm H} \leq$ 1000 GeV. The number of light neutrino species is given by the ratio of the two expressions listed above:

$$N_\nu \quad = \quad 2.9841 \pm 0.0083, \tag{2.8}$$

which is two standard deviations below the value of 3 expected from 3 observed fermion families.

Alternatively, one can assume 3 neutrino species and determine the width from additional invisible decays of the Z. This yields

$$\Delta\Gamma_{\rm inv} \quad = \quad -2.7 \pm 1.6 \text{ MeV}. \tag{2.9}$$

The measured total width is below the Standard Model expectation. If a conservative approach is taken to limit the result to only positive values of $\Delta\Gamma_{\rm inv}$ and renormalising the probability for $\Delta\Gamma_{\rm inv} \geq 0$ to be unity, then the resulting 95% CL upper limit on additional invisible decays of the Z is

$$\Delta\Gamma_{\rm inv} \quad < \quad 2.0 \text{ MeV}. \tag{2.10}$$

The theoretical error on the luminosity [14] constitutes a large part of the uncertainties on N_ν and $\Delta\Gamma_{\rm inv}$.

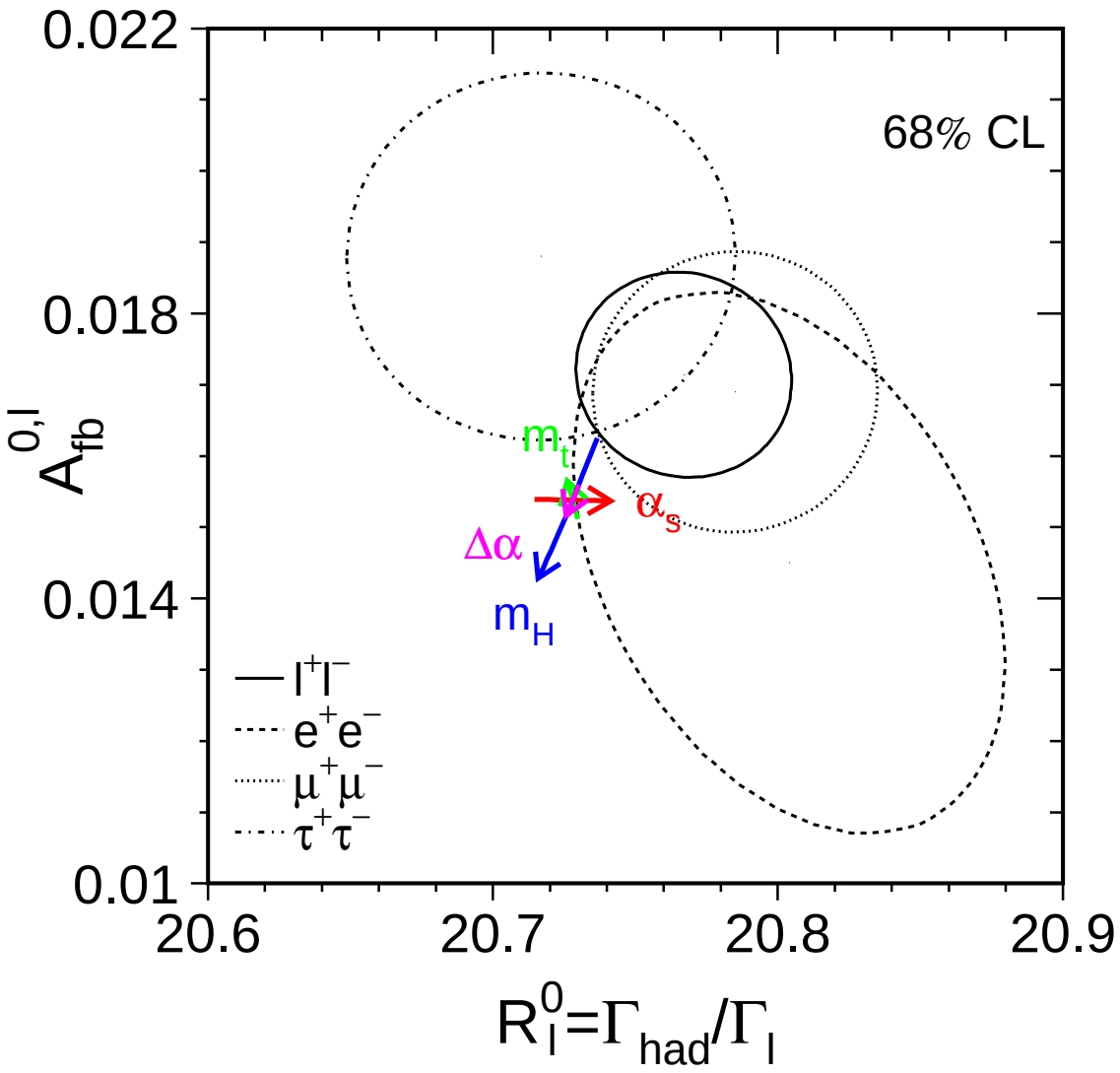

Figure 2.1: Contours of 68% probability in the R_ℓ^0-$A_{\rm FB}^{0,\ell}$ plane. For better comparison the results for the τ lepton are corrected to correspond to the massless case. The Standard Model prediction for $m_{\rm Z} = 91.1875$ GeV, $m_{\rm t} = 174.3$ GeV, $m_{\rm H} = 300$ GeV, and $\alpha_{\rm S}(m_{\rm Z}^2) = 0.118$ is also shown. The lines with arrows correspond to the variation of the Standard Model prediction when $m_{\rm t}$, $m_{\rm H}$, $\alpha_{\rm S}(m_{\rm Z}^2)$ and $\Delta\alpha_{\rm had}^{(5)}(m_{\rm Z}^2)$ are varied in the intervals $m_{\rm t} = 174.3 \pm 5.1$ GeV, $m_{\rm H} = 300^{+700}_{-186}$ GeV, $\alpha_{\rm S}(m_{\rm Z}^2) = 0.118 \pm 0.002$ and $\Delta\alpha_{\rm had}^{(5)}(m_{\rm Z}^2) = 0.02761 \pm 0.00036$, respectively. The arrows point in the direction of increasing values of $m_{\rm t}$, $m_{\rm H}$, $\alpha_{\rm S}$ and $\Delta\alpha_{\rm had}^{(5)}(m_{\rm Z}^2)$.

Chapter 3

The τ Polarisation

Updates with respect to summer 2000:
OPAL has finalised their results. While all results are now final, the combination procedure itself is still preliminary.

The longitudinal τ polarisation $\mathcal{P}_\tau$ of τ pairs produced in Z decays is defined as

$$\mathcal{P}_\tau \equiv \frac{\sigma_\mathrm{R} - \sigma_\mathrm{L}}{\sigma_\mathrm{R} + \sigma_\mathrm{L}}, \tag{3.1}$$

where σ_R and σ_L are the τ-pair cross sections for the production of a right-handed and left-handed τ^-, respectively. The distribution of $\mathcal{P}_\tau$ as a function of the polar scattering angle θ between the e^- and the τ^-, at $\sqrt{s} = m_\mathrm{Z}$, is given by

$$\mathcal{P}_\tau(\cos\theta) = -\frac{\mathcal{A}_\tau(1+\cos^2\theta) + 2\mathcal{A}_\mathrm{e}\cos\theta}{1+\cos^2\theta + 2\mathcal{A}_\tau\mathcal{A}_\mathrm{e}\cos\theta}, \tag{3.2}$$

with $\mathcal{A}_\mathrm{e}$ and $\mathcal{A}_\tau$ as defined in Equation (2.4). Equation (3.2) is valid for pure Z exchange. The effects of γ exchange, γ-Z interference and electromagnetic radiative corrections in the initial and final states are taken into account in the experimental analyses. In particular, these corrections account for the $\sqrt{s}$ dependence of the τ polarisation, which is important because the off-peak data are included in the event samples for all experiments. When averaged over all production angles $\mathcal{P}_\tau$ is a measurement of $\mathcal{A}_\tau$. As a function of $\cos\theta$, $\mathcal{P}_\tau(\cos\theta)$ provides nearly independent determinations of both $\mathcal{A}_\tau$ and $\mathcal{A}_\mathrm{e}$, thus allowing a test of the universality of the couplings of the Z to e and τ.

Each experiment makes separate $\mathcal{P}_\tau$ measurements using the five τ decay modes $\mathrm{e}\nu\overline{\nu}$, $\mu\nu\overline{\nu}$, $\pi\nu$, $\rho\nu$ and $a_1\nu$ [16–19]. The $\rho\nu$ and $\pi\nu$ are the most sensitive channels, contributing weights of about 40% each in the average. DELPHI and L3 also use an inclusive hadronic analysis. The combination is made using the results from each experiment already averaged over the τ decay modes.

3.1 Results

Tables 3.1 and 3.2 show the most recent results for $\mathcal{A}_\tau$ and $\mathcal{A}_\mathrm{e}$ obtained by the four LEP collaborations [16–19] and their combination. Although the size of the event samples used by the four experiments are roughly equal, smaller errors are quoted by ALEPH. This is largely associated with the higher angular granularity of the ALEPH electromagnetic calorimeter. Common systematic errors arise from

uncertainties in radiative corrections (decay radiation) in the $\pi\nu$ and $\rho\nu$ channels, and in the modelling of the a_1 decays [20]. These errors and their correlations need further investigation, but are already taken into account in the combination (see also Reference 18). The statistical correlation between the extracted values of $\mathcal{A}_\tau$ and $\mathcal{A}_\mathrm{e}$ is small ($\leq 5\%$).

The average values for $\mathcal{A}_\tau$ and $\mathcal{A}_\mathrm{e}$:

$$\mathcal{A}_\tau = 0.1439 \pm 0.0043 \tag{3.3}$$

$$\mathcal{A}_\mathrm{e} = 0.1498 \pm 0.0049\,, \tag{3.4}$$

with a correlation of 0.013, are compatible, in good agreement with neutral-current lepton universality. Assuming e-τ universality, the values for $\mathcal{A}_\tau$ and $\mathcal{A}_\mathrm{e}$ can be combined. This combination is performed including the small common systematic errors between $\mathcal{A}_\tau$ and $\mathcal{A}_\mathrm{e}$ within each experiment and between experiments. The combined result of $\mathcal{A}_\tau$ and $\mathcal{A}_\mathrm{e}$ is:

$$\mathcal{A}_\ell = 0.1465 \pm 0.0033\,, \tag{3.5}$$

where the error includes a systematic component of 0.0016.

Experiment		$\mathcal{A}_\tau$
ALEPH	(90 - 95), final	$0.1451 \pm 0.0052 \pm 0.0029$
DELPHI	(90 - 95), final	$0.1359 \pm 0.0079 \pm 0.0055$
L3	(90 - 95), final	$0.1476 \pm 0.0088 \pm 0.0062$
OPAL	(90 - 95), final	$0.1456 \pm 0.0076 \pm 0.0057$
LEP Average	preliminary	0.1439 ± 0.0043

Table 3.1: LEP results for $\mathcal{A}_\tau$. The first error is statistical and the second systematic. In the LEP average, statistical and systematic errors are combined in quadrature. The systematic component of the error is ± 0.0026.

Experiment		$\mathcal{A}_\mathrm{e}$
ALEPH	(90 - 95), final	$0.1504 \pm 0.0068 \pm 0.0008$
DELPHI	(90 - 95), final	$0.1382 \pm 0.0116 \pm 0.0005$
L3	(90 - 95), final	$0.1678 \pm 0.0127 \pm 0.0030$
OPAL	(90 - 95), final	$0.1454 \pm 0.0108 \pm 0.0036$
LEP Average	preliminary	0.1498 ± 0.0049

Table 3.2: LEP results for $\mathcal{A}_\mathrm{e}$. The first error is statistical and the second systematic. In the LEP average, statistical and systematic errors are combined in quadrature. The systematic component of the error is ± 0.0009.

Chapter 4

Measurement of polarised lepton asymmetries at SLC

Updates with respect to summer 2000:
Unchanged w.r.t. summer 2000: SLD has final results for $A_{\rm LR}$ and the leptonic left-right forward-backward asymmetries.

The measurement of the left-right cross section asymmetry ($A_{\rm LR}$) by SLD [21] at the SLC provides a systematically precise, statistics-dominated determination of the coupling $\mathcal{A}_{\rm e}$, and is presently the most precise single measurement, with the smallest systematic error, of this quantity. In principle the analysis is straightforward: one counts the numbers of Z bosons produced by left and right longitudinally polarised electrons, forms an asymmetry, and then divides by the luminosity-weighted $\rm e^-$ beam polarisation magnitude (the $\rm e^+$ beam is not polarised):

$$A_{\rm LR} = \frac{N_{\rm L} - N_{\rm R}}{N_{\rm L} + N_{\rm R}} \frac{1}{P_{\rm e}}. \tag{4.1}$$

Since the advent of high polarisation "strained lattice" GaAs photo-cathodes (1994), the average electron polarisation at the interaction point has been in the range 73% to 77%. The method requires no detailed final state event identification ($\rm e^+e^-$ final state events are removed, as are non-Z backgrounds) and is insensitive to all acceptance and efficiency effects. The small total systematic error of 0.64% relative is dominated by the 0.50% relative systematic error in the determination of the $\rm e^-$ polarisation. The relative statistical error on $A_{\rm LR}$ is about 1.3%.

The precision Compton polarimeter detects beam electrons that are scattered by photons from a circularly polarised laser. Two additional polarimeters that are sensitive to the Compton-scattered photons and which are operated in the absence of positron beam, have verified the precision polarimeter result and are used to set a calibration uncertainty of 0.4% relative. In 1998, a dedicated experiment was performed in order to test directly the expectation that accidental polarisation of the positron beam was negligible; the $\rm e^+$ polarisation was found to be consistent with zero $(-0.02 \pm 0.07)\%$.

The $A_{\rm LR}$ analysis includes several very small corrections. The polarimeter result is corrected for higher order QED and accelerator related effects, a total of $(-0.22 \pm 0.15)\%$ relative for 1997/98 data. The event asymmetry is corrected for backgrounds and accelerator asymmetries, a total of $(+0.15 \pm 0.07)\%$ relative, for 1997/98 data.

The translation of the $A_{\rm LR}$ result to a "pole" value is a $(-2.5 \pm 0.4)\%$ relative shift, where the uncertainty arises from the precision of the centre-of-mass energy determination. This small error due

to the beam energy measurement reflects the results of a scan of the Z peak used to calibrate the energy spectrometers to $m_{\rm Z}$ from LEP data. The pole value, $A^0_{\rm LR}$, is equivalent to a measurement of $\mathcal{A}_{\rm e}$.

The 2000 result is included in a running average of all of the SLD $A_{\rm LR}$ measurements (1992, 1993, 1994/1995, 1996, 1997 and 1998). This updated result for $A^0_{\rm LR}$ ($\mathcal{A}_{\rm e}$) is 0.1514 ± 0.0022. In addition, the left-right forward-backward asymmetries for leptonic final states are measured [22]. From these, the parameters $\mathcal{A}_{\rm e}$, $\mathcal{A}_\mu$ and $\mathcal{A}_\tau$ can be determined. The results are $\mathcal{A}_{\rm e} = 0.1544\pm0.0060$, $\mathcal{A}_\mu = 0.142\pm0.015$ and $\mathcal{A}_\tau = 0.136 \pm 0.015$. The lepton-based result for $\mathcal{A}_{\rm e}$ can be combined with the $A^0_{\rm LR}$ result to yield $\mathcal{A}_{\rm e} = 0.1516 \pm 0.0021$, including small correlations in the systematic errors. The correlation of this measurement with $\mathcal{A}_\mu$ and $\mathcal{A}_\tau$ is indicated in Table 4.1.

Assuming lepton universality, the $A_{\rm LR}$ result and the results on the leptonic left-right forward-backward asymmetries can be combined, while accounting for small correlated systematic errors, yielding

$$\mathcal{A}_\ell = 0.1513 \pm 0.0021. \tag{4.2}$$

	$\mathcal{A}_{\rm e}$	$\mathcal{A}_\mu$	$\mathcal{A}_\tau$
$\mathcal{A}_{\rm e}$	1.000		
$\mathcal{A}_\mu$	0.038	1.000	
$\mathcal{A}_\tau$	0.033	0.007	1.000

Table 4.1: Correlation coefficients between $\mathcal{A}_{\rm e}$, $\mathcal{A}_\mu$ and $\mathcal{A}_\tau$

Chapter 5

Results from b and c Quarks

Updates with respect to summer 2000:
ALEPH has updated their $A_{\rm FB}^{\rm b\overline{b}}$ jet-charge measurement using a neural net charge tag
DELPHI has presented new measurements of $A_{\rm FB}^{\rm b\overline{b}}$ using a neural net charge tag
SLD has updated $R_{\rm c}$ and most $\mathcal{A}_{\rm b}$ and $\mathcal{A}_{\rm c}$ measurements.

5.1 Introduction

The relevant quantities in the heavy quark sector at LEP-I/SLD which are currently determined by the combination procedure are:

- The ratios of the b and c quark partial widths of the Z to its total hadronic partial width: $R_{\rm b}^0 \equiv \Gamma_{\rm b\overline{b}}/\Gamma_{\rm had}$ and $R_{\rm c}^0 \equiv \Gamma_{\rm c\overline{c}}/\Gamma_{\rm had}$. (The symbols $R_{\rm b}$, $R_{\rm c}$ are used to denote the experimentally measured ratios of event rates or cross sections.)
- The forward-backward asymmetries, $A_{\rm FB}^{\rm b\overline{b}}$ and $A_{\rm FB}^{\rm c\overline{c}}$.
- The final state coupling parameters $\mathcal{A}_{\rm b}$, $\mathcal{A}_{\rm c}$ obtained from the left-right-forward-backward asymmetry at SLD.
- The semileptonic branching ratios, BR($\rm b \to \ell^-$), BR($\rm b \to c \to \ell^+$) and BR($\rm c \to \ell^+$), and the average time-integrated $\rm B^0\overline{B^0}$ mixing parameter, $\overline{\chi}$. These are often determined at the same time or with similar methods as the asymmetries. Including them in the combination greatly reduces the errors. For example the measurements of $\overline{\chi}$ act as an effective measurement of the charge tagging efficiency, so that all errors coming from the mixture of different lepton sources in $\rm b\overline{b}$ events cancel in the asymmetries.
- The probability that a c quark produces a $\rm D^+$, $\rm D_s$, $\rm D^{*+}$ meson[1] or a charmed baryon. The probability that a c quark fragments into a $\rm D^0$ is calculated from the constraint that the probabilities for the weakly decaying charmed hadrons add up to one.

A full description of the averaging procedure is published in [3]; the main motivations for the procedure are outlined here. Several analyses measure more than one parameter simultaneously, for example the

[1] Actually the product $\rm P(c \to D^{*+}) \times BR(D^{*+} \to \pi^+ D^0)$ is fitted because this quantity is needed and measured by the LEP experiments.

asymmetry measurements with leptons or D mesons. Some of the measurements of electroweak parameters depend explicitly on the values of other parameters, for example R_b depends on R_c. The common tagging and analysis techniques lead to common sources of systematic uncertainty, in particular for the double-tag measurements of R_b. The starting point for the combination is to ensure that all the analyses use a common set of assumptions for input parameters which give rise to systematic uncertainties. The input parameters are updated and extended [23] to accommodate new analyses and more recent measurements. The correlations and interdependencies of the input measurements are then taken into account in a χ^2 minimisation which results in the combined electroweak parameters and their correlation matrix.

5.2 Summary of Measurements and Averaging Procedure

All measurements are presented by the LEP and SLD collaborations in a consistent manner for the purpose of combination. The tables prepared by the experiments include a detailed breakdown of the systematic error of each measurement and its dependence on other electroweak parameters. Where necessary, the experiments apply small corrections to their results in order to use agreed values and ranges for the input parameters to calculate systematic errors. The measurements, corrected where necessary, are summarised in Appendix A in Tables A.1–A.20, where the statistical and systematic errors are quoted separately. The correlated systematic entries are from physics sources shared with one or more other results in the tables and are derived from the full breakdown of common systematic uncertainties. The uncorrelated systematic entries come from the remaining sources.

5.2.1 Averaging Procedure

A χ^2 minimisation procedure is used to derive the values of the heavy-flavour electroweak parameters, following the procedure described in Reference 3. The full statistical and systematic covariance matrix for all measurements is calculated. This correlation matrix takes into account correlations between different measurements of one experiment and between different experiments. The explicit dependence of each measurement on the other parameters is also accounted for.

Since c-quark events form the main background in the R_b analyses, the value of R_b depends on the value of R_c. If R_b and R_c are measured in the same analysis, this is reflected in the correlation matrix for the results. However the analyses do not determine R_b and R_c simultaneously but instead measure R_b for an assumed value of R_c. In this case the dependence is parameterised as

$$R_b \;=\; R_b^{\rm meas} + a(R_c)\frac{(R_c - R_c^{\rm used})}{R_c}. \qquad (5.1)$$

In this expression, $R_b^{\rm meas}$ is the result of the analysis assuming a value of $R_c = R_c^{\rm used}$. The values of $R_c^{\rm used}$ and the coefficients $a(R_c)$ are given in Table A.1 where appropriate. The dependence of all other measurements on other electroweak parameters is treated in the same way, with coefficients $a(x)$ describing the dependence on parameter x.

5.2.2 Partial Width Measurements

The measurements of R_b and R_c fall into two categories. In the first, called a single-tag measurement, a method to select b or c events is devised, and the number of tagged events is counted. This number

must then be corrected for backgrounds from other flavours and for the tagging efficiency to calculate the true fraction of hadronic Z decays of that flavour. The dominant systematic errors come from understanding the branching ratios and detection efficiencies which give the overall tagging efficiency. For the second technique, called a double-tag measurement, each event is divided into two hemispheres. With N_t being the number of tagged hemispheres, N_{tt} the number of events with both hemispheres tagged and $N_{\rm had}$ the total number of hadronic Z decays one has

$$\frac{N_t}{2N_{\rm had}} = \varepsilon_{\rm b}R_{\rm b} + \varepsilon_{\rm c}R_{\rm c} + \varepsilon_{\rm uds}(1 - R_{\rm b} - R_{\rm c}), \tag{5.2}$$

$$\frac{N_{tt}}{N_{\rm had}} = \mathcal{C}_{\rm b}\varepsilon_{\rm b}^2R_{\rm b} + \mathcal{C}_{\rm c}\varepsilon_{\rm c}^2R_{\rm c} + \mathcal{C}_{\rm uds}\varepsilon_{\rm uds}^2(1 - R_{\rm b} - R_{\rm c}), \tag{5.3}$$

where $\varepsilon_{\rm b}$, $\varepsilon_{\rm c}$ and $\varepsilon_{\rm uds}$ are the tagging efficiencies per hemisphere for b, c and light-quark events, and $\mathcal{C}_{\rm q} \neq 1$ accounts for the fact that the tagging efficiencies between the hemispheres may be correlated. In the case of $R_{\rm b}$ one has $\varepsilon_{\rm b} \gg \varepsilon_{\rm c} \gg \varepsilon_{\rm uds}$, $\mathcal{C}_{\rm b} \approx 1$. The correlations for the other flavours can be neglected. These equations can be solved to give $R_{\rm b}$ and $\varepsilon_{\rm b}$. Neglecting the c and uds backgrounds and the correlations, they are approximately given by

$$\varepsilon_{\rm b} \approx 2N_{tt}/N_t, \tag{5.4}$$

$$R_{\rm b} \approx N_t^2/(4N_{tt}N_{\rm had}). \tag{5.5}$$

The double-tagging method has the advantage that the b tagging efficiency is derived from the data, reducing the systematic error. The residual background of other flavours in the sample, and the evaluation of the correlation between the tagging efficiencies in the two hemispheres of the event are the main sources of systematic uncertainty in such an analysis.

This method can be enhanced by including more tags. All additional efficiencies can be determined from the data, reducing the statistical uncertainties without adding new systematic uncertainties.

Small corrections must be applied to the results to obtain the partial width ratios $R_{\rm b}^0$ and $R_{\rm c}^0$ from the cross section ratios $R_{\rm b}$ and $R_{\rm c}$. These corrections depend slightly on the invariant mass cutoff of the simulations used by the experiments; they are applied by the collaborations before the combination.

The partial width measurements included are:

- Lifetime (and lepton) double-tag measurements for $R_{\rm b}$ from ALEPH [24], DELPHI [25], L3 [26], OPAL [27] and SLD [28]. These are the most precise determinations of $R_{\rm b}$. Since they completely dominate the combined result, no other $R_{\rm b}$ measurements are used at present. The basic features of the double-tag technique are discussed above. In the ALEPH, DELPHI, OPAL and SLD measurements the charm rejection is enhanced by using the invariant mass information. DELPHI, OPAL and SLD also add kinematic information from the particles at the secondary vertex. The ALEPH and DELPHI measurements make use of several different tags; this improves the statistical accuracy and reduces the systematic errors due to hemisphere correlations and charm contamination, compared with the simple single/double tag.
- Analyses with $\rm D/D^{*\pm}$ mesons to measure $R_{\rm c}$ from ALEPH, DELPHI and OPAL. All measurements are constructed in such a way that no assumptions on the charm fragmentation are necessary as these are determined from the LEP-I data. The available measurements can be divided into three groups:
  - inclusive/exclusive double tag (ALEPH [29], DELPHI [30,31], OPAL [32]): In a first step $\rm D^{*\pm}$ mesons are reconstructed in several decay channels and their production rate is measured, which depends on the product $R_{\rm c} \times \mathrm{P}(\mathrm{c} \to \mathrm{D}^{*+}) \times \mathrm{BR}(\mathrm{D}^{*+} \to \pi^+\mathrm{D}^0)$. This sample

of $c\overline{c}$ (and $b\overline{b}$) events is then used to measure $P(c \to D^{*+}) \times BR(D^{*+} \to \pi^+ D^0)$ using a slow pion tag in the opposite hemisphere. In the ALEPH measurement R_c is unfolded internally in the analysis so that no explicit $P(c \to D^{*+}) \times BR(D^{*+} \to \pi^+ D^0)$ is available.

- exclusive double tag (ALEPH [29]): This analysis uses exclusively reconstructed D^{*+}, D^0 and D^+ mesons in different decay channels. It has lower statistics but better purity than the inclusive analyses.
- reconstruction of all weakly decaying charmed states (ALEPH [33], DELPHI [31], OPAL [34]): These analyses make the assumption that the production fractions of D^0, D^+, D_s and Λ_c in c-quark jets of $c\overline{c}$ events add up to one with small corrections due to unmeasured charm strange baryons. This is a single tag measurement, relying only on knowing the decay branching ratios of the charm hadrons. These analyses are also used to measure the c hadron production ratios which are needed for the R_b analyses.

- A lifetime plus mass double tag from SLD to measure R_c [35]. This analysis uses the same tagging algorithm as the SLD R_b analysis, but with the neural net tuned to tag charm. Although the charm tag has a purity of about 84%, most of the background is from b which can be measured with high precision from the b/c mixed tag rate.
- A measurement of R_c using single leptons assuming $BR(c \to \ell^+)$ from ALEPH [29].

To avoid effects from nonlinearities in the fit, for the inclusive/exclusive single/double tag and for the charm-counting analyses, the products $R_c P(c \to D^{*+}) \times BR(D^{*+} \to \pi^+ D^0)$, $R_c f_{D^0}$, $R_c f_{D^+}$, $R_c f_{D_s}$ and $R_c f_{\Lambda_c}$ that are actually measured in the analyses are directly used as inputs to the fit. The measurements of the production rates of weakly decaying charmed hadrons, especially $R_c f_{D_s}$ and $R_c f_{\Lambda_c}$ have substantial errors due to the uncertainties in the branching ratios of the decay mode used. Since these errors are relative, there is a potential bias towards lower measurements. To avoid this bias, for the production rates of weakly decaying charmed hadrons the logarithm of the production rates instead of the rates themselves are input to the fit. For $R_c f_{D^0}$ and $R_c f_{D^+}$ the difference between the results using the logarithm or the value itself is negligible. For $R_c f_{D_s}$ and $R_c f_{\Lambda_c}$ the difference in the extracted value of R_c is about one tenth of a standard deviation.

5.2.3 Asymmetry Measurements

All b and c asymmetries given by the experiments correspond to full acceptance.

The QCD corrections to the forward-backward asymmetries depend strongly on the experimental analyses. For this reason the numbers given by the collaborations are also corrected for QCD effects. A detailed description of the procedure can be found in [36] with updates reported in [23].

For the 12- and 14-parameter fits described above, the LEP peak and off-peak asymmetries are corrected to $\sqrt{s} = 91.26$ GeV using the predicted dependence from ZFITTER [37]. The slope of the asymmetry around m_Z depends only on the axial coupling and the charge of the initial and final state fermions and is thus independent of the value of the asymmetry itself, i.e., the effective electroweak mixing angle.

After calculating the overall averages, the quark pole asymmetries $A_{FB}^{0,q}$, defined in terms of effective couplings, are derived from the measured asymmetries by applying corrections as listed in Table 5.1. These corrections are due to the energy shift from 91.26 GeV to m_Z, initial state radiation, γ exchange and γ-Z interference. A very small correction due to the nonzero value of the b quark mass is included in the last correction. All corrections are calculated using ZFITTER.

Source	$\delta A_{\rm FB}^{\rm b}$	$\delta A_{\rm FB}^{\rm c}$
$\sqrt{s} = m_{\rm Z}$	-0.0013	-0.0034
QED corrections	$+0.0041$	$+0.0104$
γ, γ-Z, mass	-0.0003	-0.0008
Total	$+0.0025$	$+0.0062$

Table 5.1: Corrections to be applied to the quark asymmetries as $A_{\rm FB}^0 = A_{\rm FB}^{\rm meas} + \delta A_{\rm FB}$.

The SLD left-right-forward-backward asymmetries are also corrected for all radiative effects and are directly presented in terms of $\mathcal{A}_{\rm b}$ and $\mathcal{A}_{\rm c}$.

The measurements used are:

- Measurements of $A_{\rm FB}^{\rm b\overline{b}}$ and $A_{\rm FB}^{\rm c\overline{c}}$ using leptons from ALEPH [38], DELPHI [39], L3 [40] and OPAL [41]. These analyses measure either $A_{\rm FB}^{\rm b\overline{b}}$ only from a high p_t lepton sample or they obtain $A_{\rm FB}^{\rm b\overline{b}}$ and $A_{\rm FB}^{\rm c\overline{c}}$ from a fit to the lepton spectra. In the case of OPAL the lepton information is combined with hadronic variables in a neural net. DELPHI uses in addition lifetime information and jet-charge in the hemisphere opposite to the lepton to separate the different lepton sources. Some asymmetry analyses also measure $\overline{\chi}$.
- Measurements of $A_{\rm FB}^{\rm b\overline{b}}$ based on lifetime tagged events with a hemisphere charge measurement from ALEPH [42], DELPHI [43,44], L3 [45] and OPAL [46]. These measurements contribute roughly the same weight to the combined result as the lepton fits.
- Analyses with D mesons to measure $A_{\rm FB}^{\rm c\overline{c}}$ from ALEPH [47] or $A_{\rm FB}^{\rm c\overline{c}}$ and $A_{\rm FB}^{\rm b\overline{b}}$ from DELPHI [48] and OPAL [49].
- Measurements of $\mathcal{A}_{\rm b}$ and $\mathcal{A}_{\rm c}$ from SLD. These results include measurements using lepton [50], D meson [51] and vertex mass plus hemisphere charge [52] tags, which have similar sources of systematic errors as the LEP asymmetry measurements. SLD also uses vertex mass for bottom or charm tagging in conjunction with a kaon tag or a vertex charge tag for both $\mathcal{A}_{\rm b}$ and $\mathcal{A}_{\rm c}$ measurements [53–55].

5.2.4 Other Measurements

The measurements of the charmed hadron fractions $\mathrm{P(c \to D^{*+}) \times BR(D^{*+} \to \pi^+ D^0)}$, $f(\mathrm{D^+})$, $f(\mathrm{D_s})$ and $f(\mathrm{c_{baryon}})$ are included in the $R_{\rm c}$ measurements and are described there.

ALEPH [56], DELPHI [57], L3 [26,58] and OPAL [59] measure $\mathrm{BR(b \to \ell^-)}$, $\mathrm{BR(b \to c \to \ell^+)}$ and $\overline{\chi}$ or a subset of them from a sample of leptons opposite to a b-tagged hemisphere and from a double lepton sample. DELPHI [30] and OPAL [60] measure $\mathrm{BR(c \to \ell^+)}$ from a sample opposite to a high energy $\mathrm{D^{*\pm}}$.

5.3 Results

In a first fit the asymmetry measurements on peak, above peak and below peak are corrected to three common centre-of-mass energies and are then combined at each energy point. The results of this fit,

including the SLD results, are given in Appendix B. The dependence of the average asymmetries on centre-of-mass energy agrees with the prediction of the Standard Model, as shown in Figure 5.1. A second fit is made to derive the pole asymmetries $A_{\rm FB}^{0,\rm q}$ from the measured quark asymmetries, in which all the off-peak asymmetry measurements are corrected to the peak energy before combining. This fit determines a total of 14 parameters: the two partial widths, two LEP asymmetries, two coupling parameters from SLD, three semileptonic branching ratios, the average mixing parameter and the probabilities for c quark to fragment into a D^+, a D_s, a D^{*+}, or a charmed baryon. If the SLD measurements are excluded from the fit there are 12 parameters to be determined. Results for the non-electroweak parameters are independent of the treatment of the off-peak asymmetries and the SLD data.

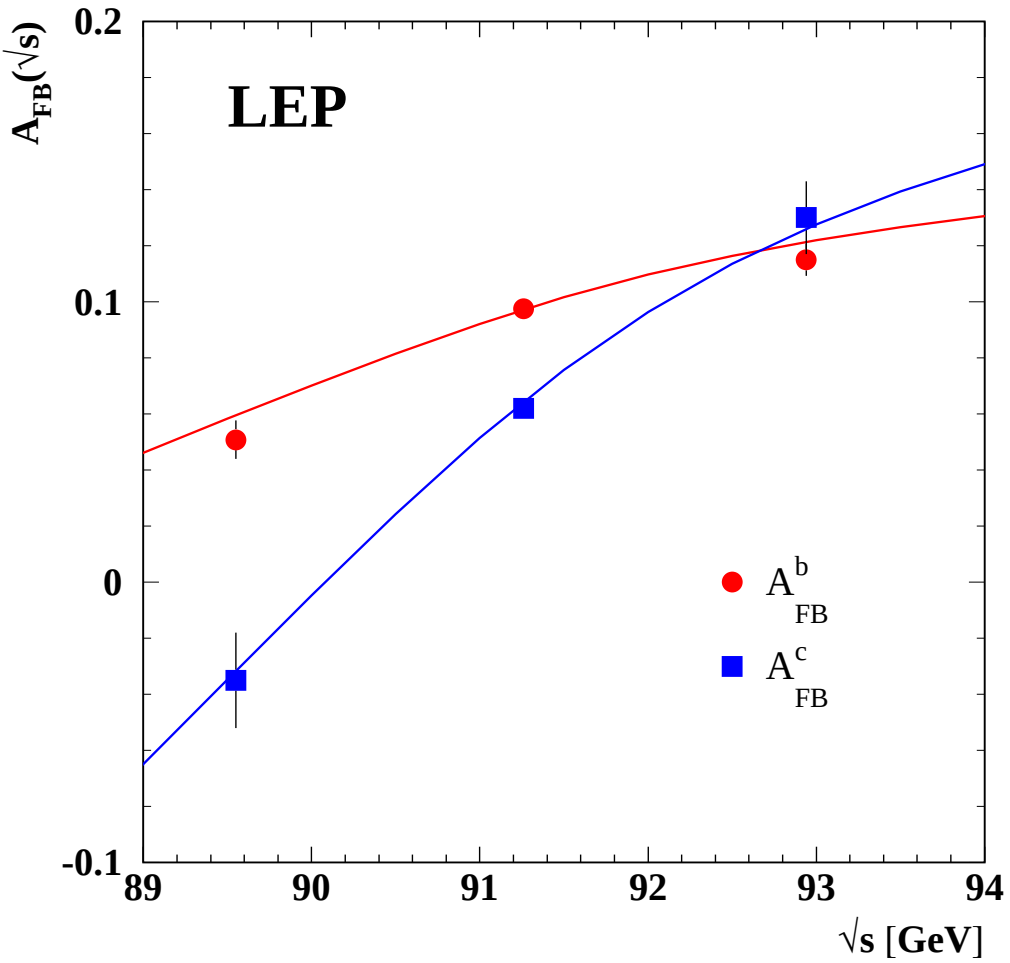

Figure 5.1: Measured asymmetries for b and c quark final states as a function of the centre-of-mass energy.

5.3.1 Results of the 12-Parameter Fit to the LEP Data

Using the full averaging procedure gives the following combined results for the electroweak parameters:

$$\begin{aligned} R_{\mathrm{b}}^{0} &= 0.21651 \pm 0.00072 \\ R_{\mathrm{c}}^{0} &= 0.1689 \pm 0.0047 \\ A_{\mathrm{FB}}^{0,\mathrm{b}} &= 0.0990 \pm 0.0017 \\ A_{\mathrm{FB}}^{0,\mathrm{c}} &= 0.0684 \pm 0.0035\,, \end{aligned} \tag{5.6}$$

where all corrections to the asymmetries and partial widths are applied. The χ^2/d.o.f. is $44/(90-12)$. The corresponding correlation matrix is given in Table 5.2.

	R_{b}^{0}	R_{c}^{0}	$A_{\mathrm{FB}}^{0,\mathrm{b}}$	$A_{\mathrm{FB}}^{0,\mathrm{c}}$
R_{b}^{0}	1.00	−0.17	−0.09	0.02
R_{c}^{0}	−0.17	1.00	0.07	−0.01
$A_{\mathrm{FB}}^{0,\mathrm{b}}$	−0.09	0.07	1.00	0.15
$A_{\mathrm{FB}}^{0,\mathrm{c}}$	0.02	−0.01	0.15	1.00

Table 5.2: The correlation matrix for the four electroweak parameters from the 12-parameter fit.

5.3.2 Results of the 14-Parameter Fit to LEP and SLD Data

Including the SLD results for R_{b}, R_{c}, $\mathcal{A}_{\mathrm{b}}$ and $\mathcal{A}_{\mathrm{c}}$ into the fit the following results are obtained:

$$\begin{aligned} R_{\mathrm{b}}^{0} &= 0.21646 \pm 0.00065\,, \\ R_{\mathrm{c}}^{0} &= 0.1719 \pm 0.0031\,, \\ A_{\mathrm{FB}}^{0,\mathrm{b}} &= 0.0990 \pm 0.0017\,, \\ A_{\mathrm{FB}}^{0,\mathrm{c}} &= 0.0685 \pm 0.0034\,, \\ \mathcal{A}_{\mathrm{b}} &= 0.922 \pm 0.020\,, \\ \mathcal{A}_{\mathrm{c}} &= 0.670 \pm 0.026\,, \end{aligned} \tag{5.7}$$

with a χ^2/d.o.f. of $47/(99-14)$. The corresponding correlation matrix is given in Table 5.3 and the largest errors for the electroweak parameters are listed in Table 5.4.

In deriving these results the parameters $\mathcal{A}_{\mathrm{b}}$ and $\mathcal{A}_{\mathrm{c}}$ are treated as independent of the forward-backward asymmetries $A_{\mathrm{FB}}^{0,\mathrm{b}}$ and $A_{\mathrm{FB}}^{0,\mathrm{c}}$ (but see Section 12.1 for a joint analysis). In Figure 5.2 the results for R_{b}^{0} and R_{c}^{0} are shown compared with the Standard Model expectation.

Amongst the non-electroweak observables the B semileptonic branching fraction ($\mathrm{BR}(\mathrm{b} \to \ell^-) = 0.1062 \pm 0.0021$) is of special interest. The dominant error source on this quantity is the dependence on the semileptonic decay models $\mathrm{b} \to \ell^-$, $\mathrm{c} \to \ell^+$ with

$$\Delta\mathrm{BR}(\mathrm{b} \to \ell^-)(\mathrm{b} \to \ell^- - \mathrm{modelling}) = 0.0011. \tag{5.8}$$

Extensive studies are made to understand the size of this error. Amongst the electroweak quantities the quark asymmetries with leptons depend also on the assumptions on the decay model while the asymmetries using other methods usually do not. The fit implicitly requires that the different methods

	R_b^0	R_c^0	$A_{FB}^{0,b}$	$A_{FB}^{0,c}$	$\mathcal{A}_b$	$\mathcal{A}_c$
R_b^0	1.00	−0.14	−0.08	0.01	−0.08	0.04
R_c^0	−0.14	1.00	0.04	−0.01	0.03	−0.05
$A_{FB}^{0,b}$	−0.08	0.04	1.00	0.15	0.02	0.00
$A_{FB}^{0,c}$	0.01	−0.01	0.15	1.00	0.00	0.01
$\mathcal{A}_b$	−0.08	0.03	0.02	0.00	1.00	0.13
$\mathcal{A}_c$	0.04	−0.05	0.00	0.01	0.13	1.00

Table 5.3: The correlation matrix for the six electroweak parameters from the 14-parameter fit.

	R_b^0 (10^{-3})	R_c^0 (10^{-3})	$A_{FB}^{0,b}$ (10^{-3})	$A_{FB}^{0,c}$ (10^{-3})	$\mathcal{A}_b$ (10^{-2})	$\mathcal{A}_c$ (10^{-2})
statistics	0.43	2.3	1.6	3.0	1.5	2.1
internal systematics	0.29	1.4	0.6	1.4	1.2	1.5
QCD effects	0.18	0.1	0.3	0.1	0.3	0.2
BR(D $\to$ neut.)	0.14	0.3	0	0	0	0
D decay multiplicity	0.13	0.3	0	0	0	0
BR($D^+ \to K^-\pi^+\pi^+$)	0.09	0.2	0	0	0	0
BR($D_s \to \phi\pi^+$)	0.03	0.5	0	0	0	0
BR($\Lambda_c \to$p $K^-\pi^+$)	0.06	0.5	0	0.1	0	0
D lifetimes	0.06	0.1	0	0.1	0	0
gluon splitting	0.22	0.1	0.1	0.1	0.1	0.1
c fragmentation	0.10	0.2	0.1	0.2	0.1	0.1
light quarks	0.07	0.2	0.1	0.1	0	0
beam polarisation	0	0	0	0	0.5	0.4
total	0.65	3.1	1.7	3.5	2.0	2.6

Table 5.4: The dominant error sources for the electroweak parameters from the 14-parameter fit.

give consistent results. This effectively constrains the decay model and thus reduces the error from this source in the fit result for BR(b $\to \ell^-$).

To get a conservative estimate of the modelling error in BR(b $\to \ell^-$) the fit is repeated removing all asymmetry measurements. The result of this fit is

$$\mathrm{BR}(b \to \ell^-) = 0.1065 \pm 0.0023 \tag{5.9}$$

with

$$\Delta\mathrm{BR}(b \to \ell^-)(b \to \ell^- - \text{modelling}) = 0.0014. \tag{5.10}$$

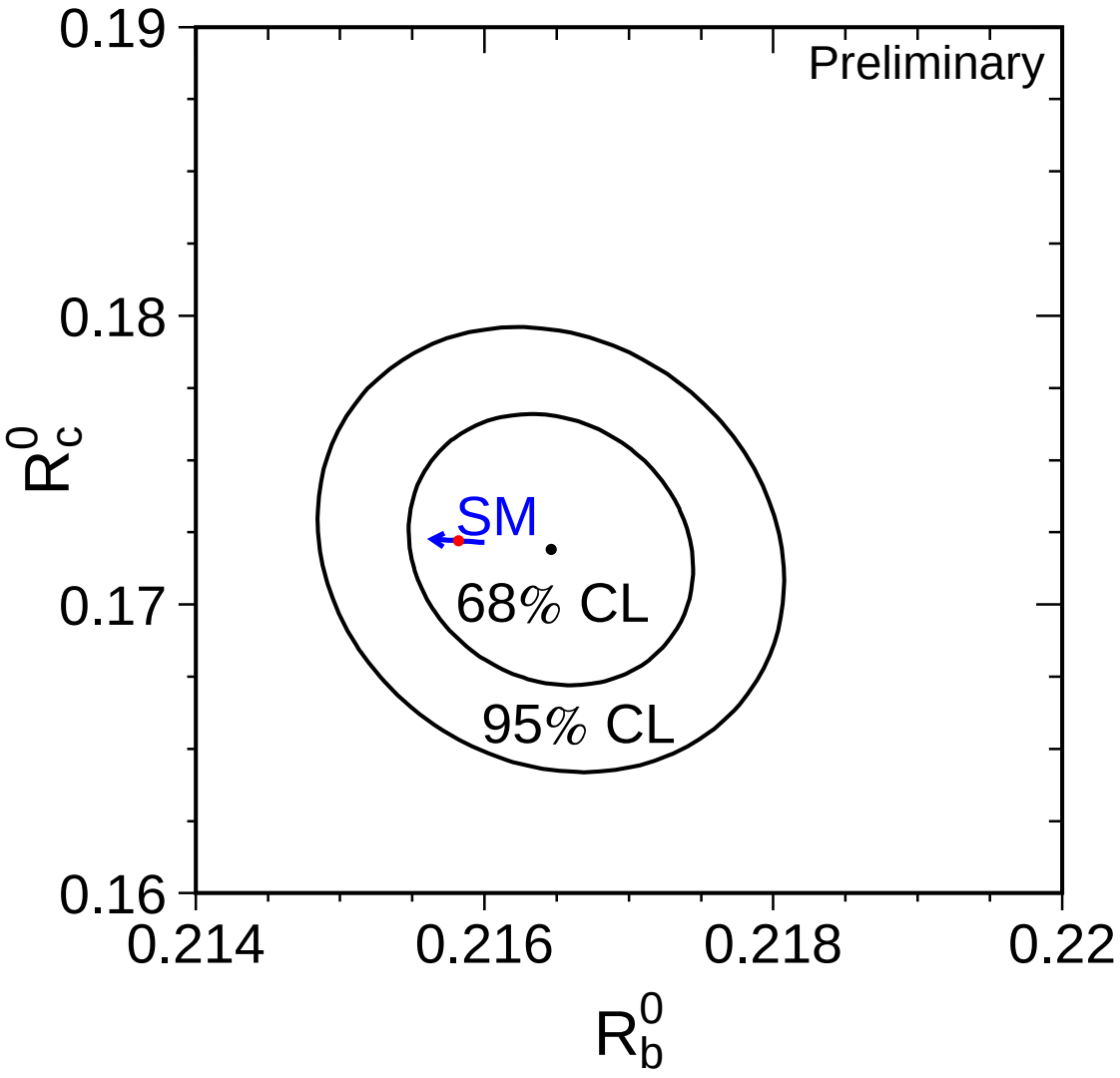

Figure 5.2: Contours in the (R_b^0,R_c^0) plane derived from the LEP+SLD data, corresponding to 68% and 95% confidence levels assuming Gaussian systematic errors. The Standard Model prediction for $m_t = 174.3 \pm 5.1$ GeV is also shown. The arrow points in the direction of increasing values of m_t.

Chapter 6

The Hadronic Charge Asymmetry $\langle Q_{\rm FB} \rangle$

Updates with respect to summer 2000:
DELPHI and OPAL revert to their published result. While all results are now final, the combination procedure itself is still preliminary.

The LEP experiments ALEPH [61], DELPHI [62], L3 [45] and OPAL [63] provide measurements of the hadronic charge asymmetry based on the mean difference in jet charges measured in the forward and backward event hemispheres, $\langle Q_{\rm FB} \rangle$. DELPHI also provides a related measurement of the total charge asymmetry by making a charge assignment on an event-by-event basis and performing a likelihood fit [62]. The experimental values quoted for the average forward-backward charge difference, $\langle Q_{\rm FB} \rangle$, cannot be directly compared as some of them include detector dependent effects such as acceptances and efficiencies. Therefore the effective electroweak mixing angle, $\sin^2\theta^{\rm lept}_{\rm eff}$, as defined in Section 12.3, is used as a means of combining the experimental results summarised in Table 6.1.

Experiment		$\sin^2\theta^{\rm lept}_{\rm eff}$
ALEPH	(90-94), final	$0.2322 \pm 0.0008 \pm 0.0011$
DELPHI	(91-91), final	$0.2345 \pm 0.0030 \pm 0.0027$
L3	(91-95), final	$0.2327 \pm 0.0012 \pm 0.0013$
OPAL	(90-91), final	$0.2326 \pm 0.0012 \pm 0.0029$
LEP Average		0.2324 ± 0.0012

Table 6.1: Summary of the determination of $\sin^2\theta^{\rm lept}_{\rm eff}$ from inclusive hadronic charge asymmetries at LEP. For each experiment, the first error is statistical and the second systematic. The latter, amounting to 0.0010 in the average, is dominated by fragmentation and decay modelling uncertainties.

The dominant source of systematic error arises from the modelling of the charge flow in the fragmentation process for each flavour. All experiments measure the required charge properties for $Z \to b\overline{b}$ events from the data. ALEPH also determines the charm charge properties from the data. The fragmentation model implemented in the JETSET Monte Carlo program [64] is used by all experiments as reference; the one of the HERWIG Monte Carlo program [65] is used for comparison. The JETSET fragmentation parameters are varied to estimate the systematic errors. The central values chosen by the experiments for these parameters are, however, not the same. The smaller of the two fragmentation errors in any pair of results is treated as common to both. The present average of $\sin^2\theta^{\rm lept}_{\rm eff}$ from $\langle Q_{\rm FB} \rangle$ and its associated error are not very sensitive to the treatment of common uncertainties. The ambiguities due to QCD corrections may cause changes in the derived value of

$\sin^2\theta^{\rm lept}_{\rm eff}$. These are, however, well below the fragmentation uncertainties and experimental errors. The effect of fully correlating the estimated systematic uncertainties from this source between the experiments has a negligible effect upon the average and its error.

There is also some correlation between these results and those for $A^{\rm b\overline{b}}_{\rm FB}$ using jet charges. The dominant source of correlation is again through uncertainties in the fragmentation and decay models used. The typical correlation between the derived values of $\sin^2\theta^{\rm lept}_{\rm eff}$ from the $\langle Q_{\rm FB}\rangle$ and the $A^{\rm b\overline{b}}_{\rm FB}$ jet charge measurements is estimated to be about 20% to 25%. This leads to only a small change in the relative weights for the $A^{\rm b\overline{b}}_{\rm FB}$ and $\langle Q_{\rm FB}\rangle$ results when averaging their $\sin^2\theta^{\rm lept}_{\rm eff}$ values (Section 12.3). Thus, the correlation between $\langle Q_{\rm FB}\rangle$ and $A^{\rm b\overline{b}}_{\rm FB}$ from jet charge has little impact on the overall Standard Model fit, and is neglected at present.

Chapter 7

Photon-Pair Production at LEP-II

Updates with respect to summer 2000:
This is a new chapter. LEP results on photon-pair production are combined. These combination results became available after the summer conferences and were first presented at Siena, in October 2001.

7.1 Introduction

The reaction $e^+e^- \to \gamma\gamma(\gamma)$ provides a clean test of QED at LEP energies and is well suited to detect the presence of non-standard physics. The differential QED cross-section at the Born level in the relativistic limit is given by:

$$\left(\frac{d\sigma}{d\Omega}\right)_{\rm Born} = \frac{\alpha^2}{s}\frac{1+\cos^2\theta}{1-\cos^2\theta}\ . \tag{7.1}$$

Since the two final state particles are identical the polar angle θ is defined such that $\cos\theta > 0$. Various models with deviations from this cross-section will be discussed in section 7.4. Results on the $\geq$2-photon final state using the high energy data collected by the four LEP collaborations are reported by the individual experiments [66]. Here the results of the LEP working group dedicated to the combination of the $e^+e^- \to \gamma\gamma(\gamma)$ measurements are reported. Results are given for the averaged total cross-section and for global fits to the differential cross-sections.

7.2 Event Selection

This channel is very clean and the event selection, which is similar for all experiments, is based on the presence of at least two energetic clusters in the electromagnetic calorimeters. A minimum energy is required, typically $(E_1+E_2)/\sqrt{s}$ larger than 0.3 to 0.6, where E_1 and E_2 are the energies of the two most energetic photons. In order to remove e^+e^- events, charged tracks are in general not allowed except when they can be associated to a photon conversion in one hemisphere.

The polar angle is defined in order to minimise effects due to initial state radiation as

$$\cos\theta = \left|\sin(\frac{\theta_1-\theta_2}{2})\right| \Big/ \sin(\frac{\theta_1+\theta_2}{2})\ ,$$

where θ_1 and θ_2 are the polar angles of the two most energetic photons. The acceptance in polar angle is in the range of 0.90 to 0.96 on $|\cos\theta|$, depending on the experiment.

With these criteria, the selection efficiencies are in the range of 68% to 95% and the residual background (from e^+e^- events and from $e^+e^- \to \tau^+\tau^-$ with $\tau^\pm \to e^\pm\nu\bar{\nu}$) is very small, 0.1% to 1%. Detailed descriptions of the event selections performed by the four collaborations can be found in [66].

7.3 Total cross-section

The total cross-sections are combined using a χ^2 minimisation. Given the different angular acceptances, only the ratios of the measured cross-sections relative to the QED expectation $r = \sigma_{\rm meas}/\sigma_{\rm QED}$ are averaged. Figure 7.1 shows the measured ratios $r_{i,k}$ of the experiments i at energies k with their statistical and systematic errors added in quadrature. Systematic errors are uncorrelated between experiments as the error on the theory is not included in the experimental errors.

Denoting with Δ the vector of residuals between the measurements and the expected ratios, three different averages are performed:

1. per energy $k = 1, \ldots, 7$: $\Delta_{i,k} = r_{i,k} - x_k$
2. per experiment $i = 1, \ldots, 4$: $\Delta_{i,k} = r_{i,k} - y_i$
3. global value: $\Delta_{i,k} = r_{i,k} - z$

The seven fit parameters per energy x_k are shown in Figure 7.1 as LEP combined cross-sections. They are correlated with correlation coefficients ranging from 10% to 20%. The four fit-parameters per experiment y_i are uncorrelated between each other, the results are given in Table 7.1 together with the single global fit parameter z.

No significant deviations from the QED expectations are found. The global ratio is below unity by 1.5σ not accounting for the error on the radiative corrections (1%) which is of similar size as the experimental error (1.2%).

Experiment	cross-section ratio
ALEPH	0.963±0.025
DELPHI	0.974±0.032
L3	0.982±0.021
OPAL	1.000±0.021
global	0.982±0.012

Table 7.1: Cross-section ratios $r = \sigma_{\rm meas}/\sigma_{\rm QED}$ for the four LEP experiments averaged over all energies and the global average over all experiments and energies. The error includes the statistical and experimental systematic error but no error from theory.

7.4 Global fit to the differential cross-sections

The global fit is based on angular distributions at energies between 183 and 207 GeV from the individual experiments. As an example angular distributions from each experiment are shown in Figure 7.2.

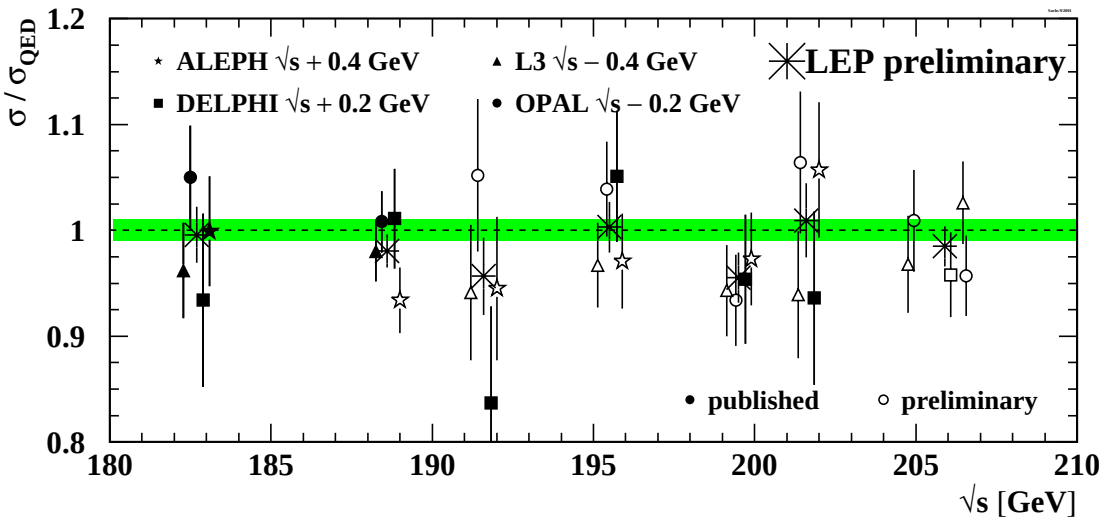

Figure 7.1: Cross-section ratios $r = \sigma_{\rm meas}/\sigma_{\rm QED}$ at different energies. The measurements of the single experiments are displaced by $\pm$ 200 or 400 MeV from the actual energy for clarity. Filled symbols indicate published results, open symbols stand for preliminary numbers. The average over the experiments at each energy is shown as a star. Measurements between 203 and 209 GeV are averaged to one energy point. The theoretical error is not included in the experimental errors but is represented as the shaded band.

	data used		sys. error [%]		$\lvert\cos\theta\rvert$
	published	preliminary	experimental	theory	
ALEPH		189 – 202	2	1	0.95
DELPHI	189 – 202	206	2.5	1	0.90
L3	183 – 189	192 – 207	2.1	1	0.96
OPAL	183 – 189	192 – 207	1.1	1	0.90

Table 7.2: The data samples used for the global fit to the differential cross-sections, the systematic errors, the assumed error on the theory and the polar angle acceptance for the LEP experiments.

Combined differential cross-sections are not available yet, since they need a common binning of the histograms. All four experiments give preliminary results; DELPHI, L3 and OPAL include the whole year 2000 data-taking, as shown in Table 7.2. The systematic errors arise from the luminosity evaluation (including theory uncertainty on the small-angle Bhabha cross-section computation), from the selection efficiency and the background evaluations and from radiative corrections. The last contribution, owing to the fact that the available $e^+e^- \to \gamma\gamma(\gamma)$ cross-section calculation is based on $\mathcal{O}(\alpha^3)$ code, is assumed to be 1% and is considered correlated among energies and experiments.

Various model predictions are fitted to these angular distributions taking into account the experimental systematic error correlated between energies for each experiment and the error on the theory. A binned log likelihood fit is performed with one free parameter for the model and five fit parameters used to keep the normalisation free within the systematic errors of the theory and the four experiments.

The following models of new physics are considered. In some cases they give rise to identical distortions of the predictions; hence their parameters can be transformed into each other.

Cut-off parameter $\Lambda_\pm$ [67,68]:

$$\left(\frac{d\sigma}{d\Omega}\right)_{\Lambda_\pm} = \left(\frac{d\sigma}{d\Omega}\right)_{\text{Born}} \pm \frac{\alpha^2 s}{2\Lambda_\pm^4}(1+\cos^2\theta) \tag{7.2}$$

Effective Lagrangian theory [69] describing anomalous $e^+e^-\gamma$ couplings in dimension 6 ($\Lambda_6^4 = \frac{2}{\alpha}\Lambda_\pm^4$) or contact interactions for dimensions 7 and 8 ($\Lambda_7 = \Lambda'$; $\Lambda_8^4 = m_e\Lambda_7^3$):

$$\left(\frac{d\sigma}{d\Omega}\right)_{\Lambda'} = \left(\frac{d\sigma}{d\Omega}\right)_{\text{Born}} + \frac{s^2}{32\pi}\frac{1}{\Lambda'^6} \tag{7.3}$$

Low scale gravity in extra dimensions [70], where M_s is related to the string scale and expected to be of order $\mathcal{O}$(TeV):

$$\left(\frac{d\sigma}{d\Omega}\right)_{M_s} = \left(\frac{d\sigma}{d\Omega}\right)_{\text{Born}} - \frac{\alpha s}{2\pi}\,\frac{\lambda}{M_s^4}\,(1+\cos^2\theta) + \frac{s^3}{16\pi^2}\,\frac{\lambda^2}{M_s^8}\,(1-\cos^4\theta)\ ,\ \lambda = \pm 1 \tag{7.4}$$

Excited electrons [71] with mass M_{e^*} and chiral magnetic coupling described by the Lagrangian

$$\mathcal{L} = \frac{1}{2\Lambda}\bar{\ell^*}\sigma^{\mu\nu}\left[gf\frac{\tau}{2}W_{\mu\nu} + g'f'\frac{Y}{2}B_{\mu\nu}\right]\ell_L + \text{h.c.}\,, \tag{7.5}$$

where g and g' are the coupling constants of $SU(2)_L$ and $U(1)_Y$, respectively. For the two photon final state this leads to the following cross-section:

$$\left(\frac{d\sigma}{d\Omega}\right)_{e^*} = \left(\frac{d\sigma}{d\Omega}\right)_{\text{Born}} + \frac{\alpha^2}{4}\frac{f_\gamma^4}{\Lambda^4}M_{e^*}^2\left[\frac{p^4}{(p^2-M_{e^*}^2)^2} + \frac{q^4}{(q^2-M_{e^*}^2)^2} + \frac{\frac{1}{2}s^2\sin^2\theta}{(p^2-M_{e^*}^2)(q^2-M_{e^*}^2)}\right]\ , \tag{7.6}$$

with $f_\gamma = -\frac{1}{2}(f+f')$, $p^2 = -\frac{s}{2}(1-\cos\theta)$ and $q^2 = -\frac{s}{2}(1+\cos\theta)$ and $\Lambda = M_{e^*}$.

7.5 Fit Results

Where possible the fit parameters are chosen such that the likelihood function is approximately Gaussian. The preliminary results of the fits to the differential cross-sections are given in Table 7.3. No significant deviations with respect to the QED expectations are found (all the parameters are compatible with zero) and therefore 95% confidence level limits are obtained by renormalising the probability distribution of the fit parameter to the physically allowed region. For limits on f_γ/Λ a scan over M_{e^*} is performed and presented in Figure 7.3. Only for M_{e^*} is the cross-section nonlinear in the fit parameter. The obtained negative log likelihood is shown in Figure 7.4 and the limit is determined at 1.92 units above the minimum.

7.6 Conclusion

The LEP collaborations study the $e^+e^- \to \gamma\gamma(\gamma)$ channel up to the highest available centre-of-mass energies. The total cross-section results are combined in terms of the ratios with respect to the QED expectations. No deviations are found. The differential cross-sections are fit following different parametrisations from models predicting deviations from QED. No evidence for deviations is found and therefore combined 95% confidence level limits are given.

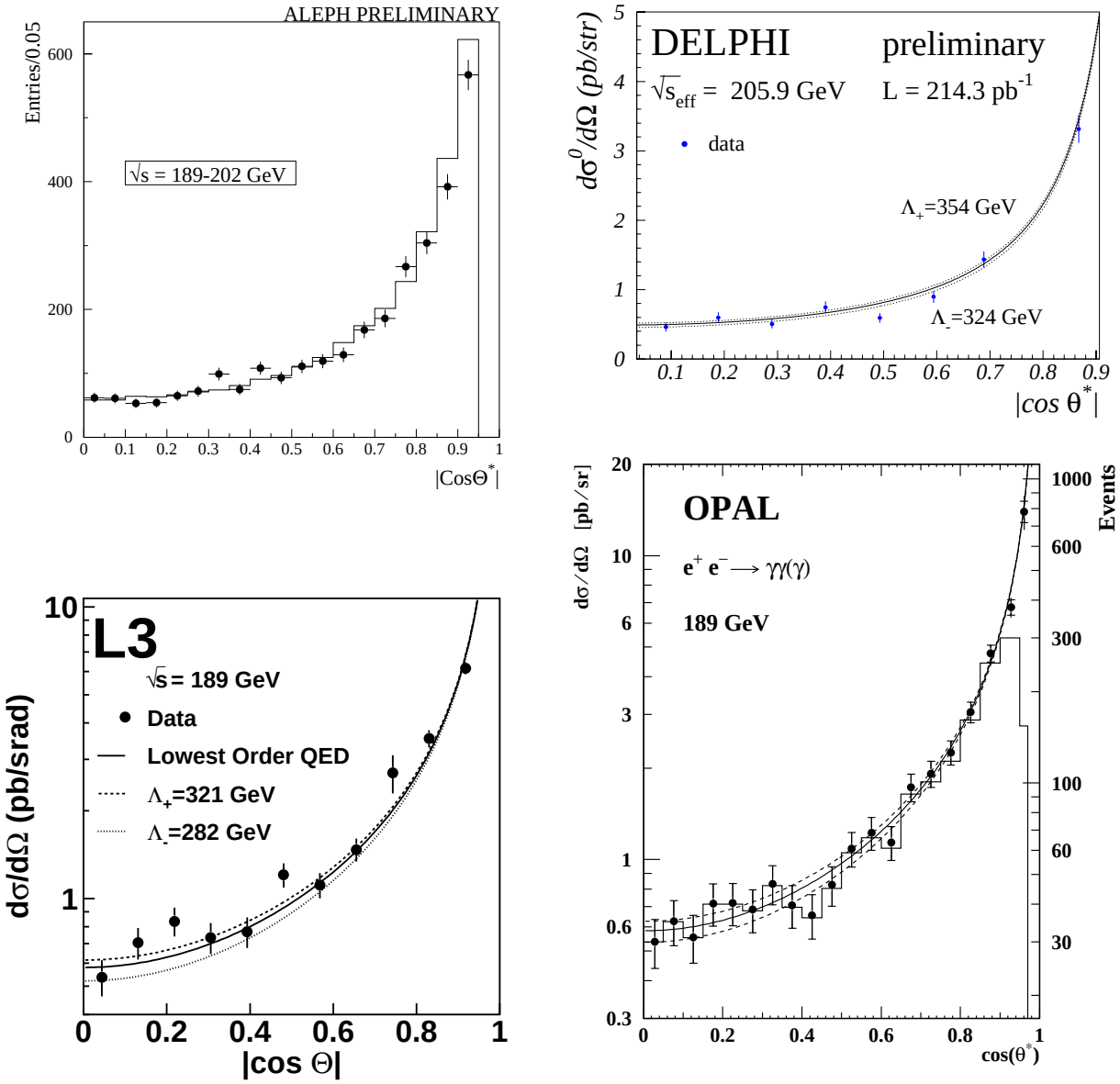

Figure 7.2: Examples for angular distributions of the four LEP experiments. Points are the data and the curves are the QED prediction (solid) and the individual fit results for $\Lambda_{\pm}$ (dashed). ALEPH shows the uncorrected number of observed events, the expectation is presented as histogram. For OPAL the histogram represents the number of observed events, before efficiency and radiative corrections are applied.

Fit parameter	Fit result	95% CL limit [GeV]
$\Lambda_{\pm}^{-4}$	$\left(4.6^{+27.0}_{-26.5}\right) \cdot 10^{-12}$ GeV^{-4}	$\Lambda_+ > 365$ $\Lambda_- > 379$
Λ_7^{-6}	$\left(0.18^{+1.95}_{-1.92}\right) \cdot 10^{-18}$ GeV^{-6}	$\Lambda_7 > 794$
derived from Λ_+		$\Lambda_6 > 1484$
derived from Λ_7		$\Lambda_8 > 22.5$
λ/M_s^4	$\left(-0.106^{+0.609}_{-0.615}\right) \cdot 10^{-12}$ GeV^{-4}	$\lambda = +1$: $M_s > 972$ $\lambda = -1$: $M_s > 940$
$f_\gamma^4(M_{e^*} = 200\text{GeV})$	$0.036^{+0.414}_{-0.400}$	$f_\gamma/\Lambda < 4.1$ TeV^{-1}

Table 7.3: The preliminary combined fit parameters and the 95% confidence level limits for the four LEP experiments.

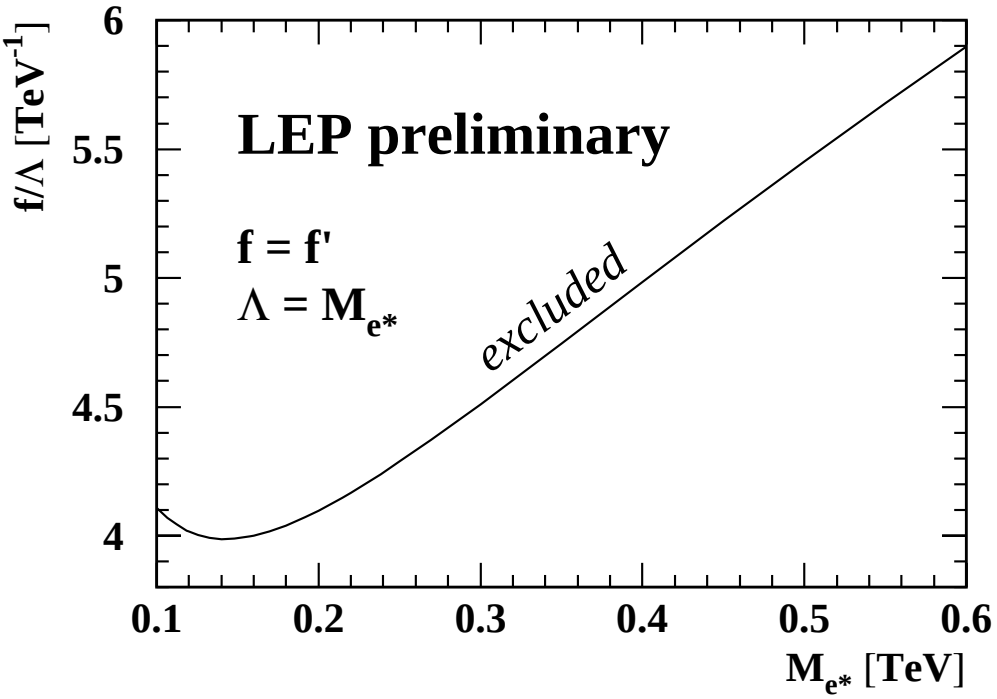

Figure 7.3: 95% CL limits on f_γ/Λ as a function of M_{e^*}. In the case of $f = f'$ it follows that $f_\gamma = f$. It is assumed that $\Lambda = M_{e^*}$.

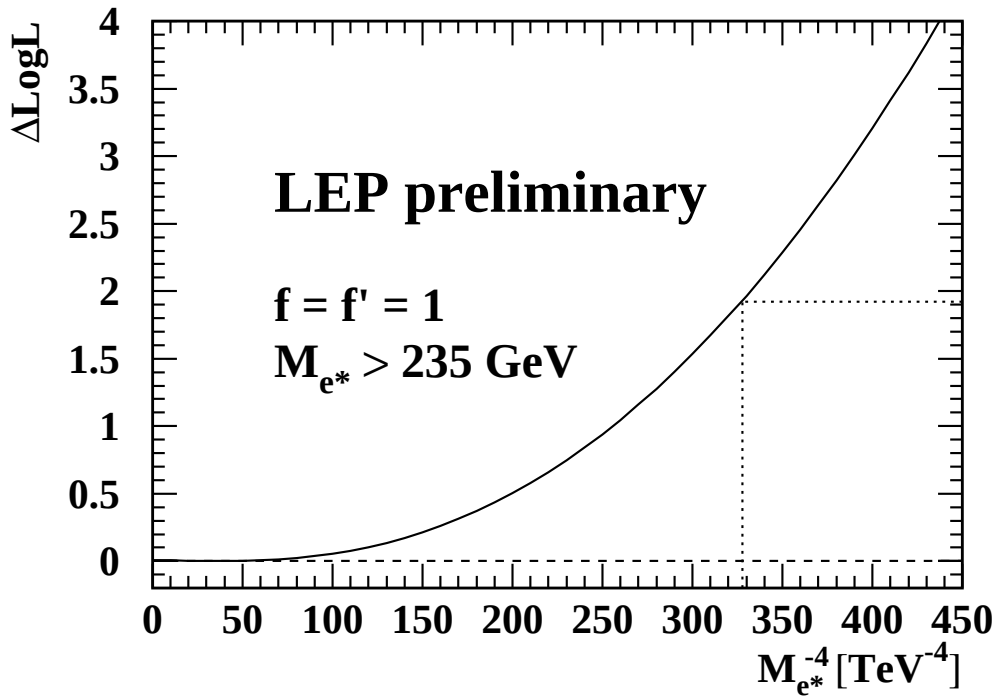

Figure 7.4: Log likelihood difference $\Delta\text{LogL} = -\ln\mathcal{L} + \ln\mathcal{L}_{\max}$ as a function of $M_{e^*}^{-4}$. The coupling is fixed at $f = f' = 1$. The value corresponding to $\Delta\text{LogL} = 1.92$ is $M_{e^*} = 235$ GeV.

Chapter 8

Fermion-Pair Production at LEP-II

Updates with respect to summer 2000:
Additional preliminary results based on the data collected in the year 2000 are included.

8.1 Introduction

Since the start of the LEP-II program LEP has delivered collisions at centre-of-mass energies from $\sim$ 130 GeV to $\sim$ 209 GeV. The four LEP experiments make measurements of the $e^+e^- \to f\bar{f}$ processes over this range of energies, and a preliminary combination of these data is discussed in this Chapter.

In the years 1995 to 1999 LEP delivered luminosity at a number of distinct centre-of-mass energy points. In 2000 most of the luminosity was delivered close to 2 distinct energies, but there was also a significant fraction of the luminosity delivered in, more-or-less, a continuum of energies. To facilitate the combination of the measurements, the four LEP experiments all divided the data they collected in 2000 into two energy bins: from 202.5 to 205.5 GeV; and 205.5 GeV and above. The nominal and actual centre-of-mass energies to which the LEP data are averaged for each year are given in Table 8.1.

A number of measurements on the process $e^+e^- \to f\bar{f}$ exist and are combined. The preliminary averages of cross-section and forward-backward asymmetry measurements are discussed in Section 8.2. The results presented in this section update those presented in [1,72–75]. Complete results of the combinations are available on the web page [76]. In Section 8.3 a preliminary average of the differential cross-section measurements, $\frac{d\sigma}{d\cos\theta}$, for the channels $e^+e^- \to \mu^+\mu^-$ and $e^+e^- \to \tau^+\tau^-$ is presented. In Section 8.4 a preliminary combination of the heavy flavour results R_b, R_c, $A_{FB}^{b\bar{b}}$ and $A_{FB}^{c\bar{c}}$ from LEP-II is presented. In Section 8.5 the combined results are interpreted in terms of contact interactions and the exchange of Z′ bosons. The results are summarised in section 8.6.

There are significant changes with respect to results presented in Summer 2000 [1,73]:

- The method of combining the cross-sections and leptonic forward-backward asymmetries is improved.
- The combinations are updated using new data:
  - updated preliminary cross-sections and leptonic forward-backward asymmetries for data taken at centre-of-mass energies of 205 and 207 GeV,

Year	Nominal Energy GeV	Actual Energy GeV	Luminosity pb^{-1}
1995	130	130.2	~ 3
	136	136.2	~ 3
	133*	133.2	~ 6
1996	161	161.3	~ 10
	172	172.1	~ 10
	167*	166.6	~ 20
1997	130	130.2	~ 2
	136	136.2	~ 2
	183	182.7	~ 50
1998	189	188.6	~ 170
1999	192	191.6	~ 30
	196	195.5	~ 80
	200	199.5	~ 80
	202	201.6	~ 40
2000	205	204.9	~ 80
	207	206.7	~ 140

Table 8.1: The nominal and actual centre-of-mass energies for data collected during LEP-II operation in each year. The approximate average luminosity analysed per experiment at each energy is also shown. Values marked with a * are average energies for 1995 and 1996 used for heavy flavour results. The data taken at nominal energies of 130 and 136 in 1995 and 1997 are combined by most experiments.

  - new preliminary differential cross-section results for $\mu^+\mu^-$ and $\tau^+\tau^-$ final states,
  - new preliminary heavy-flavour results.

- The interpretations are updated due to the changes in combined LEP results.

8.2 Averages for Cross-sections and Asymmetries

In this section the results of the preliminary combination of cross-sections and asymmetries are given. The individual experiments' analyses of cross-sections and forward-backward asymmetries are discussed in [77]. The preliminary cross-section and leptonic forward-backward asymmetry results at centre-of-mass energies of 205 and 207 GeV are updated with respect to [1, 73]. These are now obtained from analyses based on the full data set collected in 2000, improving the precision of the measurements.

Cross-section results are combined for the $e^+e^- \to q\overline{q}$, $e^+e^- \to \mu^+\mu^-$ and $e^+e^- \to \tau^+\tau^-$ channels, forward-backward asymmetry measurements are combined for the $\mu^+\mu^-$ and $\tau^+\tau^-$ final states. At LEP-II energies γ radiation is very important, leading in particular to a high rate for the radiative return to the Z. Events are classified according to the effective centre of mass energy, $\sqrt{s'}$, measured in different ways. The averages are made for the samples of events with high $\sqrt{s'}$, as discussed in the following.

Individual experiments use their own $f\overline{f}$ signal definitions; corrections are applied to bring the measurements to two common signal definitions:

- **Definition 1:** $\sqrt{s'}$ is taken to be the mass of the s-channel propagator, with the $\mathrm{f\bar{f}}$ signal being defined by the cut $\sqrt{s'/s} > 0.85$. The effects of ISR-FSR photon interference is subtracted to render the propagator mass unambiguous.
- **Definition 2:** For dilepton events, $\sqrt{s'}$ is taken to be the bare invariant mass of the outgoing difermion pair. For hadronic events, it is taken to be the mass of the s-channel propagator. In both cases, ISR-FSR photon interference is included and the signal is defined by the cut $\sqrt{s'/s} > 0.85$. When calculating the contribution to the hadronic cross-section due to ISR-FSR interference, since the propagator mass is ill-defined, it is replaced by the bare $\mathrm{q\bar{q}}$ mass.

The measurement corrected to the common signal definition, $\mathrm{M_{common}}$ is computed from the experimental measurement $\mathrm{M_{exp}}$,

$$\mathrm{M_{common}} = \mathrm{M_{exp}} + (\mathrm{P_{common}} - \mathrm{P_{exp}}),$$

where $\mathrm{P_{exp}}$ is the prediction for the measurement obtained for the experiments' signal definition and $\mathrm{P_{common}}$ is the prediction for the common signal definition. The predictions are computed with ZFITTER [78]. The theoretical uncertainties associated with the corrections are obtained by comparing ZFITTER, TOPAZ0 v4.4 [79] and the Monte Carlo generator KK v4.02 [80]. The uncertainties are approximately 0.2% for the hadronic cross-sections, 0.7% for dilepton cross-sections and 0.003 for the leptonic asymmetries [75]. These uncertainties will be updated for the final analyses, taking into account the results of Reference 81. These errors are not included in the combination. Results are presented extrapolated to full 4π angular acceptance. Events containing additional fermion pairs from radiative processes are considered to be signal, providing that the primary pair passes the cut on $\sqrt{s'/s}$ and that the secondary pair has a mass below 70 GeV.

The average is performed using the Best Linear Unbiased Estimator (BLUE) technique [82], which is based on matrix algebra and which is equivalent to a χ^2 minimisation. For the first time, all the data, from centre-of-mass energies of 130 to 207 GeV are averaged together, taking into account correlations between all LEP-II $\mathrm{e^+e^-} \to \mathrm{f\bar{f}}$ measurements. Previously [1], the data were treated as three independent subsamples at (130–189) GeV, (192–202) GeV and (205–207) GeV, ignoring correlations between the subsamples.

Particular care is taken to ensure that the correlations between the hadronic cross-sections are reasonably estimated. As in [1,73] the errors are broken down into 5 categories

1) The statistical uncertainty plus uncorrelated systematic uncertainties, combined in quadrature.
2) The systematic uncertainty for the final state X which is fully correlated between energy points for that experiment.
3) The systematic uncertainty for experiment Y which is fully correlated between different final states for this energy point but uncorrelated between energy points.
4) The systematic uncertainty for the final state X which is fully correlated between energy points and between different experiments.
5) The systematic uncertainty which is fully correlated between energy points and between different experiments for all final states.

In previous averages, uncertainties in the hadronic cross-sections arising from fragmentation models and modelling of ISR had been treated as uncorrelated between experiments. However, although

there are some differences between the models used and the methods of evaluating the errors, there are significant common elements in the estimation of these sources of uncertainty between the experiments. For the average reported here, these errors are treated as fully correlated between energy points and experiments.

Table 8.2 gives the averaged cross-sections and forward-backward asymmetries for all energies for Definition 1. The differences in the results obtained using Definition 2 are also given.

The χ^2 per degree of freedom for the average of the LEP-II $f\bar{f}$ data is 170/180. The correlations are rather small, with the largest components at any given pair of energies being between the hadronic cross-sections. The other off-diagonal terms in the correlation matrix are smaller than 10%. The correlation matrix between the averaged hadronic cross-sections at different centre-of-mass energies is given in Table 8.3.

Differences in the results with respect to previous combinations at centre-of-mass energies from 130–202 GeV [1,73,74] arise mainly from the introduction of correlations between measurements which were previously taken to be uncorrelated, and the improved treatment of the correlations themselves.

Figures 8.1 and 8.2 show the LEP averaged cross-sections and asymmetries, respectively, as a function of the centre-of-mass energy, together with the SM predictions. There is good agreement between the SM expectations and the measurements of the individual experiments and the combined averages. The measured cross-sections for hadronic final states at most of the energy points are somewhat above the SM expectations. Taking into account the correlations between the data points and also assigning an error of $\pm 0.26\%$ [81] on the absolute SM predictions, the difference of the cross-section from the SM expectations averaged over all energies is approximately 1.8 standard deviations. It is concluded that there is no significant evidence in the results for physics beyond the SM in the process $e^+e^- \to f\bar{f}$.

$\sqrt{s}$ (GeV)	Quantity	Average value	SM	Δ
130	$\sigma(q\bar{q})$ [pb]	82.124±2.232	82.803	-0.251
	$\sigma(\mu^+\mu^-)$ [pb]	8.620±0.682	8.439	-0.331
	$\sigma(\tau^+\tau^-)$ [pb]	9.036±0.930	8.435	-0.108
	$A_{fb}(\mu^+\mu^-)$	0.693±0.060	0.705	0.012
	$A_{fb}(\tau^+\tau^-)$	0.663±0.076	0.704	0.012
136	$\sigma(q\bar{q})$ [pb]	66.724±1.974	66.596	-0.224
	$\sigma(\mu^+\mu^-)$ [pb]	8.276±0.677	7.281	-0.280
	$\sigma(\tau^+\tau^-)$ [pb]	7.086±0.820	7.279	-0.091
	$A_{fb}(\mu^+\mu^-)$	0.707±0.060	0.684	0.013
	$A_{fb}(\tau^+\tau^-)$	0.752±0.088	0.683	0.014
161	$\sigma(q\bar{q})$ [pb]	37.014±1.074	35.247	-0.143
	$\sigma(\mu^+\mu^-)$ [pb]	4.608±0.364	4.613	-0.178
	$\sigma(\tau^+\tau^-)$ [pb]	5.673±0.545	4.613	-0.061
	$A_{fb}(\mu^+\mu^-)$	0.537±0.067	0.609	0.017
	$A_{fb}(\tau^+\tau^-)$	0.646±0.077	0.609	0.016
172	$\sigma(q\bar{q})$ [pb]	29.262±0.989	28.738	-0.124
	$\sigma(\mu^+\mu^-)$ [pb]	3.571±0.317	3.952	-0.157
	$\sigma(\tau^+\tau^-)$ [pb]	4.013±0.450	3.951	-0.054
	$A_{fb}(\mu^+\mu^-)$	0.674±0.077	0.591	0.018
	$A_{fb}(\tau^+\tau^-)$	0.342±0.094	0.591	0.017
183	$\sigma(q\bar{q})$ [pb]	24.609±0.426	24.200	-0.109
	$\sigma(\mu^+\mu^-)$ [pb]	3.490±0.147	3.446	-0.139
	$\sigma(\tau^+\tau^-)$ [pb]	3.375±0.174	3.446	-0.050
	$A_{fb}(\mu^+\mu^-)$	0.559±0.035	0.576	0.018
	$A_{fb}(\tau^+\tau^-)$	0.608±0.045	0.576	0.018
189	$\sigma(q\bar{q})$ [pb]	22.446±0.257	22.156	-0.101
	$\sigma(\mu^+\mu^-)$ [pb]	3.116±0.077	3.207	-0.131
	$\sigma(\tau^+\tau^-)$ [pb]	3.121±0.099	3.207	-0.048
	$A_{fb}(\mu^+\mu^-)$	0.566±0.021	0.569	0.019
	$A_{fb}(\tau^+\tau^-)$	0.584±0.028	0.569	0.018
192	$\sigma(q\bar{q})$ [pb]	22.291±0.523	21.237	-0.098
	$\sigma(\mu^+\mu^-)$ [pb]	2.943±0.175	3.097	-0.127
	$\sigma(\tau^+\tau^-)$ [pb]	2.832±0.216	3.097	-0.047
	$A_{fb}(\mu^+\mu^-)$	0.540±0.052	0.566	0.019
	$A_{fb}(\tau^+\tau^-)$	0.614±0.070	0.566	0.019
196	$\sigma(q\bar{q})$ [pb]	20.729±0.338	20.127	-0.094
	$\sigma(\mu^+\mu^-)$ [pb]	2.967±0.106	2.962	-0.123
	$\sigma(\tau^+\tau^-)$ [pb]	2.984±0.138	2.962	-0.045
	$A_{fb}(\mu^+\mu^-)$	0.580±0.031	0.562	0.019
	$A_{fb}(\tau^+\tau^-)$	0.493±0.045	0.562	0.019
200	$\sigma(q\bar{q})$ [pb]	19.372±0.319	19.085	-0.090
	$\sigma(\mu^+\mu^-)$ [pb]	3.040±0.104	2.834	-0.118
	$\sigma(\tau^+\tau^-)$ [pb]	2.966±0.134	2.833	-0.044
	$A_{fb}(\mu^+\mu^-)$	0.518±0.031	0.558	0.019
	$A_{fb}(\tau^+\tau^-)$	0.549±0.043	0.558	0.019
202	$\sigma(q\bar{q})$ [pb]	19.278±0.430	18.572	-0.088
	$\sigma(\mu^+\mu^-)$ [pb]	2.621±0.139	2.770	-0.116
	$\sigma(\tau^+\tau^-)$ [pb]	2.777±0.183	2.769	-0.044
	$A_{fb}(\mu^+\mu^-)$	0.543±0.048	0.556	0.020
	$A_{fb}(\tau^+\tau^-)$	0.583±0.060	0.556	0.019
205	$\sigma(q\bar{q})$ [pb]	18.119±0.316	17.811	-0.085
	$\sigma(\mu^+\mu^-)$ [pb]	2.449±0.100	2.674	-0.112
	$\sigma(\tau^+\tau^-)$ [pb]	2.705±0.129	2.673	-0.042
	$A_{fb}(\mu^+\mu^-)$	0.558±0.036	0.553	0.020
	$A_{fb}(\tau^+\tau^-)$	0.565±0.044	0.553	0.019
207	$\sigma(q\bar{q})$ [pb]	17.423±0.263	17.418	-0.083
	$\sigma(\mu^+\mu^-)$ [pb]	2.613±0.088	2.623	-0.111
	$\sigma(\tau^+\tau^-)$ [pb]	2.528±0.108	2.623	-0.042
	$A_{fb}(\mu^+\mu^-)$	0.540±0.029	0.552	0.020
	$A_{fb}(\tau^+\tau^-)$	0.561±0.038	0.551	0.019

Table 8.2: Preliminary combined LEP results for $e^+e^- \to f\bar{f}$. All the results correspond to the signal Definition 1. The Standard Model predictions are from ZFITTER [78]. The difference, Δ, in the averages for the measurements for Definition 2 relative to Definition 1 are given in the final column. The quoted uncertainties do not include the theoretical uncertainties on the corrections discussed in the text.

$\sqrt{s}$ GeV)	130	136	161	172	183	189	192	196	200	202	205	207
130	1.000	0.075	0.085	0.076	0.121	0.151	0.084	0.116	0.131	0.091	0.137	0.160
136		1.000	0.079	0.071	0.112	0.140	0.078	0.107	0.121	0.084	0.127	0.148
161			1.000	0.082	0.128	0.162	0.089	0.123	0.139	0.097	0.144	0.167
172				1.000	0.114	0.145	0.080	0.110	0.125	0.087	0.130	0.150
183					1.000	0.237	0.130	0.179	0.203	0.139	0.208	0.242
189						1.000	0.173	0.236	0.270	0.184	0.266	0.307
192							1.000	0.136	0.156	0.106	0.151	0.173
196								1.000	0.212	0.145	0.207	0.238
200									1.000	0.166	0.236	0.271
202										1.000	0.162	0.185
205											1.000	0.282
207												1.000

Table 8.3: The correlation coefficients between averaged hadronic cross-sections at different energies.

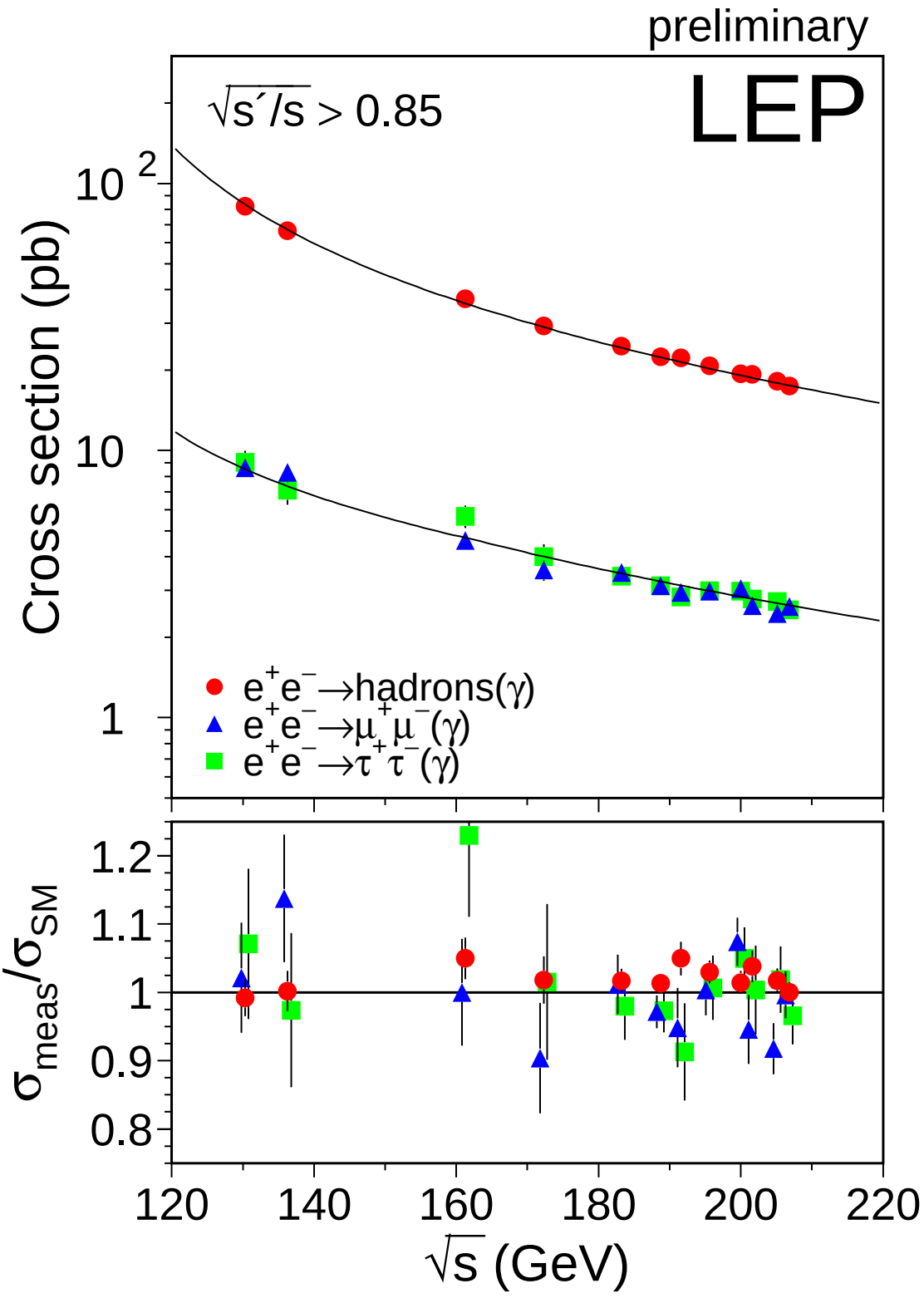

Figure 8.1: Preliminary combined LEP results on the cross-sections for $q\overline{q}$, $\mu^+\mu^-$ and $\tau^+\tau^-$ final states, as a function of centre-of-mass energy. The expectations of the SM, computed with ZFITTER [78], are shown as curves. The lower plot shows the ratio of the data divided by the SM.

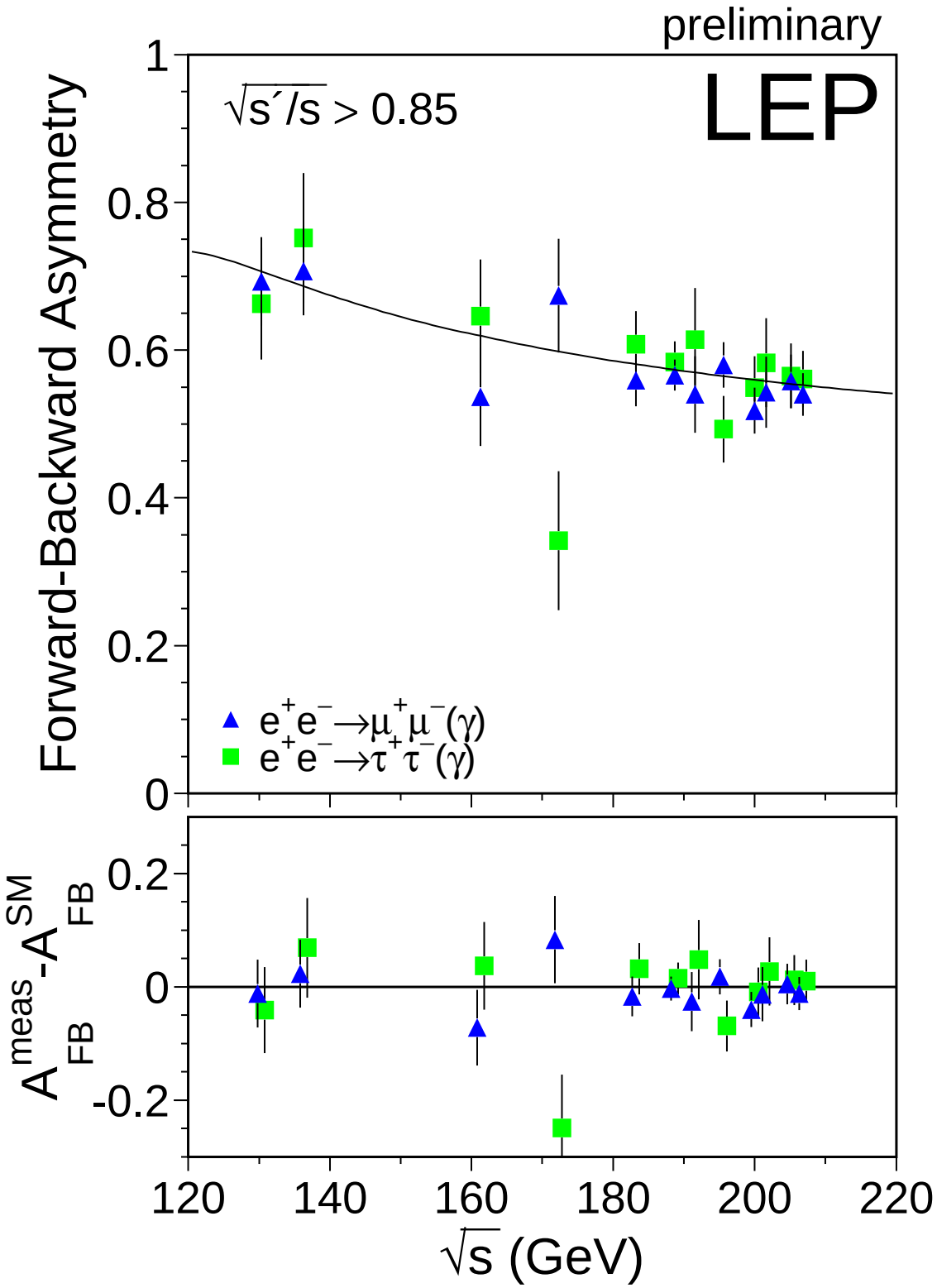

Figure 8.2: Preliminary combined LEP results on the forward-backward asymmetry for $\mu^+\mu^-$ and $\tau^+\tau^-$ final states as a function of centre-of-mass energy. The expectations of the SM computed with ZFITTER [78], are shown as curves. The lower plot shows differences between the data and the SM.

8.3 Averages for Differential Cross-sections

The LEP experiments measure the differential cross-section, $\frac{d\sigma}{d\cos\theta}$, for the $e^+e^- \to \mu^+\mu^-$ and $e^+e^- \to \tau^+\tau^-$ channels for samples of events with $\sqrt{s'/s} > 0.85$. A preliminary combination of these results is made using a χ^2 fit to the measured differential cross sections, using the expected error on the differential cross sections, computed from the expected cross sections and the expected numbers of events in each experiment. Using a Monte Carlo simulation it is shown that this method provides a good approximation to the exact likelihood method based on Poisson statistics [73].

The combination included data from 183 to 207 GeV, but not all experiments provided measurements at all energies. Since [1,73], new, preliminary, results for centre-of-mass energies of 205 and 207 GeV are made available by all experiments. In addition, new, preliminary, results for $e^+e^- \to \mu^+\mu^-$ at energies from 192–202 GeV from L3 are made available. The data used in the combination are summarised in Table 8.4.

Each experiments' data are binned in 10 bins of $\cos\theta$ at each energy, using their own signal definition. The scattering angle, θ, is the angle of the negative lepton with respect to the incoming electron direction in the lab coordinate system. The outer acceptances of the most forward and most backward bins for which the four experiments present their data are different. This is accounted for as part of the correction to a common signal definition. The ranges in $\cos\theta$ for the measurements of the individual experiments and the average are given in Table 8.5. The signal definition used corresponded to Definition 1 of Section 8.2.

Correlated small systematic errors between different experiments, channels and energies, arising from uncertainties on the overall normalisation are considered in the averaging procedure.

Three separate averages are performed; one for 183 and 189 GeV data, one for 192–202 GeV data and for 205 and 207 GeV data. The averages for the 183–189 data set are not updated with respect to [1,73]. The results of the averages are shown in Figures 8.3 and 8.4.

The correlations between bins in the average are less than 2% of the total error on the averages in each bin. The overall agreement between the averaged data and the predictions is reasonable, with a χ^2 of 191 for 160 degrees of freedom. At 202 GeV the cross-section in the most backward bin, $-1.0 < \cos\theta < -0.8$, for both muon and tau final states is above the predictions. For the muons the excess in the data corresponds to 3.4 standard deviations. For the taus the excess is 2.3 standard deviations, however, for this measurement the individual experiments are somewhat inconsistent, having a χ^2 with respect to the average of 10.5 for 2 degrees of freedom. The data at 202 GeV suffer from rather low delivered luminosity, with fewer than four events expected in each experiment in each channel in this backward $\cos\theta$ bin. The agreement between the data and the predictions in the same $\cos\theta$ bin is better at higher energies.

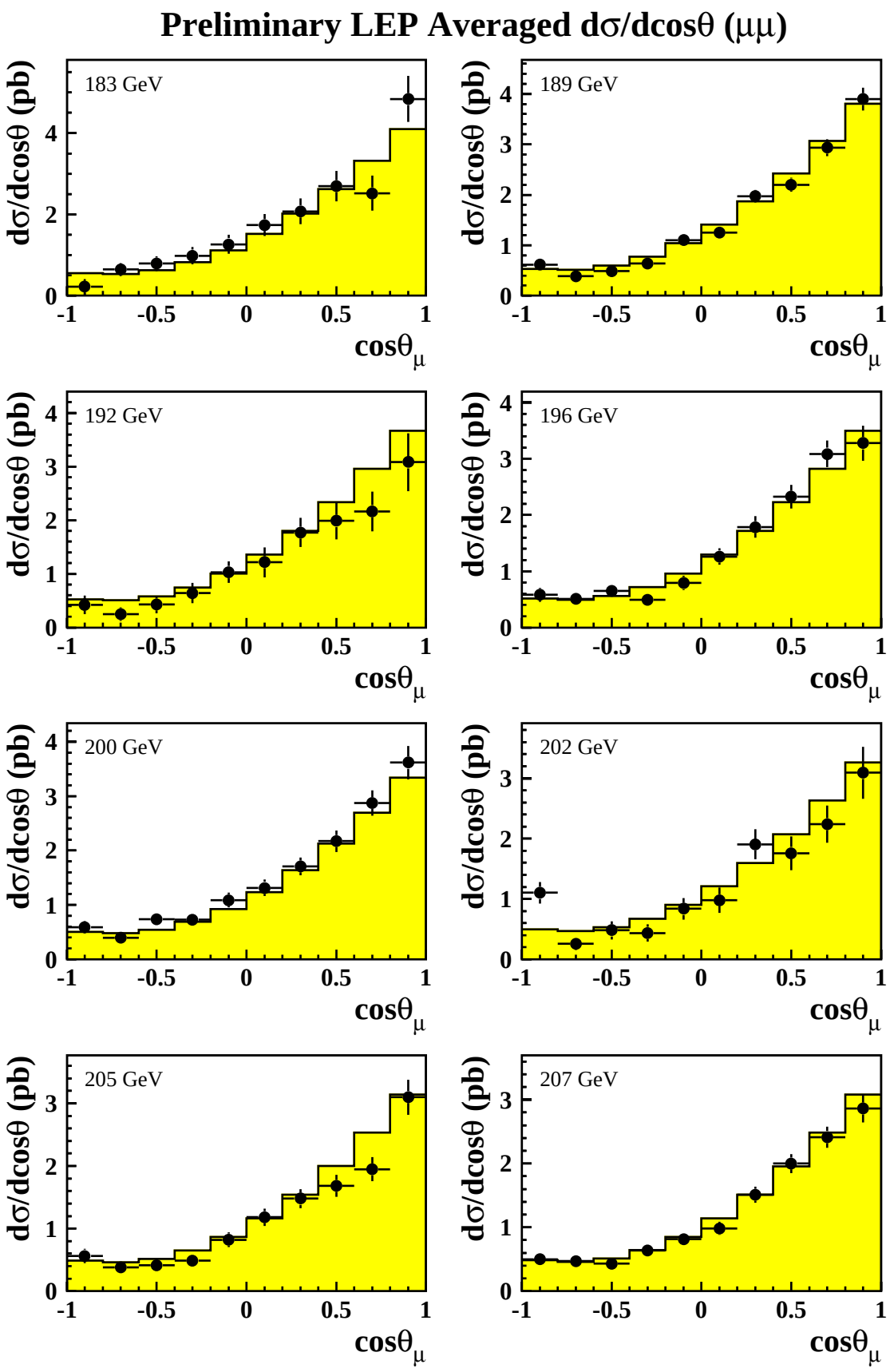

Figure 8.3: LEP averaged differential cross-sections for $e^+e^- \to \mu^+\mu^-$ at energies of 183–207 GeV. The SM predictions, shown as solid histograms, are computed with ZFITTER [78].

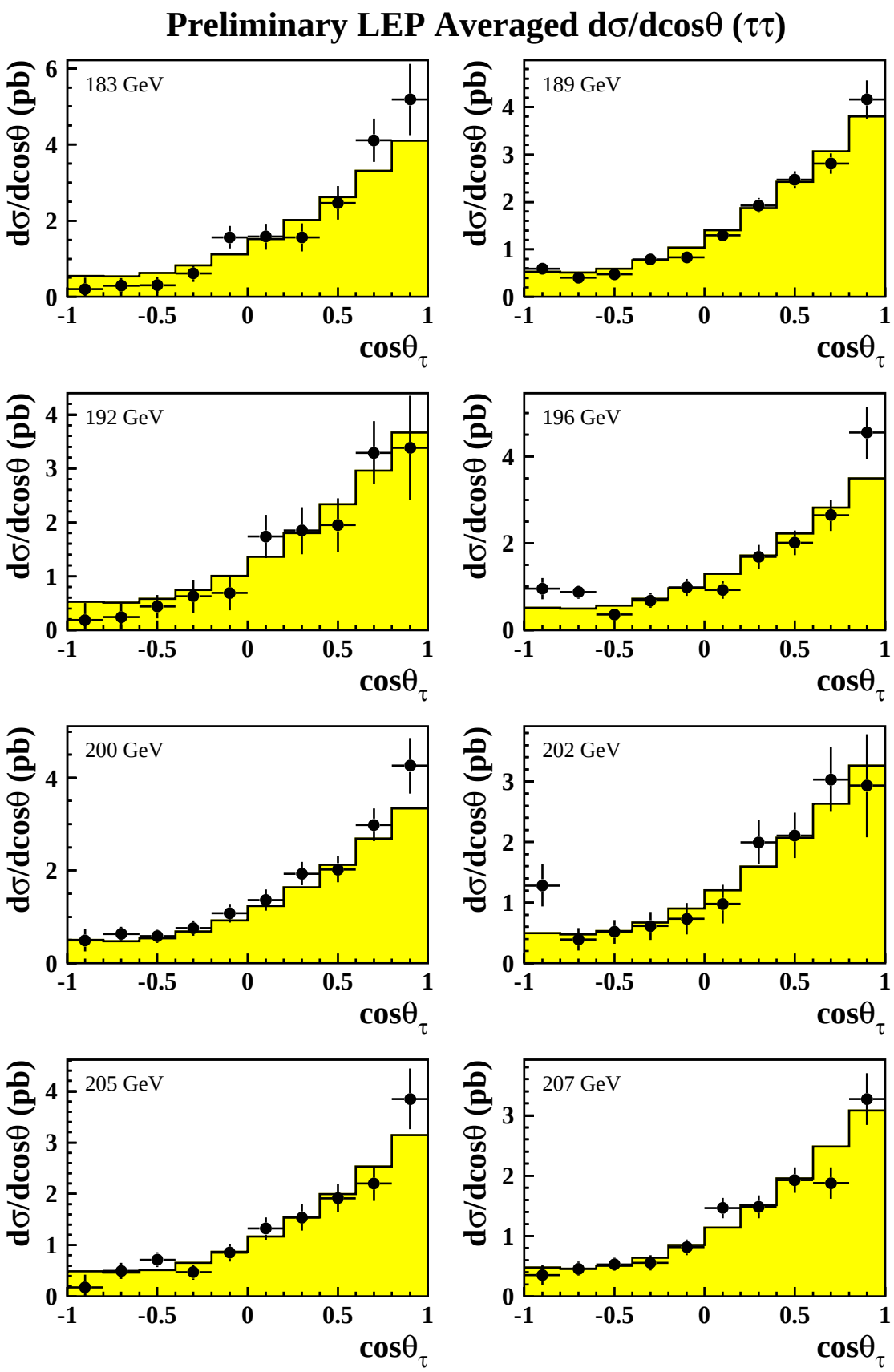

Figure 8.4: LEP averaged differential cross-sections for $e^+e^- \to \tau^+\tau^-$ at energies of 183–207 GeV. The SM predictions, shown as solid histograms, are computed with ZFITTER [78].

	$e^+e^- \to \mu^+\mu^-$				$e^+e^- \to \tau^+\tau^-$			
$\sqrt{s}$(GeV)	A	D	L	O	A	D	L	O
183	-	F	-	F	-	F	-	F
189	P	F	F	F	P	F	F	F
192–202	P	P	P	P	P	P	-	P
205–207	P	P	P	P	P	P	-	P

Table 8.4: Differential cross-section data provided by the LEP collaborations (ALEPH, DELPHI, L3 and OPAL) for $e^+e^- \to \mu^+\mu^-$ and $e^+e^- \to \tau^+\tau^-$ combination at different centre-of-mass energies. Data indicated with F are final, published data. Data marked with P are preliminary. Data marked with a - are not available for combination.

Experiment	$\cos\theta_{min}$	$\cos\theta_{max}$
ALEPH	-0.95	0.95
DELPHI ($e^+e^- \to \mu^+\mu^-$ 183)	-0.94	0.94
DELPHI ($e^+e^- \to \mu^+\mu^-$ 189–207)	-0.97	0.97
DELPHI ($e^+e^- \to \tau^+\tau^-$)	-0.96	0.96
L3	-0.90	0.90
OPAL	-1.00	1.00
Average	-1.00	1.00

Table 8.5: The acceptances for which experimental data are presented and the acceptance for the LEP average. For DELPHI the acceptance is shown for the different channels and for the muons for different centre of mass energies. For all other experiments the acceptance is the same for muon and tau-lepton channels and for all energies provided.

8.4 Averages for Heavy Flavour Measurements

This section presents a preliminary combination of both published [83] and preliminary [84] measurements of the ratios[1] R_b and R_c and the forward-backward asymmetries, $A_{FB}^{b\bar{b}}$ and $A_{FB}^{c\bar{c}}$, from the LEP collaborations at centre-of-mass energies in the range of 130 to 207 GeV. The averages are updated with respect to [1, 73]. New preliminary results from DELPHI and L3 at centre-of-mass energies of 205 and 207 GeV, based on analyses of the full 2000 data sets, are also included. New, preliminary, results from ALEPH at lower energies are also combined. Table 8.6 summarises all the inputs that are combined.

A common signal definition is defined for all the measurements, requiring:

- an effective centre-of-mass energy $\sqrt{s'} > 0.85\sqrt{s}$
- the inclusion of ISR and FSR photon interference contribution and
- extrapolation to full angular acceptance.

Systematic errors are divided into three categories: uncorrelated errors, errors correlated between the measurements of each experiment, and errors common to all experiments. Full details concerning the combination procedure can be found in [85].

The results of the combination are presented in Table 8.7 and Figures 8.5 and 8.6. The results are consistent with the Standard Model predictions of ZFITTER.

Because of the large correlation (-0.36) with R_c at 183 GeV and 189 GeV, the errors on the corresponding measurements of R_b receive an additional contribution which is absent at the other energy points. For other energies where there is no measurement of R_c, the Standard Model value of R_c is used in extracting R_b (the error on the Standard Model prediction of R_c is estimated to be negligible compared to the other uncertainties on R_b).

A list of the error contributions from the combination at 189 GeV is shown in Table 8.8.

$\sqrt{s}$ (GeV)	R_b				R_c				$A_{FB}^{b\bar{b}}$				$A_{FB}^{c\bar{c}}$			
	A	D	L	O	A	D	L	O	A	D	L	O	A	D	L	O
133	F	F	F	F	-	-	-	-	-	F	-	F	-	F	-	F
167	F	F	F	F	-	-	-	-	-	F	-	F	-	F	-	F
183	F	P	F	F	F	-	-	-	F	-	-	F	P	-	-	F
189	P	P	F	F	P	-	-	-	P	P	F	F	P	-	-	F
192 to 202	P	P	P	-	-	-	-	-	P	P	-	-	-	-	-	-
205 and 207	-	P	P	-	-	-	-	-	-	P	-	-	-	-	-	-

Table 8.6: Data provided by the ALEPH, DELPHI, L3, OPAL collaborations for combination at different centre-of-mass energies. Data indicated with F are final, published data. Data marked with P are preliminary. Data marked with a - are not supplied for combination.

[1] Unlike at LEP-I, R_q^0 is defined as $\frac{\sigma_{q\bar{q}}}{\sigma_{had}}$.

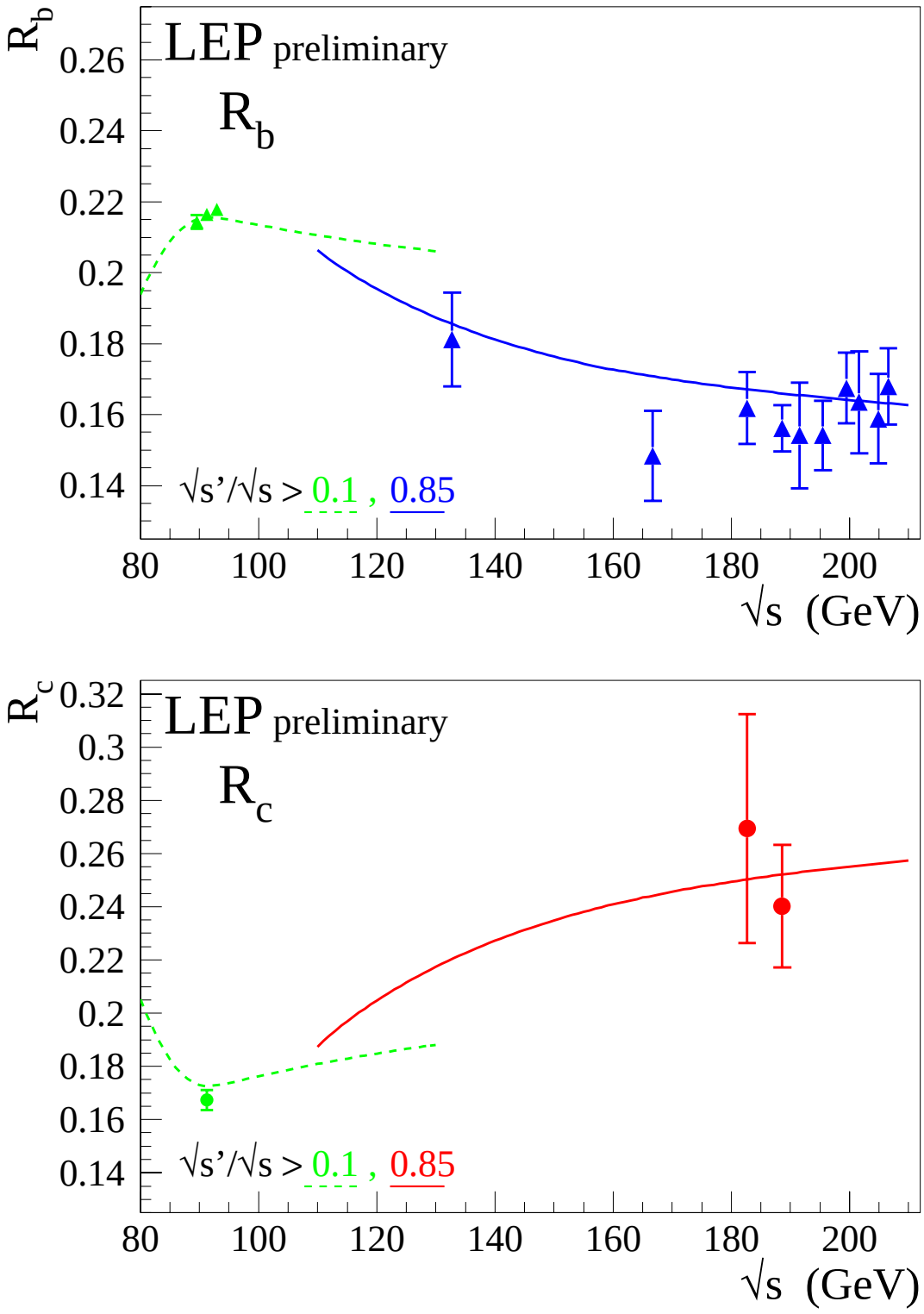

Figure 8.5: Preliminary combined LEP measurements of R_b and R_c. Solid lines represent the Standard Model prediction for the signal definition and dotted lines the inclusive prediction. Both are computed with ZFITTER[86]. The LEP-I measurements are taken from [87].

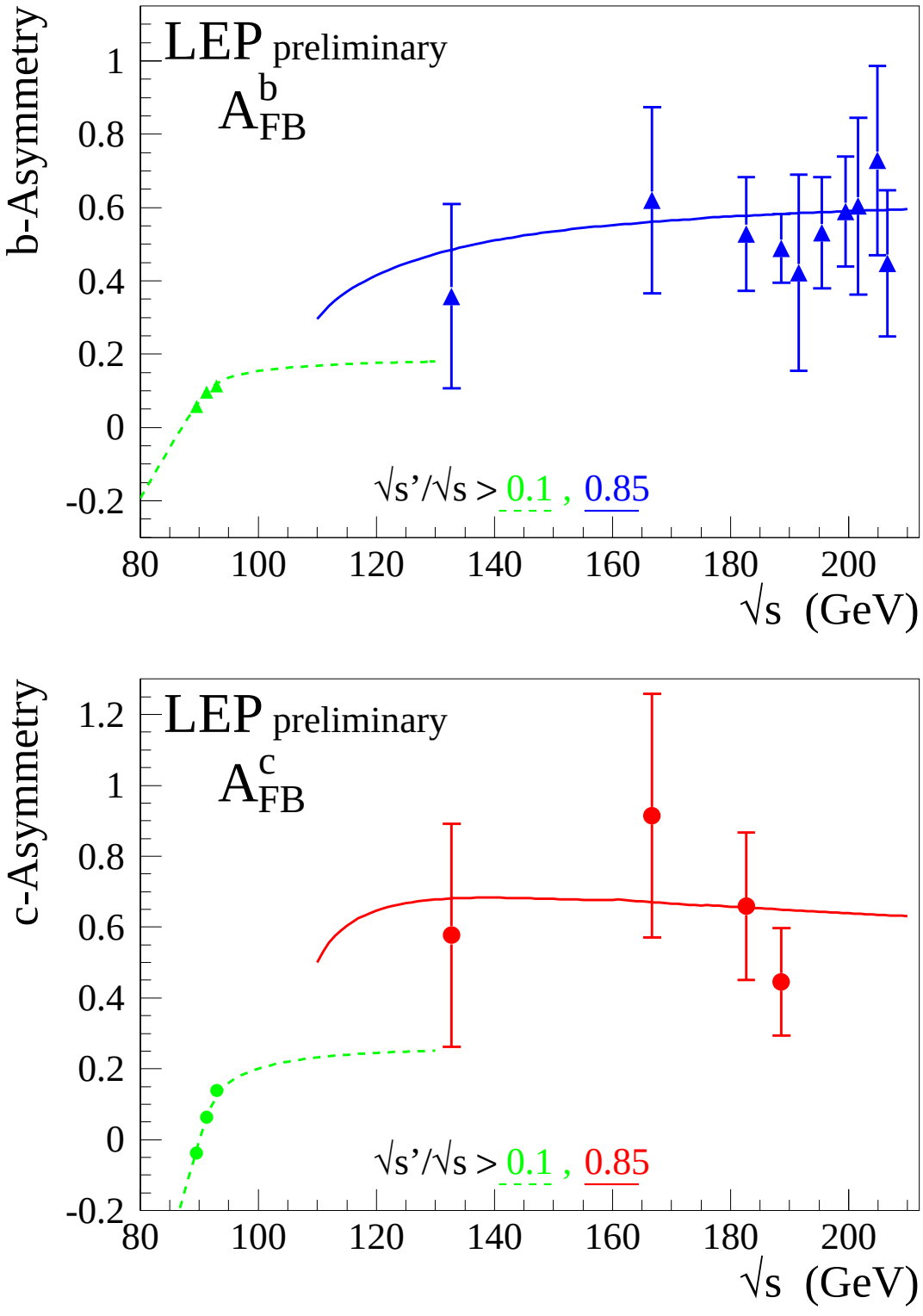

Figure 8.6: Preliminary combined LEP measurements of the forward–backward asymmetries $A_{FB}^{b\bar{b}}$ and $A_{FB}^{c\bar{c}}$. Solid lines represent the Standard Model prediction for the signal definition and dotted lines the inclusive prediction. Both are computed with ZFITTER [86]. The LEP-I measurements are taken from [87].

$\sqrt{s}$ (GeV)	R_b	R_c	$A_{FB}^{b\bar{b}}$	$A_{FB}^{c\bar{c}}$
133	0.1811 ± 0.0132	-	0.358 ± 0.251	0.577 ± 0.314
	(0.1853)	-	(0.487)	(0.681)
167	0.1484 ± 0.0127	-	0.620 ± 0.254	0.915 ± 0.344
	(0.1708)	-	(0.561)	(0.671)
183	0.1619 ± 0.0101	0.269 ± 0.043	0.528 ± 0.155	0.658 ± 0.209
	(0.1671)	(0.250)	(0.578)	(0.656)
189	0.1562 ± 0.0065	0.240 ± 0.023	0.488 ± 0.094	0.446 ± 0.151
	(0.1660)	(0.252)	(0.583)	(0.649)
192	0.1541 ± 0.0149	-	0.422 ± 0.267	-
	(0.1655)	-	(0.585)	-
196	0.1542 ± 0.0098	-	0.531 ± 0.151	-
	(0.1648)	-	(0.587)	-
200	0.1675 ± 0.0100	-	0.589 ± 0.150	-
	(0.1642)	-	(0.590)	-
202	0.1635 ± 0.0143	-	0.604 ± 0.241	-
	(0.1638)	-	(0.593)	-
205	0.1588 ± 0.0126	-	0.728 ± 0.258	-
	(0.1634)	-	(0.594)	-
207	0.1680 ± 0.0108	-	0.447 ± 0.200	-
	(0.1632)	-	(0.593)	-

Table 8.7: Results of the global fit, compared to the Standard Model predictions computed with ZFITTER [86], for the signal definition in parentheses. The quoted errors are the statistical and systematic errors added in quadrature. Because of the large correlation with R_c at 183 GeV and 189 GeV, the errors on the corresponding measurements of R_b receive an additional contribution which is absent at the other energy points.

Error list	R_b (189 GeV)	R_c (189 GeV)	$A_{FB}^{b\bar{b}}$ (189 GeV)	$A_{FB}^{c\bar{c}}$ (189 GeV)
statistics	0.00606	0.0179	0.0884	0.1229
internal syst	0.00232	0.0123	0.0296	0.0481
common syst	0.00082	0.0078	0.0138	0.0735
total syst	0.00246	0.0145	0.0327	0.0878
total error	0.00654	0.0231	0.0942	0.1510

Table 8.8: Error breakdown at 189 GeV.

8.5 Interpretation

The combined cross-sections and asymmetries and results on heavy flavour production are interpreted in a variety of models. The cross-section and asymmetry results are used to place limits on the mass of a possible additional heavy neutral boson, Z′, in several models. Limits on contact interactions between leptons and on contact interaction between electrons and b and c quarks are obtained. These results are of particular interest since they are inaccessible to $p\bar{p}$ or ep colliders. The results update those provided in [1,73].

8.5.1 Models with Z′ Bosons

The combined hadronic and leptonic cross-sections and the leptonic forward-backward asymmetries are used to fit the data to models including an additional, heavy, neutral boson, Z′. The results are updated with respect to those given in [1,73] due to the updated cross-section and leptonic forward-backward asymmetry results.

Fits are made to the mass of a Z′, $M_{Z'}$, for 4 different models referred to as χ, ψ, η and L-R [88] and for the Sequential Standard Model [89], which proposes the existence of a Z′ with exactly the same coupling to fermions as the standard Z. The LEP-II data alone does not significantly constrain the mixing angle between the Z and Z′ fields, $\Theta_{ZZ'}$. However, results from a single experiment in which LEP-I data is used in the fit show that the mixing is consistent with zero (see for example [90], giving limits of 30 mrad or less depending on model). So for these fits $\Theta_{ZZ'}$ is fixed to zero.

No significant evidence is found for the existence of a Z′ boson in any of the models. 95% confidence level lower limits on $M_{Z'}$ are obtained, by integrating the likelihood function[2]. The lower limits on the Z′ mass are shown in Table 8.9.

Model	χ	ψ	η	L-R	SSM
$M_{Z'}^{limit}$ (GeV)	678	463	436	800	1890

Table 8.9: The 95% confidence level lower limits on the Z′ mass and χ, ψ, η, L-R and SSM models.

8.5.2 Contact Interactions between Leptons

The averages of cross-sections and forward-backward asymmetries for muon-pair and tau-lepton pair final states are used to search for contact interactions between leptons. The results are updated with respect to those given in [1,73] due to the updated cross-section and leptonic forward-backward asymmetry results.

Following [91], contact interactions are parameterised by an effective Lagrangian, $\mathcal{L}_{\text{eff}}$, which is added to the Standard Model Lagrangian and has the form:

$$\mathcal{L}_{\text{eff}} = \frac{g^2}{(1+\delta)\Lambda^2} \sum_{i,j=L,R} \eta_{ij} \bar{e}_i \gamma_\mu e_i \bar{f}_j \gamma^\mu f_j,$$

[2]To be able to obtain confidence limits from the likelihood function it is necessary to convert the likelihood to a probability density function; this is done by multiplying by a prior probability function. Simply integrating the likelihood is equivalent to multiplying by a uniform prior probability function.

where $g^2/4\pi$ is taken to be 1 by convention, $\delta = 1(0)$ for $f = e$ ($f \neq e$), $\eta_{ij} = \pm 1$ or 0, Λ is the scale of the contact interactions, e_i and f_j are left or right-handed spinors. By assuming different helicity coupling between the initial state and final state currents, a set of different models can be defined from this Lagrangian [92], with either constructive (+) or destructive (−) interference between the Standard Model process and the contact interactions. The models and corresponding choices of η_{ij} are given in Table 8.10. The models LL, RR, VV, AA, LR, RL, V0, A0 are considered here since these models lead to large deviations in the $e^+e^- \to \mu^+\mu^-$ and $e^+e^- \to \tau^+\tau^-$ channels. The total hadronic cross section on its own does not allow stringent limits to be placed on contact interactions involving quarks.

For the purpose of fitting contact interaction models to the data, a new parameter $\epsilon = 1/\Lambda^2$ is defined; $\epsilon = 0$ in the limit that there are no contact interactions. This parameter is allowed to take both positive and negative values in the fits. Theoretical uncertainties on the Standard Model predictions are taken from [81], see above.

The values of ϵ extracted for each model are all compatible with the Standard Model expectation $\epsilon = 0$, at the two standard deviation level. These errors on ϵ are typically a factor of two smaller than those obtained from a single LEP experiment with the same data set. The fitted values of ϵ are converted into 95% confidence level lower limits on Λ. The limits are obtained by integrating the likelihood function over the physically allowed values, $\epsilon \geq 0$ for each Λ^+ limit and $\epsilon \leq 0$ for Λ^- limits. The fitted values of ϵ and the extracted limits are shown in Table 8.11. Figure 8.7 shows the limits obtained on the scale Λ for the different models assuming universality between contact interactions for $e^+e^- \to \mu^+\mu^-$ and $e^+e^- \to \tau^+\tau^-$.

Model	η_{LL}	η_{RR}	η_{LR}	η_{RL}
$LL^{\pm}$	± 1	0	0	0
$RR^{\pm}$	0	± 1	0	0
$VV^{\pm}$	± 1	± 1	± 1	± 1
$AA^{\pm}$	± 1	± 1	∓ 1	∓ 1
$LR^{\pm}$	0	0	± 1	0
$RL^{\pm}$	0	0	0	± 1
$V0^{\pm}$	± 1	± 1	0	0
$A0^{\pm}$	0	0	± 1	± 1

Table 8.10: Choices of η_{ij} for different contact interaction models

.

8.5.3 Contact Interactions from Heavy Flavour Averages

Limits on contact interactions between electrons and b and c quarks are obtained. The formalism for describing contact interactions including heavy flavours is identical to that described above for leptons.

All heavy flavour LEP-II combined results from 133 to 207 GeV given in Table 8.7 are used as inputs. For the purpose of fitting contact interaction models to the data, $R_{\rm b}$ and $R_{\rm c}$ are converted to cross sections $\sigma_{\rm b\overline{b}}$ and $\sigma_{\rm c\overline{c}}$ using the averaged $\rm q\overline{q}$ cross section of section 8.2 corresponding to signal Definition 2. In the calculation of errors, the correlations between $R_{\rm b}$, $R_{\rm c}$ and $\sigma_{\rm q\overline{q}}$ are assumed to be negligible.

$e^+e^- \to \mu^+\mu^-$			
Model	ϵ (TeV^{-2})	Λ^-(TeV)	Λ^+(TeV)
LL	$-0.0056^{+0.0042}_{-0.0037}$	8.8	14.4
RR	$-0.0060^{+0.0051}_{-0.0046}$	8.4	13.8
VV	$-0.0014^{+0.0016}_{-0.0012}$	15.5	22.2
AA	$-0.0025^{+0.0018}_{-0.0023}$	12.1	20.1
LR	$0.0014^{+0.0043}_{-0.0074}$	7.4	9.3
RL	$0.0014^{+0.0043}_{-0.0074}$	7.4	9.3
V0	$-0.0036^{+0.0032}_{-0.0013}$	12.2	19.9
A0	$0.0008^{+0.0020}_{-0.0031}$	12.7	13.0

$e^+e^- \to \tau^+\tau^-$			
Model	ϵ (TeV^{-2})	Λ^-(TeV)	Λ^+(TeV)
LL	$-0.0033^{+0.0056}_{-0.0050}$	8.9	11.4
RR	$-0.0036^{+0.0061}_{-0.0056}$	8.4	10.9
VV	$-0.0012^{+0.0017}_{-0.0020}$	14.0	19.1
AA	$-0.0004^{+0.0025}_{-0.0027}$	13.1	14.2
LR	$-0.0053^{+0.0079}_{-0.2210}$	2.1	9.2
RL	$-0.0053^{+0.0079}_{-0.2210}$	2.1	9.2
V0	$-0.0011^{+0.0023}_{-0.0033}$	12.3	15.7
A0	$-0.0028^{+0.0041}_{-0.0043}$	9.3	12.9

$e^+e^- \to \ell^+\ell^-$			
Model	ϵ (TeV^{-2})	Λ^-(TeV)	Λ^+(TeV)
LL	$-0.0042^{+0.0027}_{-0.0028}$	9.8	16.5
RR	$-0.0046^{+0.0037}_{-0.0034}$	9.4	15.8
VV	$-0.0014^{+0.0012}_{-0.0012}$	16.5	26.2
AA	$-0.0018^{+0.0016}_{-0.0019}$	14.0	21.7
LR	$-0.0023^{+0.0051}_{-0.0045}$	8.5	11.2
RL	$-0.0023^{+0.0051}_{-0.0045}$	8.5	11.2
V0	$-0.0020^{+0.0016}_{-0.0019}$	13.5	22.9
A0	$-0.0011^{+0.0025}_{-0.0023}$	13.2	15.6

Table 8.11: Fitted values of ϵ and 95% confidence limits on the scale, Λ, for constructive (+) and destructive interference (−) with the Standard Model, for the contact interaction models discussed in the text. Results are given for $e^+e^- \to \mu^+\mu^-$, $e^+e^- \to \tau^+\tau^-$ and $e^+e^- \to \ell^+\ell^-$, assuming universality in the contact interactions between $e^+e^- \to \mu^+\mu^-$ and $e^+e^- \to \tau^+\tau^-$.

The results are updated with respect to those given in [1,73] due to the updated hadronic cross-sections and heavy flavour results. No evidence for contact interactions between electrons and b and c is found. The fitted values of ϵ and their 68% confidence level uncertainties together with the 95% confidence level lower limit on Λ are shown in Table 8.12. Figure 8.8 shows the limits obtained on the scale, Λ, of models with different helicity combinations involved in the interactions.

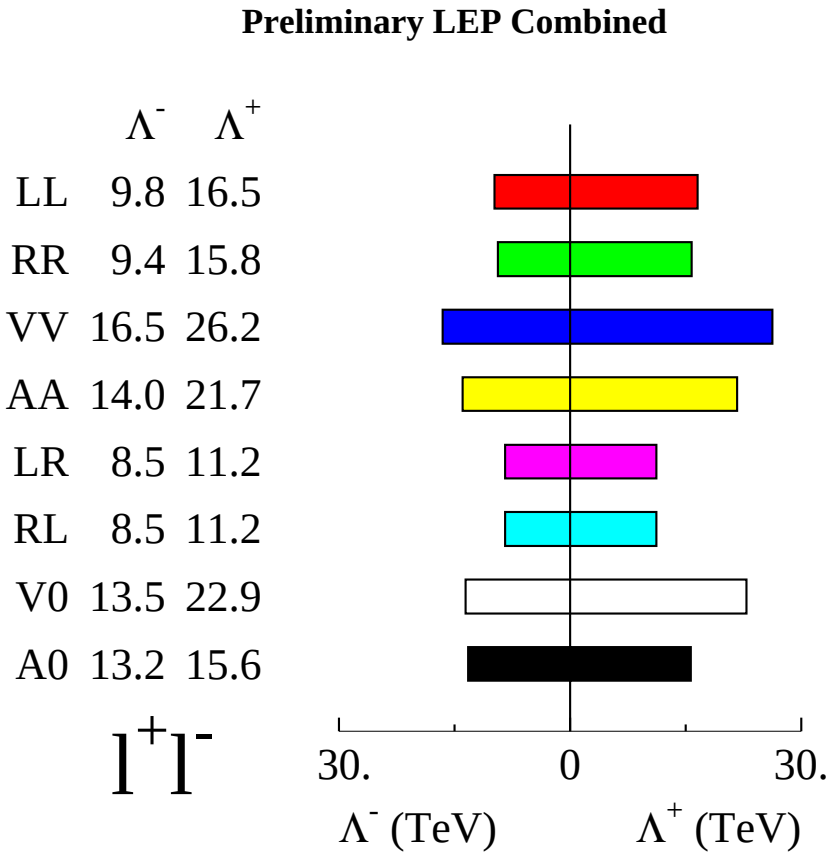

Figure 8.7: The 95% CL exclusion limits on Λ for $e^+e^- \to \ell^+\ell^-$ assuming universality in the contact interactions between $e^+e^- \to \mu^+\mu^-$ and $e^+e^- \to \tau^+\tau^-$.

8.6 Summary

A preliminary combination of the LEP-II $e^+e^- \to f\bar{f}$ cross-sections (for hadron, muon and tau final states) and forward-backward asymmetries (for muon and tau final states) from LEP running at energies from 130 to 207 GeV is made. The results from the four LEP experiments are in good agreement with each other.

The averages for all energies are shown in Table 8.2. Overall the data agree with the Standard Model predictions of ZFITTER. Preliminary differential cross-sections, $\frac{d\sigma}{d\cos\theta}$, for $e^+e^- \to \mu^+\mu^-$ and $e^+e^- \to \tau^+\tau^-$ are combined. Results are shown in Figures 8.3 and 8.4. A preliminary average of results on heavy flavour production at LEP-II is also made for measurements of R_b, R_c, $A_{FB}^{b\bar{b}}$ and $A_{FB}^{c\bar{c}}$, using results from LEP centre-of-mass energies from 130 to 207 GeV. Results are given in Table 8.7 and shown graphically in Figures 8.5 and 8.6. The results are in good agreement with the predictions of the SM.

The preliminary averaged cross-section and forward-backward asymmetry results together with the combined results on heavy flavour production are interpreted in a variety of models. The LEP-II averaged cross-sections and lepton asymmetries are used to obtain lower limits on the mass of a

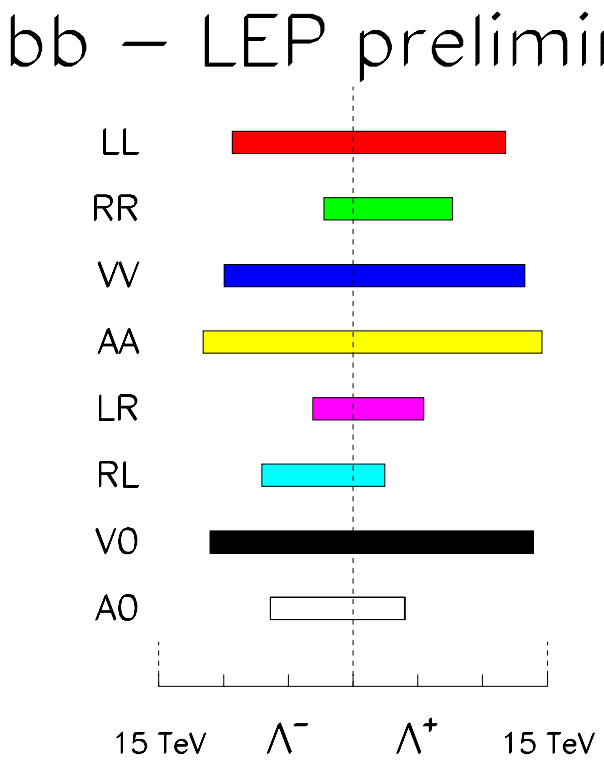

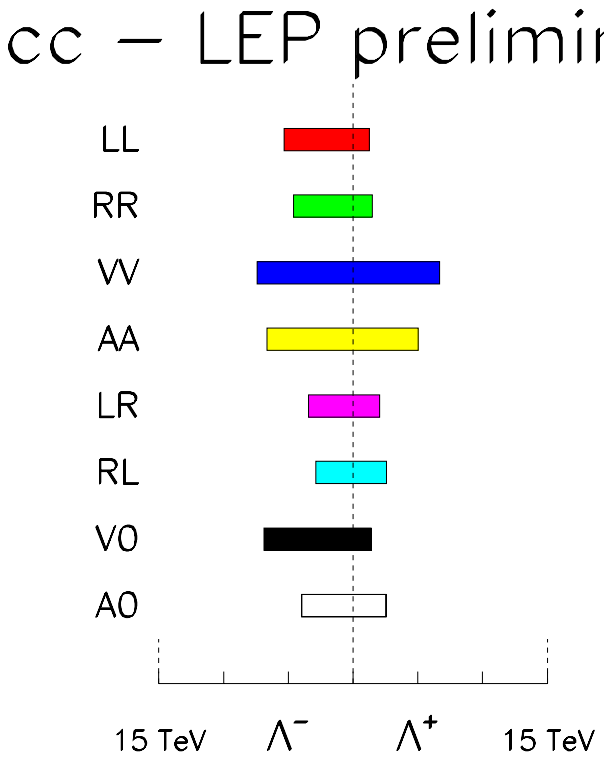

Figure 8.8: The 95% CL exclusion limits on the scale of Contact Interactions in $e^+e^- \to b\bar{b}$ and $e^+e^- \to c\bar{c}$ using Heavy Flavour LEP combined results from 133 to 207 GeV.

$e^+e^- \to b\bar{b}$			
Model	ϵ (TeV^{-2})	Λ^-(TeV)	Λ^+(TeV)
LL	$-0.0030^{+0.0045}_{-0.0047}$	9.3	11.8
RR	$-0.1755^{+0.1634}_{-0.0159}$	2.2	7.7
VV	$-0.0029^{+0.0038}_{-0.0040}$	10.0	13.3
AA	$-0.0018^{+0.0029}_{-0.0031}$	11.6	14.6
LR	$-0.0491^{+0.0555}_{-0.0384}$	3.1	5.5
RL	$0.0065^{+0.1409}_{-0.0149}$	7.0	2.5
V0	$-0.0021^{+0.0032}_{-0.0034}$	11.0	13.9
A0	$0.0305^{+0.0203}_{-0.0348}$	6.4	4.0

$e^+e^- \to c\bar{c}$			
Model	ϵ (TeV^{-2})	Λ^-(TeV)	Λ^+(TeV)
LL	$0.0146^{+0.5911}_{-0.0259}$	5.3	1.3
RR	$0.0492^{+0.3723}_{-0.0568}$	4.6	1.5
VV	$0.0008^{+0.0106}_{-0.0100}$	7.4	6.7
AA	$0.0081^{+0.0171}_{-0.0154}$	6.6	5.0
LR	$0.0913^{+0.1076}_{-0.1251}$	3.5	2.1
RL	$0.0145^{+0.0872}_{-0.0872}$	2.9	2.6
V0	$0.0047^{+0.0170}_{-0.0133}$	6.9	1.4
A0	$0.0524^{+0.0736}_{-0.0780}$	4.0	2.6

Table 8.12: Fitted values of ϵ and 95% confidence limits on the scale, Λ, for constructive (+) and destructive interference (−) with the Standard Model, for the contact interaction models discussed in the text. From combined $b\bar{b}$ and $c\bar{c}$ results with centre of mass energies from 133 to 207 GeV.

possible Z′ boson in different models. Limits range from 436 to 1890 GeV depending on the model. Limits on the scale of contact interactions between leptons and also between electrons and $b\bar{b}$ and $c\bar{c}$ final states are determined. A full set of limits are given in Tables 8.11 and 8.12.

Chapter 9

W and Four-Fermion Production at LEP-II

Updates with respect to summer 2000:
New preliminary results are presented for W-pair, Z-pair and single W production, based on the full data sample collected in the year 2000 between 202 and 209 GeV. Improved procedures are used for the combination of W-pair cross sections and W decay branching fractions. New averages of the Z-pair and single W cross sections are performed, including also preliminary updates below 205 GeV.

9.1 Introduction

This Chapter summarises the combination of published and preliminary results of the four LEP experiments on W-pair, Z-pair and single W cross sections and on W decay branching fractions, prepared for the summer 2001 conferences [1, 93]. Where available, the published final results of the analysis of data collected at centre–of–mass energies up to 209 GeV are used in the combination.

Most relevant, with respect to the results presented at the summer 2000 conferences [1, 94], are new measurements of the W-pair, Z-pair and single-W cross sections at the highest LEP-II centre–of–mass energies between 202 and 209 GeV, using the full data samples collected in the year 2000. This represents, for energies above 202 GeV, an increase in luminosity by more than a factor of two over the results presented at the summer 2000 conferences from the year 2000 data available at that time. Another significant change is an improved procedure for the combination of measured W-pair cross sections between 183 and 207 GeV and for the combination of measured W decay branching fractions, also used to derive the average ratio between the measured W-pair cross sections and the corresponding theoretical predictions from various models. Finally, new combinations of single-W and Z-pair cross sections are presented to take into account the new data available above 200 GeV, also including minor changes in the single-W combination procedure and preliminary updates of Z-pair cross sections between 192 and 202 GeV.

In the year 2000, LEP ran at centre–of–mass energies larger than 200 GeV, up to a maximum of 209 GeV. For the measurements of the W-pair, Z-pair and single-W cross section, the data collected above 202 GeV is divided [95] in two ranges of $\sqrt{s}$, below and above 205.5 GeV, to enhance the sensitivity of the cross-section measurements to possible signals of new physics at the highest e^+e^- centre–of–mass energy. The two data sets have mean centre–of–mass energies of 204.9 and 206.6 GeV, and the respective integrated luminosities used for the analyses considered in this note are approximately 80 and 130 pb^{-1} per experiment.

Results from different experiments are combined in χ^2 minimisations through matrix algebra, based on the Best Linear Unbiased Estimate (BLUE) method described in Reference 82, and taking into account, when relevant, the correlations between the systematic uncertainties, which arise mainly from the use of the same Monte Carlo codes to predict the background and to simulate the hadronisation processes. The detailed breakdown of the systematic errors for the measurements combined in this Chapter is described in Appendix C. Experimental results are compared with recent theoretical predictions, many of which were developed in the framework of the LEP-II Monte Carlo workshop [96].

9.2 W-pair production cross section

All experiments have published final results on the W-pair (CC03 [96]) production cross section for centre–of–mass energies from 161 to 189 GeV [97–109]. The preliminary results contributed by all four collaborations at $\sqrt{s} = 192$–202 GeV are unchanged with respect to the summer 2000 conferences [110–114]. All experiments contribute new preliminary results at $\sqrt{s} = 205$–207 GeV [115–118], based on the analysis of the full data sample collected in the year 2000. New LEP averages of the measurements at the eight centre–of–mass energies between 183 and 207 GeV are computed for the summer 2001 conferences, using an improved combination procedure. In particular, the LEP combined cross sections are now obtained from one global fit to the 32 measurements performed by the four experiments at each of these eight energies, taking into account inter-experiment as well as inter-energy correlations, rather than from eight individual fits at the various energies, neglecting inter-energy correlations, as in the case of the previous combination for the summer 2000 [1, 94] conferences.

In the averaging of results at and above $\sqrt{s} = 189$ GeV, the component of the systematic error from each experiment coming from the uncertainty on the 4-jet QCD background is taken to be fully correlated between experiments. This is slightly different from the procedure adopted for the summer 2000 conferences [1], where some experiments had also included in the correlated error the uncertainties due to the modelling of hadronisation and final state interactions. More importantly, this common error, ranging between 0.04 and 0.12 pb, is now taken to be also fully correlated between energies. The remaining sources of systematic errors, taken as completely uncorrelated between experiments, are split by each experiment into two categories, for which 100% and 0% correlations between different energies are assumed. The detailed inputs used for the combination are given in Appendix C. The measured statistical errors are used for the combination. After building the full 32×32 covariance matrix for the measurements, the χ^2 minimisation fit is performed as described in Reference [119]. More detailed studies on correlated systematic errors are in progress.

The results from each experiment for the W-pair production cross section are shown in Table 9.1, together with the LEP combination at each energy. All measurements are defined to represent CC03 [96] WW cross sections, and assume Standard Model values for the W decay branching fractions. The results for centre–of–mass energies between 183 and 207 GeV, for which new LEP averages are computed, supersede the ones presented in [1]: the effect of the new combination procedure is to change the LEP combined cross sections at these energies by 0.6% at most, generally towards lower values. The combined LEP cross sections at the eight energies are all positively correlated, with correlations ranging from 9% to 24%. For completeness, the measurements at 161 [97, 120] and 172 GeV [98–101, 121] are also listed in the table. All results from the four experiments listed in the table are preliminary, with the exception of those at 161–189 GeV.

Figure 9.1 shows the combined LEP W-pair cross section measured as a function of the centre–of–mass energy. The combined measurements are compared with the theoretical calculations from YFSWW [122] and RACOONWW [123] between 155 and 215 GeV for $m_{\mathrm{W}} = 80.35$ GeV. The two

$\sqrt{s}$	WW cross section (pb)					χ^2/d.o.f.
(GeV)	ALEPH	DELPHI	L3	OPAL	LEP	
161.3	$4.23 \pm 0.75^*$	$3.67 \,^{+\,0.99}_{-\,0.87}{}^*$	$2.89 \,^{+\,0.82}_{-\,0.71}{}^*$	$3.62 \,^{+\,0.94}_{-\,0.84}{}^*$	3.69 ± 0.45	} 1.3 / 3
172.1	$11.7 \pm 1.3^*$	$11.6 \pm 1.4^*$	$12.3 \pm 1.4^*$	$12.3 \pm 1.3^*$	12.0 ± 0.7	} 0.22/ 3
182.7	$15.57 \pm 0.68^*$	$15.86 \pm 0.74^*$	$16.53 \pm 0.72^*$	$15.43 \pm 0.66^*$	15.79 ± 0.36	} 27.42/24
188.6	$15.71 \pm 0.38^*$	$15.83 \pm 0.43^*$	$16.24 \pm 0.43^*$	$16.30 \pm 0.38^*$	16.00 ± 0.21	
191.6	17.23 ± 0.91	16.90 ± 1.02	16.39 ± 0.93	16.60 ± 0.98	16.72 ± 0.48	
195.5	17.00 ± 0.57	17.86 ± 0.63	16.67 ± 0.60	18.59 ± 0.74	17.43 ± 0.32	
199.5	16.98 ± 0.56	17.35 ± 0.60	16.94 ± 0.62	16.32 ± 0.66	16.84 ± 0.31	
201.6	16.16 ± 0.76	17.67 ± 0.84	16.95 ± 0.88	18.48 ± 0.91	17.23 ± 0.42	
204.9	16.57 ± 0.55	17.44 ± 0.64	17.35 ± 0.64	15.97 ± 0.64	16.71 ± 0.31	
206.6	17.32 ± 0.45	16.50 ± 0.48	17.96 ± 0.51	17.77 ± 0.57	17.33 ± 0.25	

Table 9.1: W-pair production cross section from the four LEP experiments and combined values at all recorded centre–of–mass energies. All results are preliminary and unpublished, with the exception of those indicated by *. The measurements between 183 and 207 GeV are combined in one global fit, taking into account inter-experiment as well as inter-energy correlations of systematic errors. The results for the combined LEP W-pair production cross section at 161 and 172 GeV are taken from [120, 121] respectively.

codes have been extensively compared and agree at a level better than 0.5% at the LEP-II energies [96]. The calculations above 170 GeV, based for the two programs on the so-called leading pole (LPA) or double pole approximations (DPA) [124], have theoretical uncertainties decreasing from 0.7% at 170 GeV to about 0.4% at centre–of–mass energies larger than 200 GeV, while in the threshold region a larger theoretical uncertainty of 2% is assigned [125]. This theoretical uncertainty is represented by the width of the shaded band in Figure 9.1. An error of 50 MeV on the W mass would translate into additional errors of 0.1% (3.0%) on the cross-section predictions at 200 GeV (161 GeV, respectively). All results, up to the highest centre–of–mass energies, are in agreement with the two theoretical predictions considered.

9.2.1 Ratio of measured and predicted W-pair cross sections

The agreement between the measured W-pair cross section, $\sigma_{\rm WW}^{\rm meas}$, and its expectation according to a given theoretical model, $\sigma_{\rm WW}^{\rm theo}$, can be expressed quantitatively in terms of their ratio

$$\mathcal{R}_{\rm WW} = \frac{\sigma_{\rm WW}^{\rm meas}}{\sigma_{\rm WW}^{\rm theo}},$$

averaged over the measurements performed by the four experiments at different energies in the LEP-II region. The above procedure is used to compare the measurements at the eight energies between 183 and 207 GeV to the predictions of GENTLE [126], KORALW [127], YFSWW [122] and RACOONWW [123]. The measurements at 161 and 172 GeV are not used in the combination because they were performed using data samples of low statistics and because of the high sensitivity of the cross section to the value of the W mass at these energies.

The combination of the ratio $\mathcal{R}_{\rm WW}$ is performed using as input from the four experiments the 32 cross sections measured at each of the eight energies. For each model considered, these are converted

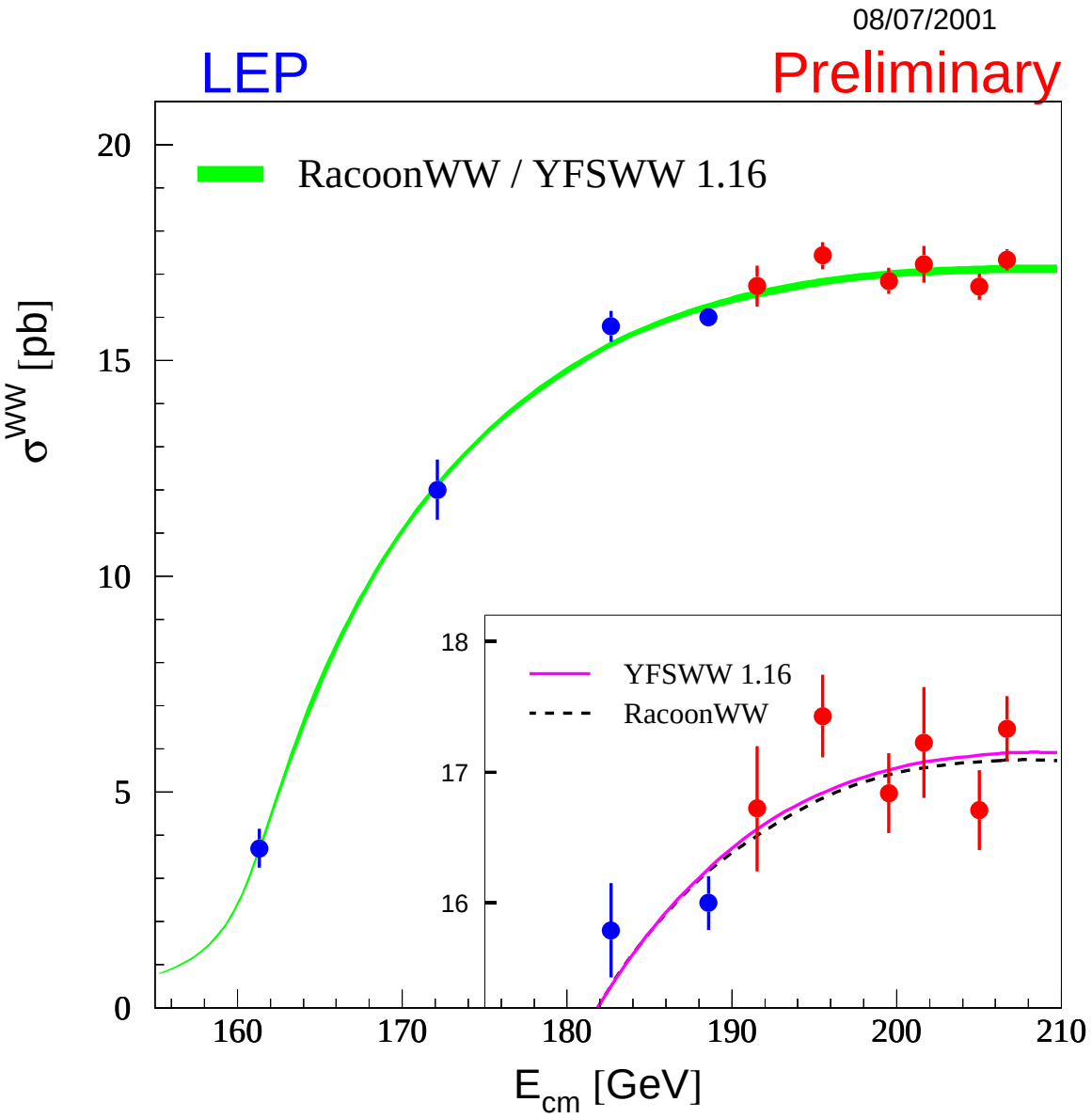

Figure 9.1: Measurements of the W-pair production cross section, compared to the predictions of RACOONWW [123] and YFSWW [122]. The shaded area represents the uncertainty on the theoretical predictions, estimated to be $\pm 2\%$ for $\sqrt{s} < 170$ GeV and ranging from 0.7 to 0.4% above 170 GeV.

into 32 ratios by dividing them by the corresponding theoretical predictions, listed in Appendix C. The full 32×32 covariance matrix for the ratios is built taking into account the same sources of systematic errors used for the combination of the W-pair cross sections at these energies. The small statistical errors on the theoretical predictions at the various energies, taken as fully correlated for the four experiments and uncorrelated between different energies, are also translated into errors on the individual measurements of $\mathcal{R}_{\mathrm{WW}}$. The theoretical errors on the predictions, due to the physical and technical precision of the generators used, are not propagated to the individual ratios and are used instead when comparing to the combined values obtained for $\mathcal{R}_{\mathrm{WW}}$. For each of the four models considered, two fits are performed: in the first, eight values of $\mathcal{R}_{\mathrm{WW}}$ at the different energies are

extracted, averaged over the four experiments; in the second, only one value of $\mathcal{R}_{\mathrm{WW}}$ is determined, representing the global agreement of measured and predicted cross sections over the whole energy range.

The results of the two fits to $\mathcal{R}_{\mathrm{WW}}$ for each of the four models considered are given in Table 9.2. As already qualitatively noted from Figure 9.1, the LEP measurements of the W-pair cross section above threshold are in very good agreement to the predictions of YFSWW and RACOONWW. In contrast, the predictions from GENTLE and KORALW are more than 2% too high with respect to the measurements. The main differences between these two sets of predictions come from non-leading $\mathcal{O}(\alpha)$ electroweak radiative corrections to the W-pair production process, which are included (in the LPA/DPA approximation [124]) in both YFSWW and RACOONWW, but not in GENTLE and KORALW. Especially interesting is the comparison between KORALW and YFSWW, as the numerical results provided by the authors for KORALW are actually those of a downgraded version of YFSWW, such that the only differences between the two calculations are the screening of Coulomb interactions according to the prescription of Reference 128 and the inclusion of non-leading $\mathcal{O}(\alpha)$ electroweak radiative corrections to W-pair production (mainly radiation off W bosons and pure weak corrections). Of these two effects, only the latter is found to be relevant to the measurement of $\mathcal{R}_{\mathrm{WW}}$, while the former has a negligible impact on the total W-pair cross section [129].

$\sqrt{s}$	Ratio of measured and expected WW cross sections			
(GeV)	$\mathcal{R}_{\mathrm{WW}}^{\mathrm{GENTLE}}$	$\mathcal{R}_{\mathrm{WW}}^{\mathrm{KORALW}}$	$\mathcal{R}_{\mathrm{WW}}^{\mathrm{YFSWW}}$	$\mathcal{R}_{\mathrm{WW}}^{\mathrm{RACOONWW}}$
182.7	1.005 ± 0.022	1.011 ± 0.023	1.028 ± 0.023	1.028 ± 0.023
188.6	0.961 ± 0.013	0.967 ± 0.013	0.984 ± 0.013	0.985 ± 0.013
191.6	0.986 ± 0.028	0.991 ± 0.028	1.009 ± 0.029	1.012 ± 0.029
195.5	1.010 ± 0.018	1.015 ± 0.018	1.035 ± 0.019	1.037 ± 0.019
199.5	0.964 ± 0.018	0.970 ± 0.018	0.990 ± 0.018	0.992 ± 0.018
201.6	0.983 ± 0.024	0.989 ± 0.024	1.009 ± 0.025	1.012 ± 0.025
204.9	0.949 ± 0.018	0.955 ± 0.018	0.976 ± 0.018	0.978 ± 0.018
206.6	0.984 ± 0.014	0.989 ± 0.014	1.011 ± 0.015	1.014 ± 0.015
χ^2/d.o.f	27.42/24	27.42/24	27.42/24	27.42/24
Average	0.973 ± 0.009	0.979 ± 0.009	0.998 ± 0.009	1.000 ± 0.009
χ^2/d.o.f	39.16/31	39.20/31	39.04/31	39.14/31

Table 9.2: Ratios of LEP combined W-pair cross-section measurements to the expectations according to GENTLE [126], KORALW [127], YFSWW [122] and RACOONWW [123]. For each of the four models, two fits are performed, one to the LEP combined values of $\mathcal{R}_{\mathrm{WW}}$ at the eight energies between 183 and 207 GeV, and another to the LEP combined average of $\mathcal{R}_{\mathrm{WW}}$ over all energies. The results of the fits are given in the table together with the resulting χ^2. Both fits take into account inter-experiment as well as inter-energy correlations of systematic errors.

The results of the fits for YFSWW and RACOONWWare also shown in Figure 9.2, where relative errors of 0.5% on the cross-section predictions are assumed. For simplicity, the energy dependence of the relative error on the W-pair cross-section predicted by each model is neglected in Figure 9.2.

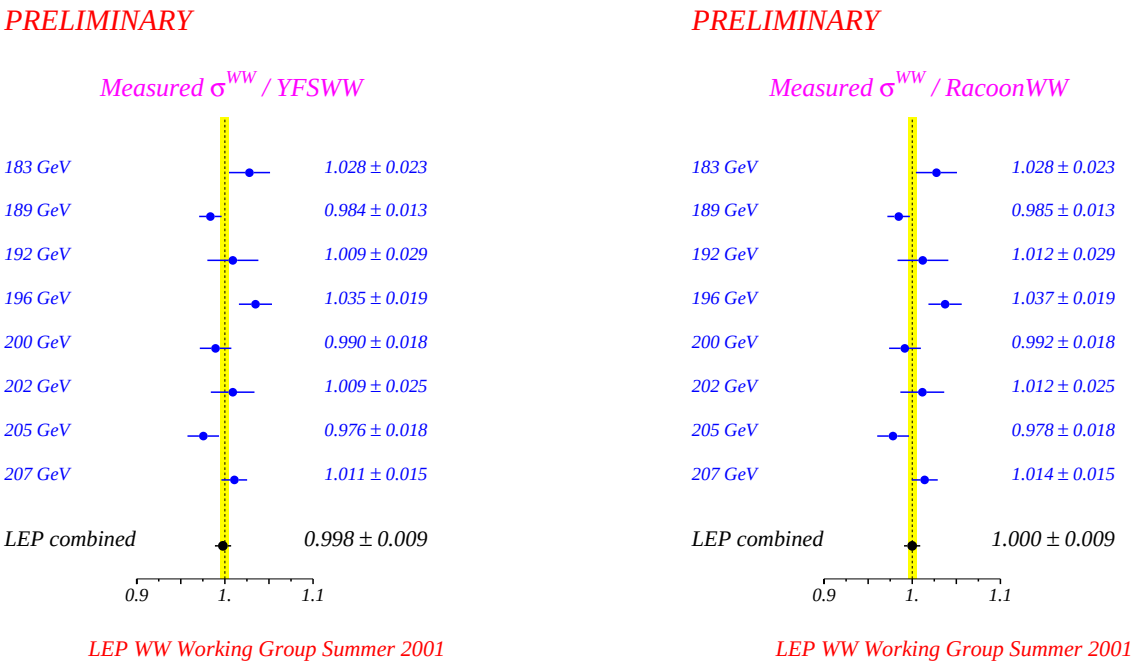

Figure 9.2: Ratios of LEP combined W-pair cross-section measurements to the expectations according to YFSWW [122] and RACOONWW [123] The yellow bands represent constant relative errors of 0.5% on the two cross-section predictions.

9.3 W decay branching fractions

From the cross sections for the individual WW→ 4f decay channels measured by the four experiments at all energies larger than 161 GeV, the W decay branching fractions $\mathcal{B}(\mathrm{W} \to \mathrm{f}\bar{\mathrm{f}}')$ are determined, with and without the assumption of lepton universality. All four experiments update their results since the summer 2000 conferences to include the full data samples collected in the year 2000 at centre–of–mass energies of 205 and 207 GeV [115–118]. The results from each experiment are given in Table 9.3 and Figure 9.3, together with the result of the LEP combination.

	Lepton non–universality			Lepton universality
Experiment	$\mathrm{B}(\mathrm{W} \to \mathrm{e}\overline{\nu}_\mathrm{e})$ [%]	$\mathrm{B}(\mathrm{W} \to \mu\overline{\nu}_\mu)$ [%]	$\mathrm{B}(\mathrm{W} \to \tau\overline{\nu}_\tau)$ [%]	$\mathrm{B}(\mathrm{W} \to \mathrm{hadrons})$ [%]
ALEPH	10.95 ± 0.31	11.11 ± 0.29	10.57 ± 0.38	67.33 ± 0.47
DELPHI	10.36 ± 0.34	10.62 ± 0.28	10.99 ± 0.47	68.10 ± 0.52
L3	10.40 ± 0.30	9.72 ± 0.31	11.78 ± 0.43	68.34 ± 0.52
OPAL	10.40 ± 0.35	10.61 ± 0.35	11.18 ± 0.48	67.91 ± 0.61
LEP	10.54 ± 0.17	10.54 ± 0.16	11.09 ± 0.22	67.92 ± 0.27
χ^2/d.o.f.	14.9/9			18.8/11

Table 9.3: Summary of leptonic and hadronic W branching fractions derived from preliminary W-pair production cross-sections measurements up to 207 GeV centre–of–mass energy. A common systematic error of (0.03–0.06)% on the leptonic branching fractions is taken into account in the combination.

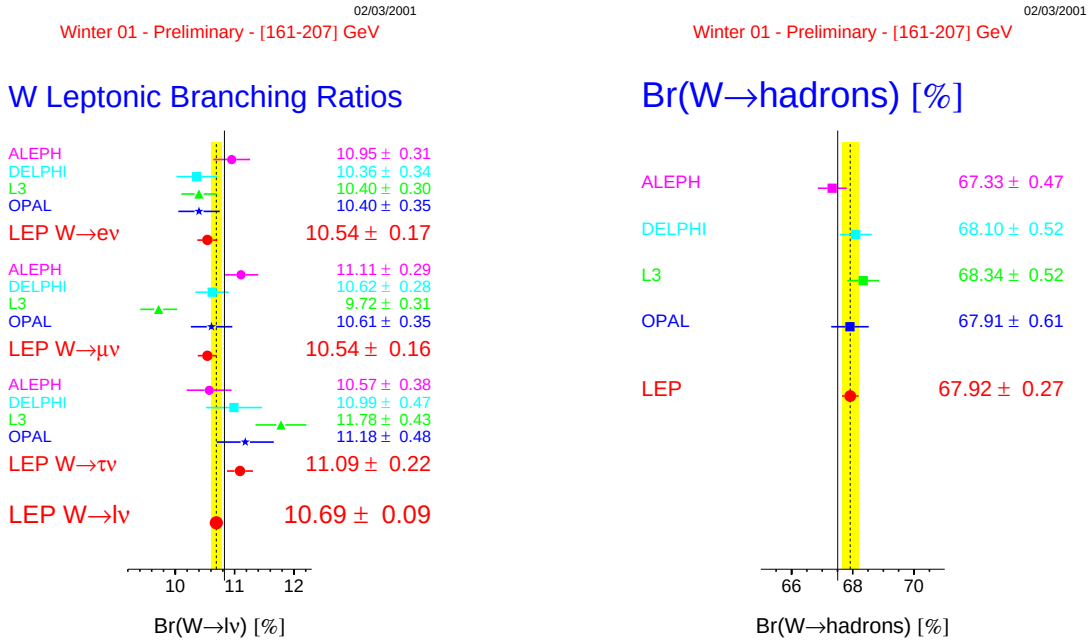

Figure 9.3: Summary of leptonic and hadronic W branching fractions derived from preliminary W-pair production cross-sections measurements up to 207 GeV centre–of–mass energy, unchanged from winter 2001. The thin vertical line denotes the Standard Model expectation.

The two combinations performed, with and without the assumption of lepton universality, both use as inputs from each of the four experiments the three leptonic branching fractions, with their systematic and observed statistical errors and their three by three correlation matrices. In the fit with lepton universality, the branching fraction to hadrons is determined from that to leptons by constraining the sum to unity. In building the full 12×12 covariance matrix, it is assumed that the 4-jet QCD background components of the systematic error are fully correlated between different experiments both for the same and for different leptonic channels, as they arise mainly from the uncertainty on the WW cross section in the channel where both W bosons decay to hadrons. The combination procedure is consistent with that used for the combination of the total W-pair cross sections and outlined in the previous section, as the same sources of inter-experiment correlations are considered, while inter-energy correlations of systematic errors are taken into account internally by each experiment when deriving their average branching ratios. The detailed inputs used for the combination are given in Appendix C.

The results of the fit which does not make use of the lepton universality assumption show a negative correlation of 21.4% (18.9%) between the $\mathrm{W}\to\tau\overline{\nu}_\tau$ and $\mathrm{W}\to\mathrm{e}\overline{\nu}_\mathrm{e}$ ($\mathrm{W}\to\mu\overline{\nu}_\mu$) branching fractions, while between the electron and muon decay channels there is a positive correlation of 6.6%. The two-by-two comparison of these branching fractions constitutes a test of lepton universality in the decay of on–shell W bosons at the level of 2.9%:

$$\begin{aligned}
\mathrm{B}(\mathrm{W}\to\mu\overline{\nu}_\mu)\,/\,\mathrm{B}(\mathrm{W}\to\mathrm{e}\overline{\nu}_\mathrm{e}) &= 1.000\pm0.021\,,\\
\mathrm{B}(\mathrm{W}\to\tau\overline{\nu}_\tau)\,/\,\mathrm{B}(\mathrm{W}\to\mathrm{e}\overline{\nu}_\mathrm{e}) &= 1.052\pm0.029\,,\\
\mathrm{B}(\mathrm{W}\to\tau\overline{\nu}_\tau)\,/\,\mathrm{B}(\mathrm{W}\to\mu\overline{\nu}_\mu) &= 1.052\pm0.028\,.
\end{aligned}$$

The branching fractions are all consistent with each other within the errors.

Assuming lepton universality, the measured hadronic branching fraction is $[67.92\pm0.17(\mathrm{stat.})\pm0.21(\mathrm{syst.})]\%$ and the leptonic one is $[10.69\pm0.06(\mathrm{stat.})\pm0.07(\mathrm{syst.})]\%$. These results are consistent

with their Standard Model expectations, of 67.51% and 10.83% respectively [130]. The systematic error receives equal contributions from the correlated and uncorrelated sources. The high χ^2 of the fit, 18.8 for 11 degrees of freedom, is mainly caused by the spread of the L3 results for W decays to muons and taus around the common average.

Within the Standard Model, the branching fractions of the W boson depend on the six matrix elements $|V_{qq'}|$ of the Cabibbo–Kobayashi–Maskawa (CKM) quark mixing matrix not involving the top quark. In terms of these matrix elements, the leptonic branching fraction of the W boson $\mathcal{B}(W \to \ell\overline{\nu}_\ell)$ is given by

$$\frac{1}{\mathcal{B}(W \to \ell\overline{\nu}_\ell)} \quad = \quad 3\left\{1 + \left[1 + \frac{\alpha_s(M_W^2)}{\pi}\right] \sum_{\substack{i\,=\,(u,\,c),\\ j\,=\,(d,\,s,\,b)}} |V_{ij}|^2\right\},$$

where $\alpha_s(M_W^2)$ is the strong coupling constant. Taking $\alpha_s(M_W^2) = 0.121 \pm 0.002$, the measured leptonic branching fraction of the W yields

$$\sum_{\substack{i\,=\,(u,\,c),\\ j\,=\,(d,\,s,\,b)}} |V_{ij}|^2 \quad = \quad 2.039 \,\pm\, 0.025\,(B_{W \to \ell\overline{\nu}_\ell}) \,\pm\, 0.001\,(\alpha_s),$$

where the first error is due to the uncertainty on the branching fraction measurement and the second to the uncertainty on α_s. Using the experimental knowledge [131] of the sum $|V_{ud}|^2 + |V_{us}|^2 + |V_{ub}|^2 + |V_{cd}|^2 + |V_{cb}|^2 = 1.0477 \pm 0.0074$, the above result can be interpreted as a measurement of $|V_{cs}|$ which is the least well determined of these matrix elements:

$$|V_{cs}| \quad = \quad 0.996 \,\pm\, 0.013.$$

The error includes a ± 0.0006 contribution from the uncertainty on α_s and a ± 0.004 contribution from the uncertainties on the other CKM matrix elements, the largest of which is that on $|V_{cd}|$. These contributions are negligible in the error on this determination of $|V_{cs}|$, which is dominated by the ± 0.013 experimental error from the measurement of the W branching fractions.

9.4 Z-pair production cross section

All experiments have published final results [132–137] on the Z-pair production cross section at $\sqrt{s} = 183$ and 189 GeV, already presented in [94]. Since the summer 2000 conferences, L3 [138] has published its updated final results between 192 and 202 GeV, OPAL [139] has provided preliminary updates of its previous measurements at those energies [140], whereas the corresponding preliminary results from ALEPH [141,142] and DELPHI [143,144] are unchanged. All experiments also contribute preliminary results at 205 and 207 GeV [139,142,145,146], based on the analysis of the full data sample collected in the year 2000.

The results of the individual experiments and the LEP averages are summarised for the different centre–of–mass energies in Table 9.4. The combination of final results at $\sqrt{s} = 183$ and 189 GeV is the same that was given for the summer 2000 conferences, while the results above 189 GeV supersede those previously presented [1], and are all preliminary with the exception of the L3 results between 192 and 202 GeV.

All numerical results presented in this Section are defined to represent NC02 [96] ZZ cross sections. The combination of results is performed using the symmetrized expected statistical error of each

$\sqrt{s}$	ZZ cross section (pb)					χ^2/d.o.f.
(GeV)	ALEPH	DELPHI	L3	OPAL	LEP	
182.7	$0.11\ ^{+\ 0.16\ *}_{-\ 0.12}$	$0.38 \pm 0.18^*$	$0.31\ ^{+\ 0.17\ *}_{-\ 0.15}$	$0.12\ ^{+\ 0.20\ *}_{-\ 0.18}$	0.23 ± 0.08	2.28/3
188.6	$0.67\ ^{+\ 0.14\ *}_{-\ 0.13}$	$0.60 \pm 0.15^*$	$0.73\ ^{+\ 0.15\ *}_{-\ 0.14}$	$0.80\ ^{+\ 0.15\ *}_{-\ 0.14}$	0.70 ± 0.08	0.97/3
191.6	$0.53\ ^{+\ 0.34}_{-\ 0.27}$	0.55 ± 0.34	$0.29 \pm 0.22^*$	$1.13\ ^{+\ 0.47}_{-\ 0.41}$	0.60 ± 0.18	2.88/3
195.5	$0.69\ ^{+\ 0.23}_{-\ 0.20}$	1.17 ± 0.29	$1.18 \pm 0.26^*$	$1.19\ ^{+\ 0.28}_{-\ 0.26}$	1.04 ± 0.13	3.23/3
199.5	$0.70\ ^{+\ 0.22}_{-\ 0.20}$	1.08 ± 0.26	$1.25 \pm 0.27^*$	$1.09\ ^{+\ 0.26}_{-\ 0.24}$	1.01 ± 0.13	2.80/3
201.6	$0.70\ ^{+\ 0.33}_{-\ 0.28}$	0.87 ± 0.33	$0.95 \pm 0.39^*$	$0.94\ ^{+\ 0.38}_{-\ 0.33}$	0.86 ± 0.18	0.32/3
204.9	$1.21\ ^{+\ 0.26}_{-\ 0.23}$	1.05 ± 0.26	0.84 ± 0.23	$1.07\ ^{+\ 0.28}_{-\ 0.26}$	1.03 ± 0.13	1.11/3
206.6	$1.01\ ^{+\ 0.19}_{-\ 0.17}$	0.98 ± 0.22	1.20 ± 0.21	$1.07\ ^{+\ 0.22}_{-\ 0.21}$	1.06 ± 0.11	0.76/3

Table 9.4: Z-pair production cross section from the four LEP experiments and combined values for the eight energies between 183 and 207 GeV. All results are preliminary with the exception of those indicated by *. A common systematic error of (0.01–0.07) pb is taken into account in the averaging procedure.

analysis, to avoid biases due to the limited number of events selected. As in the combination performed for the summer 2000 conferences [94], the component of the systematic errors that is considered as correlated between experiments includes the uncertainty on the backgrounds from $q\bar{q}$, WW, Zee and Weν processes and the uncertainty on the b quark modelling. Summing these contributions together, the common error ranges between 0.01 and 0.07 pb for the various experiments, as described in Appendix C.

The measurements are shown in Figure 9.4 as a function of the LEP centre–of–mass energy, where they are compared to the YFSZZ [147] and ZZTO [148] predictions. Both these calculations have an estimated uncertainty of $\pm 2\%$ [96]. The data do not show any significant deviation from the theoretical expectations.

9.5 Single-W production cross section

Since the summer 2000 [94] conferences, only ALEPH [149] and DELPHI [150] present new measurements of the single-W cross section, from the analysis of the full data sample collected in the year 2000 at 205 and 207 GeV, while L3 has published unchanged its results at 189 GeV [151], already presented as preliminary in the summer 2000. None of the other results previously presented by the four experiments are updated: these include the results published by ALEPH [152] and L3 [153,154] at 183 GeV, and the preliminary measurements by ALEPH at 189–202 [155], DELPHI at 189–202 [156,157], L3 at 192–202 [158] and OPAL at 189 GeV [159].

A new combination of LEP results for the summer 2001 conferences is performed not only at 205–207 GeVto include the new results by ALEPH and DELPHI, but also at all energies between 183 and 202 GeV. This is done to include the DELPHI results for the total single-W cross section at these energies [157] defined according to the common LEP prescription of Reference 160, which accounts for all decays of the W boson, including those to taus. In contrast, for the previous combination performed for the winter 2000 conferences [160], previous DELPHI results [156] had been used, accounting only for decays of the W boson to hadrons, electrons or muons. In the new average for the summer 2001 conferences, results are combined assuming uncorrelated systematic errors between experiments and

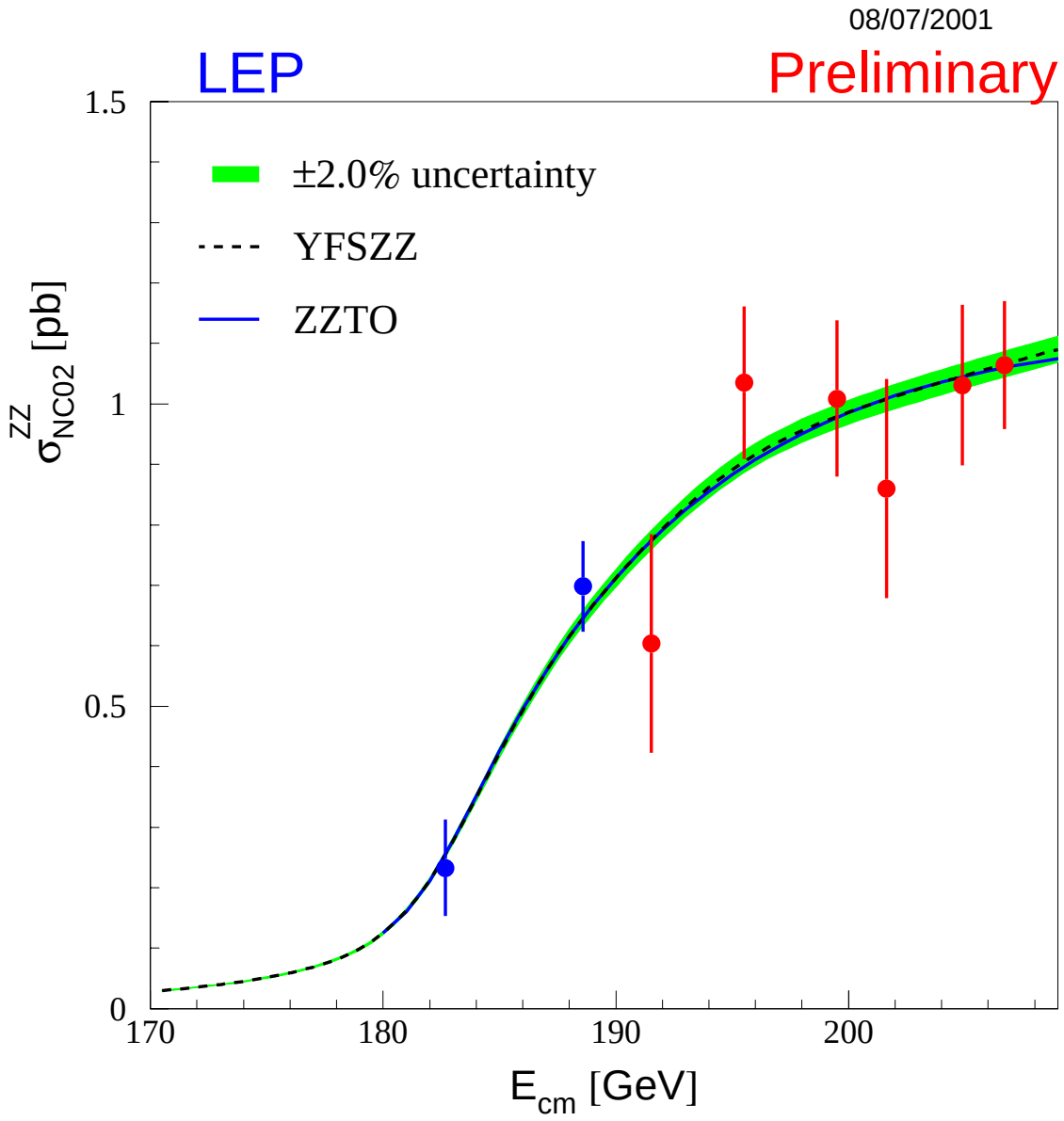

Figure 9.4: Measurements of the Z-pair production cross section, compared to the predictions of YFSZZ [147] and ZZTO [148]. The shaded area represents the ±2% uncertainty on the predictions.

consistently using expected statistical errors for all measurements, given the limited statistical precision of the single-W cross-section measurements. This also differs slightly from the procedure previously used for the winter 2000 conferences, where expected statistical errors had only been used for a few measurements on very limited data samples, reverting to measured statistical errors elsewhere.

The measurements of the hadronic and total single-W cross sections by the four LEP experiments between 183 and 207 GeVare listed in Tables 9.5 and 9.6, together with the corresponding LEP combined values. All numerical results presented in this Section represent single-W cross sections according to the common LEP definition given in [160]. Single-W production is considered as the complete t-channel subset of Feynman diagrams contributing to $e\nu_e f\bar{f}'$ final states, with additional cuts on kinematic variables to exclude the regions of phase space dominated by multiperipheral diagrams,

where the cross-section calculation is affected by large uncertainties. The kinematic cuts used in the signal definitions are: $m_{q\overline{q}} > 45$ GeV for the $e\nu_e q\overline{q}$ final states, $E_\ell > 20$ GeV for the $e\nu_e \ell\nu_e$ final states with $\ell = \mu$ or τ, and finally $|\cos\theta_{e^-}| > 0.95$, $|\cos\theta_{e^+}| < 0.95$ and $E_{e^+} > 20$ GeV (or the charge conjugate cuts) for the $e\nu_e e\nu_e$ final states. The measurements performed on the small amount of data below 183 GeV, by L3 at 130–172 GeV [154,161] and ALEPH at 161–172 GeV [152], are not converted into the single-W common LEP definition and are absent from the tables and the following plot.

The LEP measurements of the single-W cross section are shown, as a function of the LEP centre–of–mass energy, in Figure 9.5 for the hadronic decays and for all decays of the W boson. In the two figures, the measurements are compared with the expected values from WTO [162], WPHACT [163] and `grc4f` [164]. As discussed more in detail in [1] and [96], the theoretical predictions are scaled upward to correct for the implementation of QED radiative corrections at the wrong momentum transfer scale s. The full correction factor of 4%, derived [96] by the comparison to the theoretical predictions from SWAP [165], is conservatively taken as a systematic error. This uncertainty dominates the $\pm 5\%$ theoretical error currently assigned to these predictions [1,96], represented by the shaded area in Figure 9.5. All results, up to the highest centre–of–mass energies, are in agreement with the theoretical predictions.

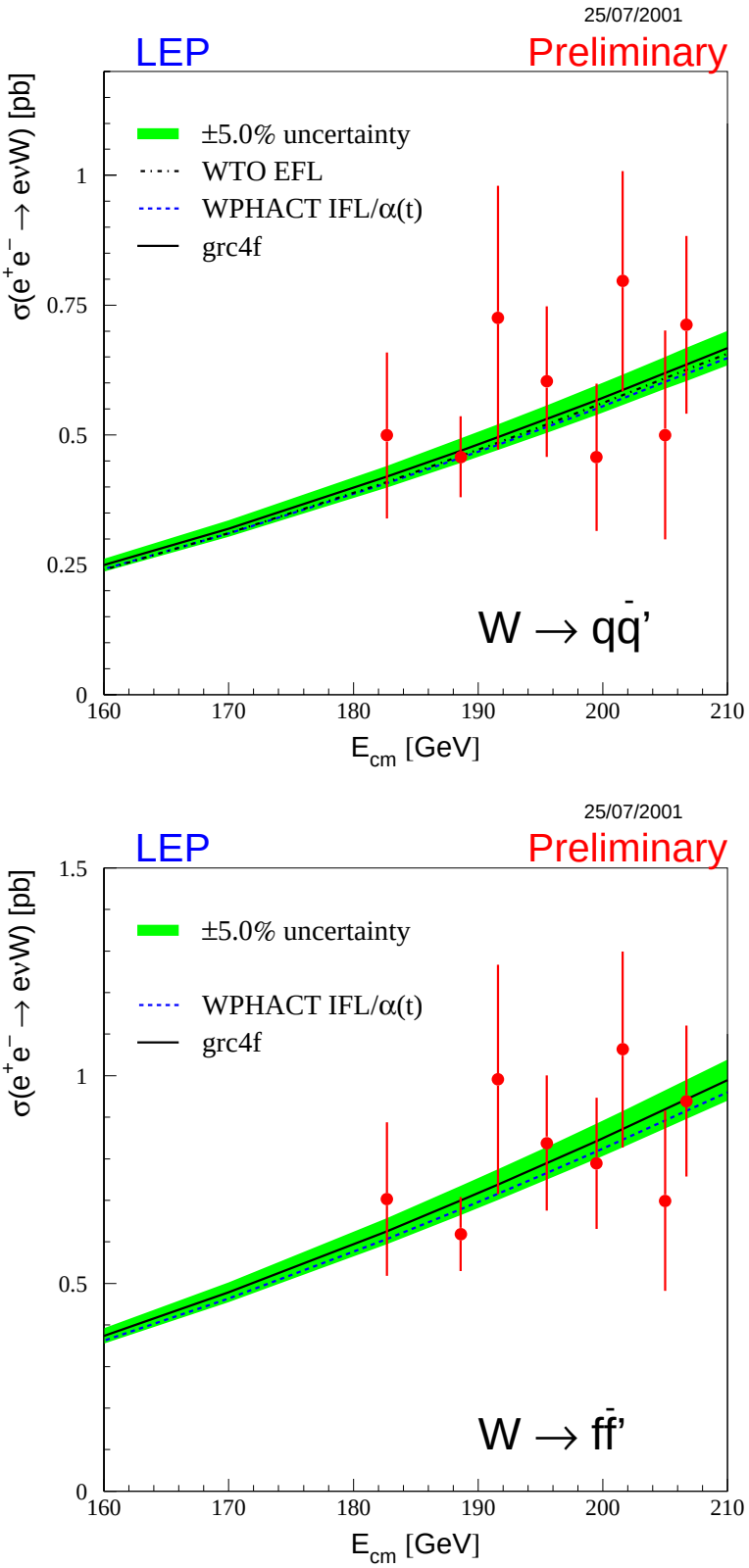

Figure 9.5: Measurements of the single-W production cross section. Top: hadronic decay channel of the W boson; bottom: total production cross section. Also shown are the predictions of WTO [162] (hadronic decay channel only), WPHACT [163] and `grc4f` [164]. The shaded area represents the ±5% uncertainty on the predictions.

$\sqrt{s}$	Single-W hadronic cross section (pb)					χ^2/d.o.f.
(GeV)	ALEPH	DELPHI	L3	OPAL	LEP	
182.7	$0.40 \pm 0.24^*$	—	$0.58 \, ^{+\,0.23\,*}_{-\,0.20}$	—	0.50 ± 0.16	0.31/1
188.6	0.31 ± 0.14	$0.44 \, ^{+\,0.28}_{-\,0.25}$	$0.52 \, ^{+\,0.14\,*}_{-\,0.13}$	$0.53 \, ^{+\,0.14}_{-\,0.13}$	0.46 ± 0.08	1.47/3
191.6	0.94 ± 0.44	$0.01 \, ^{+\,0.19}_{-\,0.07}$	$0.85 \, ^{+\,0.45}_{-\,0.37}$	—	0.73 ± 0.25	1.94/2
195.5	0.45 ± 0.23	$0.78 \, ^{+\,0.38}_{-\,0.34}$	$0.66 \, ^{+\,0.25}_{-\,0.23}$	—	0.60 ± 0.15	0.77/2
199.5	0.82 ± 0.26	$0.16 \, ^{+\,0.29}_{-\,0.17}$	$0.34 \, ^{+\,0.23}_{-\,0.20}$	—	0.46 ± 0.14	3.60/2
201.6	0.68 ± 0.35	$0.55 \, ^{+\,0.47}_{-\,0.40}$	$1.09 \, ^{+\,0.42}_{-\,0.37}$	—	0.80 ± 0.21	1.13/2
204.9	0.50 ± 0.25	$0.50 \, ^{+\,0.35}_{-\,0.31}$	—	—	0.50 ± 0.20	0.00/1
206.6	0.95 ± 0.24	$0.37 \, ^{+\,0.24}_{-\,0.21}$	—	—	0.71 ± 0.17	2.77/1

Table 9.5: Single-W production cross section from the four LEP experiments and combined values for the eight energies between 183 and 207 GeV, in the hadronic decay channel of the W boson. All results are preliminary with the exception of those indicated by *.

$\sqrt{s}$	Single-W total cross section (pb)					χ^2/d.o.f.
(GeV)	ALEPH	DELPHI	L3	OPAL	LEP	
182.7	$0.61 \pm 0.27^*$	—	$0.80 \, ^{+\,0.28\,*}_{-\,0.25}$	—	0.70 ± 0.19	0.26/1
188.6	0.45 ± 0.15	$0.75 \, ^{+\,0.30}_{-\,0.26}$	$0.69 \, ^{+\,0.16\,*}_{-\,0.15}$	$0.67 \, ^{+\,0.17}_{-\,0.15}$	0.62 ± 0.09	1.60/3
191.6	1.31 ± 0.48	$0.17 \, ^{+\,0.34}_{-\,0.18}$	$1.06 \, ^{+\,0.49}_{-\,0.42}$	—	0.99 ± 0.28	2.38/2
195.5	0.65 ± 0.25	$0.94 \, ^{+\,0.41}_{-\,0.36}$	$0.98 \, ^{+\,0.28}_{-\,0.27}$	—	0.84 ± 0.16	0.92/2
199.5	0.99 ± 0.27	$0.51 \, ^{+\,0.33}_{-\,0.32}$	$0.79 \, ^{+\,0.27}_{-\,0.24}$	—	0.79 ± 0.16	1.40/2
201.6	0.75 ± 0.36	$1.15 \, ^{+\,0.55}_{-\,0.46}$	$1.38 \, ^{+\,0.47}_{-\,0.42}$	—	1.06 ± 0.24	1.38/2
204.9	0.78 ± 0.27	$0.56 \, ^{+\,0.36}_{-\,0.32}$	—	—	0.70 ± 0.22	0.24/1
206.6	1.19 ± 0.25	$0.58 \, ^{+\,0.26}_{-\,0.23}$	—	—	0.94 ± 0.18	2.71/1

Table 9.6: Single-W total production cross section from the four LEP experiments and combined values for the eight energies between 183 and 207 GeV. All results are preliminary with the exception of those indicated by *.

Chapter 10

Electroweak Gauge Boson Self Couplings

Updates with respect to summer 2000:
Additional preliminary results based on the data collected in the year 2000 are included. No results on charged TGCs are included as the effects of newly calculated radiative corrections on the couplings results derived from W-pair production are still under investigation.

10.1 Introduction

The measurement of gauge boson couplings and the search for possible anomalous contributions due to the effects of new physics beyond the Standard Model are among the principal physics aims at LEP-II [166]. Combined preliminary measurements of the neutral triple gauge boson couplings and quartic gauge couplings are presented here. The results for the neutral couplings already include the full data set for all but the OPAL results from Zγ-production. For the quartic gauge couplings the whole data set is analysed so far only by L3, and by ALEPH for the $\nu\bar{\nu}\gamma\gamma$ -channel.

The W-pair production process, $e^+e^- \rightarrow W^+W^-$, involves the charged triple gauge boson vertices between the W^+W^- and the Z or the photon. During LEP-II operation, about 10,000 W-pair events are collected by each experiment. Single W ($e\nu W$) and single photon ($\nu\bar{\nu}\gamma$) production at LEP are also sensitive to the WWγ vertex. Results from these channels have been combined for previous summer conferences.

For the charged TGCs, new Monte Carlo calculations (RacoonWW [123] and YFSWW [122]) including $O(\alpha_{em})$ corrections to the WW production process have recently become available. They have the potential to largely affect the measurements of the charged TGCs in W-pair production. Their implications are still under investigation. Preliminary results including these $O(\alpha_{em})$ corrections are so far available only from ALEPH [167]. Therefore, as for the winter conferences this year, no new combinations are made for these measurements.

At centre-of-mass energies exceeding twice the Z boson mass, pair production of Z bosons is kinematically allowed. Here, one searches for the possible existence of triple vertices involving only neutral electroweak gauge bosons. Such vertices could also contribute to Zγ production. In contrast to triple gauge boson vertices with two charged gauge bosons, purely neutral gauge boson vertices do not occur in the Standard Model of electroweak interactions.

Within the Standard Model, quartic electroweak gauge boson vertices with at least two charged

gauge bosons do exist. In e^+e^- collisions at LEP-II centre-of-mass energies, the WWZγ and WW$\gamma\gamma$ vertices contribute to WWγ and $\nu\bar{\nu}\gamma\gamma$ production in s-channel and t-channel, respectively. The effect of the Standard Model quartic electroweak vertices is below the sensitivity of LEP-II. Thus only anomalous quartic vertices are searched for in the production of WWγ, $\nu\bar{\nu}\gamma\gamma$ and also Z$\gamma\gamma$ final states. No results from the Z$\gamma\gamma$ final state analysis are included in the combinations due to current investigations of differences in the description of the anomalous contributions to this vertex [168].

10.1.1 Neutral Triple Gauge Boson Couplings

There are two classes of Lorentz invariant structures associated with neutral TGC vertices which preserve $U(1)_{em}$ and Bose symmetry, as described in [169, 170].

The first class refers to anomalous Z$\gamma\gamma^*$ and ZγZ* couplings which are accessible at LEP in the process $e^+e^- \to Z\gamma$. The parametrisation contains eight couplings: h_i^V with $i = 1, ..., 4$ and $V = \gamma$,Z. The superscript γ refers to Z$\gamma\gamma^*$ couplings and superscript Z refers to ZγZ* couplings. The photon and the Z boson in the final state are considered as on-shell particles, while the third boson at the vertex, the s-channel internal propagator, is off shell. The couplings h_1^V and h_2^V are CP-odd while h_3^V and h_4^V are CP-even.

The second class refers to anomalous ZZγ^* and ZZZ* couplings which are accessible at LEP-II in the process $e^+e^- \to ZZ$. This anomalous vertex is parametrised in terms of four couplings: f_i^V with $i = 4, 5$ and $V = \gamma$,Z. The superscript γ refers to ZZγ^* couplings and the superscript Z refers to ZZZ* couplings, respectively. Both Z bosons in the final state are assumed to be on-shell, while the third boson at the triple vertex, the s-channel internal propagator, is off-shell. The couplings f_4^V are CP-odd whereas f_5^V are CP-even.

Note that the h_i^V and f_i^V couplings are independent of each other. They are assumed to be real and they vanish at tree level in the Standard Model.

10.1.2 Quartic Gauge Boson Couplings

Anomalous contributions to electroweak quartic vertices are treated in the framework of References [171–173]. Considered are the three lowest-dimensional operators leading to quartic vertices not causing anomalous TGCs. According to a more recent description of the QGCs [174], anomalous contributions to the WW$\gamma\gamma$ and ZZ$\gamma\gamma$ vertex are treated separately, although their structure is the same. The corresponding couplings are parametrised by $a_0^{\mathrm{V}}/\Lambda^2$ and $a_c^{\mathrm{V}}/\Lambda^2$, where Λ represents the energy scale of new physics and V=W,Z for the respective WW$\gamma\gamma$ and ZZ$\gamma\gamma$ vertices. An anomalous contribution to the WWZγ vertex is parametrised by a_n/Λ^2. The couplings $a_0^{\mathrm{V}}/\Lambda^2$ and $a_c^{\mathrm{V}}/\Lambda^2$ conserve C and P, while the coupling a_n/Λ^2 is CP-violating. The production of WWγ depends on all three $a_0^{\mathrm{W}}/\Lambda^2$, $a_c^{\mathrm{W}}/\Lambda^2$, and a_n/Λ^2 couplings. The production of $\nu\bar{\nu}\gamma\gamma$ and Z$\gamma\gamma$ depend only on $a_0^{\mathrm{V}}/\Lambda^2$ and $a_c^{\mathrm{V}}/\Lambda^2$ (for V=W,Z or Z respectively), as they do not involve the WWZγ vertex. The coupling parameters are assumed to be real and they vanish at tree level in the Standard Model. At present there are differences between the Monte Carlo descriptions of [172] and [168] of the quartic gauge coupling vertex, especially in the Z$\gamma\gamma$-final state. This issue is still under investigation as stated in [168] and currently effort is going on to repeat the measurement using the latter description. No new results are available using this framework so far and therefore no new combinations are presented for the ZZ$\gamma\gamma$ couplings. The analyses of the $\nu\bar{\nu}\gamma\gamma$ final state do not include possible contributions from the ZZ$\gamma\gamma$

vertex and hence the presented measurements here assume a vanishing ZZ$\gamma\gamma$ vertex measuring only $a_0^{\rm W}/\Lambda^2$, $a_c^{\rm W}/\Lambda^2$ and a_n/Λ^2 accordingly.

10.2 Measurements

The combined results presented here are obtained from updated neutral electroweak gauge boson coupling measurements and quartic gauge coupling measurements as discussed above. The individual references should be consulted for details about the data samples used.

The h-coupling analyses of ALEPH, DELPHI and L3 use the data collected at LEP-II up to centre-of-mass energies of 209 GeV. The OPAL measurements so far use the data at 189 GeV. The results of the f-couplings are now obtained from the whole data set above the ZZ-production threshold by all of the experiments. The experiments already pre-combine different processes and final states for each of the couplings. For the neutral TGCs, the analyses use measurements of the total cross sections of Zγ and ZZ production and the differential distributions: the h_i^V couplings [175–178] and the f_i^V couplings [175, 176, 179, 180] are determined.

For QGCs, the combined results are based on measurements from WWγ and $\nu\bar{\nu}\gamma\gamma$ production. In addition to the total cross section, the photon energy is used as a sensitive variable in the WWγ channel. The analyses in the $\nu\bar{\nu}\gamma\gamma$ channel generally restrict to low recoil masses where contributions from the Standard Model and a possible ZZ$\gamma\gamma$ vertex are small. The QGCs $a_0^{\rm V}/\Lambda^2$, $a_c^{\rm V}/\Lambda^2$ and a_n/Λ^2 [181–183] are determined, where the whole data set is analysed by L3 and ALEPH, while OPAL uses the data at 189 GeV.

10.3 Combination Procedure

The combination procedure is identical to the previous LEP combination of electroweak gauge boson couplings [184].

Each experiment provides the negative log likelihood, $\log\mathcal{L}$, as a function of the coupling parameters (one or two) to be combined. The single-parameter analyses are performed fixing all other parameters to their Standard Model values. The two-parameter analyses are performed setting the remaining parameters to their Standard Model values.

The $\log\mathcal{L}$ functions from each experiment include statistical as well as those systematic uncertainties which are considered as uncorrelated between experiments. For both single- and multi-parameter combinations, the individual $\log\mathcal{L}$ functions are added. It is necessary to use the $\log\mathcal{L}$ functions directly in the combination, since in some cases they are not parabolic, and hence it is not possible to combine the results correctly by simply taking weighted averages of the measurements.

The main contributions to the systematic uncertainties that are uncorrelated between experiments arise from detector effects, background in the selected signal samples, limited Monte Carlo statistics and the fitting method. Their importance varies for each experiment and the individual references should be consulted for details.

The systematic uncertainties arising from the theoretical cross section prediction in Zγ-production ($\simeq 1\%$ in the q$\overline{\rm q}\gamma$- and $\simeq 2\%$ in the $\nu\bar{\nu}\gamma$ channel) are treated as correlated. For ZZ production, the

uncertainty on the theoretical cross section prediction is small compared to the statistical accuracy and therefore is neglected. Smaller sources of correlated systematic uncertainties, such as those arising from the LEP beam energy, are for simplicity treated as uncorrelated.

The correlated systematic uncertainties in the h-coupling analyses are taken into account by scaling the combined log-likelihood functions by the squared ratio of the sum of statistical and uncorrelated systematic uncertainty over the total uncertainty including all correlated uncertainties. For the general case of non-Gaussian probability density functions, this treatment of the correlated errors is only an approximation; it also neglects correlations in the systematic uncertainties between the parameters in multi-parameter analyses.

The one standard deviation uncertainties (68% confidence level) are obtained by taking the coupling values for which $\Delta \log \mathcal{L} = +0.5$ above the minimum. The 95% confidence level (C.L.) limits are given by the coupling values for which $\Delta \log \mathcal{L} = +1.92$ above the minimum. These cut-off values are used for obtaining the results of both single- and multi-parameter analyses reported here. Note that in the case of the neutral TGCs, double minima structures appear in the negative log-likelihood curves. For multi-parameter analyses, the two dimensional 68% C.L. contour curves for any pair of couplings are obtained by requiring $\Delta \log \mathcal{L} = +1.15$, while for the 95% C.L. contour curves $\Delta \log \mathcal{L} = +3.0$ is required.

10.4 Results

We present results from the four LEP experiments on the various electroweak gauge boson couplings, and their combination. The results quoted for each individual experiment are calculated using the method described in Section 10.3. Thus they may differ slightly from those reported in the individual references. In particular for the h-coupling result from OPAL and DELPHI, a slightly modified estimate of the systematic uncertainty due to the theoretical cross section prediction is responsible for slightly different limits compared to the published results. Furthermore, for the QGC, L3 integrates the likelihood in order to determine the 95%CL, whereas here it is read off the $\log \mathcal{L}$-curve at $\Delta \log \mathcal{L} = 1.92$ as for Gaussian shaped likelihood functions.

10.4.1 Neutral Triple Gauge Boson Couplings in $Z\gamma$ Production

The individual analyses and results of the experiments for the h-couplings are described in [175–178].

Single-Parameter Analyses

The results for each experiment are shown in Table 10.1, where the errors include both statistical and systematic uncertainties. The individual $\log \mathcal{L}$ curves and their sum are shown in Figures 10.1 and 10.2. The results of the combination are given in Table 10.2. From Figures 10.1 and 10.2 it is clear that the sensitivity of the L3 analysis [177] is the highest amongst the LEP experiments. This is partially due to the use of a larger phase space region, which increases the statistics by about a factor two, and partially due to added information from using an Optimal Observable technique.

Parameter	ALEPH	DELPHI	L3	OPAL
h_1^γ	$[-0.14, +0.14]$	$[-0.15, +0.15]$	$[-0.06, +0.06]$	$[-0.13, +0.13]$
h_2^γ	$[-0.07, +0.07]$	$[-0.09, +0.09]$	$[-0.053, +0.024]$	$[-0.089, +0.089]$
h_3^γ	$[-0.069, +0.037]$	$[-0.047, +0.047]$	$[-0.062, -0.014]$	$[-0.16, +0.00]$
h_4^γ	$[-0.020, +0.045]$	$[-0.032, +0.030]$	$[-0.004, +0.045]$	$[+0.01, +0.13]$
h_1^Z	$[-0.23, +0.23]$	$[-0.24, +0.25]$	$[-0.17, +0.16]$	$[-0.22, +0.22]$
h_2^Z	$[-0.12, +0.12]$	$[-0.14, +0.14]$	$[-0.10, +0.09]$	$[-0.15, +0.15]$
h_3^Z	$[-0.28, +0.19]$	$[-0.32, +0.18]$	$[-0.23, +0.11]$	$[-0.29, +0.14]$
h_4^Z	$[-0.10, +0.15]$	$[-0.12, +0.18]$	$[-0.08, +0.16]$	$[-0.09, +0.19]$

Table 10.1: The 95% C.L. intervals ($\Delta \log \mathcal{L} = 1.92$) measured by the ALEPH, DELPHI, L3 and OPAL. In each case the parameter listed is varied while the remaining ones are fixed to their Standard Model values. Both statistical and systematic uncertainties are included.

Parameter	95% C.L.
h_1^γ	$[-0.056, +0.055]$
h_2^γ	$[-0.045, +0.025]$
h_3^γ	$[-0.049, -0.008]$
h_4^γ	$[-0.002, +0.034]$
h_1^Z	$[-0.13, +0.13]$
h_2^Z	$[-0.078, +0.071]$
h_3^Z	$[-0.20, +0.07]$
h_4^Z	$[-0.05, +0.12]$

Table 10.2: The 95% C.L. intervals ($\Delta \log \mathcal{L} = 1.92$) obtained combining the results from the four experiments. In each case the parameter listed is varied while the remaining ones are fixed to their Standard Model values. Both statistical and systematic uncertainties are included.

Two-Parameter Analyses

The results for each experiment are shown in Table 10.3, where the errors include both statistical and systematic uncertainties. The 68% C.L. and 95% C.L. contour curves resulting from the combinations of the two-dimensional likelihood curves are shown in Figure 10.3. The LEP average values are given in Table 10.4.

Parameter	ALEPH	DELPHI	L3
h_1^γ	$[-0.32, +0.32]$	$[-0.28, +0.28]$	$[-0.17, +0.04]$
h_2^γ	$[-0.18, +0.18]$	$[-0.17, +0.18]$	$[-0.12, +0.02]$
h_3^γ	$[-0.17, +0.38]$	$[-0.48, +0.20]$	$[-0.09, +0.13]$
h_4^γ	$[-0.08, +0.29]$	$[-0.08, +0.15]$	$[-0.04, +0.11]$
h_1^Z	$[-0.54, +0.54]$	$[-0.45, +0.46]$	$[-0.48, +0.33]$
h_2^Z	$[-0.29, +0.30]$	$[-0.29, +0.29]$	$[-0.30, +0.22]$
h_3^Z	$[-0.58, +0.52]$	$[-0.57, +0.38]$	$[-0.43, +0.39]$
h_4^Z	$[-0.29, +0.31]$	$[-0.31, +0.28]$	$[-0.23, +0.28]$

Table 10.3: The 95% C.L. intervals ($\Delta \log \mathcal{L} = 1.92$) measured by ALEPH, DELPHI and L3. In each case the two parameters listed are varied while the remaining ones are fixed to their Standard Model values. Both statistical and systematic uncertainties are included.

Parameter	95% C.L.	Correlations	
h_1^γ	$[-0.16, +0.05]$	1.00	+0.79
h_2^γ	$[-0.11, +0.02]$	+0.79	1.00
h_3^γ	$[-0.08, +0.14]$	1.00	+0.97
h_4^γ	$[-0.04, +0.11]$	+0.97	1.00
h_1^Z	$[-0.35, +0.28]$	1.00	+0.77
h_2^Z	$[-0.21, +0.17]$	+0.77	1.00
h_3^Z	$[-0.37, +0.29]$	1.00	+0.76
h_4^Z	$[-0.19, +0.21]$	+0.76	1.00

Table 10.4: The 95% C.L. intervals ($\Delta \log \mathcal{L} = 1.92$) obtained combining the results from ALEPH, DELPHI and L3. In each case the two parameters listed are varied while the remaining ones are fixed to their Standard Model values. Both statistical and systematic uncertainties are included. Since the shape of the log-likelihood is not parabolic, there is some ambiguity in the definition of the correlation coefficients and the values quoted here are approximate.

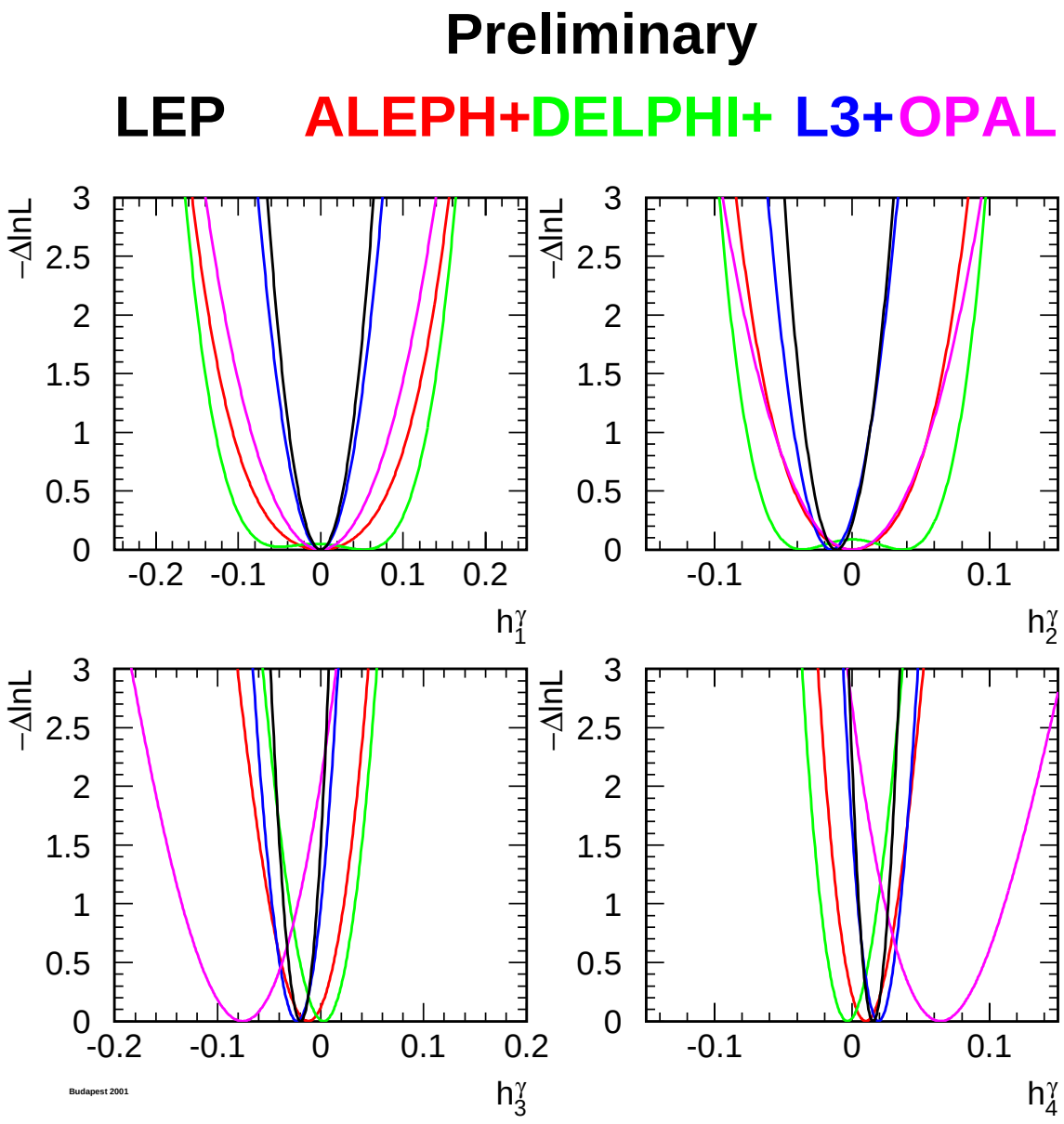

Figure 10.1: The $\log \mathcal{L}$ curves of the four experiments, and the LEP combined curve for the four neutral TGCs h_i^γ, $i = 1, 2, 3, 4$. In each case, the minimal value is subtracted.

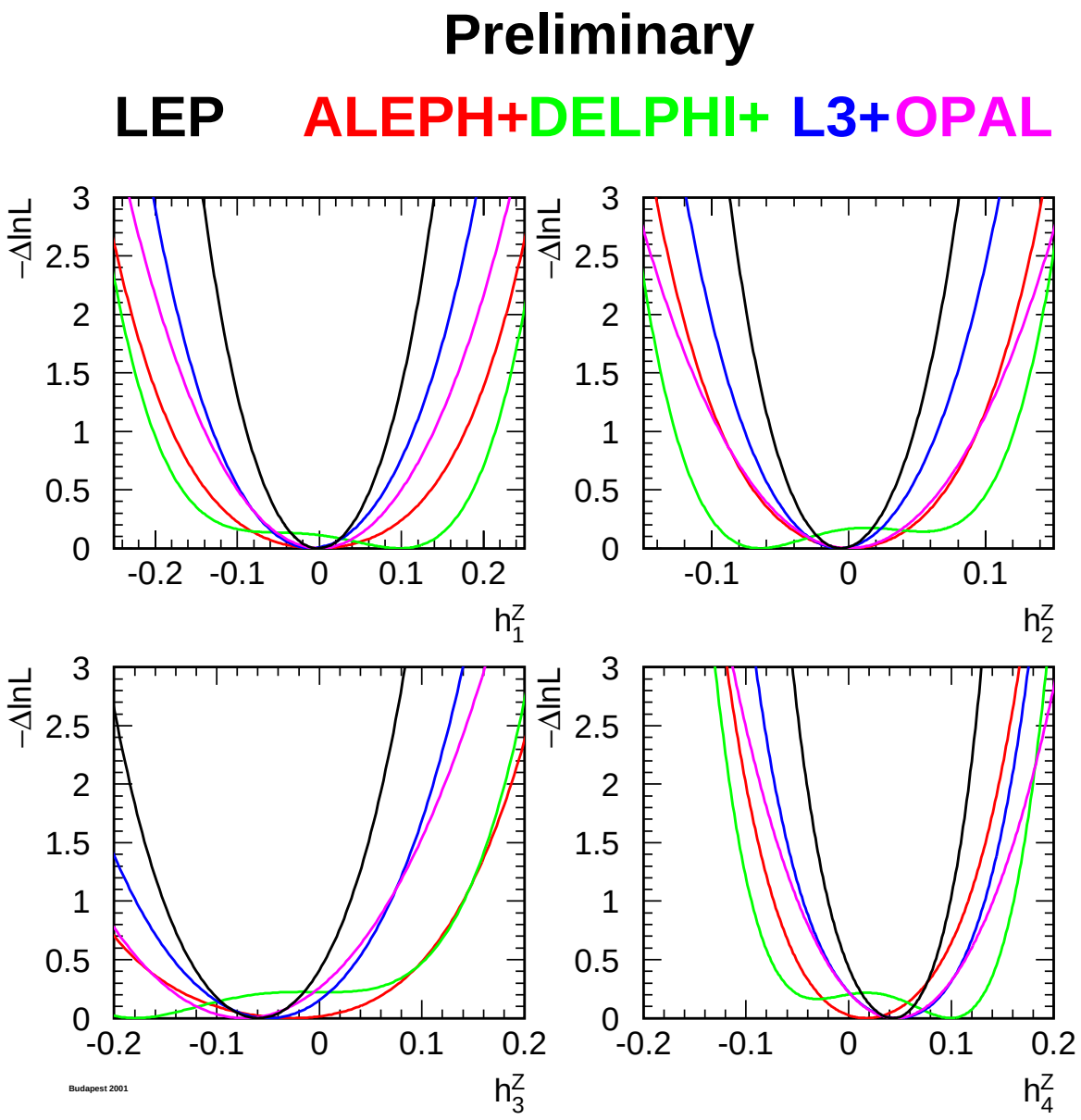

Figure 10.2: The $\log \mathcal{L}$ curves of the four experiments, and the LEP combined curve for the four neutral TGCs h_i^Z, $i = 1, 2, 3, 4$. In each case, the minimal value is subtracted.

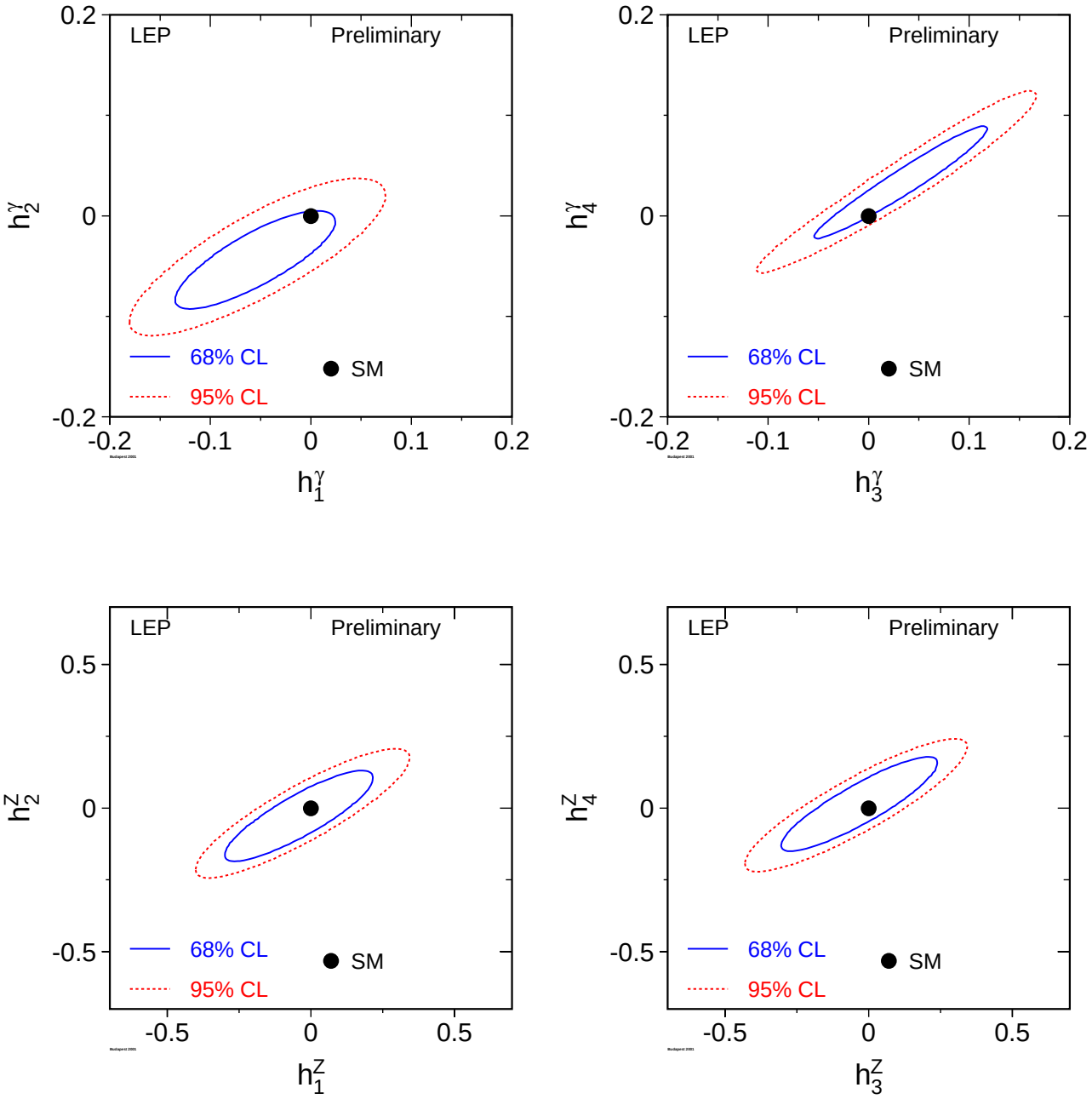

Figure 10.3: Contour curves of 68% C.L. and 95% C.L. in the planes (h_1^γ, h_2^γ), (h_3^γ, h_4^γ), (h_1^Z, h_2^Z) and (h_3^Z, h_4^Z) showing the LEP combined result.

10.4.2 Neutral Triple Gauge Boson Couplings in ZZ Production

The individual analyses and results of the experiments for the f-couplings are described in [175, 176, 179, 180].

Single-Parameter Analyses

The results for each experiment are shown in Table 10.5, where the errors include both statistical and systematic uncertainties. The individual $\log \mathcal{L}$ curves and their sum are shown in Figure 10.4. The results of the combination are given in Table 10.6.

Two-Parameter Analyses

The results from each experiment are shown in Table 10.7, where the errors include both statistical and systematic uncertainties. The 68% C.L. and 95% C.L. contour curves resulting from the combinations of the two-dimensional likelihood curves are shown in Figure 10.5. The LEP average values are given in Table 10.8.

10.4.3 Quartic Gauge Boson Couplings

The individual analyses and results of the experiments for the quartic gauge couplings are described in [181–183].

The results for each experiment are shown in Table 10.9, where the uncertainties include both statistical and systematic effects. The individual $\log \mathcal{L}$ curves and their sum are shown in Figures 10.6. The results of the combination are given in Table 10.10.

Conclusions

No significant deviation from the Standard Model prediction is seen for any of the electroweak gauge boson couplings studied.

Parameter	ALEPH	DELPHI	L3	OPAL
f_4^γ	$[-0.26, +0.26]$	$[-0.26, +0.28]$	$[-0.24, +0.26]$	$[-0.36, +0.36]$
f_4^Z	$[-0.44, +0.43]$	$[-0.49, +0.42]$	$[-0.43, +0.41]$	$[-0.55, +0.64]$
f_5^γ	$[-0.54, +0.56]$	$[-0.48, +0.61]$	$[-0.48, +0.56]$	$[-0.82, +0.72]$
f_5^Z	$[-0.73, +0.83]$	$[-0.42, +0.69]$	$[-0.46, +1.2]$	$[-0.96, +0.31]$

Table 10.5: The 95% C.L. intervals ($\Delta \log \mathcal{L} = 1.92$) measured by ALEPH, DELPHI, L3 and OPAL. In each case the parameter listed is varied while the remaining ones are fixed to their Standard Model values. Both statistical and systematic uncertainties are included.

Parameter	95% C.L.
f_4^γ	$[-0.17, +0.19]$
f_4^Z	$[-0.31, +0.28]$
f_5^γ	$[-0.36, +0.40]$
f_5^Z	$[-0.36, +0.39]$

Table 10.6: The 95% C.L. intervals ($\Delta \log \mathcal{L} = 1.92$) obtained combining the results from all four experiments. In each case the parameter listed is varied while the remaining ones are fixed to their Standard Model values. Both statistical and systematic uncertainties are included.

Parameter	ALEPH	DELPHI	L3	OPAL
f_4^γ	$[-0.26, +0.26]$	$[-0.26, +0.28]$	$[-0.24, +0.26]$	$[-0.36, +0.36]$
f_4^Z	$[-0.44, +0.43]$	$[-0.49, +0.42]$	$[-0.43, +0.41]$	$[-0.54, +0.63]$
f_5^γ	$[-0.52, +0.53]$	$[-0.52, +0.61]$	$[-0.48, +0.56]$	$[-0.77, +0.73]$
f_5^Z	$[-0.77, +0.86]$	$[-0.44, +0.69]$	$[-0.46, +1.2]$	$[-0.96, +0.44]$

Table 10.7: The 95% C.L. intervals ($\Delta \log \mathcal{L} = 1.92$) measured by ALEPH, DELPHI, L3 and OPAL. In each case the two parameters listed are varied while the remaining ones are fixed to their Standard Model values. Both statistical and systematic uncertainties are included.

Parameter	95% C.L.	Correlations	
f_4^γ	$[-0.17, +0.19]$	1.00	+0.10
f_4^Z	$[-0.30, +0.28]$	+0.10	1.00
f_5^γ	$[-0.34, +0.38]$	1.00	−0.18
f_5^Z	$[-0.36, +0.38]$	−0.18	1.00

Table 10.8: The 95% C.L. intervals ($\Delta \log \mathcal{L} = 1.92$) obtained combining the results from all four experiments. In each case the two parameters listed are varied while the remaining ones are fixed to their Standard Model values. Both statistical and systematic uncertainties are included. Since the shape of the log-likelihood is not parabolic, there is some ambiguity in the definition of the correlation coefficients and the values quoted here are approximate.

Parameter [GeV^{-2}]	ALEPH	L3	OPAL
$a_0^{\mathrm{W}}/\Lambda^2$	$[-0.029,\ +0.029]$	$[-0.017,\ +0.017]$	$[-0.065,\ +0.065]$
$a_c^{\mathrm{W}}/\Lambda^2$	$[-0.079,\ +0.080]$	$[-0.03,\ +0.05]$	$[-0.13,\ +0.17]$
a_n/Λ^2	—	$[-0.15,\ +0.14]$	$[-0.61,\ +0.57]$

Table 10.9: The 95% C.L. intervals ($\Delta \log \mathcal{L} = 1.92$) measured by ALEPH, L3 and OPAL. In each case the parameter listed is varied while the remaining ones are fixed to their Standard Model values. Both statistical and systematic uncertainties are included.

Parameter [GeV^{-2}]	95% C.L.
$a_0^{\mathrm{W}}/\Lambda^2$	$[-0.018,\ +0.018]$
$a_c^{\mathrm{W}}/\Lambda^2$	$[-0.033,\ +0.047]$
a_n/Λ^2	$[-0.17,\ +0.15]$

Table 10.10: The 95% C.L. intervals ($\Delta \log \mathcal{L} = 1.92$) obtained combining the results from ALEPH, L3 and OPAL. In each case the parameter listed is varied while the remaining ones are fixed to their Standard Model values. Both statistical and systematic uncertainties are included.

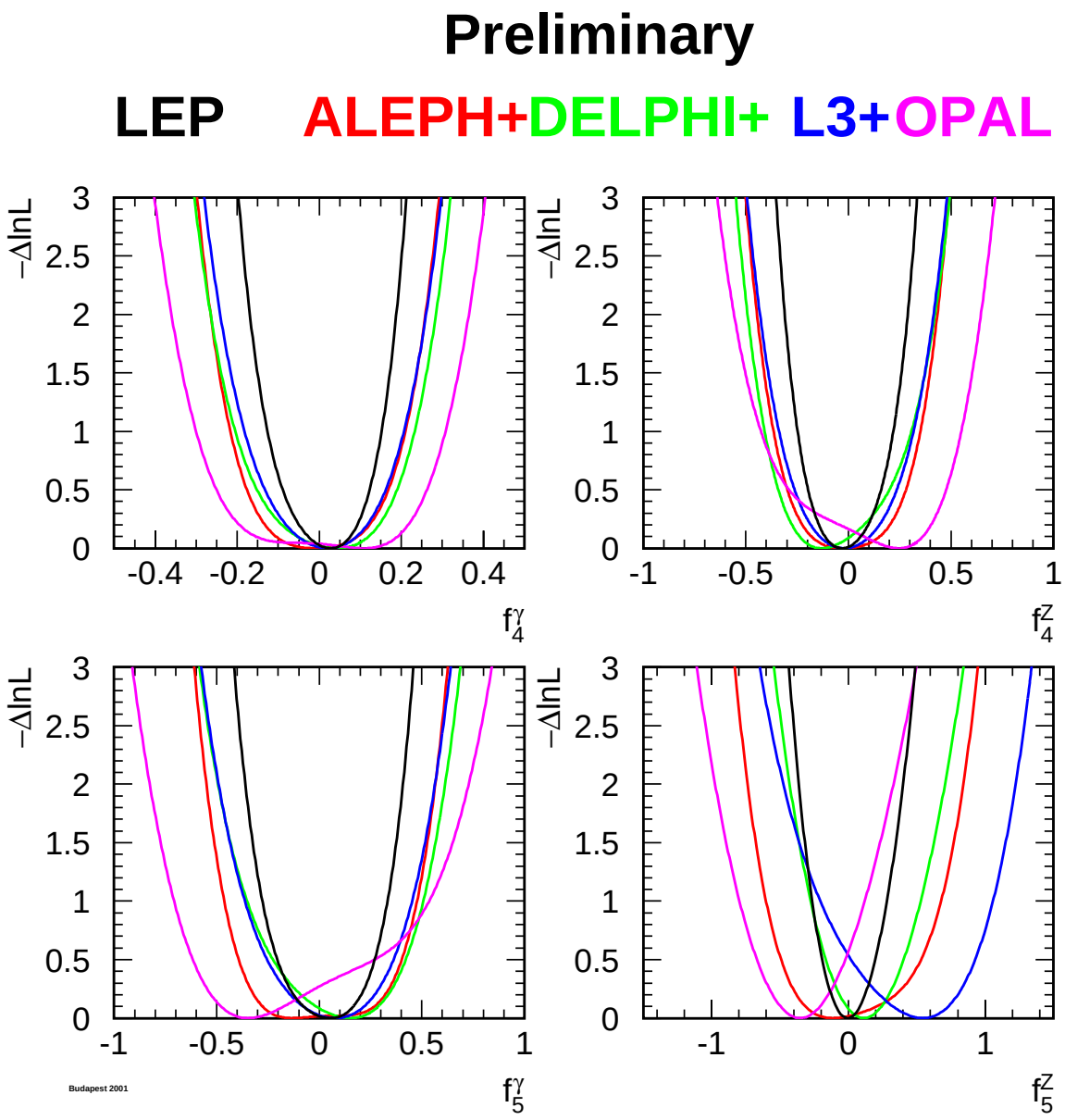

Figure 10.4: The $\log \mathcal{L}$ curves of the four experiments, and the LEP combined curve for the four neutral TGCs f_i^V, $V = \gamma, Z$, $i = 4, 5$. In each case, the minimal value is subtracted.

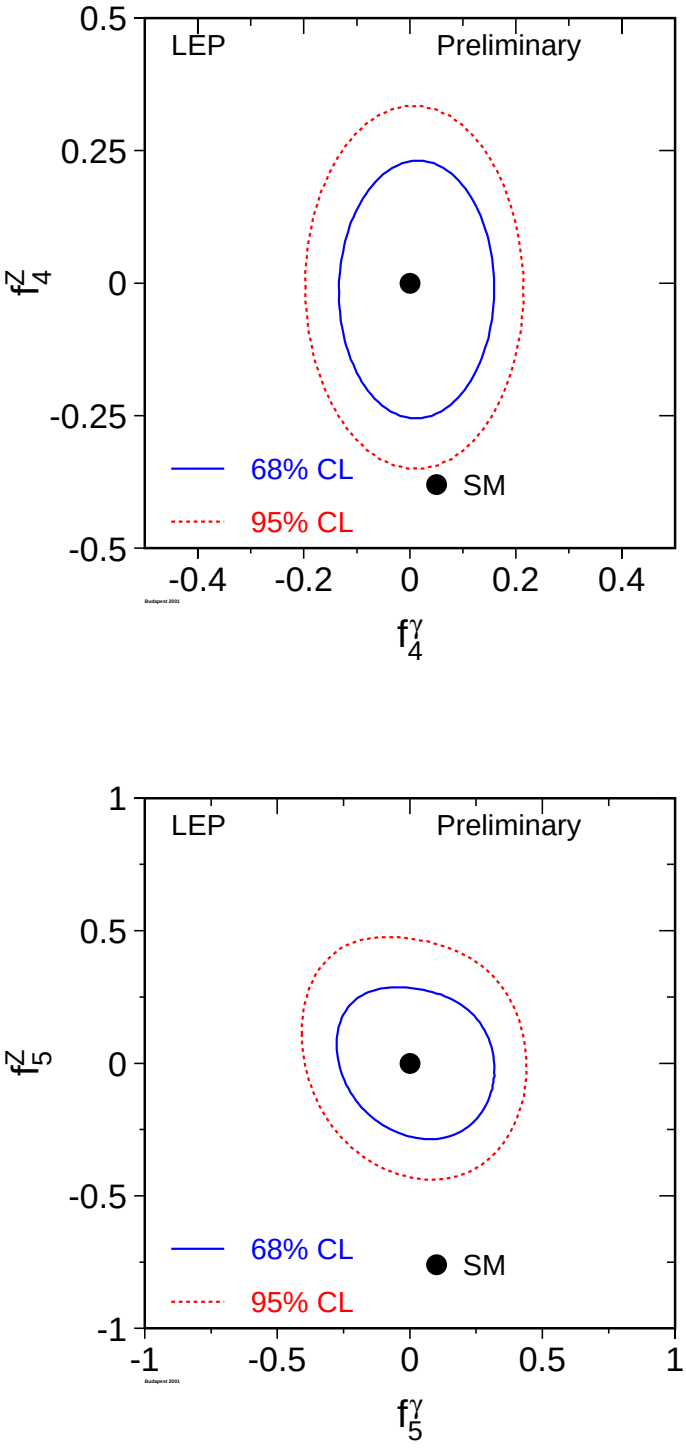

Figure 10.5: Contour curves of 68% C.L. and 95% C.L. in the plane (f_4^γ, f_4^Z) and (f_5^γ, f_5^Z)showing the LEP combined result.

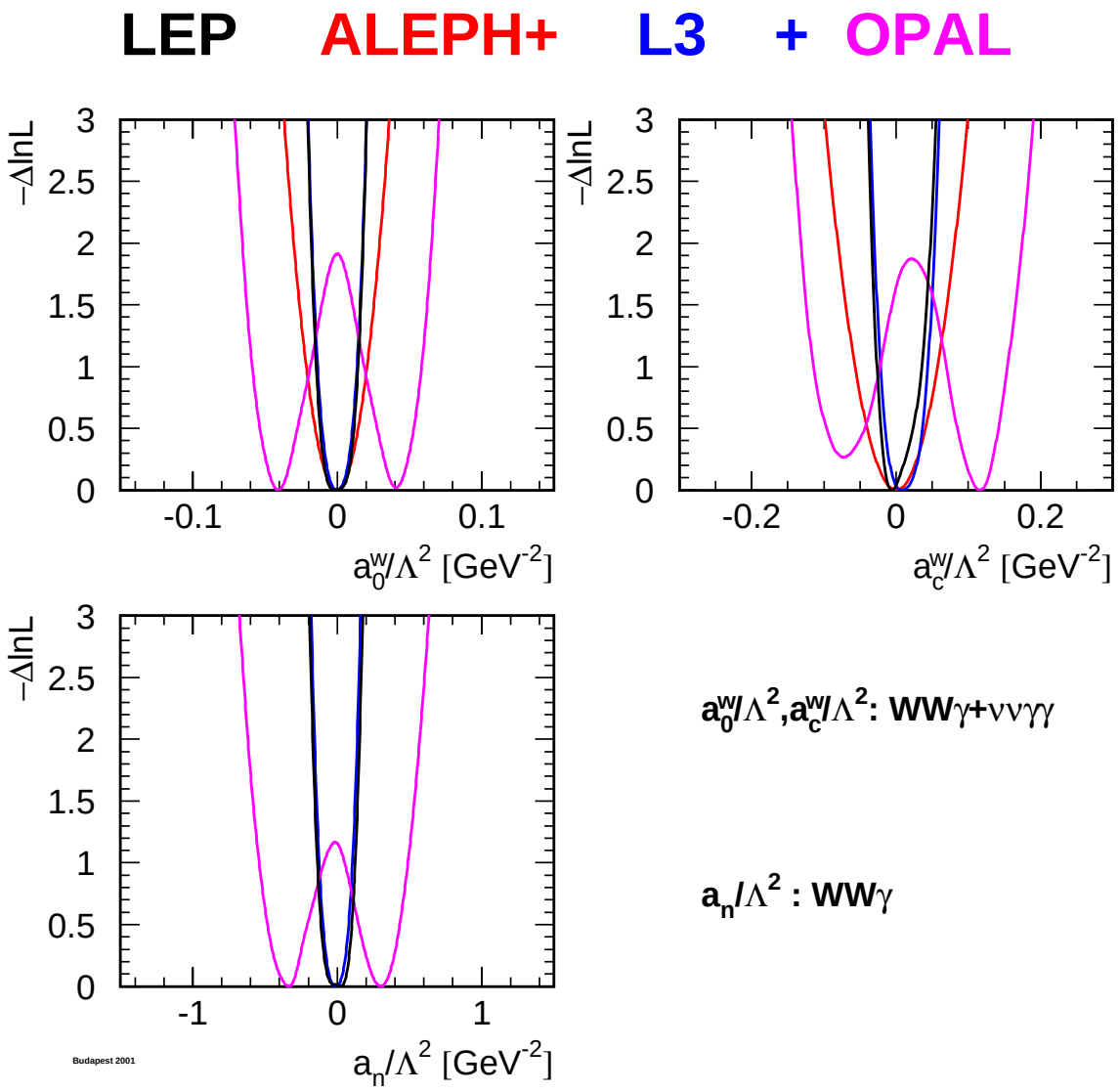

Figure 10.6: The $\log \mathcal{L}$ curves of ALEPH, L3 and OPAL, and the LEP combined curve for the QGCs a_0^W/Λ^2, a_c^W/Λ^2 and a_n/Λ^2. In each case, the minimal value is subtracted.

Chapter 11

W-Boson Mass and Width at LEP-II

Updates with respect to summer 2000:
Additional preliminary results based on the data collected in the year 2000 are included.

11.1 W Mass Measurements

The W boson mass results presented in this Chapter are obtained from data recorded over a range of centre-of-mass energies, $\sqrt{s} = 161-209$ GeV, during the 1996-2000 operation of the LEP collider. The results reported by the ALEPH, DELPHI and L3 collaborations include an analysis of the year 2000 data, and have an integrated luminosity per experiment of about 700 pb^{-1}. The OPAL collaboration has analysed the data up to and including 1999 and has an integrated luminosity of approximately 450 pb^{-1}.

The results on the W mass and width quoted below correspond to a definition based on a Breit-Wigner denominator with an s-dependent width, $|(s - m_{\mathrm{W}}^2) + is\Gamma_{\mathrm{W}}/m_{\mathrm{W}}|$.

Since 1996 the LEP $\mathrm{e^+e^-}$ collider has been operating above the threshold for $\mathrm{W^+W^-}$ pair production. Initially, 10 pb^{-1} of data were recorded close to the $\mathrm{W^+W^-}$ pair production threshold. At this energy the $\mathrm{W^+W^-}$ cross section is sensitive to the W boson mass, m_{W}. Table 11.1 summarises the W mass results from the four LEP collaborations based on these data [97].

THRESHOLD ANALYSIS [97]	
Experiment	m_{W}(threshold)/GeV
ALEPH	80.14 ± 0.35
DELPHI	80.40 ± 0.45
L3	$80.80^{+0.48}_{-0.42}$
OPAL	$80.40^{+0.46}_{-0.43}$

Table 11.1: W mass measurements from the $\mathrm{W^+W^-}$ threshold cross section at $\sqrt{s} = 161$ GeV. The errors include statistical and systematic contributions.

Subsequently LEP has operated at energies significantly above the $\mathrm{W^+W^-}$ threshold, where the $\mathrm{e^+e^-} \to \mathrm{W^+W^-}$ cross section has little sensitivity to m_{W}. For these higher energy data m_{W} is measured through the direct reconstruction of the W boson's invariant mass from the observed jets and

leptons. Table 11.2 summarises the W mass results presented individually by the four LEP experiments using the direct reconstruction method. The combined values of m_{W} from each collaboration take into account the correlated systematic uncertainties between the decay channels and between the different years of data taking. In addition to the combined numbers, each experiment presents mass measurements from $\mathrm{W^+W^-}\to\mathrm{q\overline{q}}\ell\nu_{\mathrm{e}}$ and $\mathrm{W^+W^-}\to\mathrm{q\overline{q}q\overline{q}}$ channels separately. The DELPHI and OPAL collaborations provide results from independent fits to the data in the $\mathrm{q\overline{q}}\ell\nu_{\mathrm{e}}$ and $\mathrm{q\overline{q}q\overline{q}}$ decay channels separately and hence account for correlations between years but do not include correlations between the two channels. The $\mathrm{q\overline{q}}\ell\nu_{\mathrm{e}}$ and $\mathrm{q\overline{q}q\overline{q}}$ results quoted by the ALEPH and L3 collaborations are obtained from a simultaneous fit to all data which, in addition to other correlations, takes into account the correlated systematic uncertainties between the two channels. The L3 result is unchanged when determined through separate fits. The large variation in the systematic uncertainties in the $\mathrm{W^+W^-}\to\mathrm{q\overline{q}q\overline{q}}$ channel are caused by differing estimates of the possible effects of Colour Reconnection (CR) and Bose-Einstein Correlations (BEC); this is discussed below. The systematic errors in the $\mathrm{W^+W^-}\to\mathrm{q\overline{q}}\ell\nu_{\mathrm{e}}$ channel are dominated by uncertainties from hadronisation, with estimates ranging from 15 to 30 MeV.

	DIRECT RECONSTRUCTION		
	$\mathrm{W^+W^-}\to\mathrm{q\overline{q}}\ell\nu_{\mathrm{e}}$	$\mathrm{W^+W^-}\to\mathrm{q\overline{q}q\overline{q}}$	Combined
Experiment	m_{W}/GeV	m_{W}/GeV	m_{W}/GeV
ALEPH [185–187]	$80.456 \pm 0.051 \pm 0.032$	$80.507 \pm 0.054 \pm 0.045$	$80.477 \pm 0.038 \pm 0.032$
DELPHI [99, 188–190]	$80.414 \pm 0.074 \pm 0.048$	$80.384 \pm 0.053 \pm 0.065$	$80.399 \pm 0.045 \pm 0.049$
L3 [100, 191–194]	$80.314 \pm 0.074 \pm 0.045$	$80.478 \pm 0.063 \pm 0.069$	$80.389 \pm 0.048 \pm 0.051$
OPAL [101, 195–198]	$80.516 \pm 0.067 \pm 0.030$	$80.408 \pm 0.066 \pm 0.100$	$80.491 \pm 0.053 \pm 0.038$

Table 11.2: Preliminary W mass measurements from direct reconstruction ($\sqrt{s}$ = 172 – 209 GeV). The first error is statistical and the second systematic. Results are given for the semi-leptonic, fully-hadronic channels and the combined value. The $\mathrm{W^+W^-}\to\mathrm{q\overline{q}}\ell\nu_{\mathrm{e}}$ results from the ALEPH and OPAL collaborations include mass information from the $\mathrm{W^+W^-}\to\ell\nu_{\mathrm{e}}\ell\nu_{\mathrm{e}}$ channel.

11.2 Combination Procedure

A combined LEP W mass measurement is obtained from the results of the four experiments. In order to perform a reliable combination of the measurements, a more detailed input than that given in Table 11.2 is required. Each experiment provided a W mass measurement for both the $\mathrm{W^+W^-}\to\mathrm{q\overline{q}}\ell\nu_{\mathrm{e}}$ and $\mathrm{W^+W^-}\to\mathrm{q\overline{q}q\overline{q}}$ channels for each of the data taking years (1996-2000) that it had analysed. In addition to the four threshold measurements a total of 36 direct reconstruction measurements are supplied: ALEPH and DELPHI provided 10 measurements (1996-2000), L3 gave 8 measurements (1996-2000) having already combined the 1996 and 1997 results and OPAL provided 8 measurements (1996-1999). The $\mathrm{W^+W^-}\to\ell\nu_{\mathrm{e}}\ell\nu_{\mathrm{e}}$ channel is also analysed by the ALEPH(1997-2000) and OPAL(1997-2000) collaborations; the lower precision results obtained from this channel are combined by the experiments with their $\mathrm{W^+W^-}\to\mathrm{q\overline{q}}\ell\nu_{\mathrm{e}}$ channel mass determinations.

Subdividing the results by data-taking years enables a proper treatment of the correlated systematic uncertainty from the LEP beam energy and other dependences on the centre-of-mass energy or data-taking period. A detailed breakdown of the sources of systematic uncertainty are provided for each result and the correlations specified. The inter-year, inter-channel and inter-experiment correlations are included in the combination. The main sources of correlated systematic errors are: colour reconnection, Bose-Einstein correlations, hadronisation, the LEP beam energy, and uncertainties from

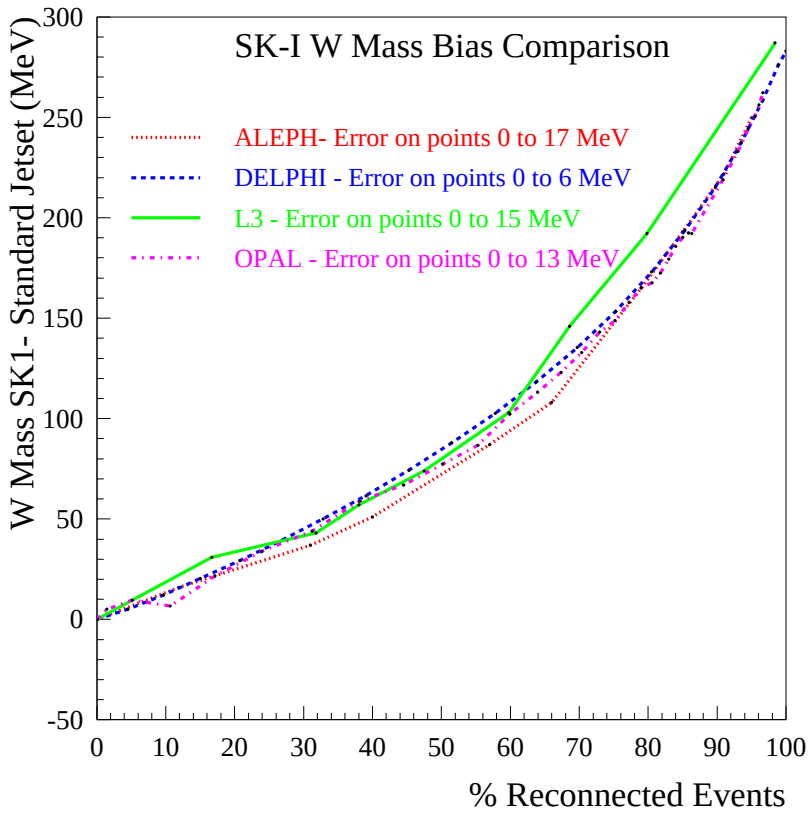

Figure 11.1: W mass bias obtained in the SK-I model of colour reconnection relative to a simulation without colour reconnection as a function of the fraction of events reconnected, at a centre of mass energy of 189 GeV and for the fully-hadronic decay channel. The analyses of the four LEP experiments show similar sensitivity to this effect. The points connected by the lines have correlated uncertainties increasing to the right in the range indicated.

initial and final state radiation. The full correlation matrix for the LEP beam energy is employed [199]. The combination is performed and the evaluation of the components of the total error assessed using the Best Linear Unbiased Estimate (BLUE) technique, see Reference 82.

The four LEP collaborations gave different estimates of the systematic errors arising from final state interactions: these varied from 30-66 MeV for colour reconnection and from 20-67 MeV for Bose-Einstein correlations. This range of estimates could be due to different experimental sensitivities to these effects or, alternatively, simply a reflection of the different phenomenological models used to assess the uncertainties. This question is resolved by comparing the results of the experiments when analysing simulation samples with and without CR effects in the SK-I model [200]. Studies of these samples demonstrate that the four experiments are equally sensitive to colour reconnection effects, *i.e.* when looking at the same CR model similar biases are seen by all experiments. This is shown in Figure 11.1 as a function of the fraction of reconnected events, a reconnection fraction of 30% of events is typically assumed by the experiments for the assessment of systematic uncertainties.

For this reason a common value of the CR systematic uncertainty is used in the combination. For Bose-Einstein Correlations, no similar test is made of the respective experimental sensitivities.

Source	Systematic Error on m_{W} (MeV)		
	$\mathrm{q\overline{q}}\ell\nu_{\mathrm{e}}$	$\mathrm{q\overline{q}q\overline{q}}$	Combined
ISR/FSR	8	9	8
Hadronisation	19	17	17
Detector Systematics	12	8	10
LEP Beam Energy	17	17	17
Colour Reconnection	–	40	11
Bose-Einstein Correlations	–	25	7
Other	4	4	3
Total Systematic	29	54	30
Statistical	33	30	26
Total	44	62	40
Statistical in absence of Systematics	32	29	22

Table 11.3: Error decomposition for the combined LEP W mass results. Detector systematics include uncertainties in the jet and lepton energy scales and resolution. The 'Other' category refers to errors, all of which are uncorrelated between experiments, arising from: simulation statistics, background estimation, four-fermion treatment, fitting method and event selection. The error decomposition in the $\mathrm{q\overline{q}}\ell\nu_{\mathrm{e}}$ and $\mathrm{q\overline{q}q\overline{q}}$ channels refers to the independent fits to the results from the two channels separately.

However, in the absence of evidence that the experiments have different sensitivities to the effect, a common value of the systematic uncertainty from BEC is assumed. In the combination a common colour reconnection error of 40 MeV and a common Bose-Einstein systematic uncertainty of 25 MeV are used. These values are chosen as representative averages of the estimates of the different LEP experiments, resulting in the same final error on m_{W} as obtained when using the BEC and CR estimates of the experiments. Applying this procedure changes the value of m_{W} from the fit by 7 MeV.

11.3 LEP Combined W Boson Mass

The combined W mass from direct reconstruction is

$$m_{\mathrm{W}}(\mathrm{direct}) = 80.450 \pm 0.026(\mathrm{stat.}) \pm 0.030(\mathrm{syst.})\ \mathrm{GeV},$$

with a χ^2/d.o.f. of 31.1/35, corresponding to a χ^2 probability of 66%. The weight of the fully-hadronic channel in the combined fit is 0.27. This reduced weight is a consequence of the relatively large size of the current estimates of the systematic errors from CR and BEC. Table 11.3 gives a breakdown of the contribution to the total error of the various sources of systematic errors. The largest contribution to the systematic error comes from hadronisation uncertainties, which are conservatively treated as correlated between the two channels, between experiments and between years. In the absence of systematic effects the current LEP statistical precision on m_{W} would be 22 MeV: the statistical error contribution in the LEP combination is larger than this (26 MeV) due to the significantly reduced weight of the fully-hadronic channel.

In addition to the above results, the W boson mass is measured at LEP from the 10 pb^{-1} per

experiment of data recorded at threshold for W pair production:

$$m_{\mathrm{W}}(\text{threshold}) = 80.40 \pm 0.20(\text{stat.}) \pm 0.07(\text{syst.}) \pm 0.03(\mathrm{E_{beam}})\ \text{GeV}.$$

When the threshold measurements are combined with the much more precise results obtained from direct reconstruction one achieves a W mass measurement of

$$m_{\mathrm{W}} = 80.450 \pm 0.026(\text{stat.}) \pm 0.030(\text{syst.})\text{GeV}.$$

The LEP beam energy uncertainty is the only correlated systematic error source between the threshold and direct reconstruction measurements. The threshold measurements have a weight of only 0.02 in the combined fit. This LEP combined result is compared with the results (threshold and direct reconstruction combined) of the four LEP experiments in Figure 11.2.

11.4 Consistency Checks

The difference between the combined W boson mass measurements obtained from the fully-hadronic and semi-leptonic channels, $\Delta m_{\mathrm{W}}(\mathrm{q\overline{q}q\overline{q}} - \mathrm{q\overline{q}}\ell\nu_{\mathrm{e}})$, is determined:

$$\Delta m_{\mathrm{W}}(\mathrm{q\overline{q}q\overline{q}} - \mathrm{q\overline{q}}\ell\nu_{\mathrm{e}}) = +9 \pm 44\ \text{MeV}.$$

A significant non-zero value for Δm_{W} could indicate that FSI effects are biasing the value of m_{W} determined from $\mathrm{W^+W^-}\rightarrow\mathrm{q\overline{q}q\overline{q}}$ events. Since Δm_{W} is primarily of interest as a check of the possible effects of final state interactions, the errors from CR and BEC are set to zero in its determination. The result is obtained from a fit where the imposed correlations are the same as those for the results given in the previous sections. This result is almost unchanged if the systematic part of the error on m_{W} from hadronisation effects is considered as uncorrelated between channels, although the uncertainty increases by 16%. The study of the mass difference and the equivalent analysis for the W width are not used to place limits on colour reconnection, for example using the study of the W mass bias in the SK-I colour reconnection model reported in Section 11.2. This is because only one model is analysed there, and, taken in isolation, the results are not sufficiently precise.

The masses from the two channels obtained from this fit with the BEC and CR errors now included are:

$$m_{\mathrm{W}}(\mathrm{W^+W^-}\rightarrow\mathrm{q\overline{q}}\ell\nu_{\mathrm{e}}) = 80.448 \pm 0.033(\text{stat.}) \pm 0.028(\text{syst.})\ \text{GeV},$$
$$m_{\mathrm{W}}(\mathrm{W^+W^-}\rightarrow\mathrm{q\overline{q}q\overline{q}}) = 80.457 \pm 0.030(\text{stat.}) \pm 0.054(\text{syst.})\ \text{GeV}.$$

These two results are correlated and have a correlation coefficient of 0.28. The value of χ^2/d.o.f is 31.1/34, corresponding to a χ^2 probability of 62%. These results and the correlation between them can be used to combine the two measurements or to form the mass difference. The LEP combined results from the two channels are compared with those quoted by the individual experiments in Figure 11.3.

Experimentally, separate m_{W} measurements are obtained from the $\mathrm{W^+W^-}\rightarrow\mathrm{q\overline{q}}\ell\nu_{\mathrm{e}}$ and $\mathrm{W^+W^-}\rightarrow\mathrm{q\overline{q}q\overline{q}}$ channels for each of the years of data. The combination using only the $\mathrm{q\overline{q}}\ell\nu_{\mathrm{e}}$ measurements yields:

$$m_{\mathrm{W}}^{\mathrm{indep}}(\mathrm{W^+W^-}\rightarrow\mathrm{q\overline{q}}\ell\nu_{\mathrm{e}}) = 80.448 \pm 0.033(\text{stat.}) \pm 0.029(\text{syst.})\ \text{GeV}.$$

The systematic error is dominated by hadronisation uncertainties ($\pm$19 MeV) and the uncertainty in the LEP beam energy ($\pm$17 MeV). The combination using only the $\mathrm{q\overline{q}q\overline{q}}$ measurements gives:

$$m_{\mathrm{W}}^{\mathrm{indep}}(\mathrm{W^+W^-}\rightarrow\mathrm{q\overline{q}q\overline{q}}) = 80.447 \pm 0.030(\mathrm{stat.}) \pm 0.054(\mathrm{syst.})\ \mathrm{GeV}.$$

where the dominant contributions to the systematic error arise from BEC/CR ($\pm$47 MeV), hadronisation ($\pm$17 MeV) and from the uncertainty in the LEP beam energy ($\pm$17 MeV).

11.5 LEP Combined W Boson Width

The method of direct reconstruction is also well suited to the direct measurement of the width of the W boson. The results of the four LEP experiments are shown in Table 11.4 and in Figure 11.2.

Experiment	Γ_{W} (GeV)
ALEPH	$2.13 \pm 0.11 \pm 0.09$
DELPHI	$2.11 \pm 0.10 \pm 0.07$
L3	$2.24 \pm 0.11 \pm 0.15$
OPAL	$2.04 \pm 0.16 \pm 0.09$

Table 11.4: Preliminary W width measurements ($\sqrt{s} = 172 - 209$ GeV) from the individual experiments. The first error is statistical and the second systematic.

Each experiment provided a W width measurement for both $\mathrm{W^+W^-}\rightarrow\mathrm{q\overline{q}}\ell\nu_{\mathrm{e}}$ and $\mathrm{W^+W^-}\rightarrow\mathrm{q\overline{q}q\overline{q}}$ channels for each of the data taking years (1996-2000) that it has analysed. A total of 25 measurements are supplied: ALEPH provided 3 $\mathrm{W^+W^-}\rightarrow\mathrm{q\overline{q}q\overline{q}}$ results (1998-2000) and two $\mathrm{W^+W^-}\rightarrow\mathrm{q\overline{q}}\ell\nu_{\mathrm{e}}$ results (1998-1999), DELPHI 8 measurements (1997-2000), L3 8 measurements (1996-2000) having already combined the 1996 and 1997 results and OPAL provided 4 measurements (1996-1998) where for the first two years the $\mathrm{W^+W^-}\rightarrow\mathrm{q\overline{q}}\ell\nu_{\mathrm{e}}$ and $\mathrm{W^+W^-}\rightarrow\mathrm{q\overline{q}q\overline{q}}$ results are already combined.

A common colour reconnection error of 65 MeV and a common Bose-Einstein correlation error of 35 MeV are used in the combination. This procedure resulted in the same error on Γ_{W} as obtained using the BEC/CR errors supplied by the experiments. The change in the value of the width is only 2 MeV.

A simultaneous fit to the results of the four LEP collaborations is performed in the same way as for the m_{W} measurement. Correlated systematic uncertainties are taken into account and the combination gives:

$$\Gamma_{\mathrm{W}} = 2.150 \pm 0.068(\mathrm{stat.}) \pm 0.060(\mathrm{syst.})\ \mathrm{GeV},$$

with a χ^2/d.o.f. of 19.7/24, corresponding to a χ^2 probability of 71%.

11.6 Summary

The results of the four LEP experiments on the mass and width of the W boson are combined taking into account correlated systematic uncertainties, giving:

$$\begin{aligned} m_{\mathrm{W}} &= 80.450 \pm 0.039\ \mathrm{GeV}, \\ \Gamma_{\mathrm{W}} &= 2.150 \pm 0.091\ \mathrm{GeV}. \end{aligned}$$

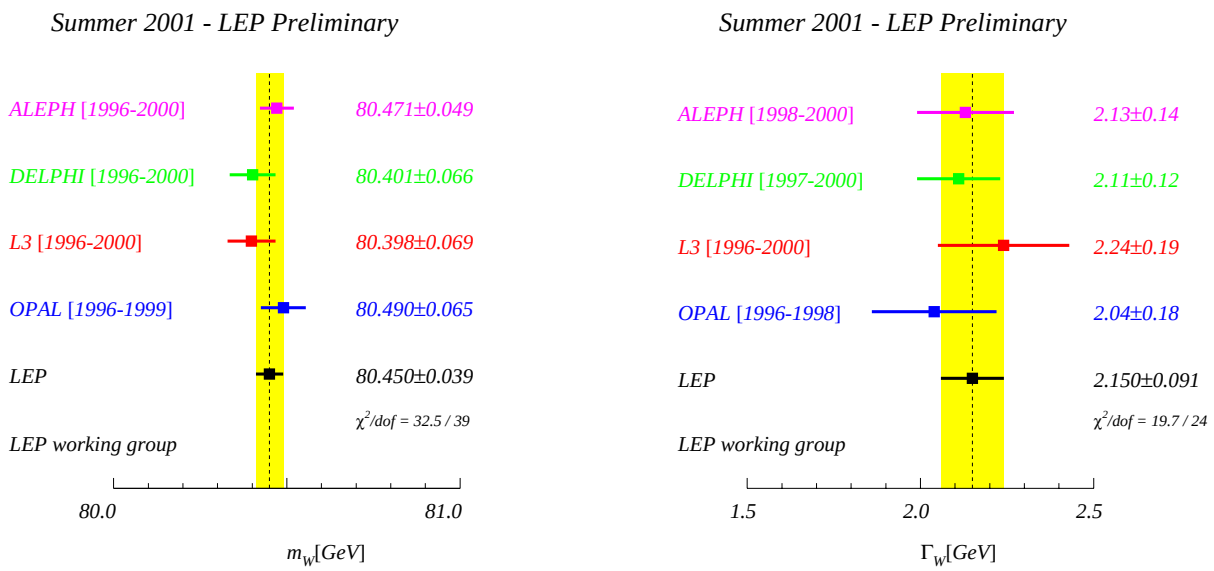

Figure 11.2: The combined results for the measurements of the W mass (left) and W width (right) compared to the results obtained by the four LEP collaborations. The combined values take into account correlations between experiments and years and hence, in general, do not give the same central value as a simple average. In the LEP combination of the $q\bar{q}q\bar{q}$ results common values (see text) for the CR and BEC errors are used. The individual and combined m_W results include the measurements from the threshold cross section.

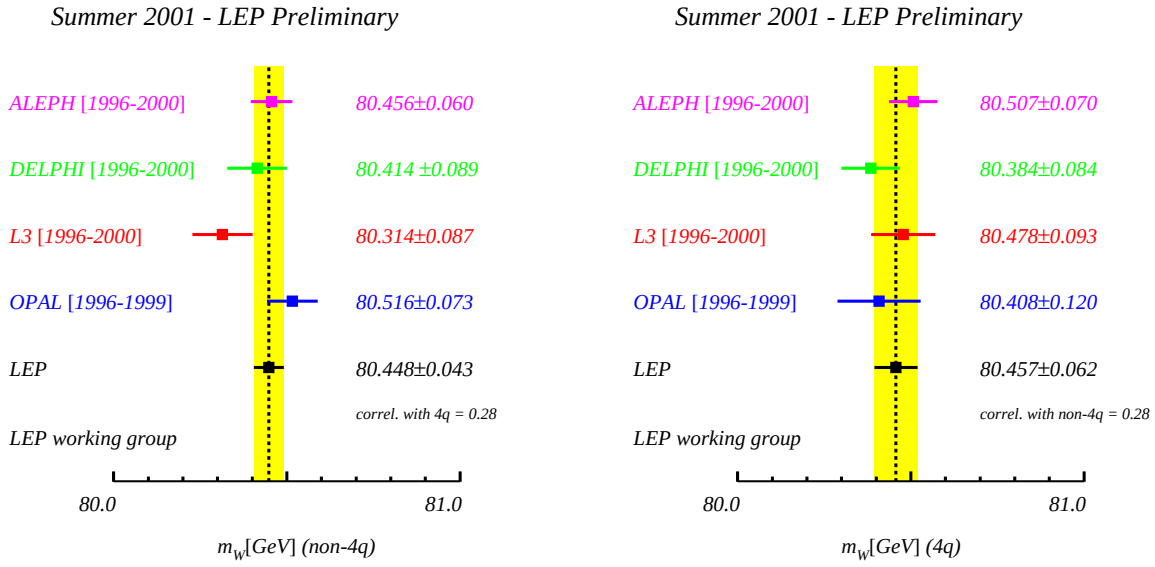

Figure 11.3: The W mass measurements from the $W^+W^- \to q\bar{q}\ell\nu_e$ (left) and $W^+W^- \to q\bar{q}q\bar{q}$ (right) channels obtained by the four LEP collaborations compared to the combined value. The combined values take into account correlations between experiments, years and the two channels. In the LEP combination of the $q\bar{q}q\bar{q}$ results common values (see text) for the CR and BEC errors are used. The ALEPH and L3 $q\bar{q}\ell\nu_e$ and $q\bar{q}q\bar{q}$ results are correlated since they are obtained from a fit to both channels taking into account inter-channel correlations.

Chapter 12

Effective Couplings of the Neutral Weak Current

Updates with respect to summer 2000:
Effective vector and axial-vector coupling constants are also determined for the heavy quark flavours.

12.1 The Coupling Parameters $\mathcal{A}_f$

The coupling parameters $\mathcal{A}_f$ are defined in terms of the effective vector and axial-vector neutral current couplings of fermions (Equation (2.4)). The LEP measurements of the forward-backward asymmetries of charged leptons (Chapter 2) and b and c quarks (Chapter 5) determine the products $A_{FB}^{0,f} = \frac{3}{4}\mathcal{A}_e\mathcal{A}_f$ (Equation (2.3)). The LEP measurements of the τ polarisation (Chapter 3), $\mathcal{P}_\tau(\cos\theta)$, determine $\mathcal{A}_\tau$ and $\mathcal{A}_e$ separately (Equation (3.2)). Owing to polarised beams at SLC, SLD measures the coupling parameters directly with the left-right and forward-backward left-right asymmetries (Chapters 4 and 5).

Table 12.1 shows the results for the leptonic coupling parameter $\mathcal{A}_\ell$ from the LEP and SLD measurements, assuming lepton universality.

Using the measurements of $\mathcal{A}_\ell$ one can extract $\mathcal{A}_b$ and $\mathcal{A}_c$ from the LEP measurements of the b and c quark asymmetries. The SLD measurements of the left-right forward-backward asymmetries for b and c quarks are direct determinations of $\mathcal{A}_b$ and $\mathcal{A}_c$. Table 12.2 shows the results on the

	$\mathcal{A}_\ell$	Cumulative Average	χ^2/d.o.f.
$A_{FB}^{0,\ell}$	0.1512 ± 0.0042		
$\mathcal{P}_\tau$	0.1465 ± 0.0033	0.1482 ± 0.0026	0.8/1
$\mathcal{A}_\ell$ (SLD)	0.1513 ± 0.0021	0.1501 ± 0.0016	1.6/2

Table 12.1: Determination of the leptonic coupling parameter $\mathcal{A}_\ell$ assuming lepton universality. The second column lists the $\mathcal{A}_\ell$ values derived from the quantities listed in the first column. The third column contains the cumulative averages of the $\mathcal{A}_\ell$ results up to and including this line. The χ^2 per degree of freedom for the cumulative averages is given in the last column.

	LEP ($\mathcal{A}_\ell = 0.1482 \pm 0.0026$)	SLD	LEP+SLD ($\mathcal{A}_\ell = 0.1501 \pm 0.0016$)	Standard Model fit
$\mathcal{A}_\mathrm{b}$	0.891 ± 0.022	0.922 ± 0.020	0.899 ± 0.013	0.935
$\mathcal{A}_\mathrm{c}$	0.615 ± 0.033	0.670 ± 0.026	0.645 ± 0.020	0.668

Table 12.2: Determination of the quark coupling parameters $\mathcal{A}_\mathrm{b}$ and $\mathcal{A}_\mathrm{c}$ from LEP data alone (using the LEP average for $\mathcal{A}_\ell$), from SLD data alone, and from LEP+SLD data (using the LEP+SLD average for $\mathcal{A}_\ell$) assuming lepton universality.

quark coupling parameters $\mathcal{A}_\mathrm{b}$ and $\mathcal{A}_\mathrm{c}$ derived from LEP measurements (Equations 5.6) and SLD measurements separately, and from the combination of LEP+SLD measurements (Equation 5.7).

The LEP extracted values of $\mathcal{A}_\mathrm{b}$ and $\mathcal{A}_\mathrm{c}$ are in agreement with the SLD measurements, but somewhat lower than the Standard Model predictions (0.935 and 0.668, respectively, essentially independent of m_t and m_H). The combination of LEP and SLD of $\mathcal{A}_\mathrm{b}$ is 2.8 sigma below the Standard Model, while $\mathcal{A}_\mathrm{c}$ agrees at the 1.2 sigma level. This is mainly because the $\mathcal{A}_\mathrm{b}$ value, deduced from the measured $A_\mathrm{FB}^{0,\,\mathrm{b}}$ and the combined $\mathcal{A}_\ell$, is significantly lower than both the Standard Model and the direct measurement of $\mathcal{A}_\mathrm{b}$, this can also be seen in Figure 12.1.

12.2 The Effective Vector and Axial-Vector Coupling Constants

The partial widths of the Z into leptons and the lepton forward-backward asymmetries (Section 2), the τ polarisation and the τ polarisation asymmetry (Section 3) are combined to determine the effective vector and axial-vector couplings for e, μ and τ. The asymmetries (Equations (2.3) and (3.2)) determine the ratio $g_{\mathrm{V}\ell}/g_{\mathrm{A}\ell}$ (Equation (2.4)), while the leptonic partial widths determine the sum of the squares of the couplings:

$$\Gamma_{\ell\ell} \;=\; \frac{G_\mathrm{F} m_\mathrm{Z}^3}{6\pi\sqrt{2}}(g_{\mathrm{V}\ell}^2 + g_{\mathrm{A}\ell}^2)(1+\delta_\ell^{QED})\,, \tag{12.1}$$

where $\delta_\ell^{QED} = 3q_\ell^2\alpha(m_\mathrm{Z}^2)/(4\pi)$, with q_ℓ denoting the electric charge of the lepton, accounts for final state photonic corrections. Corrections due to lepton masses, neglected in Equation 12.1, are taken into account for the results presented below.

The averaged results for the effective lepton couplings are given in Table 12.3 for both the LEP data alone as well as for the LEP and SLD measurements. Figure 12.2 shows the 68% probability contours in the $g_{\mathrm{A}\ell}$-$g_{\mathrm{V}\ell}$ plane for the individual lepton species. The signs of $g_{\mathrm{A}\ell}$ and $g_{\mathrm{V}\ell}$ are based on the convention $g_{\mathrm{Ae}} < 0$. With this convention the signs of the couplings of all charged leptons follow from LEP data alone. The measured ratios of the e, μ and τ couplings provide a test of lepton universality and are shown in Table 12.3. All values are consistent with lepton universality. The combined results assuming universality are also given in the table and are shown as a solid contour in Figure 12.2.

The neutrino couplings to the Z can be derived from the measured value of the invisible width of the Z, Γ_inv (see Table 2.4), attributing it exclusively to the decay into three identical neutrino generations ($\Gamma_\mathrm{inv} = 3\Gamma_{\nu\nu}$) and assuming $g_{A\nu} \equiv g_{V\nu} \equiv g_\nu$. The relative sign of g_ν is chosen to be in agreement with neutrino scattering data [201], resulting in $g_\nu = +0.50068 \pm 0.00075$.

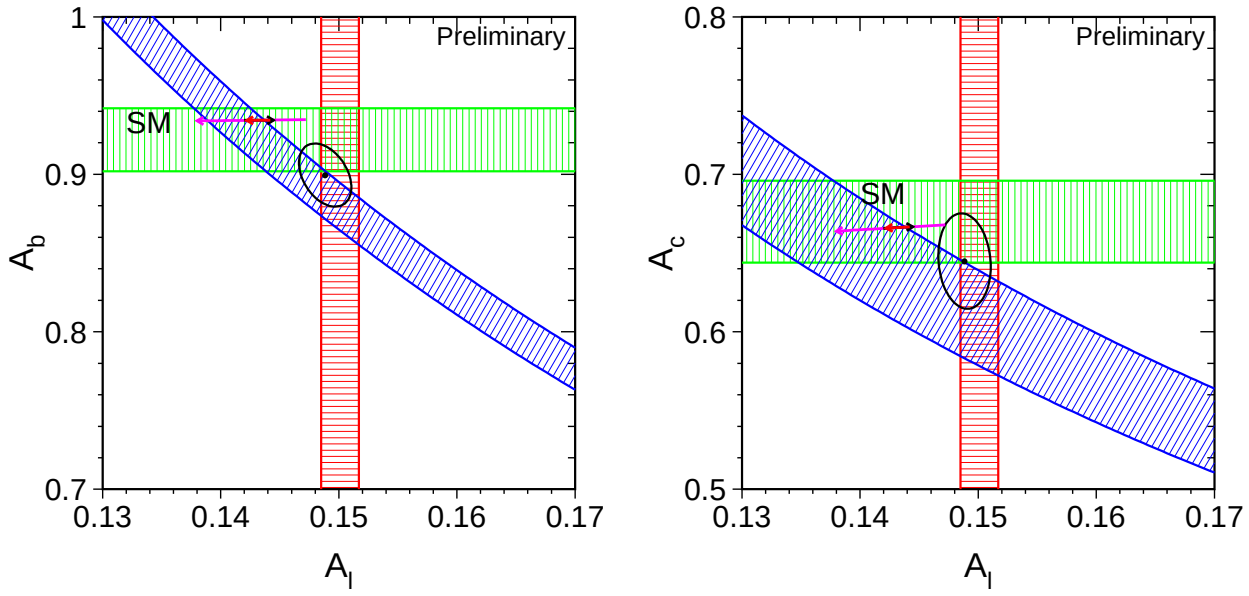

Figure 12.1: The measurements of the combined LEP+SLD $\mathcal{A}_\ell$ (vertical band), SLD $\mathcal{A}_\mathrm{b}$,$\mathcal{A}_\mathrm{c}$ (horizontal bands) and LEP $A_\mathrm{FB}^{0,\mathrm{b}}$,$A_\mathrm{FB}^{0,\mathrm{c}}$ (diagonal bands), compared to the Standard Model expectations (arrows). The arrow pointing to the left shows the variation in the Standard Model prediction for m_H in the range 300^{+700}_{-186} GeV, and the arrow pointing to the right for m_t in the range 174.3 ± 5.1 GeV. Varying the hadronic vacuum polarisation by $\Delta\alpha^{(5)}_\mathrm{had}(m_\mathrm{Z}^2) = 0.02761 \pm 0.00036$ yields an additional uncertainty on the Standard-Model prediction, oriented in direction of the Higgs-boson arrow and size corresponding to the top-quark arrow. Also shown is the 68% confidence level contour for the two asymmetry parameters resulting from the joint analyses. Although the $A_\mathrm{FB}^{0,\mathrm{b}}$ measurements prefer a high Higgs mass, the Standard Model fit to the full set of measurements prefers a low Higgs mass, for example because of the influence of $\mathcal{A}_\ell$.

In addition, the couplings analysis is extended to include also the heavy-flavour measurements as presented in Section 5.3. Assuming neutral-current lepton universality, the effective coupling constants are determined jointly for leptons as well as for b and c quarks. QCD corrections, modifying Equation 12.1, are taken from the Standard Model, as is also done to obtain the quark pole asymmetries, see Section 5.2.3.

The results are also reported in Table 12.3 and shown in Figure 12.3. The deviation of the b-quark couplings from the Standard-Model expectation is mainly caused by the combined value of $\mathcal{A}_\mathrm{b}$ being low as discussed in Section 12.1 and shown in Figure 12.1.

	Without Lepton Universality:	
	LEP	LEP+SLD
g_{Ae}	-0.50112 ± 0.00035	-0.50111 ± 0.00035
$g_{\mathrm{A}\mu}$	-0.50115 ± 0.00056	-0.50120 ± 0.00054
$g_{\mathrm{A}\tau}$	-0.50204 ± 0.00064	-0.50204 ± 0.00064
g_{Ve}	-0.0378 ± 0.0011	-0.03816 ± 0.00047
$g_{\mathrm{V}\mu}$	-0.0376 ± 0.0031	-0.0367 ± 0.0023
$g_{\mathrm{V}\tau}$	-0.0368 ± 0.0011	-0.0366 ± 0.0010
	Ratios of couplings:	
	LEP	LEP+SLD
$g_{\mathrm{A}\mu}/g_{\mathrm{Ae}}$	1.0001 ± 0.0014	1.0002 ± 0.0014
$g_{\mathrm{A}\tau}/g_{\mathrm{Ae}}$	1.0018 ± 0.0015	1.0019 ± 0.0015
$g_{\mathrm{V}\mu}/g_{\mathrm{Ve}}$	0.995 ± 0.096	0.962 ± 0.063
$g_{\mathrm{V}\tau}/g_{\mathrm{Ve}}$	0.973 ± 0.041	0.958 ± 0.029
	With Lepton Universality:	
	LEP	LEP+SLD
$g_{\mathrm{A}\ell}$	-0.50126 ± 0.00026	-0.50123 ± 0.00026
$g_{\mathrm{V}\ell}$	-0.03736 ± 0.00066	-0.03783 ± 0.00041
g_{ν}	$+0.50068 \pm 0.00075$	$+0.50068 \pm 0.00075$
	With Lepton Universality and Heavy Flavour Results:	
	LEP	LEP+SLD
$g_{\mathrm{A}\ell}$	-0.50126 ± 0.00026	-0.50125 ± 0.00026
g_{Ab}	-0.5179 ± 0.0078	-0.5146 ± 0.0051
g_{Ac}	$+0.5032 \pm 0.0079$	$+0.5043 \pm 0.0052$
$g_{\mathrm{V}\ell}$	-0.03736 ± 0.00066	-0.03751 ± 0.00037
g_{Vb}	-0.317 ± 0.012	-0.3221 ± 0.0077
g_{Vc}	$+0.173 \pm 0.011$	$+0.1843 \pm 0.0067$

Table 12.3: Results for the effective vector and axial-vector couplings derived from the LEP data and the combined LEP and SLD data without and with the assumption of lepton universality. Note that the results, in particular for b quarks, are highly correlated.

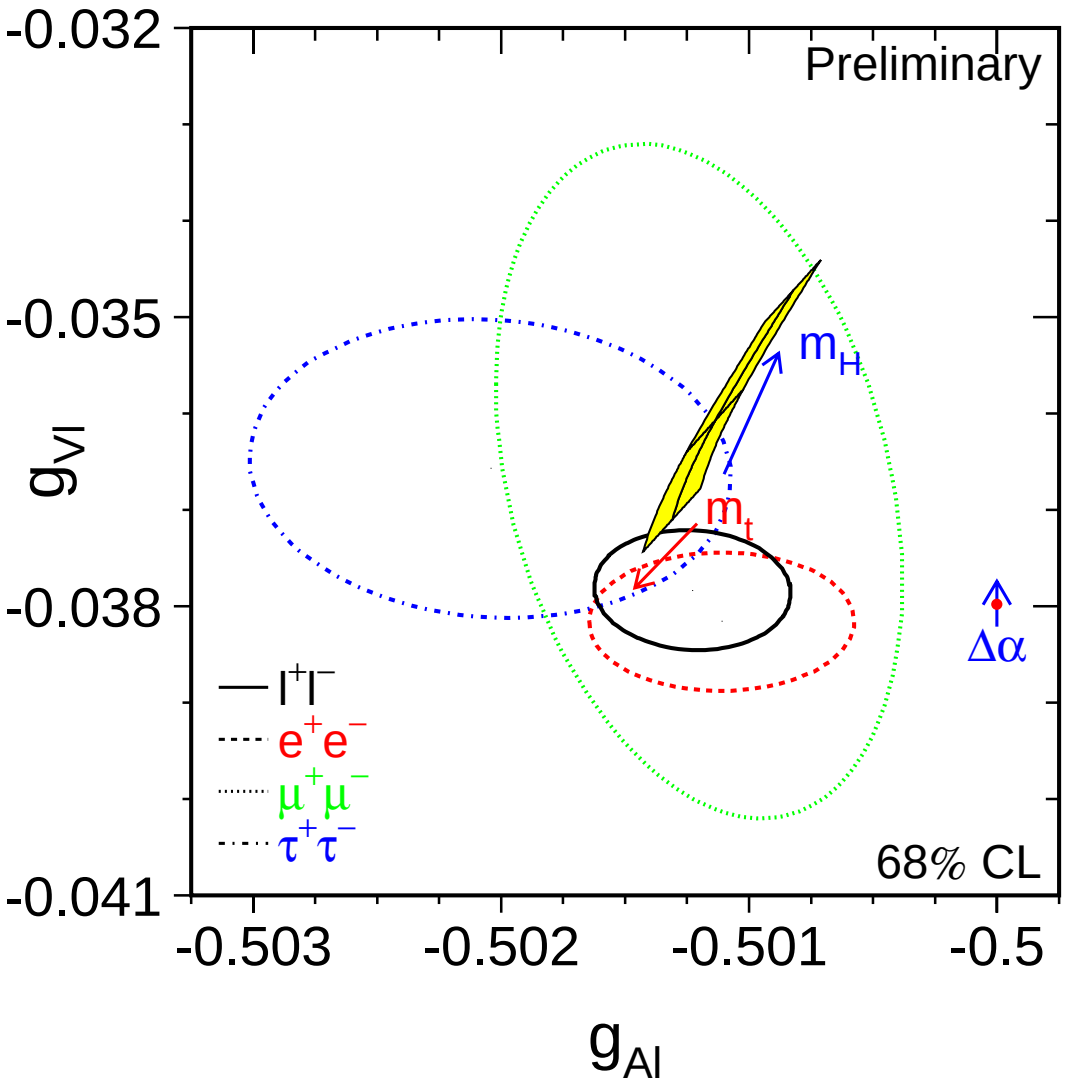

Figure 12.2: Contours of 68% probability in the $(g_{V\ell}, g_{A\ell})$ plane from LEP and SLD measurements. The solid contour results from a fit to the LEP and SLD results assuming lepton universality. The shaded region corresponds to the Standard Model prediction for $m_t = 174.3 \pm 5.1$ GeV and $m_H = 300^{+700}_{-186}$ GeV. The arrows point in the direction of increasing values of m_t and m_H. Varying the hadronic vacuum polarisation by $\Delta\alpha^{(5)}_{had}(m_Z^2) = 0.02761 \pm 0.00036$ yields an additional uncertainty on the Standard-Model prediction indicated by the corresponding arrow.

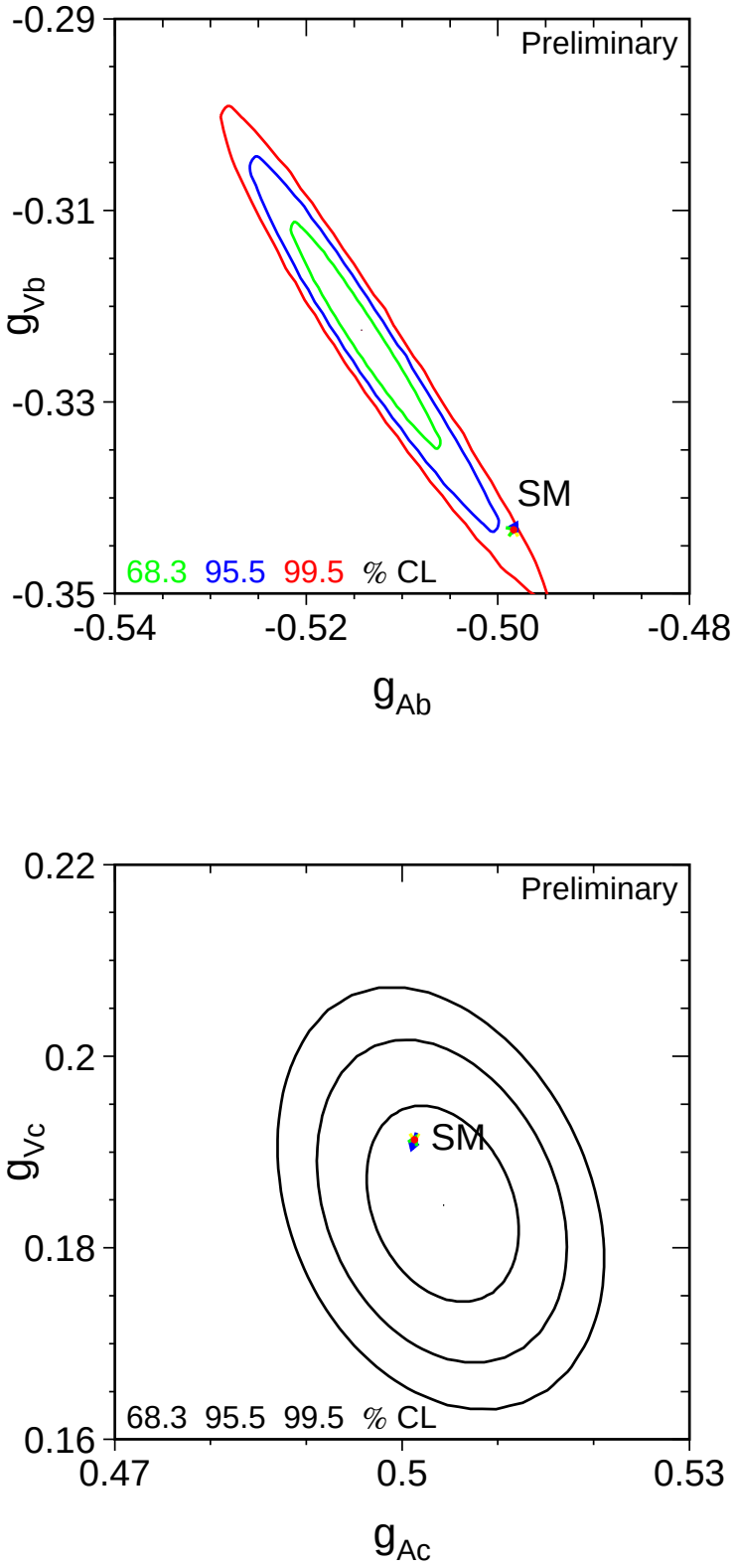

Figure 12.3: Contours of 68.3, 95.5 and 99.5% probability in the (g_{Vq}, g_{Aq}) plane from LEP and SLD measurements for b and c quarks and assuming lepton universality. The dot corresponds to the Standard Model prediction for $m_t = 174.3 \pm 5.1$ GeV, $m_H = 300^{+700}_{-186}$ GeV and $\Delta\alpha^{(5)}_{had}(m_Z^2) = 0.02761 \pm 0.00036$.

12.3 The Leptonic Effective Electroweak Mixing Angle $\sin^2\theta^{\rm lept}_{\rm eff}$

The asymmetry measurements from LEP and SLD can be combined into a single parameter, the effective electroweak mixing angle, $\sin^2\theta^{\rm lept}_{\rm eff}$, defined as:

$$\sin^2\theta^{\rm lept}_{\rm eff} \equiv \frac{1}{4}\left(1-\frac{g_{{\rm V}\ell}}{g_{{\rm A}\ell}}\right), \tag{12.2}$$

without making strong model-specific assumptions.

For a combined average of $\sin^2\theta^{\rm lept}_{\rm eff}$ from $A^{0,\ell}_{\rm FB}$, $\mathcal{A}_\tau$ and $\mathcal{A}_{\rm e}$ only the assumption of lepton universality, already inherent in the definition of $\sin^2\theta^{\rm lept}_{\rm eff}$, is needed. Also the value derived from the measurements of $\mathcal{A}_\ell$ from SLD is given. We also include the hadronic forward-backward asymmetries, assuming the difference between $\sin^2\theta^{\rm f}_{\rm eff}$ for quarks and leptons to be given by the Standard Model. This is justified within the Standard Model as the hadronic asymmetries $A^{0,\rm b}_{\rm FB}$ and $A^{0,\rm c}_{\rm FB}$ have a reduced sensitivity to the small non-universal corrections specific to the quark vertex. The results of these determinations of $\sin^2\theta^{\rm lept}_{\rm eff}$ and their combination are shown in Table 12.4 and in Figure 12.4. The combinations based on the leptonic results plus $\mathcal{A}_\ell$(SLD) and on the hadronic forward-backward asymmetries differ by 3.3 standard deviations, mainly caused by the two most precise measurements of $\sin^2\theta^{\rm lept}_{\rm eff}$, $\mathcal{A}_\ell$ (SLD) dominated by $A^0_{\rm LR}$, and $A^{0,\rm b}_{\rm FB}$ (LEP). This is the same effect as discussed already in sections 12.1 and 12.2 and shown in Figures 12.1 and 12.3: the deviation in $\mathcal{A}_{\rm b}$ as extracted from $A^{0,\rm b}_{\rm FB}$ discussed above is reflected in the value of $\sin^2\theta^{\rm lept}_{\rm eff}$ extracted from $A^{0,\rm b}_{\rm FB}$ in this analysis.

	$\sin^2\theta^{\rm lept}_{\rm eff}$	Average by Group of Observations	Cumulative Average	χ^2/d.o.f.
$A^{0,\ell}_{\rm FB}$	0.23099 ± 0.00053			
$\mathcal{A}_\ell$ $(\mathcal{P}_\tau)$	0.23159 ± 0.00041	0.23137 ± 0.00033		
$\mathcal{A}_\ell$ (SLD)	0.23098 ± 0.00026		0.23113 ± 0.00021	0.8/1
$A^{0,\rm b}_{\rm FB}$	0.23226 ± 0.00031			
$A^{0,\rm c}_{\rm FB}$	0.23272 ± 0.00079			
$\langle Q_{\rm FB}\rangle$	0.2324 ± 0.0012	0.23230 ± 0.00029	0.23152 ± 0.00017	12.8/5

Table 12.4: Determinations of $\sin^2\theta^{\rm lept}_{\rm eff}$ from asymmetries. The second column lists the $\sin^2\theta^{\rm lept}_{\rm eff}$ values derived from the quantities listed in the first column. The third column contains the averages of these numbers by groups of observations, where the groups are separated by the horizontal lines. The fourth column shows the cumulative averages. The χ^2 per degree of freedom for the cumulative averages is also given. The averages are performed including the small correlation between $A^{0,\rm b}_{\rm FB}$ and $A^{0,\rm c}_{\rm FB}$.

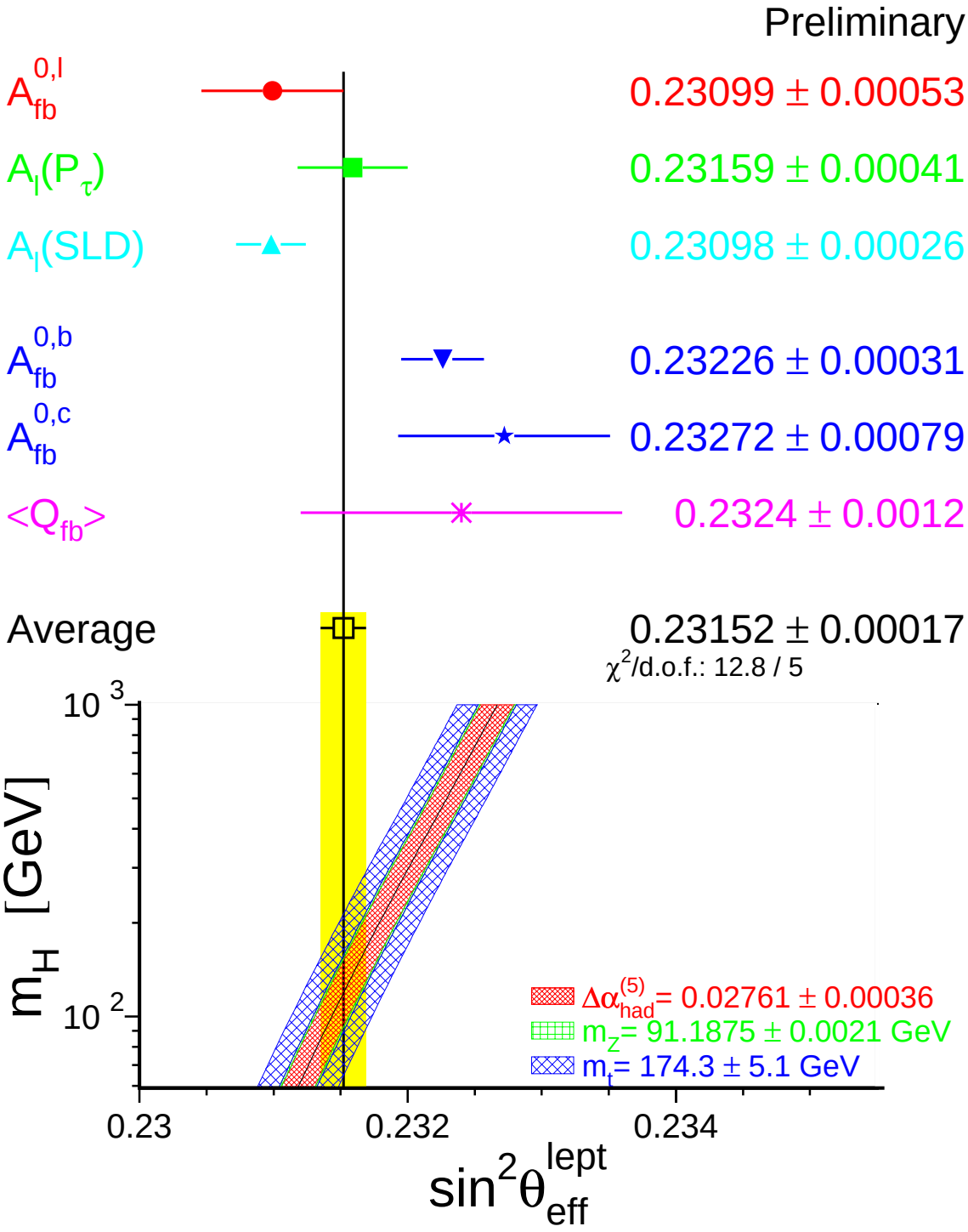

Figure 12.4: Comparison of several determinations of $\sin^2\theta_{\rm eff}^{\rm lept}$ from asymmetries. In the average, the small correlation between $A_{\rm FB}^{0,\rm b}$ and $A_{\rm FB}^{0,\rm c}$ is included. Also shown is the prediction of the Standard Model as a function of $m_{\rm H}$. The width of the Standard Model band is due to the uncertainties in $\Delta\alpha_{\rm had}^{(5)}(m_{\rm Z}^2)$ (see Chapter 13), $m_{\rm Z}$ and $m_{\rm t}$. The total width of the band is the linear sum of these effects.

Chapter 13

Constraints on the Standard Model

Updates with respect to summer 2000:
A new determination of the hadronic vacuum polarisation is used. For the first time, the atomic parity violation parameter measured in cesium is included in the analysis.

13.1 Introduction

The precise electroweak measurements performed at LEP and SLC and elsewhere can be used to check the validity of the Standard Model and, within its framework, to infer valuable information about its fundamental parameters. The accuracy of the measurements makes them sensitive to the mass of the top quark m_{t}, and to the mass of the Higgs boson m_{H} through loop corrections. While the leading m_{t} dependence is quadratic, the leading m_{H} dependence is logarithmic. Therefore, the inferred constraints on m_{H} are much weaker than those on m_{t}.

13.2 Measurements

The LEP and SLD measurements used are summarised in Table 13.1 together with the results of the Standard Model fit. Also shown are the results of measurements of m_{W} from UA2 [202], CDF [203,204], and DØ [205][1], measurements of the top quark mass by CDF [207] and DØ [208][2], measurements of the neutrino-nucleon neutral to charged current ratios from CCFR [210] and NuTeV [211], and measurements of atomic parity violation in cesium [212,213] with the numerical result taken from [214,215]. Although the combined preliminary[3] $\nu\mathcal{N}$ result is quoted in terms of $\sin^2\theta_{\mathrm{W}} = 1 - m_{\mathrm{W}}^2/m_{\mathrm{Z}}^2$, radiative corrections result in small m_{t} and m_{H} dependences[4] that are included in the fit. An additional input parameter, not shown in the table, is the Fermi constant G_F, determined from the μ lifetime, $G_F = 1.16637(1)\cdot 10^{-5}\mathrm{GeV}^{-2}$ [217]. The relative error of G_F is comparable to that of m_{Z}; both errors have negligible effects on the fit results.

[1] See Reference 206 for a combination of these m_{W} measurements.
[2] See Reference 209 for a combination of these m_{t} measurements.
[3] The final NuTeV result [216] is not used in this report as it was published only after the 2001 summer conferences.
[4] The formula used is $\delta\sin^2\theta_W = -0.00142\frac{m_{\mathrm{t}}^2-(175\mathrm{GeV})^2}{(100\mathrm{GeV})^2} + 0.00048\ln(\frac{m_{\mathrm{H}}}{150\mathrm{GeV}})$. See Reference 211 for details.

	Measurement with Total Error	Systematic Error	Standard Model fit	Pull
$\Delta\alpha^{(5)}_{\rm had}(m^2_{\rm Z})$ [218]	0.02761 ± 0.00036	0.00035	0.02774	-0.3
a) LEP				
line-shape and				
lepton asymmetries:				
$m_{\rm Z}$ [GeV]	91.1875 ± 0.0021	[a] 0.0017	91.1874	0.0
$\Gamma_{\rm Z}$ [GeV]	2.4952 ± 0.0023	[a] 0.0012	2.4963	-0.5
$\sigma^0_{\rm h}$ [nb]	41.540 ± 0.037	[b] 0.028	41.481	1.6
R^0_ℓ	20.767 ± 0.025	[b] 0.007	20.739	1.1
$A^{0,\ell}_{\rm FB}$	0.0171 ± 0.0010	[b] 0.0003	0.0165	0.7
+ correlation matrix Table 2.3				
τ polarisation:				
$\mathcal{A}_\ell$ ($\mathcal{P}_\tau$)	0.1465 ± 0.0033	0.0016	0.1483	-0.5
$q\overline{q}$ charge asymmetry:				
$\sin^2\theta^{\rm lept}_{\rm eff}$ ($\langle Q_{\rm FB}\rangle$)	0.2324 ± 0.0012	0.0010	0.2314	0.9
$m_{\rm W}$ [GeV]	80.450 ± 0.039	0.030	80.398	1.3
b) SLD [219]				
$\mathcal{A}_\ell$ (SLD)	0.1513 ± 0.0021	0.0010	0.1483	1.5
c) LEP and SLD Heavy Flavour				
$R^0_{\rm b}$	0.21646 ± 0.00065	0.00053	0.215743	1.1
$R^0_{\rm c}$	0.1719 ± 0.0031	0.0022	0.1723	-0.1
$A^{0,{\rm b}}_{\rm FB}$	0.0990 ± 0.0017	0.0009	0.1039	-2.9
$A^{0,{\rm c}}_{\rm FB}$	0.0685 ± 0.0034	0.0017	0.0743	-1.7
$\mathcal{A}_{\rm b}$	0.922 ± 0.020	0.016	0.935	-0.6
$\mathcal{A}_{\rm c}$	0.670 ± 0.026	0.016	0.668	0.1
+ correlation matrix Table 5.3				
d) $p\overline{p}$ and νN				
$m_{\rm W}$ [GeV] ($p\overline{p}$ [206])	80.454 ± 0.060	0.050	80.398	0.9
$\sin^2\theta_{\rm W}$ ($\nu\mathcal{N}$ [210,211])	0.2255 ± 0.0021	0.0010	0.2226	1.2
$m_{\rm t}$ [GeV] ($p\overline{p}$ [209])	174.3 ± 5.1	4.0	175.8	-0.3
$Q_{\rm W}$(Cs) [215]	-72.5 ± 0.7	0.6	-72.9	0.6

Table 13.1: Summary of measurements included in the combined analysis of Standard Model parameters. Section a) summarises LEP averages, Section b) SLD results ($\sin^2\theta^{\rm lept}_{\rm eff}$ includes $A_{\rm LR}$ and the polarised lepton asymmetries), Section c) the LEP and SLD heavy flavour results and Section d) electroweak measurements from $p\overline{p}$ colliders and νN scattering. The total errors in column 2 include the systematic errors listed in column 3. Although the systematic errors include both correlated and uncorrelated sources, the determination of the systematic part of each error is approximate. The Standard Model results in column 4 and the pulls (difference between measurement and fit in units of the total measurement error) in column 5 are derived from the Standard Model fit including all data (Table 13.2, column 5) with the Higgs mass treated as a free parameter.

[a] The systematic errors on $m_{\rm Z}$ and $\Gamma_{\rm Z}$ contain the errors arising from the uncertainties in the LEP energy only.

[b] Only common systematic errors are indicated.

13.3 Theoretical and Parametric Uncertainties

Detailed studies of the theoretical uncertainties in the Standard Model predictions due to missing higher-order electroweak corrections and their interplay with QCD corrections are carried out in the working group on 'Precision calculations for the Z resonance' [220], and more recently in [15]. Theoretical uncertainties are evaluated by comparing different but, within our present knowledge, equivalent treatments of aspects such as resummation techniques, momentum transfer scales for vertex corrections and factorisation schemes. The effects of these theoretical uncertainties are reduced by the inclusion of higher-order corrections [221,222] in the electroweak libraries [223].

The recently calculated complete fermionic two-loop corrections on $m_{\rm W}$ [224] are currently only used in the determination of the theoretical uncertainty. Their effect on $m_{\rm W}$ is small compared to the current experimental uncertainty on $m_{\rm W}$, however, the naive propagation of this new $m_{\rm W}$ to $\sin^2\theta^{\rm lept}_{\rm eff} = \kappa(1 - m^2_{\rm W}/m^2_{\rm Z})$, keeping the electroweak form-factor κ unmodified, shows a more visible effect as $\sin^2\theta^{\rm lept}_{\rm eff}$ is measured very precisely. Thus the corresponding calculations for $\sin^2\theta^{\rm lept}_{\rm eff}$ (or κ) and for the partial Z widths are urgently needed; in particular since partial cancellations of these new corrections in the product $\kappa(1 - m^2_{\rm W}/m^2_{\rm Z}) = \sin^2\theta^{\rm lept}_{\rm eff}$ are expected [225].

The use of the new QCD corrections [222] increases the value of $\alpha_{\rm S}(m^2_{\rm Z})$ by 0.001, as expected. The effects of missing higher-order QCD corrections on $\alpha_{\rm S}(m^2_{\rm Z})$ covers missing higher-order electroweak corrections and uncertainties in the interplay of electroweak and QCD corrections and is estimated to be at least 0.002 [226]. A discussion of theoretical uncertainties in the determination of $\alpha_{\rm S}$ can be found in References 220 and 226. The determination of the size of remaining theoretical uncertainties is under continued study.

The theoretical errors discussed above are not included in the results presented in Table 13.2. At present the impact of theoretical uncertainties on the determination of Standard Model parameters from the precise electroweak measurements is small compared to the error due to the uncertainty in the value of $\alpha(m^2_{\rm Z})$, which is included in the results.

The uncertainty in $\alpha(m^2_{\rm Z})$ arises from the contribution of light quarks to the photon vacuum polarisation ($\Delta\alpha^{(5)}_{\rm had}(m^2_{\rm Z})$):

$$\alpha(m^2_{\rm Z}) = \frac{\alpha(0)}{1 - \Delta\alpha_\ell(m^2_{\rm Z}) - \Delta\alpha^{(5)}_{\rm had}(m^2_{\rm Z}) - \Delta\alpha_{\rm top}(m^2_{\rm Z})}\,, \tag{13.1}$$

where $\alpha(0) = 1/137.036$. The top contribution, $-0.00007(1)$, depends on the mass of the top quark, and is therefore determined inside the electroweak libraries [223]. The leptonic contribution is calculated to third order [227] to be 0.03150, with negligible uncertainty.

For the hadronic contribution, we no longer use the value 0.02804 ± 0.00065 [228], but rather the new evaluation 0.02761 ± 0.0036 [218] which takes into account the recently published results on electron-positron annihilations into hadrons at low centre-of-mass energies by the BES collaboration [229]. This reduced uncertainty still causes an error of 0.00013 on the Standard Model prediction of $\sin^2\theta^{\rm lept}_{\rm eff}$, and errors of 0.2 GeV and 0.1 on the fitted values of $m_{\rm t}$ and $\log(m_{\rm H})$, all included in the results presented below. The effect on the Standard Model prediction for $\Gamma_{\ell\ell}$ is negligible. The $\alpha_{\rm S}(m^2_{\rm Z})$ values for the Standard Model fits presented in this Section are stable against a variation of $\alpha(m^2_{\rm Z})$ in the interval quoted.

There are also several evaluations of $\Delta\alpha^{(5)}_{\rm had}(m^2_{\rm Z})$ [230–237] which are more theory-driven. One of the most recent of these (Reference 236) also includes the new results from BES, yielding $0.02738 \pm$

0.00020. To show the effects of the uncertainty of $\alpha(m_Z^2)$, we also use this evaluation of the hadronic vacuum polarisation. Note that all these evaluations obtain values for $\Delta\alpha^{(5)}_{\rm had}(m_Z^2)$ consistently lower than - but still in agreement with - the old value of 0.02804 ± 0.00065.

13.4 Selected Results

Figure 13.1 shows a comparison of the leptonic partial width from LEP (Table 2.4) and the effective electroweak mixing angle from asymmetries measured at LEP and SLD (Table 12.4), with the Standard Model. Good agreement with the Standard Model prediction is observed. The point with the arrow shows the prediction if among the electroweak radiative corrections only the photon vacuum polarisation is included, which shows an that LEP+SLD data are sensitive to non-trivial electroweak corrections. Note that the error due to the uncertainty on $\alpha(m_Z^2)$ (shown as the length of the arrow) is not much smaller than the experimental error on $\sin^2\theta^{\rm lept}_{\rm eff}$ from LEP and SLD. This underlines the continued importance of a precise measurement of $\sigma(e^+e^- \to \text{hadrons})$ at low centre-of-mass energies.

Of the measurements given in Table 13.1, R^0_ℓ is one of the most sensitive to QCD corrections. For $m_Z = 91.1875$ GeV, and imposing $m_t = 174.3 \pm 5.1$ GeV as a constraint, $\alpha_S = 0.1224 \pm 0.0038$ is obtained. Alternatively, σ^0_ℓ (see Table 2.4) which has higher sensitivity to QCD corrections and less dependence on m_H yields: $\alpha_S = 0.1180 \pm 0.0030$. Typical errors arising from the variation of m_H between 100 GeV and 200 GeV are of the order of 0.001, somewhat smaller for σ^0_ℓ. These results on α_S, as well as those reported in the next section, are in very good agreement with recently determined world averages ($\alpha_S(m_Z^2) = 0.118 \pm 0.002$ [131], or $\alpha_S(m_Z^2) = 0.1178 \pm 0.0033$ based solely on NNLO QCD results excluding the LEP lineshape results and accounting for correlated errors [238]).

13.5 Standard Model Analyses

In the following, several different Standard Model fits to the data reported in Table 13.2 are discussed. The χ^2 minimisation is performed with the program MINUIT [239], and the predictions are calculated with TOPAZ0 [240] and ZFITTER [37]. The large χ^2/d.o.f. for all of these fits is caused by the same effect as discussed in the previous chapter, namely the large dispersion in the values of the leptonic effective electroweak mixing angle measured through the various asymmetries. For the analyses presented here, this dispersion is interpreted as a fluctuation in one or more of the input measurements, and thus we neither modify nor exclude any of them.

To test the agreement between the LEP data and the Standard Model, a fit to the data (including the LEP-II m_W determination) leaving the top quark mass and the Higgs mass as free parameters is performed. The result is shown in Table 13.2, column 1. This fit shows that the LEP data predicts the top mass in good agreement with the direct measurements. In addition, the data prefer an intermediate Higgs boson mass, albeit with very large errors. The strongly asymmetric errors on m_H are due to the fact that to first order, the radiative corrections in the Standard Model are proportional to $\log(m_H)$.

The data can also be used within the Standard Model to determine the top quark and W masses indirectly, which can be compared to the direct measurements performed at the $p\overline{p}$ colliders and LEP-II. In the second fit, all the results in Table 13.1, except the LEP-II and $p\overline{p}$ colliders m_W and m_t results are used. The results are shown in column 2 of Table 13.2. The indirect measurements of m_W and m_t from this data sample are shown in Figure 13.2, compared with the direct measurements. Also shown are the Standard Model predictions for Higgs masses between 114 and 1000 GeV. As can

be seen in the figure, the indirect and direct measurements of $m_{\rm W}$ and $m_{\rm t}$ are in good agreement, and both sets prefer a low value of the Higgs mass.

For the third fit, the direct $m_{\rm t}$ measurement is used to obtain the best indirect determination of $m_{\rm W}$. The result is shown in column 3 of Table 13.2 and in Figure 13.3. Also here, the indirect determination of W boson mass 80.373 ± 0.023 GeV is in agreement with the combination of direct measurements from LEP-II and $\rm p\overline{p}$ colliders [206] of $m_{\rm W} = 80.451 \pm 0.033$ GeV. For the next fit, (column 4 of Table 13.2 and Figure 13.4), the direct $m_{\rm W}$ measurements from LEP and $\rm p\overline{p}$ colliders are included to obtain $m_{\rm t} = 181^{+11}_{-9}$ GeV, in very good agreement with the direct measurement of $m_{\rm t} = 174.3 \pm 5.1$ GeV. Compared to the second fit, the error on $\log m_{\rm H}$ increases due to effects from higher-order terms.

Finally, the best constraints on $m_{\rm H}$ are obtained when all data are used in the fit. The results of this fit are shown in column 5 of Table 13.2 and Figure 13.5. In Figure 13.5 the observed value of $\Delta\chi^2 \equiv \chi^2 - \chi^2_{\rm min}$ as a function of $m_{\rm H}$ is plotted for the fit including all data. The solid curve is the result using ZFITTER, and corresponds to the last column of Table 13.2. The shaded band represents the uncertainty due to uncalculated higher-order corrections, as estimated by ZFITTER and TOPAZ0. Compared to previous analyses, its width is enlarged towards lower Higgs-boson masses due to the effects of the complete fermionic two-loop calculation of $m_{\rm W}$ discussed above. The 95% confidence level upper limit on $m_{\rm H}$ (taking the band into account) is 196 GeV. The lower limit on $m_{\rm H}$ of approximately 114 GeV obtained from direct searches [241] is not used in the determination of this limit. Also shown is the result (dashed curve) obtained when using $\Delta\alpha^{(5)}_{\rm had}(m^2_{\rm Z})$ of Reference 236. That fit results in $\log(m_{\rm H}/{\rm GeV}) = 2.03 \pm 0.19$ corresponding to $m_{\rm H} = 106^{+57}_{-38}$ GeV and an upper limit on $m_{\rm H}$ of approximately 222 GeV at 95% confidence level.

In Figures 13.6 to 13.8 the sensitivity of the LEP and SLD measurements to the Higgs mass is shown. As can be seen, the most sensitive measurements are the asymmetries, *i.e.*, $\sin^2\theta^{\rm lept}_{\rm eff}$. A reduced uncertainty for the value of $\alpha(m^2_{\rm Z})$ would therefore result in an improved constraint on $\log m_{\rm H}$ and thus $m_{\rm H}$, as already shown in Figures 13.1 and 13.5.

	- 1 - LEP including LEP-II m_{W}	- 2 - all data except m_{W} and m_{t}	- 3 - all data except m_{W}	- 4 - all data except m_{t}	- 5 - all data
m_{t} [GeV]	186^{+13}_{-11}	169^{+12}_{-9}	$173.3^{+4.7}_{-4.6}$	181^{+11}_{-9}	$175.8^{+4.4}_{-4.3}$
m_{H} [GeV]	260^{+404}_{-155}	81^{+109}_{-40}	108^{+70}_{-44}	126^{+182}_{-69}	88^{+53}_{-35}
$\log(m_{\mathrm{H}}/\mathrm{GeV})$	$2.42^{+0.41}_{-0.39}$	$1.91^{+0.37}_{-0.29}$	$2.03^{+0.22}_{-0.23}$	$2.10^{+0.39}_{-0.34}$	$1.94^{+0.21}_{-0.22}$
$\alpha_{\mathrm{S}}(m_{\mathrm{Z}}^2)$	0.1201 ± 0.0030	0.1187 ± 0.0027	0.1189 ± 0.0027	0.1186 ± 0.0028	0.1183 ± 0.0027
χ^2/d.o.f.	15.5/8	18.9/12	19.1/13	22.6/14	22.9/15
$\sin^2\theta_{\mathrm{eff}}^{\mathrm{lept}}$	0.23162	0.23150	0.23151	0.23139	0.23136
	± 0.00018	± 0.00016	± 0.00016	± 0.00015	± 0.00014
$\sin^2\theta_{\mathrm{W}}$	0.22282	0.22333	0.22313	0.22248	0.22263
	± 0.00051	± 0.00063	± 0.00045	± 0.00045	± 0.00036
m_{W} [GeV]	80.389 ± 0.026	80.363 ± 0.032	80.373 ± 0.023	80.406 ± 0.023	80.398 ± 0.019

Table 13.2: Results of the fits to: (1) LEP data alone, (2) all data except the direct determinations of m_{t} and m_{W} ($\mathrm{p\overline{p}}$ collider and LEP-II), (3) all data except direct m_{W} determinations, (4) all data except direct m_{t} determinations, and (5) all data. As the sensitivity to m_{H} is logarithmic, both m_{H} as well as $\log(m_{\mathrm{H}}/\mathrm{GeV})$ are quoted. The bottom part of the table lists derived results for $\sin^2\theta_{\mathrm{eff}}^{\mathrm{lept}}$, $\sin^2\theta_{\mathrm{W}}$ and m_{W}. See text for a discussion of theoretical errors not included in the errors above.

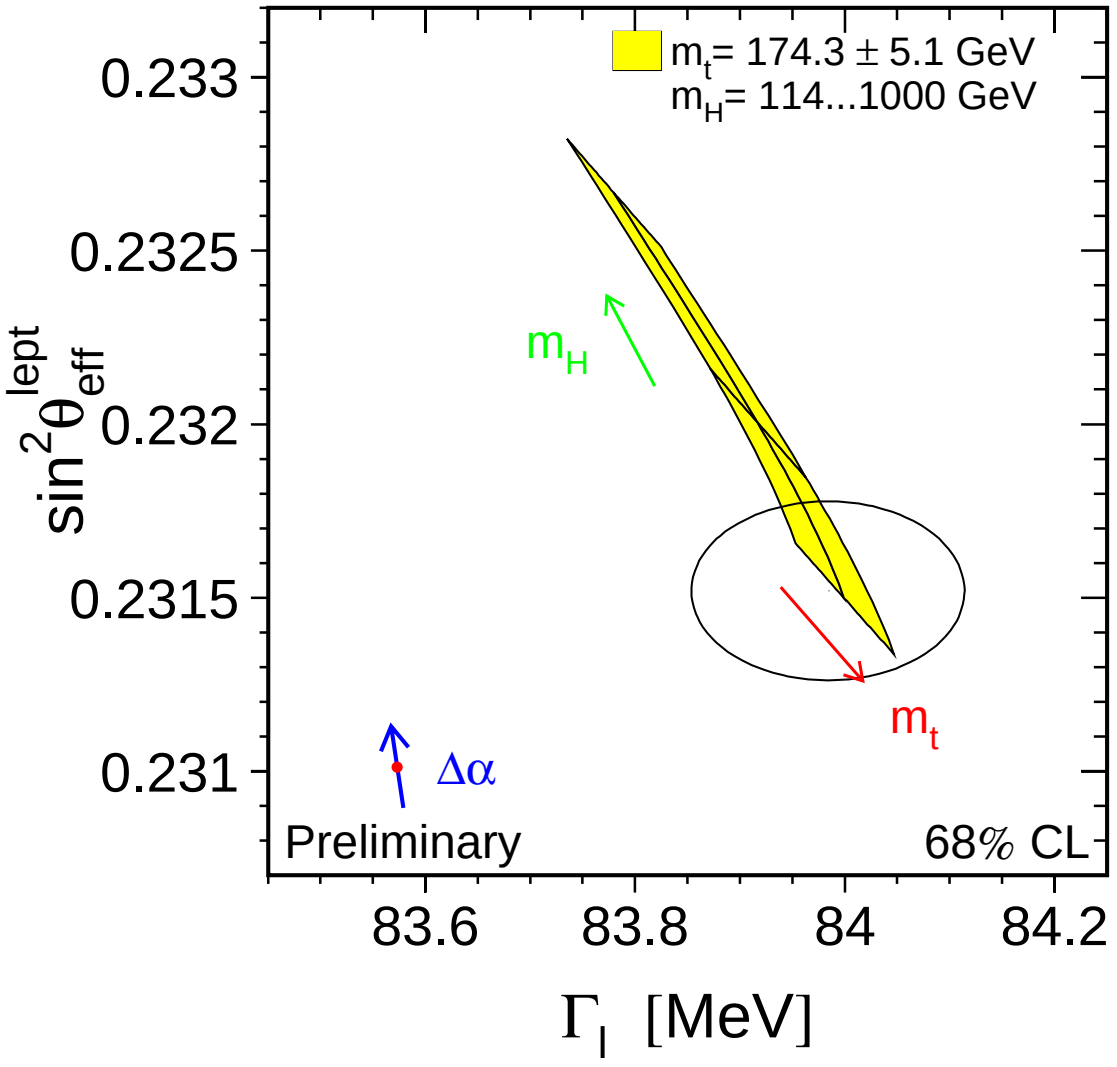

Figure 13.1: LEP-I+SLD measurements of $\sin^2\theta^{\rm lept}_{\rm eff}$ (Table 12.4) and $\Gamma_{\ell\ell}$ (Table 2.4) and the Standard Model prediction. The point shows the predictions if among the electroweak radiative corrections only the photon vacuum polarisation is included. The corresponding arrow shows variation of this prediction if $\alpha(m_{\rm Z}^2)$ is changed by one standard deviation. This variation gives an additional uncertainty to the Standard Model prediction shown in the figure.

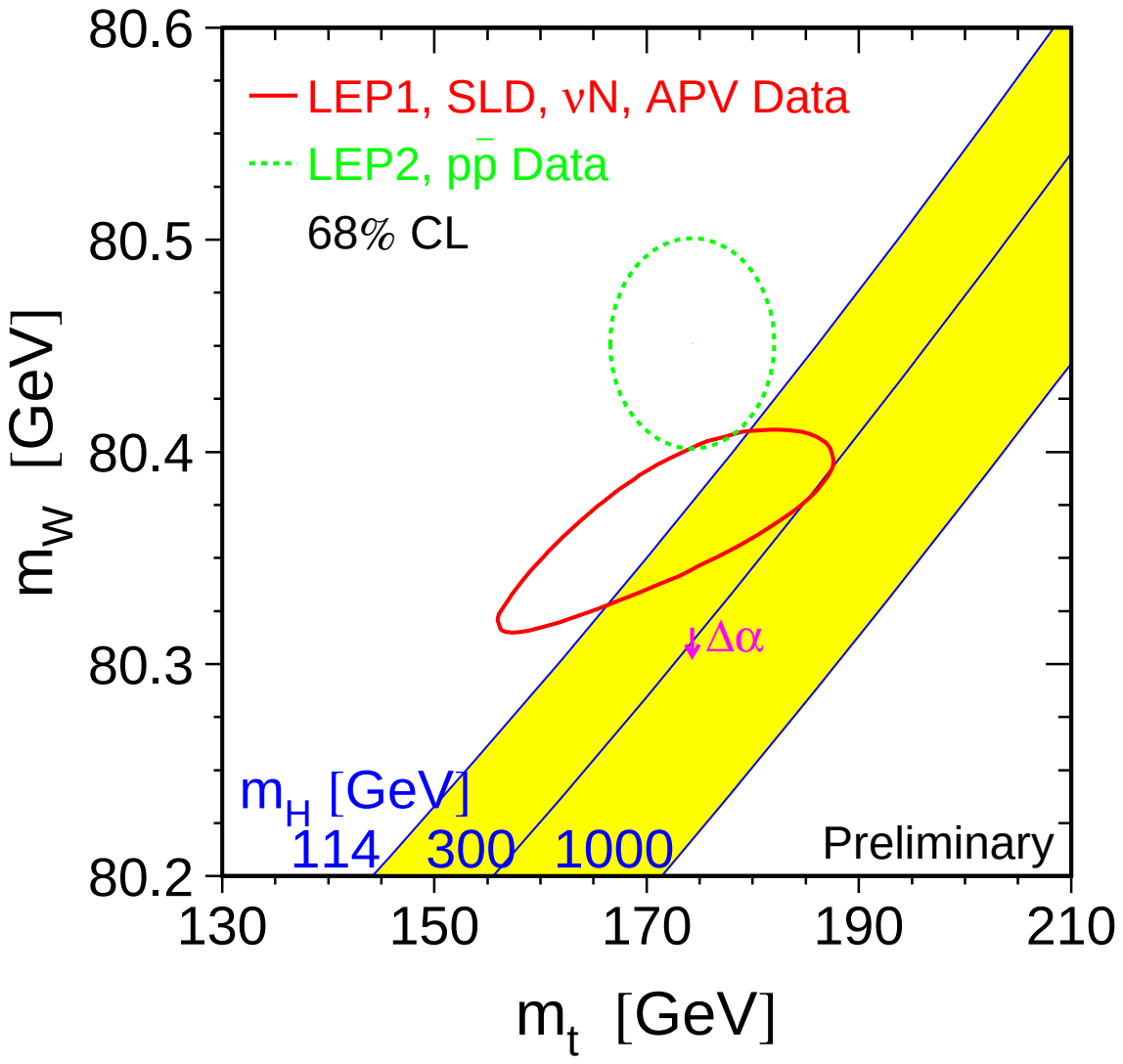

Figure 13.2: The comparison of the indirect measurements of m_{W} and m_{t} (LEP-I+SLD+νN+APV data) (solid contour) and the direct measurements ($\mathrm{p\overline{p}}$ colliders and LEP-II data) (dashed contour). In both cases the 68% CL contours are plotted. Also shown is the Standard Model relationship for the masses as a function of the Higgs mass.

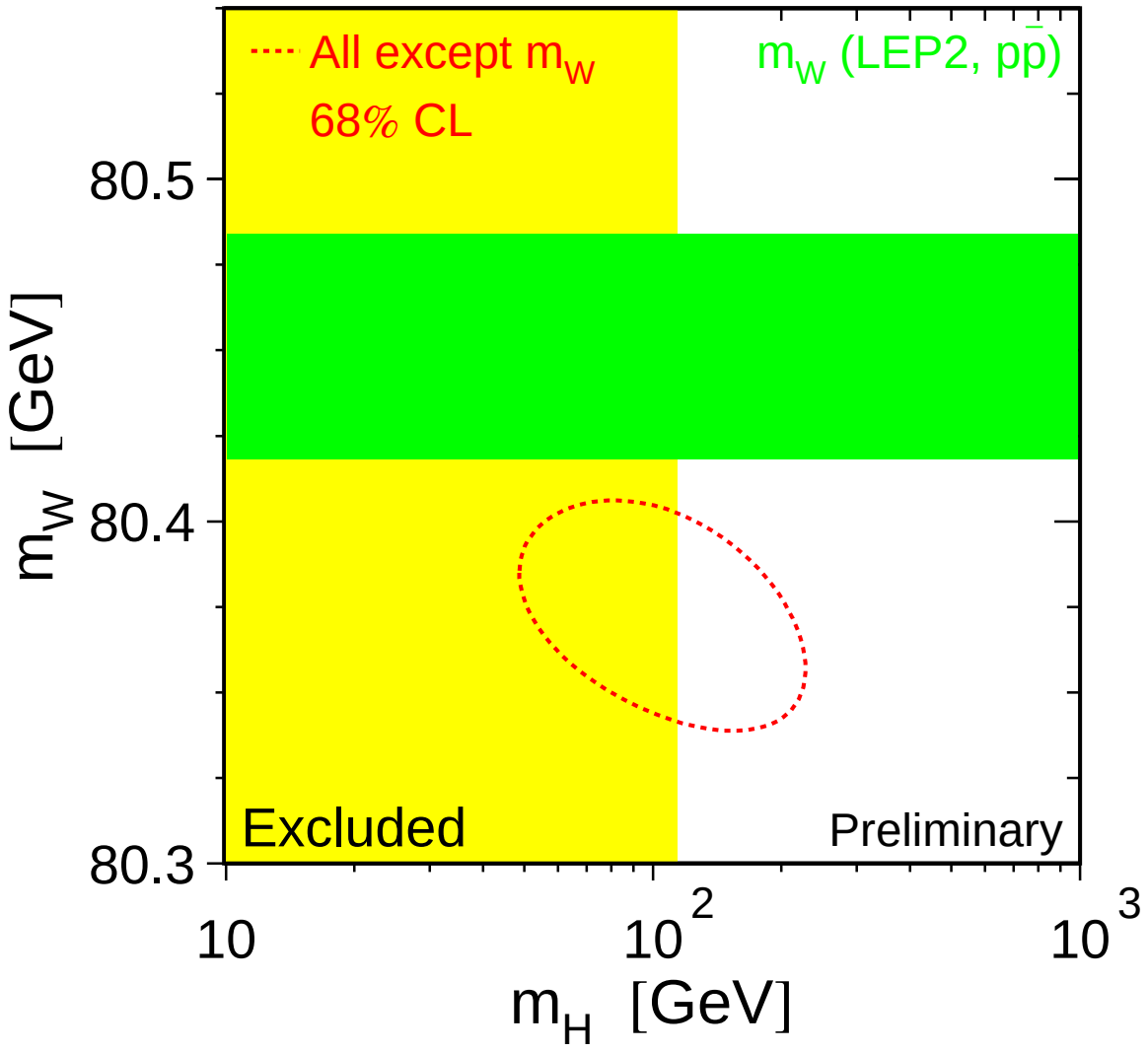

Figure 13.3: The 68% confidence level contour in m_{t} and m_{W} for the fit to all data except the direct measurement of m_{W}, indicated by the shaded horizontal band of ± 1 sigma width. The vertical band shows the 95% CL exclusion limit on m_{H} from the direct search.

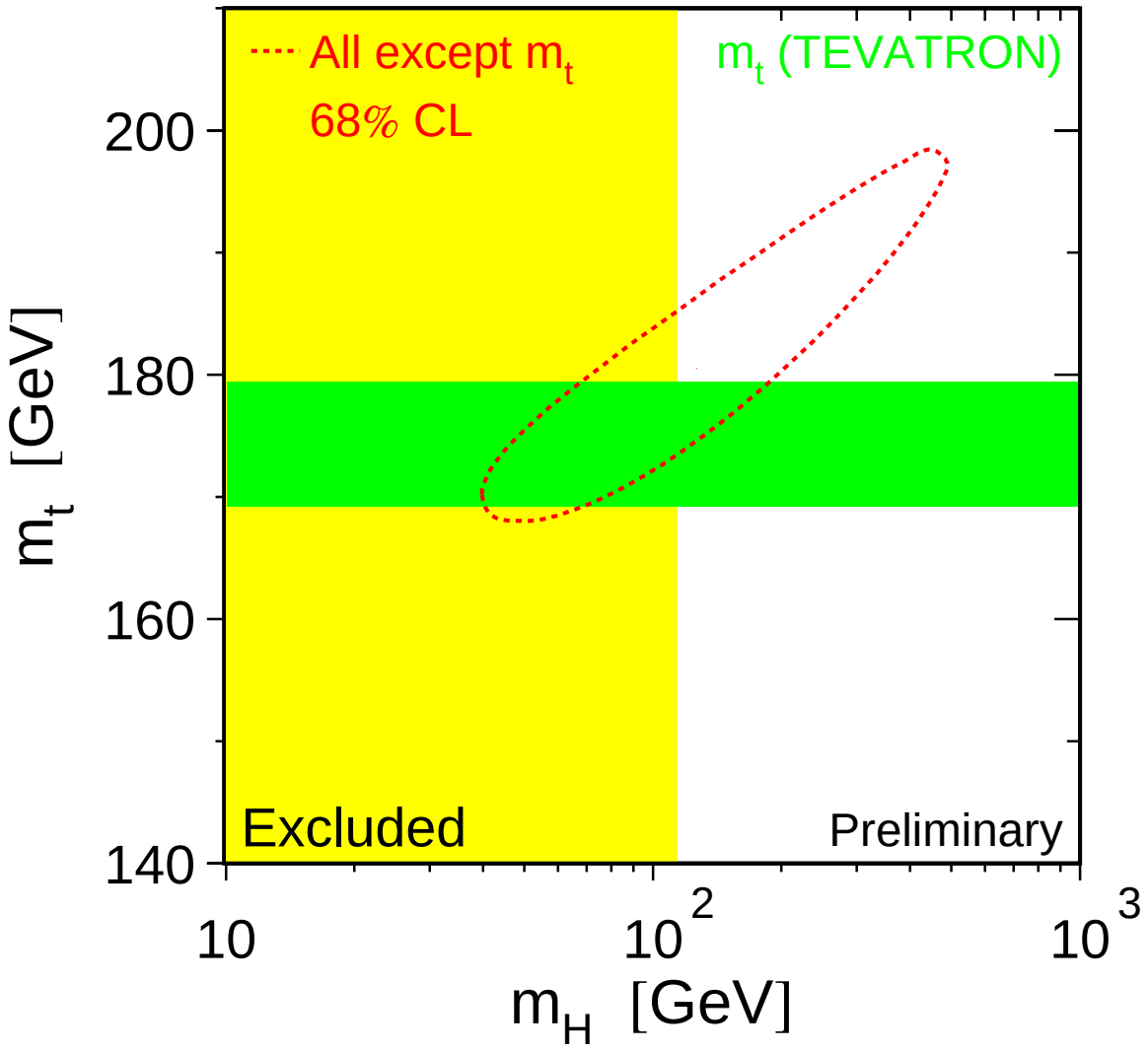

Figure 13.4: The 68% confidence level contour in $m_{\rm t}$ and $m_{\rm H}$ for the fit to all data except the direct measurement of $m_{\rm t}$, indicated by the shaded horizontal band of ± 1 sigma width. The vertical band shows the 95% CL exclusion limit on $m_{\rm H}$ from the direct search.

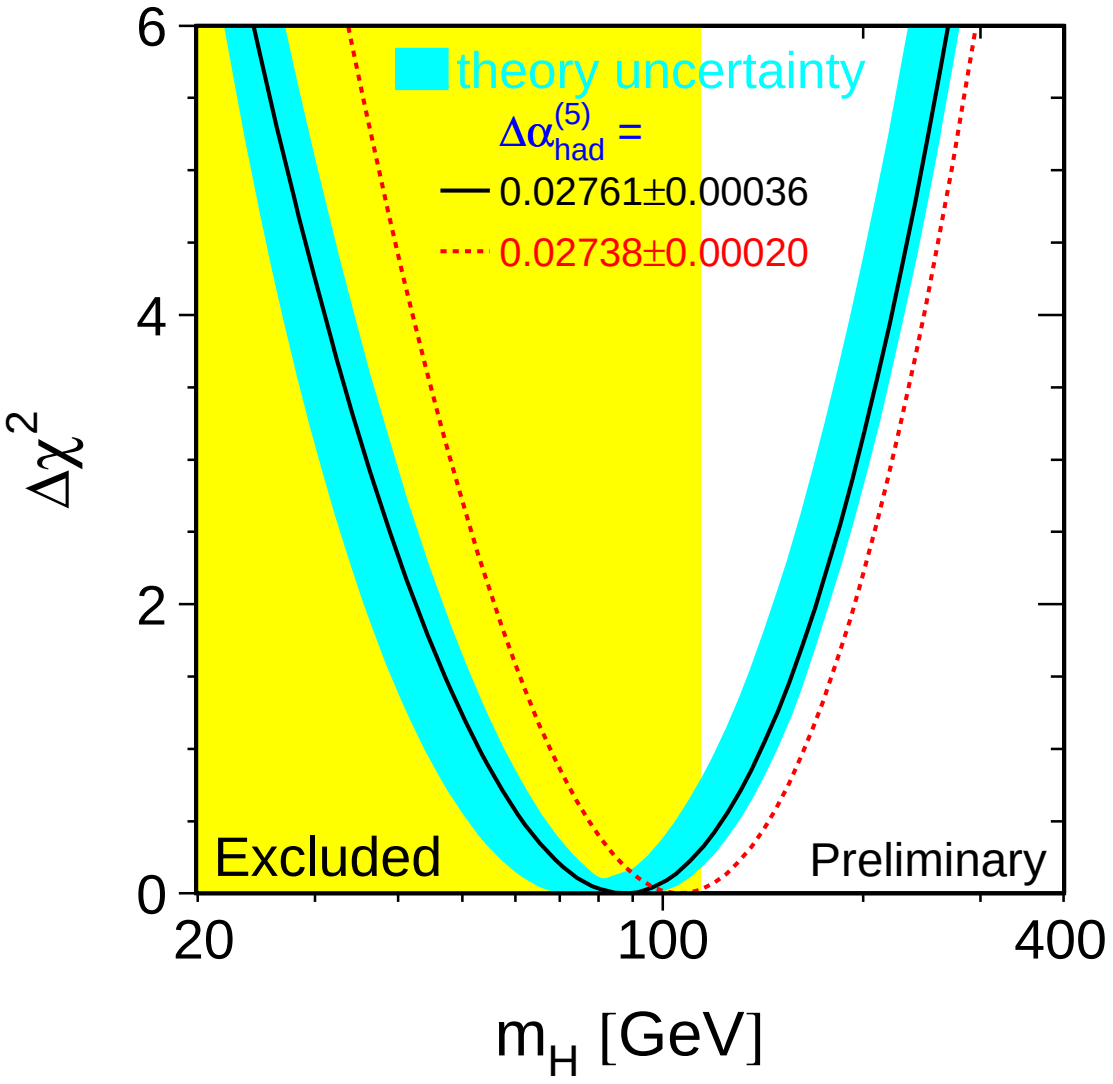

Figure 13.5: $\Delta\chi^2 = \chi^2 - \chi^2_{min}$ *vs.* $m_{\rm H}$ curve. The line is the result of the fit using all data (last column of Table 13.2); the band represents an estimate of the theoretical error due to missing higher order corrections. The vertical band shows the 95% CL exclusion limit on $m_{\rm H}$ from the direct search. The dashed curve is the result obtained using the evaluation of $\Delta\alpha^{(5)}_{\rm had}(m^2_{\rm Z})$ from Reference 236.

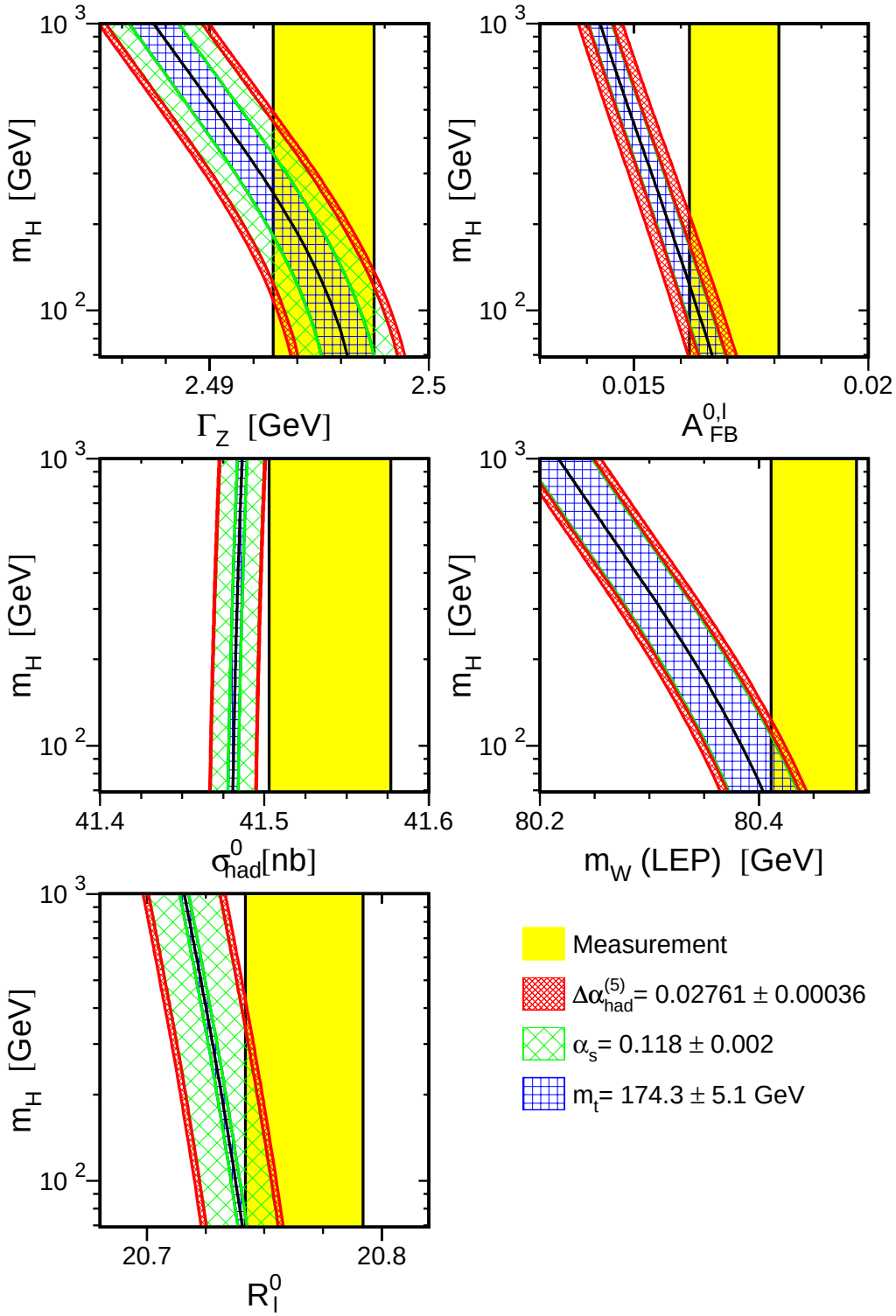

Figure 13.6: Comparison of LEP-I measurements with the Standard Model prediction as a function of m_{H}. The measurement with its error is shown as the vertical band. The width of the Standard Model band is due to the uncertainties in $\Delta\alpha^{(5)}_{\mathrm{had}}(m^2_{\mathrm{Z}})$, $\alpha_{\mathrm{S}}(m^2_{\mathrm{Z}})$ and m_{t}. The total width of the band is the linear sum of these effects.

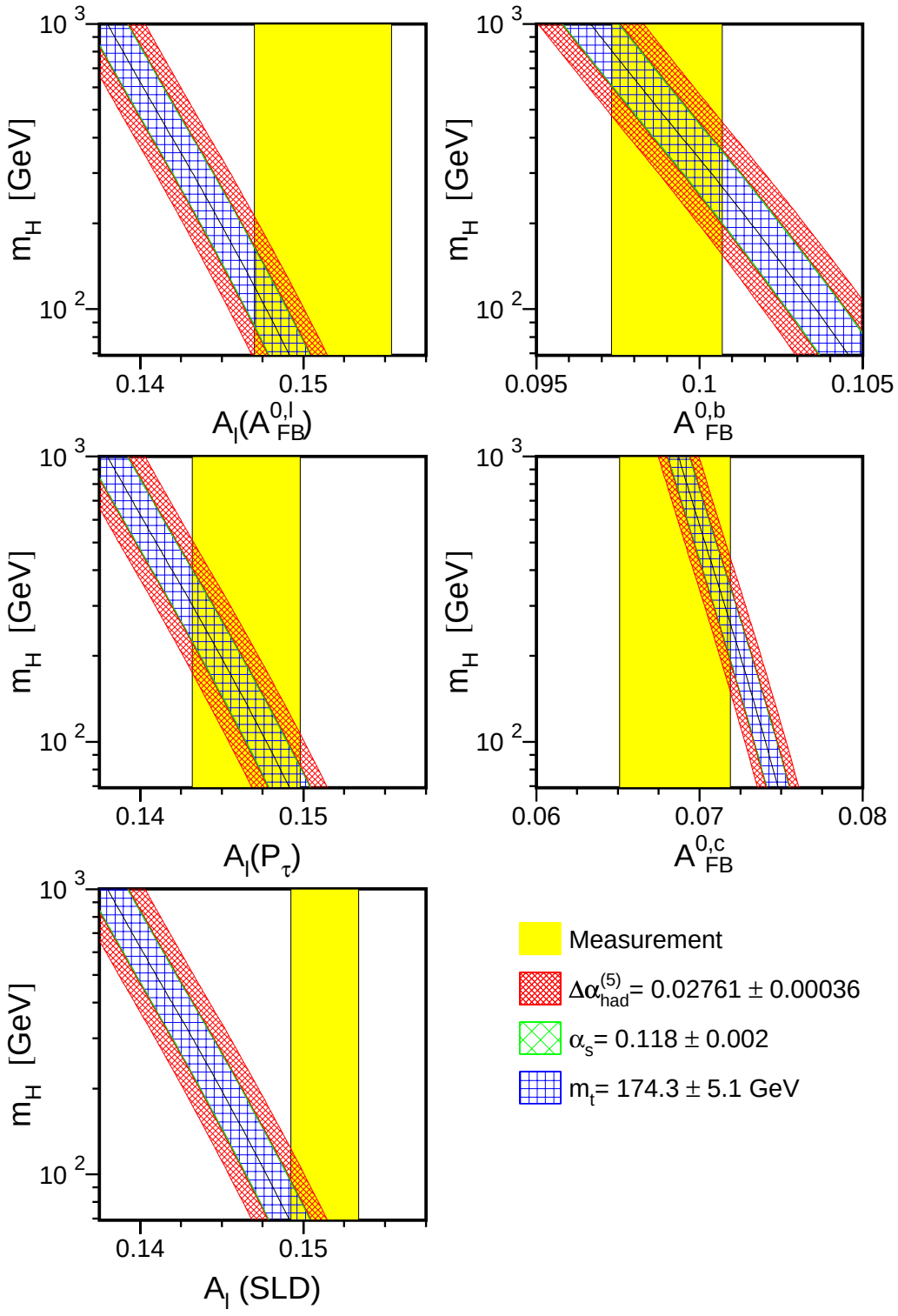

Figure 13.7: Comparison of LEP-I measurements with the Standard Model prediction as a function of $m_{\rm H}$. The measurement with its error is shown as the vertical band. The width of the Standard Model band is due to the uncertainties in $\Delta\alpha^{(5)}_{\rm had}(m^2_{\rm Z})$, $\alpha_{\rm S}(m^2_{\rm Z})$ and $m_{\rm t}$. The total width of the band is the linear sum of these effects. Also shown is the comparison of the SLD measurement of $\mathcal{A}_\ell$, dominated by $A^0_{\rm LR}$, with the Standard Model.

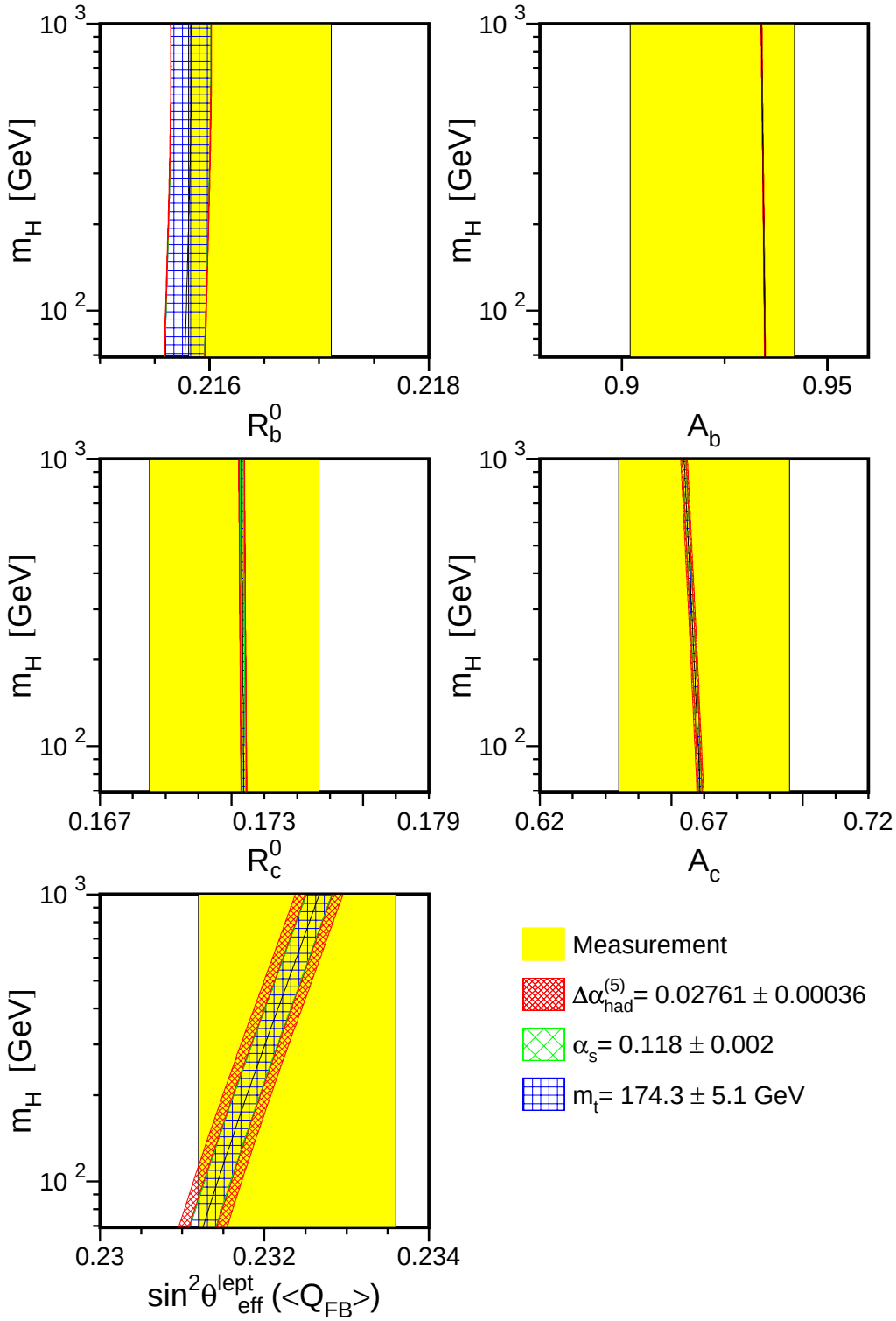

Figure 13.8: Comparison of LEP-I and SLD measurements with the Standard Model prediction as a function of $m_{\rm H}$. The measurement with its error is shown as the vertical band. The width of the Standard Model band is due to the uncertainties in $\Delta\alpha^{(5)}_{\rm had}(m_{\rm Z}^2)$, $\alpha_{\rm S}(m_{\rm Z}^2)$ and $m_{\rm t}$. The total width of the band is the linear sum of these effects.

Chapter 14

Conclusions

The combination of the many precise electroweak results yields stringent constraints on the Standard Model. In addition, the results are sensitive to the Higgs mass. Most measurements agree well with the predictions. The spread in values of the various determinations of the effective electroweak mixing angle is larger than expected. Within the Standard Model analysis, this seems to be caused by the measurement of the forward-backward asymmetry in b-quark production, showing the largest deviation w.r.t. the Standard-Model expectation.

The experiments wish to stress that this report reflects a preliminary status at the time of the 2001 summer conferences. A definitive statement on these results must wait for publication by each collaboration.

Prospects for the Future

Most of the measurements from data taken at or near the Z resonance, both at LEP as well as at SLC, that are presented in this report are either final or are being finalised. The main improvements will therefore take place in the high energy data, with more than 700 pb^{-1} per experiment. The measurements of m_{W} are likely to reach a precision not too far from the uncertainty on the prediction obtained via the radiative corrections of the Z data, providing a further important test of the Standard Model. In the measurement of the triple and quartic electroweak gauge boson self couplings, the analysis of the complete LEP-II statistics, together with the increased sensitivity at higher beam energies, will lead to an improvement in the current precision.

Acknowledgements

We would like to thank the CERN accelerator divisions for the efficient operation of the LEP accelerator, the precise information on the absolute energy scale and their close cooperation with the four experiments. The SLD collaboration would like to thank the SLAC accelerator department for the efficient operation of the SLC accelerator. We would also like to thank members of the CDF, DØ and NuTeV Collaborations for making preliminary results available to us in advance of the conferences and for useful discussions concerning their combination. Finally, the results of the section on Standard Model constraints would not be possible without the close collaboration of many theorists.

Appendix A

The Measurements used in the Heavy-Flavour Averages

In the following 20 tables the results used in the combination are listed. In each case an indication of the dataset used and the type of analysis is given. Preliminary results are indicated by the symbol "†". The values of centre-of-mass energy are given where relevant. In each table, the result used as input to the average procedure is given followed by the statistical error, the correlated and uncorrelated systematic errors, the total systematic error, and any dependence on other electroweak parameters. In the case of the asymmetries, the measurement moved to a common energy (89.55 GeV, 91.26 GeV and 92.94 GeV, respectively, for peak-2, peak and peak$+2$ results) is quoted as *corrected* asymmetry.

Contributions to the correlated systematic error quoted here are from any sources of error shared with one or more other results from different experiments in the same table, and the uncorrelated errors from the remaining sources. In the case of $\mathcal{A}_c$ and $\mathcal{A}_b$ from SLD the quoted correlated systematic error has contributions from any source shared with one or more other measurements from LEP experiments. Constants such as $a(x)$ denote the dependence on the assumed value of $x^{\rm used}$, which is also given.

	ALEPH	DELPHI	L3	OPAL	SLD
	92-95 [24]	92-95 [25]	94-95 [26]	92-95 [27]	93-98† [28]
R_b^0	0.2158	0.2163	0.2173	0.2174	0.2164
Statistical	0.0009	0.0007	0.0015	0.0011	0.0009
Uncorrelated	0.0007	0.0004	0.0015	0.0009	0.0006
Correlated	0.0006	0.0004	0.0018	0.0008	0.0005
Total Systematic	0.0009	0.0005	0.0023	0.0012	0.0007
$a(R_c)$	-0.0033	-0.0041	-0.0376	-0.0122	-0.0057
R_c^{used}	0.1720	0.1720	0.1734	0.1720	0.1710
$a(\text{BR}(c \to \ell^+))$			-0.0133	-0.0067	
$\text{BR}(c \to \ell^+)^{\text{used}}$			9.80	9.80	
$a(f(D^+))$	-0.0010	-0.0010	-0.0086	-0.0029	-0.0008
$f(D^+)^{\text{used}}$	0.2330	0.2330	0.2330	0.2380	0.2370
$a(f(D_s))$	-0.0001	0.0001	-0.0005	-0.0001	-0.0003
$f(D_s)^{\text{used}}$	0.1020	0.1030	0.1030	0.1020	0.1140
$a(f(\Lambda_c))$	0.0002	0.0003	0.0008	0.0003	-0.0003
$f(\Lambda_c)^{\text{used}}$	0.0650	0.0630	0.0630	0.0650	0.0730

Table A.1: The measurements of R_b^0. All measurements use a lifetime tag enhanced by other features like invariant mass cuts or high p_T leptons.

	ALEPH			DELPHI		OPAL		SLD
	91-95 c-count [33]	91-95 D meson [29]	92-95 lepton [29]	92-95 c-count [31]	92-95 D meson [30,31]	91-94 c-count [34]	90-95 D meson [32]	93-97† vtx-mass [35]
R_c^0	0.1735	0.1682	0.1670	0.1693	0.1610	0.1642	0.1760	0.1738
Statistical	0.0051	0.0082	0.0062	0.0050	0.0104	0.0122	0.0095	0.0031
Uncorrelated	0.0057	0.0077	0.0059	0.0050	0.0064	0.0126	0.0102	0.0019
Correlated	0.0094	0.0028	0.0009	0.0077	0.0060	0.0099	0.0062	0.0008
Total Systematic	0.0110	0.0082	0.0059	0.0092	0.0088	0.0161	0.0120	0.0021
$a(R_b)$		-0.0050						-0.0433
R_b^{used}		0.2159						0.2166
$a(\text{BR}(c \to \ell^+))$			-0.1646					
$\text{BR}(c \to \ell^+)^{\text{used}}$			9.80					

Table A.2: The measurements of R_c^0. "c-count" denotes the determination of R_c^0 from the sum of production rates of weakly decaying charmed hadrons. "D meson" denotes any single/double tag analysis using exclusive and/or inclusive D meson reconstruction.

	ALEPH				DELPHI			L3	OPAL		
	90-95 lepton [38]	90-95 lepton [38]	90-95 lepton [38]	91-95 multi [42]	93-95† lepton [39]	92-95 D-meson [48]	92-95 jet charge [43]	90-95 lepton [40]	91-95 jet charge [46]	90-95† lepton [41]	90-95 D-meson [49]
$\sqrt{s}$ (GeV)	88.380	89.380	90.210	89.470	89.433	89.434	89.550	89.500	89.440	89.490	89.490
$A_{\mathrm{FB}}^{\mathrm{b\bar{b}}}(-2)$	-3.53	5.47	9.10	4.36	5.90	5.64	6.80	6.15	4.10	3.56	-9.20
$A_{\mathrm{FB}}^{\mathrm{b\bar{b}}}(-2)$Corrected		5.87		4.55	6.18	5.92	6.80	6.27	4.36	3.70	-9.06
Statistical		1.90		1.19	2.20	7.59	1.80	2.93	2.10	1.73	10.80
Uncorrelated		0.39		0.05	0.08	0.91	0.12	0.37	0.25	0.16	2.51
Correlated		0.70		0.01	0.08	0.08	0.01	0.19	0.02	0.04	1.41
Total Systematic		0.80		0.05	0.12	0.91	0.13	0.41	0.25	0.16	2.87
$a(R_{\mathrm{b}})$		-0.3069		-9.5	-1.1543		-0.1962	-1.4467	-0.7300	-0.1000	
$R_{\mathrm{b}}^{\mathrm{used}}$		0.2192		0.2150	0.2164		0.2158	0.2170	0.2150	0.2155	
$a(R_{\mathrm{c}})$		0.0362		0.3100	1.0444		0.3200	0.3612	0.0700	0.1000	
$R_{\mathrm{c}}^{\mathrm{used}}$		0.1710		0.1725	0.1671		0.1720	0.1734	0.1730	0.1720	
$a(A_{\mathrm{FB}}^{\mathrm{c\bar{c}}}(-2))$		-0.2244		-0.2955				-0.1000	-0.3156		
$A_{\mathrm{FB}}^{\mathrm{c\bar{c}}}(-2)^{\mathrm{used}}$		-2.34		-2.87				-2.50	-2.81		
$a(\mathrm{BR}(\mathrm{b}\to\ell^-))$		-0.2486			-1.0154			-1.0290		0.3406	
$\mathrm{BR}(\mathrm{b}\to\ell^-)^{\mathrm{used}}$		11.34			10.56			10.50		10.90	
$a(\mathrm{BR}(\mathrm{b}\to\mathrm{c}\to\ell^+))$		-0.1074			-0.1424			-0.1440		-0.5298	
$\mathrm{BR}(\mathrm{b}\to\mathrm{c}\to\ell^+)^{\mathrm{used}}$		7.86			8.07			8.00		8.30	
$a(\mathrm{BR}(\mathrm{c}\to\ell^+))$		-0.0474			0.7224			0.5096		0.1960	
$\mathrm{BR}(\mathrm{c}\to\ell^+)^{\mathrm{used}}$		9.80			9.90			9.80		9.80	
$a(\overline{\chi})$		5.259			1.3054						
$\overline{\chi}^{\mathrm{used}}$		0.12460			0.11770						
$a(f(\mathrm{D}^+))$						0.5083	0.0949				
$f(\mathrm{D}^+)^{\mathrm{used}}$						0.2210	0.2330				
$a(f(\mathrm{D_s}))$						0.1742	0.0035				
$f(\mathrm{D_s})^{\mathrm{used}}$						0.1120	0.1020				
$a(f(\Lambda_{\mathrm{c}}))$						-0.0191	-0.0225				
$f(\Lambda_{\mathrm{c}})^{\mathrm{used}}$						0.0840	0.0630				
$a(\mathrm{P}(\mathrm{c}\to\mathrm{D}^{*+})\times\mathrm{BR}(\mathrm{D}^{*+}\to\pi^+\mathrm{D}^0))$				-0.1100							
$\mathrm{P}(\mathrm{c}\to\mathrm{D}^{*+})\times\mathrm{BR}(\mathrm{D}^{*+}\to\pi^+\mathrm{D}^0)^{\mathrm{used}}$				0.1830							

Table A.3: The measurements of $A_{\mathrm{FB}}^{\mathrm{b\bar{b}}}(-2)$. All numbers are given in %.

	ALEPH	DELPHI		OPAL	
	91-95 D-meson [47]	93-95† lepton [39]	92-95 D-meson [48]	90-95† lepton [41]	90-95 D-meson [49]
$\sqrt{s}$ (GeV)	89.370	89.433	89.434	89.490	89.490
$A_{\mathrm{FB}}^{\mathrm{c\bar{c}}}(-2)$	-1.10	1.12	-5.02	-6.91	3.90
$A_{\mathrm{FB}}^{\mathrm{c\bar{c}}}(-2)$Corrected	-0.02	1.82	-4.32	-6.55	4.26
Statistical	4.30	3.60	3.69	2.44	5.10
Uncorrelated	1.00	0.53	0.40	0.38	0.80
Correlated	0.09	0.16	0.09	0.23	0.30
Total Systematic	1.00	0.55	0.41	0.44	0.86
$a(R_{\mathrm{b}})$		-0.2886		-3.4000	
$R_{\mathrm{b}}^{\mathrm{used}}$		0.2164		0.2155	
$a(R_{\mathrm{c}})$		1.0096		3.2000	
$R_{\mathrm{c}}^{\mathrm{used}}$		0.1671		0.1720	
$a(A_{\mathrm{FB}}^{\mathrm{b\bar{b}}}(-2))$	-1.3365				
$A_{\mathrm{FB}}^{\mathrm{b\bar{b}}}(-2)^{\mathrm{used}}$	6.13				
$a(\mathrm{BR}(\mathrm{b}\to\ell^-))$		-1.0966		-1.7031	
$\mathrm{BR}(\mathrm{b}\to\ell^-)^{\mathrm{used}}$		10.56		10.90	
$a(\mathrm{BR}(\mathrm{b}\to\mathrm{c}\to\ell^+))$		1.1156		-1.4128	
$\mathrm{BR}(\mathrm{b}\to\mathrm{c}\to\ell^+)^{\mathrm{used}}$		8.07		8.30	
$a(\mathrm{BR}(\mathrm{c}\to\ell^+))$		1.0703		3.3320	
$\mathrm{BR}(\mathrm{c}\to\ell^+)^{\mathrm{used}}$		9.90		9.80	
$a(\overline{\chi})$		-0.0856			
$\overline{\chi}^{\mathrm{used}}$		0.11770			
$a(f(\mathrm{D}^+))$			-0.3868		
$f(\mathrm{D}^+)^{\mathrm{used}}$			0.2210		
$a(f(\mathrm{D_s}))$			-0.1742		
$f(\mathrm{D_s})^{\mathrm{used}}$			0.1120		
$a(f(\Lambda_{\mathrm{c}}))$			-0.0878		
$f(\Lambda_{\mathrm{c}})^{\mathrm{used}}$			0.0840		

Table A.4: The measurements of $A_{\mathrm{FB}}^{\mathrm{c\bar{c}}}(-2)$. All numbers are given in %.

	ALEPH		DELPHI					L3		OPAL		
	91-95† lepton [38]	91-95 multi [42]	91-92 lepton [39]	93-95† lepton [39]	92-95 D-meson [48]	92-95 jet charge [43]	92-95† multi [44]	91-95 jet charge [45]	90-95 lepton [40]	91-95 multi [46]	90-95† lepton [41]	90-95 D-meson [49]
$\sqrt{s}$ (GeV)	91.210	91.230	91.270	91.223	91.235	91.260	91.260	91.240	91.260	91.210	91.240	91.240
$A_{\mathrm{FB}}^{\mathrm{b\bar{b}}}(\mathrm{pk})$	9.71	10.00	10.89	9.86	7.58	9.83	9.72	9.31	9.85	10.06	9.14	9.00
$A_{\mathrm{FB}}^{\mathrm{b\bar{b}}}(\mathrm{pk})$Corrected	9.81	10.06	10.87	9.93	7.63	9.83	9.72	9.35	9.85	10.15	9.18	9.04
Statistical	0.40	0.27	1.30	0.64	1.97	0.47	0.35	1.01	0.67	0.52	0.44	2.70
Uncorrelated	0.16	0.11	0.33	0.15	0.76	0.13	0.21	0.51	0.27	0.41	0.14	2.14
Correlated	0.12	0.02	0.27	0.14	0.10	0.06	0.05	0.21	0.14	0.20	0.15	0.45
Total Systematic	0.20	0.11	0.43	0.20	0.77	0.15	0.22	0.55	0.31	0.46	0.20	2.19
$a(R_{\mathrm{b}})$	-0.9545	-9.5	-2.8933	-2.0201		-0.1962	0.0637	-9.1622	-2.1700	-7.6300	-0.7000	
$R_{\mathrm{b}}^{\mathrm{used}}$	0.2172	0.2158	0.2170	0.2164		0.2158	0.2164	0.2170	0.2170	0.2150	0.2155	
$a(R_{\mathrm{c}})$	0.6450	0.3100	1.0993	1.1488		0.8400	0.0595	1.0831	1.3005	0.4600	0.6000	
$R_{\mathrm{c}}^{\mathrm{used}}$	0.1720	0.1715	0.1710	0.1671		0.1720	0.1731	0.1733	0.1734	0.1730	0.1720	
$a(A_{\mathrm{FB}}^{\mathrm{c\bar{c}}}(\mathrm{pk}))$		0.6849					0.2756	1.1603	0.9262	0.6870		
$A_{\mathrm{FB}}^{\mathrm{c\bar{c}}}(\mathrm{pk})^{\mathrm{used}}$		6.66					6.89	6.91	7.41	6.19		
$a(\mathrm{BR}(\mathrm{b}\to\ell^-))$	-1.8480		-3.8824	-2.0308					-2.0160		-0.3406	
$\mathrm{BR}(\mathrm{b}\to\ell^-)^{\mathrm{used}}$	10.78		11.00	10.56					10.50		10.90	
$a(\mathrm{BR}(\mathrm{b}\to\mathrm{c}\to\ell^+))$	0.4233		0.4740	-0.3798					-0.1280		-0.3532	
$\mathrm{BR}(\mathrm{b}\to\mathrm{c}\to\ell^+)^{\mathrm{used}}$	8.14		7.90	8.07					8.00		8.30	
$a(\mathrm{BR}(\mathrm{c}\to\ell^+))$	0.5096		0.7840	1.0703					1.5288		0.5880	
$\mathrm{BR}(\mathrm{c}\to\ell^+)^{\mathrm{used}}$	9.80		9.80	9.90					9.80		9.80	
$a(\overline{\chi})$	2.9904		3.4467	1.6692								
$\overline{\chi}^{\mathrm{used}}$	0.12460		0.12100	0.11770								
$a(f(\mathrm{D}^+))$					0.0442	0.2761	-0.0175					
$f(\mathrm{D}^+)^{\mathrm{used}}$					0.2210	0.2330	0.2330					
$a(f(\mathrm{D_s}))$					-0.0788	0.0106	-0.0260					
$f(\mathrm{D_s})^{\mathrm{used}}$					0.1120	0.1020	0.1300					
$a(f(\Lambda_{\mathrm{c}}))$					-0.0115	-0.0495	0.0221					
$f(\Lambda_{\mathrm{c}})^{\mathrm{used}}$					0.0840	0.0630	0.0960					
$a(\mathrm{P}(\mathrm{c}\to\mathrm{D}^{*+})\times\mathrm{BR}(\mathrm{D}^{*+}\to\pi^+\mathrm{D}^0))$		-0.2500										
$\mathrm{P}(\mathrm{c}\to\mathrm{D}^{*+})\times\mathrm{BR}(\mathrm{D}^{*+}\to\pi^+\mathrm{D}^0)^{\mathrm{used}}$		0.1830										

Table A.5: The measurements of $A_{\mathrm{FB}}^{\mathrm{b\bar{b}}}(\mathrm{pk})$. All numbers are given in %.

	ALEPH		DELPHI			L3	OPAL	
	91-95† lepton [38]	91-95 D-meson [47]	91-92 lepton [39]	93-95† lepton [39]	92-95 D-meson [48]	90-95 lepton [40]	90-95† lepton [41]	90-95 D-meson [49]
$\sqrt{s}$ (GeV)	91.210	91.220	91.270	91.223	91.235	91.240	91.240	91.240
$A_{\mathrm{FB}}^{\mathrm{c\bar{c}}}(\mathrm{pk})$	5.68	6.13	8.05	6.29	6.58	7.94	5.95	6.50
$A_{\mathrm{FB}}^{\mathrm{c\bar{c}}}(\mathrm{pk})$Corrected	5.93	6.32	8.00	6.47	6.70	8.04	6.05	6.60
Statistical	0.53	0.90	2.26	1.00	0.97	3.70	0.59	1.20
Uncorrelated	0.24	0.23	1.25	0.53	0.25	2.40	0.37	0.49
Correlated	0.36	0.17	0.49	0.27	0.04	0.49	0.32	0.23
Total Systematic	0.44	0.28	1.35	0.60	0.25	2.45	0.49	0.54
$a(R_{\mathrm{b}})$	1.4318		2.8933	-2.3087		4.3200	4.1000	
$R_{\mathrm{b}}^{\mathrm{used}}$	0.2172		0.2170	0.2164		0.2160	0.2155	
$a(R_{\mathrm{c}})$	-2.9383		-6.4736	5.4307		-6.7600	-3.8000	
$R_{\mathrm{c}}^{\mathrm{used}}$	0.1720		0.1710	0.1671		0.1690	0.1720	
$a(A_{\mathrm{FB}}^{\mathrm{b\bar{b}}}(\mathrm{pk}))$		-2.1333				6.4274		
$A_{\mathrm{FB}}^{\mathrm{b\bar{b}}}(\mathrm{pk})^{\mathrm{used}}$		9.79				8.84		
$a(\mathrm{BR}(\mathrm{b}\to\ell^-))$	1.8993		4.8529	-2.7618		3.5007	5.1094	
$\mathrm{BR}(\mathrm{b}\to\ell^-)^{\mathrm{used}}$	10.78		11.00	10.56		10.50	10.90	
$a(\mathrm{BR}(\mathrm{b}\to\mathrm{c}\to\ell^+))$	-1.0745		-3.9500	2.2786		-3.2917	-1.7660	
$\mathrm{BR}(\mathrm{b}\to\mathrm{c}\to\ell^+)^{\mathrm{used}}$	8.14		7.90	8.07		7.90	8.30	
$a(\mathrm{BR}(\mathrm{c}\to\ell^+))$	-3.2732		-7.2520	4.8965		-6.5327	-3.9200	
$\mathrm{BR}(\mathrm{c}\to\ell^+)^{\mathrm{used}}$	9.80		9.80	9.90		9.80	9.80	
$a(\overline{\chi})$	0.0453			0.3852				
$\overline{\chi}^{\mathrm{used}}$	0.12460			0.11770				
$a(f(\mathrm{D}^+))$					-0.0221			
$f(\mathrm{D}^+)^{\mathrm{used}}$					0.2210			
$a(f(\mathrm{D_s}))$					0.0788			
$f(\mathrm{D_s})^{\mathrm{used}}$					0.1120			
$a(f(\Lambda_{\mathrm{c}}))$					0.0115			
$f(\Lambda_{\mathrm{c}})^{\mathrm{used}}$					0.0840			

Table A.6: The measurements of $A_{\mathrm{FB}}^{\mathrm{c\bar{c}}}(\mathrm{pk})$. All numbers are given in %.

	ALEPH				DELPHI			L3	OPAL		
	90-95 lepton [38]	90-95 lepton [38]	90-95 lepton [38]	91-95 multi [42]	93-95† lepton [39]	92-95 D-meson [48]	92-95 jet charge [43]	90-95 lepton [40]	91-95 jet charge [46]	90-95† lepton [41]	90-95 D-meson [49]
$\sqrt{s}$ (GeV)	92.050	92.940	93.900	92.950	92.990	92.990	92.940	93.100	92.910	92.950	92.950
$A_{\mathrm{FB}}^{\mathrm{b\bar{b}}}(+2)$	3.93	10.60	9.03	11.72	10.10	8.77	12.30	13.79	14.60	10.76	-3.10
$A_{\mathrm{FB}}^{\mathrm{b\bar{b}}}(+2)$Corrected	10.03			11.71	10.05	8.72	12.30	13.63	14.63	10.75	-3.11
Statistical	1.51			0.98	1.80	6.37	1.60	2.40	1.70	1.43	9.00
Uncorrelated	0.14			0.12	0.14	0.97	0.24	0.34	0.64	0.25	2.03
Correlated	0.24			0.02	0.16	0.14	0.08	0.19	0.34	0.28	1.69
Total Systematic	0.28			0.13	0.21	0.98	0.26	0.39	0.73	0.37	2.65
$a(R_{\mathrm{b}})$	-1.964			-9.5	-2.8859		-0.1962	-3.3756	-12.9000	-0.8000	
$R_{\mathrm{b}}^{\mathrm{used}}$	0.2192			0.2156	0.2164		0.2158	0.2170	0.2150	0.2155	
$a(R_{\mathrm{c}})$	1.575			0.3100	1.3577		1.2000	1.9869	0.6900	0.8000	
$R_{\mathrm{c}}^{\mathrm{used}}$	0.1710			0.1719	0.1671		0.1720	0.1734	0.1730	0.1720	
$a(A_{\mathrm{FB}}^{\mathrm{c\bar{c}}}(+2))$	1.081			1.2793				0.5206	1.3287		
$A_{\mathrm{FB}}^{\mathrm{c\bar{c}}}(+2)^{\mathrm{used}}$	12.51			12.42				12.39	12.08		
$a(\mathrm{BR}(\mathrm{b}\to\ell^-))$	-1.762				-2.3557			-2.0790		-1.3625	
$\mathrm{BR}(\mathrm{b}\to\ell^-)^{\mathrm{used}}$	11.34				10.56			10.50		10.90	
$a(\mathrm{BR}(\mathrm{b}\to\mathrm{c}\to\ell^+))$	-0.2478				-0.7595			-1.1200		0.7064	
$\mathrm{BR}(\mathrm{b}\to\mathrm{c}\to\ell^+)^{\mathrm{used}}$	7.86				8.07			8.00		8.30	
$a(\mathrm{BR}(\mathrm{c}\to\ell^+))$	1.524				1.0703			1.9796		0.7840	
$\mathrm{BR}(\mathrm{c}\to\ell^+)^{\mathrm{used}}$	9.80				9.90			9.80		9.80	
$a(\overline{\chi})$	6.584				1.6050						
$\overline{\chi}^{\mathrm{used}}$	0.12460				0.11770						
$a(f(\mathrm{D}^+))$						0.3978	0.4229				
$f(\mathrm{D}^+)^{\mathrm{used}}$						0.2210	0.2330				
$a(f(\mathrm{D_s}))$						-0.0788	0.0211				
$f(\mathrm{D_s})^{\mathrm{used}}$						0.1120	0.1020				
$a(f(\Lambda_{\mathrm{c}}))$						0.0573	-0.0855				
$f(\Lambda_{\mathrm{c}})^{\mathrm{used}}$						0.0840	0.0630				
$a(\mathrm{P}(\mathrm{c}\to\mathrm{D}^{*+})\times\mathrm{BR}(\mathrm{D}^{*+}\to\pi^+\mathrm{D}^0))$				-0.2800							
$\mathrm{P}(\mathrm{c}\to\mathrm{D}^{*+})\times\mathrm{BR}(\mathrm{D}^{*+}\to\pi^+\mathrm{D}^0)^{\mathrm{used}}$				0.1830							

Table A.7: The measurements of $A_{\mathrm{FB}}^{\mathrm{b\bar{b}}}(+2)$. All numbers are given in %.

	ALEPH	DELPHI		OPAL	
	91-95 D-meson [47]	93-95† lepton [39]	92-95 D-meson [48]	90-95† lepton [41]	90-95 D-meson [49]
$\sqrt{s}$ (GeV)	92.960	92.990	92.990	92.950	92.950
$A_{\rm FB}^{\rm c\bar{c}}(+2)$	10.82	10.50	11.78	15.62	16.50
$A_{\rm FB}^{\rm c\bar{c}}(+2)$Corrected	10.77	10.37	11.65	15.59	16.47
Statistical	3.30	2.90	3.20	2.02	4.10
Uncorrelated	0.79	0.41	0.52	0.57	0.92
Correlated	0.18	0.28	0.07	0.62	0.43
Total Systematic	0.81	0.50	0.52	0.84	1.02
$a(R_{\rm b})$		-4.0402		9.6000	
$R_{\rm b}^{\rm used}$		0.2164		0.2155	
$a(R_{\rm c})$		7.5891		-8.9000	
$R_{\rm c}^{\rm used}$		0.1671		0.1720	
$a(A_{\rm FB}^{\rm b\bar{b}}(+2))$	-2.6333				
$A_{\rm FB}^{\rm b\bar{b}}(+2)^{\rm used}$	12.08				
$a({\rm BR}({\rm b}\to\ell^-))$		-3.2492		9.5375	
${\rm BR}({\rm b}\to\ell^-)^{\rm used}$		10.56		10.90	
$a({\rm BR}({\rm b}\to{\rm c}\to\ell^+))$		1.5191		-1.5894	
${\rm BR}({\rm b}\to{\rm c}\to\ell^+)^{\rm used}$		8.07		8.30	
$a({\rm BR}({\rm c}\to\ell^+))$		8.1341		-9.2120	
${\rm BR}({\rm c}\to\ell^+)^{\rm used}$		9.90		9.80	
$a(\overline{\chi})$		-0.2140			
$\overline{\chi}^{\rm used}$		0.11770			
$a(f({\rm D}^+))$			-0.2984		
$f({\rm D}^+)^{\rm used}$			0.2210		
$a(f({\rm D_s}))$			0.0539		
$f({\rm D_s})^{\rm used}$			0.1120		
$a(f(\Lambda_{\rm c}))$			0.0764		
$f(\Lambda_{\rm c})^{\rm used}$			0.0840		

Table A.8: The measurements of $A_{\rm FB}^{\rm c\bar{c}}(+2)$. All numbers are given in %.

	SLD			
	93-98† lepton [50]	93-98† jet charge [52]	94-95† $K^{\pm}$ [53]	96-98† multi [54]
$\sqrt{s}$ (GeV)	91.280	91.280	91.280	91.280
$\mathcal{A}_{\rm b}$	0.924	0.907	0.855	0.921
Statistical	0.030	0.020	0.088	0.018
Uncorrelated	0.018	0.023	0.102	0.018
Correlated	0.008	0.001	0.006	0.001
Total Systematic	0.020	0.023	0.102	0.018
$a(R_{\rm b})$	-0.1237		-0.0139	-0.7283
$R_{\rm b}^{\rm used}$	0.2164		0.2180	0.2158
$a(R_{\rm c})$	0.0308		0.0060	0.0359
$R_{\rm c}^{\rm used}$	0.1674		0.1710	0.1722
$a(\mathcal{A}_{\rm c})$	0.0534	0.0211	-0.0112	0.0095
$\mathcal{A}_{\rm c}^{\rm used}$	0.667	0.670	0.666	0.667
$a(\mathrm{BR}(\mathrm{b} \to \ell^-))$	-0.1999			
$\mathrm{BR}(\mathrm{b} \to \ell^-)^{\rm used}$	10.62			
$a(\mathrm{BR}(\mathrm{b} \to \mathrm{c} \to \ell^+))$	0.0968			
$\mathrm{BR}(\mathrm{b} \to \mathrm{c} \to \ell^+)^{\rm used}$	8.07			
$a(\mathrm{BR}(\mathrm{c} \to \ell^+))$	0.0369			
$\mathrm{BR}(\mathrm{c} \to \ell^+)^{\rm used}$	9.85			
$a(\overline{\chi})$	0.2951			
$\overline{\chi}^{\rm used}$	0.11860			

Table A.9: The measurements of $\mathcal{A}_{\rm b}$.

	SLD		
	93-98† lepton [50]	93-98† D-meson [51]	96-98† K+vertex [55]
$\sqrt{s}$ (GeV)	91.280	91.280	91.280
$\mathcal{A}_c$	0.589	0.688	0.673
Statistical	0.055	0.035	0.029
Uncorrelated	0.045	0.020	0.024
Correlated	0.021	0.003	0.002
Total Systematic	0.050	0.021	0.024
$a(R_b)$	0.1855		0.5395
R_b^{used}	0.2164		0.2158
$a(R_c)$	-0.4053		-0.0682
R_c^{used}	0.1674		0.1722
$a(\mathcal{A}_b)$	0.2137	-0.0673	-0.0187
$\mathcal{A}_b^{used}$	0.935	0.935	0.935
$a(\mathrm{BR}(b \to \ell^-))$	0.2874		
$\mathrm{BR}(b \to \ell^-)^{used}$	10.62		
$a(\mathrm{BR}(b \to c \to \ell^+))$	-0.1743		
$\mathrm{BR}(b \to c \to \ell^+)^{used}$	8.07		
$a(\mathrm{BR}(c \to \ell^+))$	-0.3971		
$\mathrm{BR}(c \to \ell^+)^{used}$	9.85		
$a(\overline{\chi})$	0.0717		
$\overline{\chi}^{used}$	0.11860		

Table A.10: The measurements of $\mathcal{A}_c$.

	ALEPH	DELPHI	L3		OPAL
	91-95† multi [56]	94-95† multi [57]	92 lepton [58]	94-95† multi [26]	92-95 multi [59]
BR($b \to \ell^-$)	10.70	10.70	10.68	10.22	10.85
Statistical	0.10	0.08	0.11	0.13	0.10
Uncorrelated	0.16	0.20	0.36	0.19	0.20
Correlated	0.23	0.45	0.22	0.31	0.21
Total Systematic	0.28	0.49	0.42	0.36	0.29
$a(R_b)$			-9.2571		-0.1808
R_b^{used}			0.2160		0.2169
$a(R_c)$				1.4450	0.4867
R_c^{used}				0.1734	0.1770
$a(BR(b \to c \to \ell^+))$			-1.1700	0.1618	
$BR(b \to c \to \ell^+)^{used}$			9.00	8.09	
$a(BR(c \to \ell^+))$	-0.3078	-0.1960	-2.5480	0.9212	
$BR(c \to \ell^+)^{used}$	9.85	9.80	9.80	9.80	
$a(\overline{\chi})$	0.7683				
$\overline{\chi}^{used}$	0.1178				
$a(f(D^+))$				0.5523	0.1445
$f(D^+)^{used}$				0.2330	0.2380
$a(f(D_s))$				0.0213	0.0055
$f(D_s)^{used}$				0.1030	0.1020
$a(f(\Lambda_c))$				-0.0427	-0.0157
$f(\Lambda_c)^{used}$				0.0630	0.0650

Table A.11: The measurements of BR($b \to \ell^-$). All numbers are given in %.

	ALEPH	DELPHI	OPAL
	91-95† multi [56]	94-95† multi [57]	92-95 multi [59]
BR(b $\to$ c $\to \ell^+$)	8.18	7.98	8.41
Statistical	0.15	0.22	0.16
Uncorrelated	0.19	0.21	0.19
Correlated	0.15	0.19	0.34
Total Systematic	0.24	0.28	0.39
$a(R_b)$			-0.1808
R_b^{used}			0.2169
$a(R_c)$	0.5026		0.3761
R_c^{used}	0.1709		0.1770
$a(\mathrm{BR}(c \to \ell^+))$	0.3078		
$\mathrm{BR}(c \to \ell^+)^{used}$	9.85		
$a(\overline{\chi})$	-1.3884		
$\overline{\chi}^{used}$	0.11940		
$a(f(D^+))$			0.1190
$f(D^+)^{used}$			0.2380
$a(f(D_s))$			0.0028
$f(D_s)^{used}$			0.1020
$a(f(\Lambda_c))$			-0.0110
$f(\Lambda_c)^{used}$			0.0660

Table A.12: The measurements of BR(b $\to$ c $\to \ell^+$). All numbers are given in %.

	DELPHI	OPAL
	92-95 D+lepton [30]	90-95 D+lepton [60]
BR(c $\to \ell^+$)	9.64	9.58
Statistical	0.42	0.60
Uncorrelated	0.24	0.49
Correlated	0.13	0.43
Total Systematic	0.27	0.65
$a(\mathrm{BR}(b \to \ell^-))$	-0.5600	-1.4335
$\mathrm{BR}(b \to \ell^-)^{used}$	11.20	10.99
$a(\mathrm{BR}(b \to c \to \ell^+))$	-0.4100	-0.7800
$\mathrm{BR}(b \to c \to \ell^+)^{used}$	8.20	7.80

Table A.13: The measurements of BR(c $\to \ell^+$). All numbers are given in %.

	ALEPH	DELPHI	L3	OPAL
	90-95 multi [38]	94-95† multi [57]	90-95 lepton [40]	90-95† lepton [41]
$\overline{\chi}$	0.12446	0.12700	0.11920	0.11380
Statistical	0.00515	0.01300	0.00680	0.00540
Uncorrelated	0.00252	0.00484	0.00214	0.00306
Correlated	0.00394	0.00431	0.00252	0.00324
Total Systematic	0.00468	0.00648	0.00330	0.00445
$a(R_{\mathrm{b}})$	0.0341			
$R_{\mathrm{b}}^{\mathrm{used}}$	0.2192			
$a(R_{\mathrm{c}})$	0.0009		0.0004	
$R_{\mathrm{c}}^{\mathrm{used}}$	0.1710		0.1734	
$a(\mathrm{BR}(\mathrm{b} \to \ell^-))$	0.0524		0.0550	0.0170
$\mathrm{BR}(\mathrm{b} \to \ell^-)^{\mathrm{used}}$	11.34		10.50	10.90
$a(\mathrm{BR}(\mathrm{b} \to \mathrm{c} \to \ell^+))$	-0.0440		-0.0466	-0.0318
$\mathrm{BR}(\mathrm{b} \to \mathrm{c} \to \ell^+)^{\mathrm{used}}$	7.86		8.00	8.30
$a(\mathrm{BR}(\mathrm{c} \to \ell^+))$	0.0035	-0.0020	0.0006	0.0039
$\mathrm{BR}(\mathrm{c} \to \ell^+)^{\mathrm{used}}$	9.80	9.80	9.80	9.80

Table A.14: The measurements of $\overline{\chi}$.

	DELPHI	OPAL
	92-95 D-meson [30]	90-95 D-meson [32]
$\mathrm{P}(\mathrm{c} \to \mathrm{D}^{*+}) \times \mathrm{BR}(\mathrm{D}^{*+} \to \pi^+\mathrm{D}^0)$	0.1740	0.1514
Statistical	0.0100	0.0096
Uncorrelated	0.0040	0.0088
Correlated	0.0007	0.0011
Total Systematic	0.0041	0.0089
$a(R_{\mathrm{b}})$	0.0293	
$R_{\mathrm{b}}^{\mathrm{used}}$	0.2166	
$a(R_{\mathrm{c}})$	-0.0158	
$R_{\mathrm{c}}^{\mathrm{used}}$	0.1735	

Table A.15: The measurements of $\mathrm{P}(\mathrm{c} \to \mathrm{D}^{*+}) \times \mathrm{BR}(\mathrm{D}^{*+} \to \pi^+\mathrm{D}^0)$.

	ALEPH	DELPHI	OPAL
	91-95 D meson [33]	92-95 D meson [31]	91-94 D meson [34]
$R_c f_{D^+}$	0.0406	0.0384	0.0391
Statistical	0.0013	0.0013	0.0050
Uncorrelated	0.0014	0.0015	0.0042
Correlated	0.0032	0.0025	0.0031
Total Systematic	0.0035	0.0030	0.0052
$a(f(D^+))$		0.0008	
$f(D^+)^{used}$		0.2210	
$a(f(D_s))$		-0.0002	
$f(D_s)^{used}$		0.1120	

Table A.16: The measurements of $R_c f_{D^+}$.

	ALEPH	DELPHI	OPAL
	91-95 D meson [33]	92-95 D meson [31]	91-94 D meson [34]
$R_c f_{D_s}$	0.0207	0.0213	0.0160
Statistical	0.0033	0.0017	0.0042
Uncorrelated	0.0011	0.0010	0.0016
Correlated	0.0053	0.0054	0.0043
Total Systematic	0.0054	0.0055	0.0046
$a(f(D^+))$		0.0007	
$f(D^+)^{used}$		0.2210	
$a(f(D_s))$		-0.0009	
$f(D_s)^{used}$		0.1120	
$a(f(\Lambda_c))$		-0.0001	
$f(\Lambda_c)^{used}$		0.0840	

Table A.17: The measurements of $R_c f_{D_s}$.

	ALEPH	DELPHI	OPAL
	91-95 D meson [33]	92-95 D meson [31]	91-94 D meson [34]
$R_c f_{\Lambda_c}$	0.0157	0.0170	0.0091
Statistical	0.0016	0.0035	0.0050
Uncorrelated	0.0005	0.0016	0.0015
Correlated	0.0044	0.0045	0.0035
Total Systematic	0.0045	0.0048	0.0038
$a(f(D^+))$		0.0002	
$f(D^+)^{used}$		0.2210	
$a(f(D_s))$		-0.0001	
$f(D_s)^{used}$		0.1120	
$a(f(\Lambda_c))$		-0.0002	
$f(\Lambda_c)^{used}$		0.0840	

Table A.18: The measurements of $R_c f_{\Lambda_c}$.

	ALEPH	DELPHI	OPAL
	91-95 D meson [33]	92-95 D meson [31]	91-94 D meson [34]
$R_c f_{D^0}$	0.0965	0.0928	0.1000
Statistical	0.0029	0.0026	0.0070
Uncorrelated	0.0040	0.0038	0.0057
Correlated	0.0045	0.0023	0.0041
Total Systematic	0.0060	0.0044	0.0070
$a(f(D^+))$		0.0021	
$f(D^+)^{used}$		0.2210	
$a(f(D_s))$		-0.0004	
$f(D_s)^{used}$		0.1120	
$a(f(\Lambda_c))$		-0.0004	
$f(\Lambda_c)^{used}$		0.0840	

Table A.19: The measurements of $R_c f_{D^0}$.

	DELPHI	OPAL
	92-95 D meson [31]	90-95 D-meson [32]
$R_c P(c \to D^{*+}) \times BR(D^{*+} \to \pi^+ D^0)$	0.0282	0.0268
Statistical	0.0007	0.0005
Uncorrelated	0.0010	0.0010
Correlated	0.0007	0.0009
Total Systematic	0.0012	0.0013
$a(f(D^+))$	0.0006	
$f(D^+)^{\text{used}}$	0.2210	
$a(f(D_s))$	-0.0001	
$f(D_s)^{\text{used}}$	0.1120	
$a(f(\Lambda_c))$	-0.0004	
$f(\Lambda_c)^{\text{used}}$	0.0840	

Table A.20: The measurements of $R_c P(c \to D^{*+}) \times BR(D^{*+} \to \pi^+ D^0)$.

Appendix B

Heavy-Flavour Fit including Off-Peak Asymmetries

The full 18 parameter fit to the LEP and SLD data gave the following results:

$$
\begin{aligned}
R_{\mathrm{b}}^{0} &= 0.21647 \pm 0.00068 \\
R_{\mathrm{c}}^{0} &= 0.1719 \pm 0.0031 \\
A_{\mathrm{FB}}^{\mathrm{b\overline{b}}}(-2) &= 0.0508 \pm 0.0068 \\
A_{\mathrm{FB}}^{\mathrm{c\overline{c}}}(-2) &= -0.035 \pm 0.017 \\
A_{\mathrm{FB}}^{\mathrm{b\overline{b}}}(\mathrm{pk}) &= 0.0975 \pm 0.0018 \\
A_{\mathrm{FB}}^{\mathrm{c\overline{c}}}(\mathrm{pk}) &= 0.0620 \pm 0.0036 \\
A_{\mathrm{FB}}^{\mathrm{b\overline{b}}}(+2) &= 0.1150 \pm 0.0057 \\
A_{\mathrm{FB}}^{\mathrm{c\overline{c}}}(+2) &= 0.130 \pm 0.013 \\
\mathcal{A}_{\mathrm{b}} &= 0.922 \pm 0.020 \\
\mathcal{A}_{\mathrm{c}} &= 0.670 \pm 0.026 \\
\mathrm{BR}(\mathrm{b} \to \ell^{-}) &= 0.1067 \pm 0.0021 \\
\mathrm{BR}(\mathrm{b} \to \mathrm{c} \to \ell^{+}) &= 0.0807 \pm 0.0017 \\
\mathrm{BR}(\mathrm{c} \to \ell^{+}) &= 0.0979 \pm 0.0031 \\
\overline{\chi} &= 0.1195 \pm 0.0040 \\
f(\mathrm{D}^{+}) &= 0.234 \pm 0.016 \\
f(\mathrm{D_s}) &= 0.125 \pm 0.023 \\
f(\mathrm{c_{baryon}}) &= 0.096 \pm 0.023 \\
\mathrm{P}(\mathrm{c} \to \mathrm{D}^{*+}) \times \mathrm{BR}(\mathrm{D}^{*+} \to \pi^{+}\mathrm{D}^{0}) &= 0.1620 \pm 0.0048
\end{aligned}
$$

with a χ^2/d.o.f. of $43/(99-18)$. The corresponding correlation matrix is given in Table B.1. The energy for the peak-2, peak and peak$+2$ results are respectively 89.55 GeV, 91.26 GeV and 92.94 GeV. Note that the asymmetry results shown here are not the pole asymmetries shown in Section 5.3.2. The non-electroweak parameters do not depend on the treatment of the asymmetries.

	1) R_b	2) R_c	3) $A_{FB}^{b\bar{b}}$ (−2)	4) $A_{FB}^{c\bar{c}}$ (−2)	5) $A_{FB}^{b\bar{b}}$ (pk)	6) $A_{FB}^{c\bar{c}}$ (pk)	7) $A_{FB}^{b\bar{b}}$ (+2)	8) $A_{FB}^{c\bar{c}}$ (+2)	9) $\mathcal{A}_b$	10) $\mathcal{A}_c$	11) BR (1)	12) BR (2)	13) BR (3)	14) $\overline{\chi}$	15) $f(D^+)$	16) $f(D_s)$	17) $f(c_{bar.})$	18) PcDst
1)	1.00	−0.14	−0.02	0.00	−0.07	0.01	−0.03	0.00	−0.08	0.04	−0.09	−0.02	−0.01	−0.03	−0.16	−0.04	0.13	0.10
2)	−0.14	1.00	0.01	0.01	0.04	−0.01	0.02	−0.01	0.03	−0.05	0.06	−0.03	−0.30	0.04	−0.13	0.17	0.16	−0.44
3)	−0.02	0.01	1.00	0.16	0.03	0.01	0.01	0.00	0.00	0.00	0.02	−0.02	0.00	0.05	0.00	0.00	0.00	−0.01
4)	0.00	0.01	0.16	1.00	0.01	0.01	0.00	0.00	0.00	0.00	0.02	−0.01	0.02	0.01	0.00	0.01	0.00	0.00
5)	−0.07	0.04	0.03	0.01	1.00	0.15	0.07	0.01	0.01	0.00	0.04	−0.08	0.00	0.13	0.01	0.02	0.00	−0.03
6)	0.01	−0.01	0.01	0.01	0.15	1.00	0.01	0.09	0.00	0.01	0.13	−0.14	−0.08	0.15	0.00	0.00	−0.01	0.00
7)	−0.03	0.02	0.01	0.00	0.07	0.01	1.00	0.17	0.01	0.00	0.01	−0.03	0.01	0.06	0.01	0.01	−0.01	−0.01
8)	0.00	−0.01	0.00	0.00	0.01	0.09	0.17	1.00	0.00	0.00	0.02	−0.04	−0.03	0.02	0.00	−0.01	0.00	0.01
9)	−0.08	0.03	0.00	0.00	0.01	0.00	0.01	0.00	1.00	0.13	−0.02	0.01	0.03	0.06	0.00	0.00	0.00	−0.02
10)	0.04	−0.05	0.00	0.00	0.00	0.01	0.00	0.00	0.13	1.00	0.02	−0.04	−0.02	0.01	0.00	0.00	0.00	0.02
11)	−0.09	0.06	0.02	0.02	0.04	0.13	0.01	0.02	−0.02	0.02	1.00	−0.21	0.01	0.37	0.03	0.01	−0.01	−0.01
12)	−0.02	−0.03	−0.02	−0.01	−0.08	−0.14	−0.03	−0.04	0.01	−0.04	−0.21	1.00	0.08	−0.31	0.02	−0.01	−0.01	0.01
13)	−0.01	−0.30	0.00	0.02	0.00	−0.08	0.01	−0.03	0.03	−0.02	0.01	0.08	1.00	0.14	0.01	−0.03	−0.02	0.13
14)	−0.03	0.04	0.05	0.01	0.13	0.15	0.06	0.02	0.06	0.01	0.37	−0.31	0.14	1.00	0.01	0.01	0.00	−0.03
15)	−0.16	−0.13	0.00	0.00	0.01	0.00	0.01	0.00	0.00	0.00	0.03	0.02	0.01	0.01	1.00	−0.39	−0.26	0.10
16)	−0.04	0.17	0.00	0.01	0.02	0.00	0.01	−0.01	0.00	0.00	0.01	−0.01	−0.03	0.01	−0.39	1.00	−0.50	−0.08
17)	0.13	0.16	0.00	0.00	0.00	−0.01	−0.01	0.00	0.00	0.00	−0.01	−0.01	−0.02	0.00	−0.26	−0.50	1.00	−0.14
18)	0.10	−0.44	−0.01	0.00	−0.03	0.00	−0.01	0.01	−0.02	0.02	−0.01	0.01	0.13	−0.03	0.10	−0.08	−0.14	1.00

Table B.1: The correlation matrix for the set of the 18 heavy flavour parameters. BR(1), BR(2) and BR(3) denote BR($b \to \ell^-$), BR($b \to c \to \ell^+$) and BR($c \to \ell^+$) respectively, PcDst denotes P($c \to D^{*+}$) $\times$ BR($D^{*+} \to \pi^+ D^0$).

Appendix C

Detailed inputs and results on W-boson and four-fermion averages

Tables C.1, C.2, C.3, C.4, C.5, C.6, C.7 and C.8 give the details of the inputs and of the results for the calculation of LEP averages of the WW cross section, of the WW cross section ratio $\mathcal{R}_{\mathrm{WW}}$, of W decay branching fractions, of the ZZ cross section, and of the total and hadronic single W cross sections. For both inputs and results, whenever relevant, the splitup of the errors into their various components is given in the table. For each measurement, the Collaborations provide additional information which is necessary for the combination of LEP results, such as the expected statistical error or the splitup of the systematic uncertainty into its correlated and uncorrelated components.

$\sqrt{s}$	$\sigma_{\rm WW}$	$\Delta\sigma^{\rm stat}_{\rm WW}$	(LCEC) $\Delta\sigma^{\rm syst}_{\rm WW}$	(LUEU) $\Delta\sigma^{\rm syst}_{\rm WW}$	(LUEC) $\Delta\sigma^{\rm syst}_{\rm WW}$	$\Delta\sigma^{\rm syst}_{\rm WW}$	$\Delta\sigma_{\rm WW}$	
ALEPH [102, 106, 110, 115]								
182.7 GeV	15.57	±0.62	±0.09	±0.09	±0.26	±0.29	±0.68	
188.6 GeV	15.71	±0.34	±0.05	±0.09	±0.15	±0.18	±0.38	
191.6 GeV	17.23	±0.89	±0.05	±0.09	±0.15	±0.18	±0.91	
195.5 GeV	17.00	±0.54	±0.05	±0.09	±0.15	±0.18	±0.57	
199.5 GeV	16.98	±0.53	±0.05	±0.09	±0.15	±0.18	±0.56	
201.6 GeV	16.16	±0.74	±0.05	±0.09	±0.15	±0.18	±0.76	
204.9 GeV	16.57	±0.52	±0.05	±0.09	±0.15	±0.18	±0.55	
206.6 GeV	17.32	±0.41	±0.05	±0.09	±0.15	±0.18	±0.45	
DELPHI [103, 107, 111, 116]								
182.7 GeV	15.86	±0.69	±0.09	±0.07	±0.24	±0.27	±0.74	
188.6 GeV	15.83	±0.38	±0.07	±0.05	±0.18	±0.20	±0.43	
191.6 GeV	16.90	±1.00	±0.07	±0.06	±0.20	±0.22	±1.02	
195.5 GeV	17.86	±0.59	±0.07	±0.06	±0.20	±0.22	±0.63	
199.5 GeV	17.35	±0.56	±0.07	±0.06	±0.20	±0.22	±0.60	
201.6 GeV	17.67	±0.81	±0.08	±0.07	±0.21	±0.23	±0.84	
204.9 GeV	17.44	±0.60	±0.06	±0.05	±0.21	±0.22	±0.64	
206.6 GeV	16.50	±0.43	±0.06	±0.05	±0.20	±0.21	±0.48	
L3 [104, 108, 114, 117]								
182.7 GeV	16.53	±0.67	±0.08	±0.14	±0.21	±0.26	±0.72	
188.6 GeV	16.24	±0.37	±0.04	±0.08	±0.20	±0.22	±0.43	
191.6 GeV	16.39	±0.90	±0.08	±0.08	±0.21	±0.24	±0.93	
195.5 GeV	16.67	±0.55	±0.08	±0.08	±0.21	±0.24	±0.60	
199.5 GeV	16.94	±0.57	±0.08	±0.08	±0.21	±0.24	±0.62	
201.6 GeV	16.95	±0.85	±0.08	±0.08	±0.21	±0.24	±0.88	
204.9 GeV	17.35	±0.59	±0.08	±0.08	±0.21	±0.24	±0.64	
206.6 GeV	17.96	±0.45	±0.08	±0.08	±0.21	±0.24	±0.51	
OPAL [105, 109, 112, 113, 118]								
182.7 GeV	15.43	±0.61	±0.14	±0.00	±0.22	±0.26	±0.66	
188.6 GeV	16.30	±0.34	±0.07	±0.00	±0.17	±0.18	±0.38	
191.6 GeV	16.60	±0.88	±0.12	±0.00	±0.40	±0.42	±0.98	
195.5 GeV	18.59	±0.60	±0.12	±0.00	±0.41	±0.43	±0.74	
199.5 GeV	16.32	±0.54	±0.10	±0.00	±0.37	±0.38	±0.66	
201.6 GeV	18.48	±0.81	±0.12	±0.00	±0.40	±0.42	±0.91	
204.9 GeV	15.97	±0.52	±0.10	±0.00	±0.36	±0.37	±0.64	
206.6 GeV	17.77	±0.42	±0.09	±0.00	±0.37	±0.38	±0.57	
LEP Averages								χ^2/d.o.f.
182.7 GeV	15.79	±0.32	±0.10	±0.04	±0.11	±0.15	±0.36	
188.6 GeV	16.00	±0.18	±0.05	±0.03	±0.08	±0.10	±0.21	
191.6 GeV	16.72	±0.46	±0.07	±0.03	±0.11	±0.13	±0.48	
195.5 GeV	17.43	±0.29	±0.07	±0.04	±0.10	±0.13	±0.32	
199.5 GeV	16.84	±0.28	±0.07	±0.04	±0.10	±0.13	±0.31	27.42/24
201.6 GeV	17.23	±0.40	±0.07	±0.04	±0.10	±0.13	±0.42	
204.9 GeV	16.71	±0.28	±0.07	±0.04	±0.10	±0.13	±0.31	
206.6 GeV	17.33	±0.22	±0.06	±0.04	±0.10	±0.12	±0.25	

Table C.1: W-pair production cross section (in pb) for different centre–of–mass energies. The first column contains the centre–of–mass energy, and the second, the measurements. Observed statistical uncertainties are used in the fit and are listed in the third column; when asymmetric errors are quoted by the Collaborations, the positive error is listed in the table and used in the fit. The fourth, fifth and sixth columns contain the components of the systematic errors, as subdivided by the Collaborations into LEP-correlated energy-correlated (LCEC), LEP-uncorrelated energy-uncorrelated (LUEU), LEP-uncorrelated energy-correlated (LUEC). The total systematic error is given in the seventh column, the total error in the eighth. For the LEP averages, the χ^2 of the fit is also given in the ninth column.

$\sqrt{s}$/ GeV	182.7	188.6	191.6	195.5	199.5	201.6	204.9	206.6
182.7	1.000	0.197	0.113	0.169	0.169	0.128	0.166	0.201
188.6	0.197	1.000	0.134	0.200	0.200	0.150	0.196	0.239
191.6	0.113	0.134	1.000	0.119	0.119	0.090	0.118	0.143
195.5	0.169	0.200	0.119	1.000	0.177	0.133	0.174	0.211
199.5	0.169	0.200	0.119	0.177	1.000	0.133	0.175	0.212
201.6	0.128	0.150	0.090	0.133	0.133	1.000	0.131	0.159
204.9	0.166	0.196	0.118	0.174	0.175	0.131	1.000	0.209
206.6	0.201	0.239	0.143	0.211	0.212	0.159	0.209	1.000

Table C.2: Correlation matrix for the LEP combined W-pair cross sections listed at the bottom of Table C.1. Correlations are all positive and range from 9% to 24%.

$\sqrt{s}$	WW cross section (pb)			
(GeV)	$\sigma_{\mathrm{WW}}^{\mathrm{GENTLE}}$	$\sigma_{\mathrm{WW}}^{\mathrm{KORALW}}$	$\sigma_{\mathrm{WW}}^{\mathrm{YFSWW}}$	$\sigma_{\mathrm{WW}}^{\mathrm{RACOONWW}}$
182.7	15.710 ± 0.020	15.619 ± 0.002	15.361 ± 0.005	15.368 ± 0.008
188.6	16.647 ± 0.020	16.554 ± 0.002	16.266 ± 0.005	16.249 ± 0.011
191.6	16.961 ± 0.020	16.865 ± 0.002	16.568 ± 0.006	16.519 ± 0.009
195.5	17.262 ± 0.020	17.165 ± 0.002	16.841 ± 0.006	16.801 ± 0.009
199.5	17.462 ± 0.020	17.361 ± 0.002	17.017 ± 0.007	16.979 ± 0.009
201.6	17.532 ± 0.020	17.428 ± 0.002	17.076 ± 0.006	17.032 ± 0.009
204.9	17.602 ± 0.020	17.497 ± 0.002	17.128 ± 0.006	17.079 ± 0.009
206.6	17.621 ± 0.020	17.516 ± 0.001	17.145 ± 0.006	17.087 ± 0.009

Table C.3: W-pair cross section predictions (in pb) for different centre–of–mass energies, according to GENTLE [126], KORALW [127], YFSWW [122] and RACOONWW [123], for $m_{\mathrm{W}} = 80.35$ GeV. The errors listed in the table are only the statistical errors from the numerical integration of the cross section.

$\sqrt{s}$	$\mathcal{R}_{\rm WW}$	$\Delta\mathcal{R}^{\rm stat}_{\rm WW}$	(LCEU) $\Delta\mathcal{R}^{\rm syst}_{\rm WW}$	(LCEC) $\Delta\mathcal{R}^{\rm syst}_{\rm WW}$	(LUEU) $\Delta\mathcal{R}^{\rm syst}_{\rm WW}$	(LUEC) $\Delta\mathcal{R}^{\rm syst}_{\rm WW}$	$\Delta\mathcal{R}_{\rm WW}$	χ^2/d.o.f.
GENTLE [126]								
182.7 GeV	1.005	±0.021	±0.001	±0.006	±0.003	±0.007	±0.023	
188.6 GeV	0.961	±0.011	±0.001	±0.003	±0.002	±0.005	±0.013	
191.6 GeV	0.986	±0.027	±0.001	±0.004	±0.002	±0.006	±0.028	
195.5 GeV	1.010	±0.017	±0.001	±0.004	±0.002	±0.006	±0.018	
199.5 GeV	0.964	±0.016	±0.001	±0.004	±0.002	±0.006	±0.018	27.42/24
201.6 GeV	0.983	±0.023	±0.001	±0.004	±0.002	±0.006	±0.024	
204.9 GeV	0.949	±0.016	±0.001	±0.004	±0.002	±0.006	±0.018	
206.6 GeV	0.984	±0.012	±0.001	±0.004	±0.002	±0.006	±0.014	
Average	0.973	±0.006	±0.001	±0.004	±0.001	±0.006	±0.009	39.16/31
KORALW [127]								
182.7 GeV	1.011	±0.021	±0.000	±0.006	±0.003	±0.007	±0.023	
188.6 GeV	0.967	±0.011	±0.000	±0.003	±0.002	±0.005	±0.013	
191.6 GeV	0.991	±0.027	±0.000	±0.004	±0.002	±0.006	±0.028	
195.5 GeV	1.015	±0.017	±0.000	±0.004	±0.002	±0.006	±0.018	
199.5 GeV	0.970	±0.016	±0.000	±0.004	±0.002	±0.006	±0.018	27.42/24
201.6 GeV	0.989	±0.023	±0.000	±0.004	±0.002	±0.006	±0.024	
204.9 GeV	0.955	±0.016	±0.000	±0.004	±0.002	±0.006	±0.018	
206.6 GeV	0.989	±0.012	±0.000	±0.004	±0.002	±0.006	±0.014	
Average	0.979	±0.006	±0.000	±0.004	±0.001	±0.006	±0.009	39.20/31
YFSWW [122]								
182.7 GeV	1.028	±0.021	±0.000	±0.006	±0.003	±0.007	±0.023	
188.6 GeV	0.984	±0.011	±0.000	±0.003	±0.002	±0.005	±0.013	
191.6 GeV	1.009	±0.028	±0.000	±0.004	±0.002	±0.006	±0.029	
195.5 GeV	1.035	±0.017	±0.000	±0.004	±0.002	±0.006	±0.019	
199.5 GeV	0.990	±0.016	±0.000	±0.004	±0.002	±0.006	±0.018	27.42/24
201.6 GeV	1.009	±0.024	±0.000	±0.004	±0.002	±0.006	±0.025	
204.9 GeV	0.976	±0.016	±0.000	±0.004	±0.002	±0.006	±0.018	
206.6 GeV	1.011	±0.013	±0.000	±0.004	±0.002	±0.006	±0.015	
Average	0.998	±0.006	±0.000	±0.004	±0.001	±0.006	±0.009	39.04/31
RACOONWW [123]								
182.7 GeV	1.028	±0.021	±0.001	±0.006	±0.003	±0.007	±0.023	
188.6 GeV	0.985	±0.011	±0.001	±0.003	±0.002	±0.005	±0.013	
191.6 GeV	1.012	±0.028	±0.001	±0.004	±0.002	±0.006	±0.029	
195.5 GeV	1.037	±0.017	±0.001	±0.004	±0.002	±0.006	±0.019	
199.5 GeV	0.992	±0.016	±0.001	±0.004	±0.002	±0.006	±0.018	27.42/24
201.6 GeV	1.012	±0.024	±0.001	±0.004	±0.002	±0.006	±0.025	
204.9 GeV	0.978	±0.016	±0.001	±0.004	±0.002	±0.006	±0.018	
206.6 GeV	1.014	±0.013	±0.001	±0.004	±0.002	±0.006	±0.015	
Average	1.000	±0.006	±0.000	±0.004	±0.001	±0.006	±0.009	39.14/31

Table C.4: Ratios of LEP combined W-pair cross section measurements to the expectations of the four theoretical models considered, for different centre–of–mass energies and for all energies combined. The first column contains the centre–of–mass energy, the second the combined ratios, the third the statistical errors. The fourth, fifth, sixth and seventh columns contain the sources of systematic errors that are considered as LEP-correlated energy-uncorrelated (LCEU), LEP-correlated energy-correlated (LCEC), LEP-uncorrelated energy-uncorrelated (LUEU), LEP-uncorrelated energy-correlated (LUEC). The total error is given in the eighth column. The only LCEU systematic sources considered are the statistical errors on the cross section theoretical predictions, while the LCEC, LUEU and LUEC sources are those coming from the corresponding errors on the cross section measurements.

Decay channel	B	ΔB^{stat}	(unc) ΔB^{syst}	(cor) ΔB^{syst}	ΔB^{syst}	ΔB	3×3 correlation for ΔB
ALEPH [115]							
$\mathcal{B}(W \to e\overline{\nu}_e)$	10.95	±0.27	±0.15	±0.04	±0.16	±0.31	1.000 -0.048 -0.271
$\mathcal{B}(W \to \mu\overline{\nu}_\mu)$	11.11	±0.25	±0.14	±0.04	±0.15	±0.29	-0.048 1.000 -0.253
$\mathcal{B}(W \to \tau\overline{\nu}_\tau)$	10.57	±0.32	±0.20	±0.04	±0.20	±0.38	-0.271 -0.253 1.000
DELPHI [116]							
$\mathcal{B}(W \to e\overline{\nu}_e)$	10.36	±0.30	±0.15	±0.05	±0.16	±0.34	1.000 -0.050 -0.330
$\mathcal{B}(W \to \mu\overline{\nu}_\mu)$	10.62	±0.26	±0.09	±0.05	±0.10	±0.28	-0.050 1.000 -0.250
$\mathcal{B}(W \to \tau\overline{\nu}_\tau)$	10.99	±0.39	±0.26	±0.03	±0.26	±0.47	-0.330 -0.250 1.000
L3 [117]							
$\mathcal{B}(W \to e\overline{\nu}_e)$	10.40	±0.26	±0.13	±0.06	±0.14	±0.30	1.000 -0.016 -0.279
$\mathcal{B}(W \to \mu\overline{\nu}_\mu)$	9.72	±0.27	±0.14	±0.06	±0.15	±0.31	-0.016 1.000 -0.295
$\mathcal{B}(W \to \tau\overline{\nu}_\tau)$	11.78	±0.38	±0.20	±0.06	±0.21	±0.43	-0.279 -0.295 1.000
OPAL [118]							
$\mathcal{B}(W \to e\overline{\nu}_e)$	10.40	±0.25	±0.24	±0.05	±0.25	±0.35	1.000 0.141 -0.179
$\mathcal{B}(W \to \mu\overline{\nu}_\mu)$	10.61	±0.25	±0.23	±0.06	±0.24	±0.35	0.141 1.000 -0.174
$\mathcal{B}(W \to \tau\overline{\nu}_\tau)$	11.18	±0.31	±0.37	±0.05	±0.37	±0.48	-0.179 -0.174 1.000
LEP Average (without lepton universality assumption)							
$\mathcal{B}(W \to e\overline{\nu}_e)$	10.54	±0.13	±0.08	±0.05	±0.10	±0.17	1.000 0.066 -0.214
$\mathcal{B}(W \to \mu\overline{\nu}_\mu)$	10.54	±0.13	±0.08	±0.05	±0.09	±0.16	0.066 1.000 -0.189
$\mathcal{B}(W \to \tau\overline{\nu}_\tau)$	11.09	±0.17	±0.13	±0.04	±0.14	±0.22	-0.214 -0.189 1.000
χ^2/d.o.f.	14.9/9						
LEP Average (with lepton universality assumption)							
$\mathcal{B}(W \to \ell\overline{\nu}_\ell)$	10.69	±0.06	±0.05	±0.05	±0.07	±0.09	
$\mathcal{B}(W \to$ had.$)$	67.92	±0.17	±0.15	±0.15	±0.21	±0.27	
χ^2/d.o.f.	18.8/11						

Table C.5: W branching fraction measurements (in %). The first column contains the decay channel, the second the measurements, the third the statistical uncertainty. The fourth and fifth column list the uncorrelated and correlated components of the systematic errors, as provided by the Collaborations. The total systematic error is given in the sixth column and the total error in the seventh. Correlation matrices for the three leptonic branching fractions are given in the last column. This table is identical to Table 7 of Ref. [95], because results are not updated with respect to those presented for the winter 2001 conferences.

$\sqrt{s}$	σ_{ZZ}	$\Delta\sigma_{ZZ}^{stat}$	$\Delta\sigma_{ZZ}^{syst\,(unc)}$	$\Delta\sigma_{ZZ}^{syst\,(cor)}$	$\Delta\sigma_{ZZ}^{syst}$	$\Delta\sigma_{ZZ}$	$\Delta\sigma_{ZZ}^{stat\,(exp)}$
ALEPH [132, 141, 142]							
182.7 GeV	0.11	$^{+0.16}_{-0.11}$	±0.04	±0.01	±0.04	$^{+0.16}_{-0.12}$	±0.14
188.6 GeV	0.67	$^{+0.13}_{-0.12}$	±0.04	±0.01	±0.04	$^{+0.14}_{-0.13}$	±0.13
191.6 GeV	0.53	$^{+0.34}_{-0.27}$	±0.02	±0.01	±0.02	$^{+0.34}_{-0.27}$	±0.33
195.5 GeV	0.69	$^{+0.23}_{-0.20}$	±0.03	±0.01	±0.03	$^{+0.23}_{-0.20}$	±0.23
199.5 GeV	0.70	$^{+0.22}_{-0.20}$	±0.03	±0.01	±0.03	$^{+0.22}_{-0.20}$	±0.23
201.6 GeV	0.70	$^{+0.33}_{-0.28}$	±0.02	±0.01	±0.02	$^{+0.33}_{-0.28}$	±0.35
204.9 GeV	1.21	$^{+0.26}_{-0.23}$	±0.03	±0.01	±0.03	$^{+0.26}_{-0.23}$	±0.27
206.6 GeV	1.01	$^{+0.19}_{-0.17}$	±0.02	±0.01	±0.02	$^{+0.19}_{-0.17}$	±0.18
DELPHI [133, 143–145]							
182.7 GeV	0.38	±0.18	±0.04	±0.01	±0.04	±0.18	±0.15
188.6 GeV	0.60	±0.13	±0.07	±0.02	±0.07	±0.15	±0.14
191.6 GeV	0.55	±0.33	±0.08	±0.02	±0.08	±0.34	±0.40
195.5 GeV	1.17	±0.27	±0.09	±0.03	±0.10	±0.29	±0.24
199.5 GeV	1.08	±0.24	±0.10	±0.03	±0.11	±0.26	±0.23
201.6 GeV	0.87	±0.31	±0.11	±0.03	±0.11	±0.33	±0.34
204.9 GeV	1.05	±0.23	±0.12	±0.04	±0.12	±0.26	±0.23
206.6 GeV	0.98	±0.18	±0.11	±0.03	±0.12	±0.22	±0.19
L3 [134–136, 138, 146]							
182.7 GeV	0.31	$^{+0.16}_{-0.15}$	±0.05	±0.01	±0.05	$^{+0.17}_{-0.15}$	±0.16
188.6 GeV	0.73	$^{+0.15}_{-0.14}$	±0.03	±0.02	±0.04	$^{+0.15}_{-0.14}$	±0.15
191.6 GeV	0.29	±0.22	±0.01	±0.02	±0.02	±0.22	±0.34
195.5 GeV	1.18	±0.24	±0.06	±0.07	±0.09	±0.26	±0.22
199.5 GeV	1.25	±0.25	±0.06	±0.07	±0.09	±0.27	±0.24
201.6 GeV	0.95	±0.38	±0.05	±0.05	±0.07	±0.39	±0.35
204.9 GeV	0.84	±0.22	±0.05	±0.05	±0.07	±0.23	±0.23
206.6 GeV	1.20	±0.18	±0.07	±0.07	±0.10	±0.21	±0.17
OPAL [137, 139]							
182.7 GeV	0.12	$^{+0.20}_{-0.18}$	±0.03	±0.01	±0.03	$^{+0.20}_{-0.18}$	±0.19
188.6 GeV	0.80	$^{+0.14}_{-0.13}$	±0.06	±0.02	±0.06	$^{+0.15}_{-0.14}$	±0.14
191.6 GeV	1.13	$^{+0.46}_{-0.39}$	±0.11	±0.03	±0.11	$^{+0.47}_{-0.41}$	±0.36
195.5 GeV	1.19	$^{+0.27}_{-0.24}$	±0.09	±0.03	±0.09	$^{+0.28}_{-0.26}$	±0.25
199.5 GeV	1.09	$^{+0.25}_{-0.23}$	±0.08	±0.02	±0.08	$^{+0.26}_{-0.24}$	±0.25
201.6 GeV	0.94	$^{+0.37}_{-0.32}$	±0.07	±0.03	±0.08	$^{+0.38}_{-0.33}$	±0.37
204.9 GeV	1.07	$^{+0.26}_{-0.24}$	±0.09	±0.03	±0.09	$^{+0.28}_{-0.26}$	±0.26
206.6 GeV	1.07	$^{+0.20}_{-0.19}$	±0.07	±0.03	±0.08	$^{+0.22}_{-0.21}$	±0.21
LEP Averages							χ^2/d.o.f.
182.7 GeV	0.23	±0.08	±0.02	±0.01	±0.02	±0.08	2.28/3
188.6 GeV	0.70	±0.07	±0.03	±0.02	±0.03	±0.08	0.97/3
191.6 GeV	0.60	±0.18	±0.03	±0.02	±0.04	±0.18	2.88/3
195.5 GeV	1.04	±0.12	±0.03	±0.03	±0.05	±0.13	3.23/3
199.5 GeV	1.01	±0.12	±0.04	±0.03	±0.05	±0.13	2.80/3
201.6 GeV	0.86	±0.18	±0.04	±0.03	±0.05	±0.18	0.32/3
204.9 GeV	1.03	±0.12	±0.04	±0.03	±0.05	±0.13	1.11/3
206.6 GeV	1.06	±0.09	±0.04	±0.03	±0.05	±0.11	0.76/3

Table C.6: Z-pair production cross section (in pb) at different energies. The first column contains the LEP centre–of–mass energy, the second the measurements and the third the statistical uncertainty. The fourth and the fifth columns list the uncorrelated and correlated components of the systematic errors, as provided by the Collaborations. The total systematic error is given in the sixth column, the total error in the seventh. The eighth column lists, for the four LEP measurements, the symmetrized expected statistical error, and for the LEP combined value, the χ^2 of the fit.

$\sqrt{s}$	$\sigma_{We\nu\ (tot)}$	$\Delta\sigma^{stat}_{We\nu\ (tot)}$	$\Delta\sigma^{syst}_{We\nu\ (tot)}$	$\Delta\sigma_{We\nu\ (tot)}$	$\Delta\sigma^{stat\,(exp)}_{We\nu\ (tot)}$
ALEPH [149, 152, 155]					
182.7 GeV	0.61	± 0.26	± 0.06	± 0.27	± 0.25
188.6 GeV	0.45	± 0.14	± 0.04	± 0.15	± 0.16
191.6 GeV	1.31	± 0.47	± 0.11	± 0.48	± 0.40
195.5 GeV	0.65	± 0.24	± 0.06	± 0.25	± 0.25
199.5 GeV	0.99	± 0.25	± 0.10	± 0.27	± 0.24
201.6 GeV	0.75	± 0.35	± 0.08	± 0.36	± 0.36
204.9 GeV	0.78	± 0.26	± 0.07	± 0.27	± 0.26
206.6 GeV	1.19	± 0.22	± 0.12	± 0.25	± 0.21
DELPHI [150, 157]					
188.6 GeV	0.75	$^{+0.29}_{-0.25}$	± 0.07	$^{+0.30}_{-0.26}$	± 0.26
191.6 GeV	0.17	$^{+0.33}_{-0.17}$	± 0.07	$^{+0.34}_{-0.18}$	± 0.61
195.5 GeV	0.94	$^{+0.40}_{-0.35}$	± 0.07	$^{+0.41}_{-0.36}$	± 0.36
199.5 GeV	0.51	$^{+0.32}_{-0.31}$	± 0.07	$^{+0.33}_{-0.32}$	± 0.30
201.6 GeV	1.15	$^{+0.55}_{-0.45}$	± 0.07	$^{+0.55}_{-0.46}$	± 0.47
204.9 GeV	0.56	$^{+0.36}_{-0.31}$	± 0.06	$^{+0.36}_{-0.32}$	± 0.35
206.6 GeV	0.58	$^{+0.25}_{-0.22}$	± 0.06	$^{+0.26}_{-0.23}$	± 0.28
L3 [151, 153, 154, 158]					
182.7 GeV	0.80	$^{+0.28}_{-0.25}$	± 0.05	$^{+0.28}_{-0.25}$	± 0.26
188.6 GeV	0.69	$^{+0.16}_{-0.14}$	± 0.04	$^{+0.16}_{-0.15}$	± 0.15
191.6 GeV	1.06	$^{+0.48}_{-0.41}$	± 0.09	$^{+0.49}_{-0.42}$	± 0.45
195.5 GeV	0.98	$^{+0.27}_{-0.25}$	± 0.09	$^{+0.28}_{-0.27}$	± 0.24
199.5 GeV	0.79	$^{+0.26}_{-0.23}$	± 0.06	$^{+0.27}_{-0.24}$	± 0.25
201.6 GeV	1.38	$^{+0.45}_{-0.40}$	± 0.13	$^{+0.47}_{-0.42}$	± 0.38
OPAL [159]					
188.6 GeV	0.67	$^{+0.16}_{-0.14}$	± 0.06	$^{+0.17}_{-0.15}$	± 0.16
LEP Averages					χ^2/d.o.f.
182.7 GeV	0.70	± 0.18	± 0.04	± 0.19	0.26/1
188.6 GeV	0.62	± 0.09	± 0.03	± 0.09	1.60/3
191.6 GeV	0.99	± 0.27	± 0.06	± 0.28	2.38/2
195.5 GeV	0.84	± 0.16	± 0.05	± 0.16	0.92/2
199.5 GeV	0.79	± 0.15	± 0.05	± 0.16	1.40/2
201.6 GeV	1.06	± 0.23	± 0.06	± 0.24	1.38/2
204.9 GeV	0.70	± 0.21	± 0.05	± 0.22	0.24/1
206.6 GeV	0.94	± 0.17	± 0.08	± 0.18	2.71/1

Table C.7: Single-W total production cross section (in pb) at different energies. The first column contains the LEP centre–of–mass energy, and the second the measurements. The third and fourth column list the statistical and systematic uncertainties, and the fifth the total error. The sixth column lists, for the four LEP measurements, the symmetrized expected statistical error, and for the LEP combined value, the χ^2 of the fit.

$\sqrt{s}$	$\sigma_{\mathrm{We\nu}\ (\mathrm{had})}$	$\Delta\sigma^{\mathrm{stat}}_{\mathrm{We\nu}\ (\mathrm{had})}$	$\Delta\sigma^{\mathrm{syst}}_{\mathrm{We\nu}\ (\mathrm{had})}$	$\Delta\sigma_{\mathrm{We\nu}\ (\mathrm{had})}$	$\Delta\sigma^{\mathrm{stat\,(exp)}}_{\mathrm{We\nu}\ (\mathrm{had})}$
ALEPH [149, 152, 155]					
182.7 GeV	0.40	± 0.23	± 0.06	± 0.24	± 0.23
188.6 GeV	0.31	± 0.13	± 0.04	± 0.14	± 0.14
191.6 GeV	0.94	± 0.43	± 0.11	± 0.44	± 0.37
195.5 GeV	0.45	± 0.22	± 0.06	± 0.23	± 0.23
199.5 GeV	0.82	± 0.24	± 0.10	± 0.26	± 0.22
201.6 GeV	0.68	± 0.34	± 0.08	± 0.35	± 0.33
204.9 GeV	0.50	± 0.24	± 0.07	± 0.25	± 0.24
206.6 GeV	0.95	± 0.21	± 0.12	± 0.24	± 0.19
DELPHI [150, 157]					
188.6 GeV	0.44	$^{+0.27}_{-0.24}$	± 0.07	$^{+0.28}_{-0.25}$	± 0.25
191.6 GeV	0.01	$^{+0.18}_{-0.01}$	± 0.07	$^{+0.19}_{-0.07}$	± 0.57
195.5 GeV	0.78	$^{+0.37}_{-0.33}$	± 0.07	$^{+0.38}_{-0.34}$	± 0.33
199.5 GeV	0.16	$^{+0.28}_{-0.16}$	± 0.07	$^{+0.29}_{-0.17}$	± 0.27
201.6 GeV	0.55	$^{+0.46}_{-0.39}$	± 0.07	$^{+0.47}_{-0.40}$	± 0.43
204.9 GeV	0.50	$^{+0.34}_{-0.30}$	± 0.06	$^{+0.35}_{-0.31}$	± 0.33
206.6 GeV	0.37	$^{+0.23}_{-0.20}$	± 0.06	$^{+0.24}_{-0.21}$	± 0.26
L3 [151, 153, 154, 158]					
182.7 GeV	0.58	$^{+0.23}_{-0.20}$	± 0.04	$^{+0.23}_{-0.20}$	± 0.21
188.6 GeV	0.52	$^{+0.14}_{-0.13}$	± 0.03	$^{+0.14}_{-0.13}$	± 0.14
191.6 GeV	0.85	$^{+0.45}_{-0.37}$	± 0.06	$^{+0.45}_{-0.37}$	± 0.41
195.5 GeV	0.66	$^{+0.24}_{-0.22}$	± 0.05	$^{+0.25}_{-0.23}$	± 0.21
199.5 GeV	0.34	$^{+0.23}_{-0.20}$	± 0.03	$^{+0.23}_{-0.20}$	± 0.22
201.6 GeV	1.09	$^{+0.41}_{-0.36}$	± 0.08	$^{+0.42}_{-0.37}$	± 0.35
OPAL [159]					
188.6 GeV	0.53	$^{+0.13}_{-0.12}$	± 0.05	$^{+0.14}_{-0.13}$	± 0.13
LEP Averages					χ^2/d.o.f.
182.7 GeV	0.50	± 0.16	± 0.04	± 0.16	0.31/1
188.6 GeV	0.46	± 0.08	± 0.02	± 0.08	1.47/3
191.6 GeV	0.73	± 0.25	± 0.06	± 0.25	1.94/2
195.5 GeV	0.60	± 0.14	± 0.03	± 0.15	0.77/2
199.5 GeV	0.46	± 0.14	± 0.04	± 0.14	3.60/2
201.6 GeV	0.80	± 0.21	± 0.05	± 0.21	1.13/2
204.9 GeV	0.50	± 0.20	± 0.05	± 0.20	0.00/1
206.6 GeV	0.71	± 0.15	± 0.08	± 0.17	2.77/1

Table C.8: Single-W hadronic production cross section (in pb) at different energies. The first column contains the LEP centre–of–mass energy, and the second the measurements. The third and fourth column list the statistical and systematic uncertainties, and the fifth the total error. The sixth column lists, for the four LEP measurements, the symmetrized expected statistical error, and for the LEP combined value, the χ^2 of the fit.

Bibliography

[1] The LEP Collaborations ALEPH, DELPHI, L3, OPAL and the LEP Electroweak Working Group, and the SLD Heavy Flavour and Electroweak Groups, *A Combination of Preliminary Electroweak Measurements and Constraints on the Standard Model*, CERN–EP-2001-21, hep-ex/0103048.

[2] The LEP Collaborations ALEPH, DELPHI, L3 and OPAL and the LEP Electroweak working group, *Combination procedure for the precise determination of Z boson parameters from results of the LEP experiments*, CERN–EP-2000-153, hep-ex/0101027.

[3] The LEP Experiments: ALEPH, DELPHI, L3 and OPAL, Nucl. Inst. Meth. **A378** (1996) 101.

[4] ALEPH Collaboration, D. Decamp *et al.*, Z. Phys. **C48** (1990) 365;
ALEPH Collaboration, D. Decamp *et al.*, Z. Phys. **C53** (1992) 1;
ALEPH Collaboration, D. Buskulic *et al.*, Z. Phys. **C60** (1993) 71;
ALEPH Collaboration, D. Buskulic *et al.*, Z. Phys. **C62** (1994) 539;
ALEPH Collaboration, R. Barate *et al.*, Eur. Phys. J. **C 14** (2000) 1.

[5] DELPHI Collaboration, P. Aarnio *et al.*, Nucl. Phys. **B367** (1991) 511;
DELPHI Collaboration, P. Abreu *et al.*, Nucl. Phys. **B417** (1994) 3;
DELPHI Collaboration, P. Abreu *et al.*, Nucl. Phys. **B418** (1994) 403;
DELPHI Collaboration, P. Abreu *et al.*, Eur. Phys. J. **C 16** (2000) 371.

[6] L3 Collaboration, B. Adeva *et al.*, Z. Phys. **C51** (1991) 179;
L3 Collaboration, O. Adriani *et al.*, Phys. Rep. **236** (1993) 1;
L3 Collaboration, M. Acciarri *et al.*, Z. Phys. **C62** (1994) 551;
L3 Collaboration, M. Acciarri *et al.*, Eur. Phys. J. **C16** (2000) 1-40.

[7] OPAL Collaboration, G. Alexander *et al.*, Z. Phys. **C52** (1991) 175;
OPAL Collaboration, P.D. Acton *et al.*, Z. Phys. **C58** (1993) 219;
OPAL Collaboration, R. Akers *et al.*, Z. Phys. **C61** (1994) 19;
OPAL Collaboration, G. Abbiendi *et al.*, Eur. Phys. J. **C14** (2000) 373;
OPAL Collaboration, G. Abbiendi *et al.*, Eur. Phys. J. **C19** (2001) 587.

[8] F.A. Berends *et al.*, in *Z Physics at LEP 1, Vol. 1*, ed. G. Altarelli, R. Kleiss and C. Verzegnassi, (CERN Report: CERN 89-08, 1989), p. 89.
M. Böhm *et al.*, in *Z Physics at LEP 1, Vol. 1*, ed. G. Altarelli, R. Kleiss and C. Verzegnassi, (CERN Report: CERN 89-08, 1989), p. 203.

[9] See, for example, M. Consoli *et al.*, in *Z Physics at LEP 1, Vol. 1*, ed G. Altarelli, R. Kleiss and C. Verzegnassi, (CERN Report: CERN 89-08, 1989), p. 7.

[10] S. Jadach, *et al.*, Phys. Lett. **B257** (1991) 173.

[11] M. Skrzypek, Acta Phys. Pol. **B23** (1992) 135.

[12] G. Montagna, *et al.*, Phys. Lett. **B406** (1997) 243.

[13] G. Montagna *et al.*, Nucl. Phys. **B547** (1999) 39;
G. Montagna *et al.*, Phys. Rev. Lett. **459** (1999) 649.

[14] B.F.L Ward *et al.*, Phys. Lett. **B450** (1999) 262.

[15] D. Bardin, M. Grünewald and G. Passarino, *Precision Calculation Project Report*, hep-ph/9902452.

[16] ALEPH Collaboration, D. Buskulic *et al.*, Zeit. Phys. **C69** (1996) 183;
ALEPH Collaboration, A. Heister *et al.*, CERN-EP/2001-027 and Eur. Phys. J. **C20** (2001) 401.

[17] DELPHI Collaboration, P. Abreu *et al.*, Eur. Phys. J. **C14** (2000) 585.

[18] L3 Collaboration, M. Acciarri *et al.*, Phys. Lett. **B429** (1998) 387.

[19] OPAL Collaboration, G. Abbiendi *et al.*, *Precision Neutral Current Asymmetry Parameter Measurements from the Tau Polarization at LEP*, CERN-EP-2001-023, Submitted to Eur. Phys. J. C.

[20] The LEP Collaborations ALEPH, DELPHI, L3, OPAL and the LEP Electroweak Working Group, *Combined Preliminary Data on Z Parameters from the LEP Experiments and Constraints on the Standard Model*, CERN–PPE/94-187.

[21] SLD Collaboration, K. Abe *et al.*, Phys. Rev. Lett. **84** (2000) 5945.

[22] SLD Collaboration, K. Abe *et al.*, SLAC-PUB-8618, (2000). Submitted to Phys.Rev.Lett.

[23] The LEP Heavy Flavour Group, *Final input parameters for the LEP/SLD heavy flavour analyses,* LEPHF/01-01,
http://www.cern.ch/LEPEWWG/heavy/lephf0101.ps.gz.

[24] ALEPH Collaboration, R. Barate *et al.*, Physics Letters **B 401** (1997) 150;
ALEPH Collaboration, R. Barate *et al.*, Physics Letters **B 401** (1997) 163.

[25] DELPHI Collaboration, P.Abreu *et al.*, Eur. Phys. J. **C10** (1999) 415.

[26] L3 Collaboration, M. Acciarri *et al.*, Eur. Phys. J. **C13** (2000) 47.

[27] OPAL Collaboration, G. Abbiendi *et al.*, Eur. Phys. J. **C8** (1999) 217.

[28] SLD Collaboration, K. Abe *et al.*, Phys. Rev. Lett. **80** (1998) 660;
see also [242].

[29] ALEPH Collaboration, R. Barate *et al.*, Eur. Phys. J. **C4** (1998) 557.

[30] DELPHI Collaboration, P.Abreu *et al.*, Eur. Phys. J. **C12** (2000) 209.

[31] DELPHI Collaboration, P.Abreu *et al.*, Eur. Phys. J. **C12** (2000) 225.

[32] OPAL Collaboration, K. Ackerstaff *et al.*, Eur. Phys. J. **C1** (1998) 439.

[33] ALEPH Collaboration, R. Barate *et al.*, Eur. Phys. J. **C16** (2000) 597.

[34] OPAL Collaboration, G. Alexander *et al.*, Z. Phys. **C72** (1996) 1.

[35] SLD Collaboration, *A Measurement of R_c with the SLD Detector* SLAC–PUB–7880, contributed paper to ICHEP 98 Vancouver **ICHEP'98 #174** ;
see also [242].

[36] D. Abbaneo *et al.*, Eur. Phys. J. **C4** (1998) 185.

[37] D. Bardin *et al.*, Z. Phys. **C44** (1989) 493; Comp. Phys. Comm. **59** (1990) 303; Nucl. Phys. **B351**(1991) 1; Phys. Lett. **B255** (1991) 290 and CERN-TH 6443/92 (May 1992); the most recent version of ZFITTER (6.21) is described in DESY 99-070, hep-ph/9908433 (Aug 1999) published in Comp. Phys. Comm. **133** (2001) 229.

[38] ALEPH Collaboration, D. Buskulic *et al.*, Phys. Lett. **B384** (1996)414;
ALEPH Collaboration, *Measurement of the b and c forward-backward asymmetries using leptons* ALEPH 99-076 CONF 99-048, contributed paper to EPS 99 Tampere **HEP'99 #6-65**.

[39] DELPHI Collaboration, P.Abreu *et al.*, Z. Phys **C65** (1995) 569;
DELPHI Collaboration, *Measurement of the Forward-Backward Asymmetries of $e^+e^- \to Z \to b\bar{b}$ and $e^+e^- \to Z \to c\bar{c}$ using prompt leptons* DELPHI 2000-101 CONF 400, contributed paper to ICHEP 2000 Osaka **ICHEP'00 #377** .
Delphi notes are available at http://wwwcn.cern.ch/~pubxx/www/delsec/delnote/.

[40] L3 Collaboration, O. Adriani *et al.*, Phys. Lett. **B292** (1992) 454;
L3 Collaboration, *L3 Results on $A_{\rm FB}^{\rm b\overline{b}}$, $A_{\rm FB}^{\rm c\overline{c}}$ and χ for the Glasgow Conference,* L3 Note 1624;
L3 Collaboration, M. Acciarri *et al.*, Phys. Lett. **B448** (1999) 152.

[41] OPAL Collaboration, G. Alexander *et al.*, Z. Phys. **C70** (1996) 357;
OPAL Collaboration, R. Akers *et al.*, *Updated Measurement of the Heavy Quark Forward-Backward Asymmetries and Average B Mixing Using Leptons in Multihadronic Events*, OPAL Physics Note PN226 contributed paper to ICHEP96, Warsaw, 25-31 July 1996 **PA05-007**
OPAL Collaboration, R. Akers *et al.*, *QCD corrections to the bottom and charm forward-backward asymmetries* OPAL Physics Note PN284.

[42] ALEPH Collaboration, A. Heister *et al.*, *Measurement of A_{FB}^b using Inclusive b-hadron Decays*, CERN-EP/2001-047 and Eur. Phys. J. C DOI 10.1007/s100520100812.

[43] DELPHI Collaboration, P.Abreu *et al.*, Eur. Phys. J. **C9** (1999) 367.

[44] DELPHI Collaboration, *Determination of A_{FB}^b using inclusive charge reconstruction and lifetime tagging at LEP 1*, DELPHI 2001-027 CONF 468.

[45] L3 Collaboration, M. Acciarri *et al.*, Phys. Lett. **B439** (1998) 225.

[46] OPAL Collaboration, K.Ackerstaff *et al.*, Z. Phys. **C75** (1997) 385.

[47] ALEPH Collaboration, R. Barate *et al.*, Phys. Lett. **B434** (1998) 415.

[48] DELPHI Collaboration, P.Abreu *et al.*, Eur. Phys. J. **C10** (1999) 219.

[49] OPAL Collaboration, G. Alexander *et al.*, Z. Phys. **C73** (1996) 379.

[50] SLD Collaboration, K. Abe *et al.*, Phys. Rev. Lett. **30** (1999) 3384; SLD Collaboration, K. Abe *et al.*, SLAC-PUB-8951, to be submitted to Phys. Rev. Lett.

[51] SLD Collaboration, K. Abe, *et al.*, Phys Rev. **D63** 032005 (2001);
see also [242].

[52] SLD Collaboration, K. Abe, *et al.*, Phys Rev. Lett. **81** 942 (1998);
see also [242].

[53] SLD Collaboration, K. Abe et al, Phys. Rev. Lett. **83**, 1902 (1999).

[54] SLD Collaboration, *Direct measurement of $\mathcal{A}_b$ using charged kaons at the SLD detector*, SLAC-PUB-8200, contributed paper to EPS 99 Tampere **HEP'99 #6_473** ;
SLD Collaboration, *Direct measurement of Ab using charged vertices*, SLAC-PUB-8542, Contributed Paper to ICHEP2000 , **# 743**;
see also [242].

[55] SLD Collaboration, *Direct measurement of $\mathcal{A}_c$ using inclusive charm tagging at the SLD detector*, SLAC-PUB-8199, contributed paper to EPS 99 Tampere **HEP'99 #6_474** ;
see also [242].

[56] ALEPH Collaboration. , *Inclusive semileptonic branching ratios of b hadrons produced in Z decays*, CERN-EP/2001-057.

[57] DELPHI Collaboration, *Measurement of the semileptonic b branching ratios in Z decays* DELPHI 99-111 CONF 298, contributed paper to EPS 99 Tampere **HEP'99 #5_522** .

[58] L3 Collaboration, M. Acciarri *et al.*, Z Phys. **C71** 379 (1996).

[59] OPAL Collaboration, G. Abbiendi *et al.*, Eur. Phys. J. **C13** (2000) 225.

[60] OPAL Collaboration, G. Abbiendi *et al.*, Eur. Phys. J. **C8** (1999) 573.

[61] ALEPH Collaboration, D. Buskulic *et al.*, Z. Phys. **C71** (1996) 357.

[62] DELPHI Collaboration, P. Abreu *et al.*, Phys. Lett. **B277** (1992) 371.

[63] OPAL Collaboration, P. D. Acton *et al.*, Phys. Lett. **B294** (1992) 436.

[64] T. Sjöstrand, Comp. Phys. Comm. **82** (1994) 74.

[65] G. Marchesini *et al.*, Comp. Phys. Comm. **67** (1992) 465.

[66] ALEPH Collab., ALEPH 2000-008 CONF 2000-005 and ref. therein;
DELPHI Collab., DELPHI 2001-093 CONF 521 and ref. therein;
L3 Collab., L3 Note 2650 and ref. therein;
OPAL Collab. OPAL PN469.

[67] S. D. Drell, Ann. Phys. **4** (1958) 75.

[68] F. E. Low, Phys. Rev. Lett. **14** (1965) 238.

[69] O. J. P. Eboli, A. A. Natale, and S. F. Novaes, Phys. Lett. **B271** (1991) 274.

[70] K. Agashe and N. G. Deshpande, Phys. Lett. **B456** (1999) 60.

[71] B. Vachon. Excited electron contribution to the $e^+e^- \to \gamma\gamma$ cross-section. hep-ph/0103132, 2001.

[72] LEPEWWG $f\bar{f}$ Subgroup, D. Bourilkov *et. al.*, LEP2FF/01-01,ALEPH 2001-039 PHYSIC 2000-013, DELPHI 2001-108 PHYS 896, L3 note 2663, OPAL TN690.

[73] LEPEWWG $f\bar{f}$ Subgroup, C. Geweniger *et. al.*, LEP2FF/00-03,ALEPH 2000-088 PHYSIC 2000-034, DELPHI 2000-168 PHYS 881, L3 note 2624, OPAL TN673.

[74] LEPEWWG $f\bar{f}$ Subgroup, D. Bourilkov *et. al.*, LEP2FF/00-01,ALEPH 2000-026 PHYSIC 2000-005, DELPHI 2000-046 PHYS 855, L3 note 2527, OPAL TN647.

[75] LEPEWWG $f\bar{f}$ Subgroup, D. Bourilkov *et. al.*, LEP2FF/99-01,ALEPH 99-082 PHYSIC 99-030, DELPHI 99-143 PHYS 829, L3 note 2443, OPAL TN616.

[76] LEPEWWG $f\bar{f}$ subgroup: http://www.cern.ch/LEPEWWG/lep2/ .

[77] ALEPH Collaboration "Study of Fermion Pair Production in e^+e^- Collisions at 130-183 GeV", Eur. Phys. J. **C12** (2000) 183;
ALEPH Collaboration, "Fermion Pair Production in e^+e^- Collisions at 189 GeV and Limits on Physics Beyond the Standard Model", ALEPH 99-018 CONF 99-013;
ALEPH Collaboration, "Fermion Pair Production in e^+e^- Collisions from 192 to 202 GeV", ALEPH 2000-025 CONF 2000-021;
ALEPH Collaboration, "Fermion Pair Production in e^+e^- Collisions at high energy and Limits on Physics beyond the Standard Model ", ALEPH 2001-019 CONF 2001-016;
DELPHI Collaboration,"Measurement and Interpretation of Fermion-Pair Production at LEP energies from 130 to 172 GeV", Eur. Phys. J. **C11** (1999), 383;
DELPHI Collaboration, "Measurement and Interpretation of Fermion-Pair Production at LEP Energies from 183 to 189 GeV", Phys.Lett. **B485** (2000), 45;
DELPHI Collaboration, "Results on Fermion-Pair Production at LEP running from 192 to 202 GeV", DELPHI 2000-128 OSAKA CONF 427;
DELPHI Collaboration, "Results on Fermion-Pair Production at LEP running in 2000", DELPHI 2001-094 CONF 522;
L3 Collaboration, "Measurement of Hadron and Lepton-Pair Production at 161 GeV $< \sqrt{s} <$ 172 GeV at LEP", Phys. Lett. **B407** (1997) 361;
L3 Collaboration, "Measurement of Hadron and Lepton-Pair Production at 130 GeV $< \sqrt{s} <$ 189 GeV at LEP", Phys. Lett. **B479** (2000), 101.
L3 Collaboration, "Preliminary L3 Results on Fermion-Pair Production in 1999", L3 note 2563;
L3 Collaboration,"Preliminary L3 Results on Fermion-Pair Production in 2000", L3 note 2648;
OPAL Collaboration, "Tests of the Standard Model and Constraints on New Physics from Measurements of Fermion Pair Production at 130 - 172 GeV at LEP", Euro. Phys. J. **C2** (1998) 441;
OPAL Collaboration, "Tests of the Standard Model and Constraints on New Physics from Measurements of Fermion Pair Production at 183 GeV at LEP", Euro. Phys. J. **C6** (1999) 1;
OPAL Collaboration, "Tests of the Standard Model and Constraints on New Physics from Measurements of Fermion Pair Production at 189 GeV at LEP", Euro. Phys. J. **C13** (2000) 553;
OPAL Collaboration, "Tests of the Standard Model and Constraints on New Physics from Measurements of Fermion Pair Production at 192-202 GeV at LEP", OPAL PN424 (2000);
OPAL Collaboration, "Measurement of Standard Model Processes in e+e- Collisions at sqrts 203-209 GeV", OPAL PN469 (2001).

[78] D. Bardin *et al.*, CERN-TH 6443/92; http://www.ifh.de/∼riemann/Zfitter/zf.html .
Predictions are from ZFITTER versions 6.04 or later.
Definition 1 corresponds to the ZFITTER flags FINR=0 and INTF=0; definition 2 corresponds to FINR=0 and INTF=1 for hadrons, FINR=1 and INTF=1 for leptons.

[79] G. Montagna *et al.*, Comput. Phys. Commun. **117** (1999) 278.

[80] S. Jadach *et al.*, http://home.cern.ch/∼jadach/KKindex.html .

[81] M. Kobel *et al.*, "Two-Fermion Production in Electron Positron Collisions" in S. Jadach *et al.* [eds] , "Reports of the Working Groups on Precision Calculations for LEP2 Physics: proceedings" CERN 2000-009, hep-ph/0007180.

[82] L. Lyons, D. Gibaut and P. Clifford, Nucl. Instr. Meth. **A270** (1988) 110.

[83] ALEPH Collaboration, Euro. Phys J. **C12** (2000) 183;
DELPHI Collaboration, P.Abreu *et al.*, Euro. Phys J. **C11**(1999);
L3 Collaboration, M.Acciarri *et al.*, Phys. Lett. **B485** (2000) 71;
OPAL Collaboration, G.Abbiendi *et al.*, Euro. Phys. J. **C16** (2000) 41.

[84] ALEPH Collaboration, ALEPH 99-018 CONF 99-013;
ALEPH Collaboration, ALEPH 2000-046 CONF 2000-029;
ALEPH Collaboration, ALEPH 2000-047 CONF 2000-030;
ALEPH Collaboration, ALEPH 2001-019 CONF 2001-016;
DELPHI Collaboration, DELPHI 2001-095 CONF 523;
L3 Collaboration, L3 Internal Note 2640, 1 March 2001.

[85] LEPEWWG Heavy Flavour at LEP2 Subgroup, "Combination of Heavy Flavour Measurements at LEP2", LEP2FF/00-02.

[86] ZFITTER V6.23 is used.
D. Bardin *et al.*, Preprint hep-ph/9908433.
Relevant ZFITTER settings used are FINR=0 and INTF=1.

[87] DELPHI Collaboration, P.Abreu *et al.*, Euro Phys J. **C10**(1999) 415.
The LEP collaborations *et al.*, CERN-EP/2000-016.

[88] P. Langacker, R.W. Robinett and J.L. Rosner, Phys. Rev. **D30** (1984) 1470;
D. London and J.L. Rosner, Phys. Rev. **D34** (1986) 1530;
J.C. Pati and A. Salam, Phys. Rev. **D10** (1974) 275;
R.N. Mohapatra and J.C. Pati, Phys. Rev. **D11** (1975) 566.

[89] G. Altarelli *et al.*, Z. Phys. **C45** (1989) 109;
erratum Z. Phys. **C47** (1990) 676.

[90] DELPHI Collaboration, P. Abreu *et al.*, Zeit. Phys. **C65** (1995) 603.

[91] E. Eichten, K. Lane, and M. Peskin, Phys. Rev. Lett. **50** (1983) 811.

[92] H. Kroha, Phys. Rev. **D46** (1992) 58.

[93] The LEP WW Working Group, LEPEWWG/XSEC/2001-03, note prepared for the summer 2001 conferences, `http://lepewwg.web.cern.ch/LEPEWWG/lepww/4f/Summer01`.

[94] The LEP WW Working Group, LEPEWWG/XSEC/2000-01, note prepared for the summer 2000 conferences, `http://lepewwg.web.cern.ch/LEPEWWG/lepww/4f/Summer00`.

[95] The LEP WW Working Group, LEPEWWG/XSEC/2001-01, note prepared for the winter 2001 conferences, `http://lepewwg.web.cern.ch/LEPEWWG/lepww/4f/Winter01`.

[96] M.W. Grünewald, G. Passarino *et al.*, *"Four fermion production in electron positron collisions"*, Four fermion working group report of the LEP2 Monte Carlo Workshop 1999/2000, in *"Reports of the working groups on precision calculations for LEP2 Physics"* CERN 2000–009, `http://arXiv.org/abs/hep-ph/0005309`.

[97] ALEPH Collaboration, R. Barate *et al.*, Phys. Lett. **B401** (1997) 347.
DELPHI Collaboration, P. Abreu *et al.*, Phys. Lett. **B397** (1997) 158.
L3 Collaboration, M. Acciarri *et al.*, Phys. Lett. **B398** (1997) 223.
OPAL Collaboration, K. Ackerstaff *et al.*, Phys. Lett. **B389** (1996) 416.

[98] ALEPH Collaboration, R. Barate *et al.*, Phys. Lett. **B415** (1997) 435.

[99] DELPHI Collaboration, P. Abreu *et al.*, Eur. Phys. J. **C2** (1998) 581.

[100] L3 Collaboration, M. Acciarri *et al.*, Phys. Lett. **B407** (1997) 419.

[101] OPAL Collaboration, K. Ackerstaff *et al.*, Eur. Phys. J. **C1** (1998) 395.

[102] ALEPH Collaboration, R. Barate *et al.*, Phys. Lett. **B453** (1999) 107.

[103] DELPHI Collaboration, P. Abreu *et al.*, Phys. Lett. **B456** (1999) 310.

[104] L3 Collaboration, M. Acciarri *et al.*, Phys. Lett. **B436** (1998) 437.

[105] OPAL Collaboration, G. Abbiendi *et al.*, Eur. Phys. Jour. **C8** (1999) 191.

[106] ALEPH Collaboration, R. Barate *et al.*, Phys. Lett. **B484** (2000) 205.

[107] DELPHI Collaboration, P. Abreu *et al.*, Phys. Lett. **B479** (2000) 89.

[108] L3 Collaboration, M. Acciarri *et al.*, Phys. Lett. **B496** (2000) 19.

[109] OPAL Collaboration, G. Abbiendi *et al.*, Phys. Lett. **B493** (2000) 249.

[110] ALEPH Collaboration, ALEPH 2000–005 CONF 2000–002, ICHEP 2000 abstract 288.

[111] DELPHI Collaboration, DELPHI 2000–140 CONF 439, ICHEP 2000 abstract 458.

[112] OPAL Collaboration, OPAL Physics Note PN420, ICHEP 2000 abstract 184. The W-pair production cross sections at $\sqrt{s} = 200$–202 GeV results have been updated in [113].

[113] OPAL Collaboration, OPAL Physics Note PN437, ICHEP 2000 abstract 168.

[114] L3 Collaboration, L3 Note 2514, ICHEP 2000 abstract 512.

[115] ALEPH Collaboration, ALEPH 2001–013 CONF 2001–010, submitted to the Winter 2001 Conferences.

[116] DELPHI Collaboration, DELPHI 2001–024 CONF 465, submitted to the Winter 2001 Conferences.

[117] L3 Collaboration, L3 Note 2638, submitted to the Winter 2001 Conferences.

[118] OPAL Collaboration, OPAL Physics Note PN469, submitted to the Winter 2001 Conferences.

[119] The LEP WW Working Group, LEPEWWG/XSEC/2001-02, note prepared for the 2001 update of the PDG Review, `http://lepewwg.web.cern.ch/LEPEWWG/lepww/4f/PDG01`.

[120] The LEP Collaborations ALEPH, DELPHI, L3, OPAL, the LEP Electroweak Working Group and the SLD Heavy Flavour Working Group, *"A Combination of Preliminary Electroweak Measurements and Constraints on the Standard Model"*, CERN–PPE/97–154.

[121] The LEP Collaborations ALEPH, DELPHI, L3, OPAL, the LEP Electroweak Working Group and the SLD Heavy Flavour Working Group, *"A Combination of Preliminary Electroweak Measurements and Constraints on the Standard Model"*, CERN–EP/99–15.

[122] S. Jadach, W. Płaczek, M. Skrzypek, B.F.L. Ward, Phys. Rev. **D54** (1996) 5434.
S. Jadach, W. Płaczek, M. Skrzypek, B.F.L. Ward, Z. Wąs, Phys. Lett. **B417** (1998) 326.
S. Jadach, W. Płaczek, M. Skrzypek, B.F.L. Ward, Z. Wąs, Phys. Rev. **D61** (2000) 113010; preprint CERN-TH-99-222, hep-ph/9907346.
S. Jadach, W. Płaczek, M. Skrzypek, B.F.L. Ward, Z. Wąs, preprint CERN-TH/2000-337, hep-ph/0007012; submitted to Phys. Lett. B.
S. Jadach, W. Płaczek, M. Skrzypek, B.F.L. Ward, Z. Wąs, *The Monte Carlo Event Generator* `YFSWW3` *version* `1.16` *for W-Pair Production and Decay at LEP2/LC Energies*, preprint CERN-TH/2001-017, UTHEP-01-0101, hep-ph/0103163, accepted for publication by Comput. Phys. Commun.
The YFSWW cross-sections at 155–215 GeV have been kindly provided by the authors.

[123] A. Denner, S. Dittmaier, M. Roth and D. Wackeroth, Nucl. Phys. **B560** (1999) 33.
A. Denner, S. Dittmaier, M. Roth and D. Wackeroth, Nucl. Phys. **B587** (2000) 67.
A. Denner, S. Dittmaier, M. Roth and D. Wackeroth, Phys. Lett. **B475** (2000) 127.
A. Denner, S. Dittmaier, M. Roth and D. Wackeroth, hep-ph/0101257.
The RACOONWW cross-sections at 155–215 GeV have been kindly provided by the authors.

[124] See [96] and references therein for a discussion of complete $\mathcal{O}(\alpha)$ radiative corrections to W-pair production in the LPA/DPA approximations.

[125] The theoretical uncertainty $\Delta\sigma/\sigma$ on the W-pair production cross section calculated in the LPA/DPA above 170 GeV can be parametrised as $\Delta\sigma/\sigma = 0.4 \oplus 0.072 \cdot t_1 \cdot t_2$, where $t_1 = (200 - 2 \cdot m_{\rm W})/(\sqrt{s} - 2 \cdot m_{\rm W})$ and $t_2 = (1 - (\frac{2 \cdot M_{\rm W}}{200})^2)/(1 - (\frac{2 \cdot M_{\rm W}}{\sqrt{s}})^2)$. In the threshold region, a 2% uncertainty is assigned. Private communication from the authors of [122, 123], March 2001.

[126] D. Bardin, J. Biebel, D. Lehner, A. Leike, A. Olchevski and T. Riemann, Comp. Phys. Comm. **104** (1997) 161. See also [96].
The GENTLE cross-sections at 155–215 GeV have been kindly provided by E. Lançon and A. Ealet.

[127] M. Skrzypek, S. Jadach, M. Martinez, W. Płaczek, Z. Wąs, Phys. Lett. **B372** (1996) 289.
S. Jadach, W. Płaczek, M. Skrzypek, Z. Wąs, Comput. Phys. Commun. **94** (1996) 216.
S. Jadach, W. Płaczek, M. Skrzypek, B.F.L. Ward, Z. Wąs, Comput. Phys. Commun. **119** (1999) 272.
S. Jadach, W. Płaczek, M. Skrzypek, B.F.L. Ward, Z. Wąs, preprint hep-ph/0104049, submitted to Comput. Phys. Commun.
The "KORALW" cross-sections at 155–215 GeV have been kindly provided by the authors. They have actually been computed using YFSWW [122], switching off non-leading $\mathcal{O}(\alpha)$ radiative corrections and the screening of the Coulomb correction, to reproduce the calculation from KORALW.

[128] A. P. Chapovsky and V. A. Khoze, Eur. Phys. J. **C9** (1999) 449.

[129] K. Melnikov and O. Yakovlev, Phys. Lett. **B324** (1994) 217;
V. S. Fadin, V. A. Khoze and A. D. Martin, Phys. Rev. **D49** (1994) 2247.

[130] W. Beenakker *et al.*, *"WW Cross-Sections and Distributions"*, in *"Physics at LEP2"*, eds. G. Altarelli *et al.*, CERN 96-01.

[131] Particle Data Group, D.E. Groom *et al.*, E. Phys. J. 1520001.

[132] ALEPH Collaboration, R. Barate *et al.*, Phys. Lett. **B469** (1999) 287.

[133] DELPHI Collaboration, P. Abreu *et al.*, Phys. Lett. **B497** (2001) 199.

[134] L3 Collaboration, M. Acciarri *et al.*, Phys. Lett. **B450** (1999) 281. The Z-pair cross-section at 183 GeV therein follows the L3 definition: the corresponding NC02 cross-section is given in [135].

[135] L3 Collaboration, L3 Note 2366, submitted to the Winter 1999 Conferences.

[136] L3 Collaboration, M. Acciarri *et al.*, Phys. Lett. **B465** (1999) 363.

[137] OPAL Collaboration, G. Abbiendi *et al.*, Phys. Lett. **B476** (2000) 256.

[138] L3 Collaboration, M. Acciarri *et al.*, Phys. Lett. **B497** (2001) 23.

[139] OPAL Collaboration, OPAL Physics Note PN482, submitted to the Summer 2001 Conferences.

[140] OPAL Collaboration, OPAL Physics Note PN423, ICHEP 2000 abstract 154.

[141] ALEPH Collaboration, ALEPH 2000–004 CONF 2000–001, ICHEP 2000 abstract 287. Systematic errors on the measurement were not quoted in this note and have only been made available in [142].

[142] ALEPH Collaboration, ALEPH 2001–006 CONF 2001–003, submitted to the Winter 2001 Conferences.

[143] DELPHI Collaboration, DELPHI 2000–145 CONF 444, ICHEP 2000 abstract 659. Systematic errors on the ZZ measurement at 192–202 GeV, not quoted in this note, are scaled linearly [144] from those estimated at 189 GeV.

[144] DELPHI Collaboration, private communication by P. Bambade, March 2001.

[145] DELPHI Collaboration, DELPHI 2001-015 CONF 456, submitted to the Winter 2001 Conferences.

[146] L3 Collaboration, L3 Note 2696, submitted to the Summer 2001 Conferences.

[147] S. Jadach, W. Płaczek, B.F.L. Ward, Phys. Rev. **D56** (1997) 6939.

[148] G. Passarino, in [96].

[149] ALEPH Collaboration, ALEPH 2001–017 CONF 2001–014, submitted to the Winter 2001 Conferences.

[150] DELPHI Collaboration, DELPHI 2001–099 CONF 527, submitted to the Summer 2001 Conferences.

[151] L3 Collaboration, M. Acciarri *et al.*, Phys. Lett. **B487** (2000) 229. See also [153].

[152] ALEPH Collaboration, R. Barate *et al.*, Phys. Lett. **B462** (1999) 389. The single W cross section at 183 GeV therein follows the ALEPH definition: the corresponding value using the common LEP definition is given in [155].

[153] L3 Collaboration, private communication by S. Schmidt-Kaerst, March 2001. The single W cross-sections at 183, 189 and 192–202 GeV in [151, 154, 158] all follow the L3 definition. The corresponding values using the common LEP definition, computed by applying a conversion factor determined for each result with `grc4f` [164], have all been provided in private communications.

[154] L3 Collaboration, M. Acciarri *et al.*, Phys. Lett. **B436** (1998) 417. See also [153].

[155] ALEPH Collaboration, ALEPH 2000–022 CONF 2000–019, submitted to the Winter 2000 Conferences.

[156] DELPHI Collaboration, DELPHI 2000-047 CONF 362, submitted to the Winter 2000 Conferences. The decays of the W boson to taus are not included in the total single W cross section at 189–202 GeV. A new definition has been adopted in [157].

[157] DELPHI Collaboration, DELPHI 2000-143 CONF 442/2, contributed paper for ICHEP 2000. The decays of the W boson to taus are here included in the total single W cross section at 189–202 GeV. A different definition was used in [156].

[158] L3 Collaboration, L3 Note 2518, submitted to the Winter 2000 Conferences. See also [153].

[159] OPAL Collaboration, OPAL Physics Note PN427, March 2000.

[160] The LEP WW Working Group, LEPEWWG/WW/00–02, *LEP Single W Cross Section for Winter 2000 Conferences*,
`http://lepewwg.web.cern.ch/LEPEWWG/lepww/4f/Winter00/ww-0002.ps`.

[161] L3 Collaboration, M. Acciarri *et al.*, Phys. Lett. **B403** (1997) 168. This measurement of the single W cross-section at 161–172 GeV is superseded by that published for 130–183 GeV [154].

[162] G. Passarino, Nucl. Phys. **B578** (2000) 3.
G. Passarino, Nucl. Phys. **B574** (2000) 451.
The WTO cross-sections at 160–210 GeV have been kindly provided by the author.

[163] E. Accomando and A. Ballestrero, Comp. Phys. Comm. **99** (1999) 270.
The WPHACT cross-sections at 160–210 GeV have been kindly provided by A. Ballestrero.

[164] J. Fujimoto *et al.*, Comp. Phys. Comm. **100** (1997) 74.
Y. Kurihara *et al.*, Prog. Theor. Phys. **103** (2000) 1199.
The `grc4f` cross-sections at 160–210 GeV have been kindly computed by R. Tanaka.

[165] G. Montagna *et al.*, *"Higher–order QED corrections to single W production in electron–positron collisions"*, FNT/T–2000/08, `http://arXiv.org/abs/hep-ph/0006307`.

[166] G. Gounaris *et al.*, in *Physics at LEP 2*, Report CERN 96-01 (1996), eds G. Altarelli, T. Sjöstrand, F. Zwirner, Vol. 1, p. 525.

[167] ALEPH Collaboration, *Measurement of Triple Gauge-Boson Couplings in e^+e^- collisions up to 208GeV*, ALEPH 2001-027 CONF 2001-021.

[168] G. Montagna, M. Moretti, O. Nicrosini, M. Osmo, and F. Piccinini, Phys. Lett. **B515** (2001) 197–205.

[169] K. Hagiwara, R. D. Peccei, D. Zeppenfeld, and K. Hikasa, Nucl. Phys. **B282** (1987) 253.

[170] G. J. Gounaris, J. Layssac, and F. M. Renard, Phys. Rev. **D62** (2000) 073013.

[171] G. Belanger and F. Boudjema, Phys. Lett. **B288** (1992) 210–220.

[172] W. J. Stirling and A. Werthenbach, Eur. Phys. J. **C14** (2000) 103–110.

[173] W. J. Stirling and A. Werthenbach, Phys. Lett. **B466** (1999) 369.

[174] G. Belanger, F. Boudjema, Y. Kurihara, D. Perret-Gallix, and A. Semenov, Eur. Phys. J. **C13** (2000) 283–293.

[175] ALEPH Collaboration, *Limits on anomalous neutral gauge couplings using data from ZZ and $Z\gamma$ production between 183-208 GeV*, ALEPH 2001-061 (July 2001) CONF 2001-041.

[176] DELPHI Collaboration, *Study of Trilinear Gauge Boson Couplings ZZZ, $ZZ\gamma$ and $Z\gamma\gamma$*, DELPHI 2001-097 (July 2001) CONF 525.

[177] L3 Collaboration, M. Acciari *et al.*, Phys. Lett. **B 436** (1999) 187;
L3 Collaboration, M. Acciari *et al.*, Phys. Lett. **B 489** (2000) 55.
L3 Collaboration, *Search for anomalous ZZg and Zgg couplings in the process ee$\rightarrow$Zg at LEP*, L3 Note 2672 (July 2001).

[178] OPAL Collaboration, G. Abbiendi *et al.*, Eur. Phys. J. **C 17** (2000) 13.

[179] See references [134, 136, 146].

[180] See references [137, 139].

[181] ALEPH Collaboration, *Constraints on Anomalous Quartic Gauge Boson Couplings*, ALEPH 2001-069 CONF 2001-049.

[182] Collaboration, M.Acciarri *et al.*, Phys. Lett. **B 490** (2000) 187;
L3 Collaboration, *Measurement of the W^+W^-g Cross Section and Direct Limits on Anomalous Quartic Gauge Boson Couplings at LEP*, L3 Note 2675 (June 2001).

[183] OPAL Collaboration, G. Abbiendi *et al.*, Phys. Lett. **B 471** (1999) 293.

[184] The LEP-TGC combination group, LEPEWWG/TGC/2001-01, March 2001.

[185] ALEPH Collaboration, R. Barate et al., Phys. Lett. **B453** (1999) 121–137.

[186] ALEPH Collaboration, R. Barate et al., Eur. Phys. J. **C17** (2000) 241–261.

[187] ALEPH Collaboration, *Measurement of the W Mass and Width in e^+e^- Collisions at $\sqrt{s} \sim 192 - 208$ GeV*, ALEPH note 2001-020 CONF 2001-017.

[188] DELPHI Collaboration, P. Abreu et al., Phys. Lett. **B462** (1999) 410–424.

[189] DELPHI Collaboration, P. Abreu et al., Phys. Lett. **B511** (2001) 159–177.

[190] DELPHI Collaboration, *Measurement of the mass and width of the W Boson in e^+e^- collisions at $\sqrt{s} = 192 - 209$ GeV*, DELPHI 2001-103 CONF 531.

[191] L3 Collaboration, M. Acciarri et al., Phys. Lett. **B454** (1999) 386–398.

[192] L3 Collaboration, *Preliminary Results on the Measurement of Mass and Width of the W Boson at LEP*, L3 Note 2377, March 1999.

[193] L3 Collaboration, *Preliminary Results on the Measurement of Mass and Width of the W Boson at LEP*, L3 Note 2575, July 2000.

[194] L3 Collaboration, *Preliminary Results on the Measurement of Mass and Width of the W Boson at LEP*, L3 Note 2637, February 2001.

[195] OPAL Collaboration, G. Abbiendi et al., Phys. Lett. **B453** (1999) 138–152.

[196] OPAL Collaboration, G. Abbiendi *et al.*, Phys. Lett. **B507** (2001) 29.

[197] OPAL Collaboration, *Measurement of the Mass of the W Boson in e^+e^- annihilations at 192-202 GeV*, OPAL Physics Note PN422 (updated July 2000).

[198] OPAL Collaboration, *Determination of the W mass in the fully leptonic channel using an unbinned maximum likelihood fit*, OPAL Physics Note PN480, July 2001.

[199] LEP Energy Working Group, LEPEWG 01/01, March 2001.

[200] Torbjorn Sjostrand and Valery A. Khoze, Z. Phys. **C62** (1994) 281–310.

[201] CHARM II Collaboration, P. Vilain *et al.*, Phys. Lett. **B335** (1994) 246.

[202] UA2 Collaboration, J. Alitti *et al.*, Phys. Lett. **B276** (1992) 354.

[203] CDF Collaboration, F. Abe *et al.*, Phys. Rev. Lett. **65** (1990) 2243;
CDF Collaboration, F. Abe *et al.*, Phys. Rev. **D43** (1991) 2070.

[204] CDF Collaboration, F. Abe *et al.*, Phys. Rev. Lett. **75** (1995) 11;
CDF Collaboration, F. Abe *et al.*, Phys. Rev. **D52** (1995) 4784.
A. Gordon, talk presented at XXXIInd Rencontres de Moriond, Les Arcs, 16-22 March 1997, to appear in the proceedings.

[205] DØ Collaboration, S. Abachi *et al.*, Phys. Rev. Lett. 842000222.

[206] `http://www-cdf.fnal.gov/physics/ewk/wmass_new.htm`.

[207] CDF Collaboration, W. Yao, *t Mass at CDF*, talk presented at ICHEP 98, Vancouver, B.C., Canada, 23-29 July, 1998.

[208] DØ Collaboration, B. Abbott *et al.*, Phys. Rev. Lett. 842000222.

[209] The Top Averaging Group, L.Demortier *et al.*, for the CDF and DØ Collaborations, FERMILAB-TM-2084 (1999).

[210] CCFR/NuTeV Collaboration, K. McFarland *et al.*, Eur. Phys. Jour. **C1** (1998) 509.

[211] NuTeV Collaboration, K. McFarland, talk presented at the XXXIIIth Rencontres de Moriond, Les Arcs, France, 15-21 March, 1998, hep-ex/9806013. The preliminary result quoted is a combination of the NuTeV and CCFR results.

[212] C. S. Wood et al., Science **275** (1997) 1759.

[213] S. C. Bennett and C. E. Wieman, Phys. Rev. Lett. **82** (1999) 2484–2487.

[214] A. Derevianko, Phys. Rev. Lett. **85** (2000) 1618.

[215] S. G. Porsev M. G. Kozlov and I. I. Tupitsyn, Phys. Rev. Lett. **86** (2001) 3260.

[216] NuTeV Collaboration, G.P. Zeller *et al.*, *A Precise Determination of Electroweak Parameters in Neutrino-Nucleon Scattering*, preprint hep-ex/0110059.

[217] T. van Ritbergen and R.G. Stuart, Phys. Rev. Lett. **82** (1999) 488.

[218] H. Burkhardt and B. Pietrzyk, Phys. Lett. **B513** (2001) 46.

[219] SLD Collaboration, J. Brau, *Electroweak Precision Measurements with Leptons*, talk presented at EPS-HEP-99, Tampere, Finland, 15-21 July 1999.

[220] *Reports of the working group on precision calculations for the Z resonance*, eds. D. Bardin, W. Hollik and G. Passarino, CERN Yellow Report 95-03, Geneva, 31 March 1995.

[221] G. Degrassi, S. Fanchiotti and A. Sirlin, Nucl. Phys. **B351** (1991) 49;
G. Degrassi and A. Sirlin, Nucl. Phys. **B352** (1991) 342;
G. Degrassi, P. Gambino and A. Vicini, Phys. Lett. **B383** (1996) 219;
G. Degrassi, P. Gambino and A. Sirlin, Phys. Lett. **B394** (1997) 188;
G. Degrassi and P. Gambino, Nucl. Phys. **B567** (2000) 3.

[222] A. Czarnecki and J. Kühn, Phys. Rev. Lett. **77** (1996) 3955;
R. Harlander, T. Seidensticker and M. Steinhauser, Phys. Lett. **B426** (1998) 125.

[223] Electroweak libraries:
ZFITTER: see Reference 37;
BHM (G. Burgers, W. Hollik and M. Martinez): W. Hollik, Fortschr. Phys. **38** (1990) 3, 165; M. Consoli, W. Hollik and F. Jegerlehner: Proceedings of the Workshop on Z physics at LEP I, CERN Report 89-08 Vol.I,7 and G. Burgers, F. Jegerlehner, B. Kniehl and J. Kühn: the same proceedings, CERN Report 89-08 Vol.I, 55;
TOPAZ0 Version 4.0i: G. Montagna, O. Nicrosini, G. Passarino, F. Piccinni and R. Pittau, Nucl. Phys. **B401** (1993) 3; Comp. Phys. Comm. **76** (1993) 328.
These computer codes have upgraded by including the results of [220] and references therein. ZFITTER and TOPAZ0 have been further updated using the results of references 221 and 222. See, D. Bardin and G. Passarino, *Upgrading of Precision Calculations for Electroweak Observables*, CERN-TH/98-92, hep-ph/9803425.

[224] A. Freitas, W. Hollik, W. Walter and G. Weiglein, Phys. Lett. **B495** (2000) 338.

[225] D. Bardin, P. Gambino, G. Passarino, G. Weiglein, private communication, spring 2001.

[226] T. Hebbeker, M. Martinez, G. Passarino and G. Quast, Phys. Lett. **B331** (1994) 165;
P.A. Raczka and A. Szymacha, Phys. Rev. **D54** (1996) 3073;
D.E. Soper and L.R. Surguladze, Phys. Rev. **D54** (1996) 4566.

[227] M. Steinhauser, Phys. Lett. **B429** (1998) 158.

[228] S. Eidelmann and F. Jegerlehner, Z. Phys. **C67** (1995) 585.

[229] The BES Collaboration, J.Z.Bai *et al.*, *Measurements of the Cross Section for $e^+e^- \to$ hadrons at Center-of-Mass Energies from 2 to 5 GeV*, hep-ex/0102003.

[230] M. L. Swartz, Phys. Rev. **D53** (1996) 5268.

[231] A.D. Martin and D. Zeppenfeld, Phys. Lett. **B345** (1994) 558.

[232] R. Alemany, *et al.*, Eur. Phys. J. **C2** (1998) 123.

[233] M. Davier and A. Höcker, Phys. Lett. **B419** (1998) 419.

[234] J.H. Kühn and M. Steinhauser, Phys. Lett. **B437** (1998) 425.

[235] J. Erler, Phys. Rev. **D59**, (1999) 054008.

[236] A. D. Martin, J. Outhwaite and M. G. Ryskin, Phys. Lett. **B492** (2000) 69.

[237] F. Jegerlehner, *Hadronic Effects in (g-2) and $\alpha_{QED}(M_Z)$: Status and Perspectives*, Proc. of Int. Symp. on Radiative Corrections, Barcelona, Sept. 1998, page 75.

[238] S. Bethke, hep-ex/0004021, J. Phys. G26 (2000) R27.

[239] F. James and M. Roos, Comput. Phys. Commun. **10** (1975) 343.

[240] G. Montagna *et al.*, Comput. Phys. Commun. **117** (1999) 278;
http://www.to.infn.it/~giampier/topaz0.html .

[241] K.Hoffman, *Year 2000 update for OPAL and LEP HIGGSWG results"*, talk presented at ICHEP2000, Osaka, July 27 - August 2,2000, to appear in the proceedings.

[242] N. De Groot *Electroweak results from SLD*, talk presented at XXXVIth Rencontres de Moriond, Electroweak Interactions and Unified Theories, Les Arcs, March 2001, hep-ex/0105058;
Serbo V. Presented at Int. Europhys. Conf. High Energy Phys., July 2001, Budapest, Hungary.

Links to LEP results on the World Wide Web

The physics notes describing the preliminary results of the four LEP experiments submitted to the summer 2001 conferences, as well as additional documentation from the LEP electroweak working group are available on the World Wide Web at:

ALEPH:	http://alephwww.cern.ch/ALPUB/oldconf/summer01/summer.html
DELPHI:	http://delphiwww.cern.ch/~pubxx/www/delsec/conferences/summer01/
L3:	http://l3www.cern.ch/conferences/Budapest2001/
OPAL:	http://opal.web.cern.ch/Opal/physnote.html
LEP-EWWG:	http://lepewwg.web.cern.ch/LEPEWWG/